UNIVERSITÀ DI PISA

Scuola di Dottorato in Ingegneria "Leonardo da Vinci"

Corso di Dottorato di Ricerca in
SICUREZZA NUCLEARE E INDUSTRIALE

Tesi di Dottorato di Ricerca

AN INTEGRATED APPROACH TO ACCIDENT ANALYSIS IN PWR

Autore:

Eugenio Coscarelli *Firma*_____

Relatori:

Prof. Ing. Francesco D'Auria *Firma*_____

Ing. Giorgio M. Galassi *Firma*_____

Ing. Alessandro Del Nevo *Firma*_____

Anno 2013

A Ada e Antonio

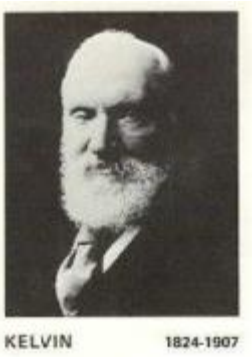

KELVIN 1824-1907

When you measure what you are speaking about, and express it in numbers, you know something about it; but when you cannot measure it, when you cannot not express it in numbers, your knowledge is of a meager and unsatisfactory kind: it may be the beginning of knowledge, but you have scarcely, in your thoughts, advanced to the stage of the science.

William Thomson, Lord Kelvin, from Popular Lectures and Addresses, 1891-1894

RINGRAZIAMENTI

Vorrei ringraziare quanti hanno permesso con la loro fattiva collaborazione ed il loro prezioso aiuto la realizzazione di questo lavoro. In primo luogo vorrei ringraziare il Prof. Ing. Francesco D'Auria per aver messo a disposizione il suo enorme bagaglio di esperienza e competenza tecnica nel campo della termoidraulica contribuendo in questo modo alla definizione degli obiettivi di questa ricerca.

Vorrei ringraziare i miei relatori, il Dott. Ing Giorgio Galassi ed il Dott. Ing. Alessandro Del Nevo che mi hanno supportato (ma soprattutto sopportato) in questo percorso, fornendomi preziosi suggerimenti attraverso i quali sono riuscito a superare le non poche difficoltà che sono emerse durante l'attività di ricerca.

Un ringraziamento particolare lo vorrei rivolgere ad un guru della termoidraulica, il Dott. Herbert Staedtke con il quale ho avuto interessanti e profondi scambi di idee che hanno illuminato il mio cammino nel complesso ed affascinante mondo della fluidodinamica bifase.

Ringrazio il Prof. Walter Ambrosini e Juan Carlos Ferreri che stimo per la profonda competenza tecnica, ma soprattutto perché ognuno di loro ha rappresentato un punto di riferimento per la mia attività di ricerca.

Vorrei ringraziare i miei più cari amici che mi sono stati vicini in questo lungo periodo di studio: Andrea, Cesare e Paola, Giancarlo e Alessandro. Un ringraziamento particolare va all'Ing. Daniele Martelli compagno di mille esami e collega dello stesso corso di dottorato.

Un profondo ringraziamento va ai miei genitori: Ada e Antonio per la loro incrollabile fiducia che hanno sempre risposto in me. Ringrazio anche i mie due nipoti Angelo e Antonio, le mie sorelle Silvana e Filomena, i miei cognati Alessandro e Carmine, per essere stati sempre presenti.

Un ringraziamento particolarmente affettuoso va, infine a mia moglie Rosa che mi è stata vicina nei momenti più difficili di questo lavoro sostenendomi materialmente e moralmente.

ABSTRACT

The purpose of the present doctoral research is to provide a contribute to the TH-SYS codes assessment for nuclear reactor applications, and particularly for the predictive analysis of PWR transient behavior, such as MSLB accident scenario, in which strong coolant flow asymmetries and multi-dimensional turbulent mixing effects strongly influence two relevant safety issues: recriticality and PTS.

The contribution consists in proposing and developing of an integrated analytical approach for TH-SYS code (TRACE-V5) assessment in relation to the investigation of the coolant transient flow processes in the reactor coolant system. The developed approach is focused on set up a methodology able to assess the accuracy of the numerical predictions based on the use of reliable experimental database that covers all relevant thermal hydraulic processes observed to occur simultaneously at system and component phenomenological levels during a selected accident scenario in a PWR system. To achieve this goal the first phase was to perform an independent assessment through the formulation of an independent assessment matrix for two classes of tests (basic test and integral effect test). The aim was to evaluate the capabilities of the code and models in reproducing the relevant thermal-hydraulic phenomena which characterize the simulated experiments. The second phase has concerned the development of the integrated methodology by defining a specific transient scenario important for PWR system safety (namely MSLB). Once the specific scenario has been identified, the methodology was oriented to define the relevant phenomena and processes that drive the system response. After the definition of all phenomena and interactions during the selected scenario, a corresponding process for establishing a test matrix was developed. The construction of the test matrix was carried out identifying a set of tests performed in integral and separate effects tests facilities achieved in a complementary way. Finally, the suitability of code in predicting the results of the complementary tests was obtained splitting the quantification of the accuracy in two phases. The first phase concerned the evaluation of the accuracy in a integral sense that is assess the code results at the system level (analysis of the overall thermal hydraulic response of the PWR system) against experimental data of the integral test performed in PKL-III facility. The second phase was oriented to measure the code discrepancies focusing the attention to the component level phenomena identified in the PWR system during the accident scenario under investigation and not experimental captured by the integral test. This last phase is connected, from the experimental point of view, with the tests carried out in the ROCOM test facility. In this way it is possible to cover experimentally the overall spectrum of phenomena expected to occur during the MSLB transient and assess the computational results using the same code (TRACE-V5 TH-SYS code) to simulate both tests: integral and separate effects tests.

Therefore, the methodology addresses also the issue of the validation of the 3-dimensional modules existing as an option in the codes like TRACE-V5 in simulating complex multi-dimensional flow patterns, such as mixing flow present in the RPV during the transient scenario (MSLB).

In view of the methodology goals, the work is supported by code validation and application results obtained in the frame of OECD/NEA CSNI PKL-2 project. It consists of an experimental program of eight tests (G series) carried out in integral test facility. The third test, identified as G3.1, has been selected for the application of the integrated approach, since the results of this PKL test, which is oriented PWR system behavior, also provide the boundary conditions for complementary tests in the ROCOM facility on mixing cold and hot water in the RPV downcomer as well as in the lower plenum and for determining the fluid state at the core inlet.

Within the proposed approach, the relevant modelling issues are identified and discussed, so as to point out the main capabilities and limitations in the present state-of-the-art tools and methods.

INDEX

ABBREVIATIONS

3-D	Three Dimensional
AM	Accident Management
BE	Best Estimate
BEPU	Best Estimate Plus Uncertainty
BC	Boundary Conditions
BIC	Boundary Initial Conditions
CET	Core Exit Temperature/Component Effect Test
CFD	Computational Fluid Dynamics
CFR	Code of Federal Regulation
CHF	Critical Heat Flux
CL	Cold Leg
COMBO	Continuous Measurement of Boron Concentration
CPh	Conditioning Phase
CSNI	Committee on the Safety of Nuclear Installations
CSP	Core Support Plate
DBA	Design Basis Accident
DIMNP	Department of Mechanical, Nuclear and Production Engineering of University of Pisa, Italy
ECCS	Emergency Core Cooling System
FA	Fuel Assembly
FC	Fuel Channel
FFT	Fast Fourier Transform
FFTBM	Fast Fourier Transform Based Method
FP	Fission product
FSAR	Final Safety Analysis Report
GRNSPG	San Piero a Grado Nuclear Research Group
GT	Guide Tube
HL	Hot Leg
I & C	Instrumentation and control
IAEA	International Atomic Energy Agency
IAM	Independent Assessment Matrix
IC	Initial Conditions
ITF	Integral Test Facility
LB-LOCA	Large Break LOCA
LOCA	Loss of Coolant Accident
LS	Loop Seal
MSL	Main Steam Line
MSLB	Main Steam Line Break
MSRCV	Main Steam Relieve Control Valve
NEA	Nuclear Energy Agency
NPP	Nuclear Power Plant
OECD	Organization for the Economic Cooperation and Development
PCT	Peak Cladding Temperature
Ph.W.	Phenomenological Window
PMI	Primary Mass Inventory

PRZ	Pressurizer
PS	Primary Side
PWR	Pressurized Water Reactor
RBV	Rod Bundle Vessel
RC	Reflux Condensation
RCS	Reactor Coolant System
RCL	Reactor Coolant Loop
RPV	Reactor Pressure Vessel
SBLOCA	Small Break LOCA
SETF	Separate Effect Test Facility
SETS	Stability Enhancing Two Step
SG	Steam Generator
SoT	Start of Transient
SPNC	Single Phase Natural Circulation
SS	Secondary Side
SYS	System
TH	Thermal-Hydraulic
THS	Thermal-Hydraulics Safety
TMF	Turbulent Mixing Flow
TPNC	Two Phase Natural Circulation
UNIPI	University of Pisa

LIST OF FIGURES

LIST OF TABLES

1 INTRODUCTION

Arguably no other field of engineering depends so strongly on the development and assessment of numerical simulation tools (like TH-SYS or CFD codes) as nuclear technology and especially nuclear safety. The applications of the *numerical process simulation* in the framework of safety and licensing is mainly due to the impracticability of executing full-scale safety related experiments and the absence of simplified scaling criteria for the important physical processes (occurring during the scenarios of interest) which would allow a direct transfer of results from small scale test facilities to the nuclear power plant. The main objective of developing numerical simulation tools (TRACE, RELAP5, CATHARE, etc.) was to replace the *evaluation model* (EM) approach which includes the definition of a limited number of worst case scenarios in combination with conservative assumption by *best-estimate* (BE) methodologies. Best-estimate approach, aimed to provide a detailed realistic description of postulated accident scenarios based on best-available modelling methodologies and numerical solution strategies, is the current strategy adopted in nuclear thermal hydraulic safety analysis. A consequence extensive experimental programs in scaled down integral and separate effect test facilities are conducted for solving open issues of current nuclear power plant designs, for demonstrating the technical feasibility of innovative designs, and for generating reference databases in order to support codes development and assessment [1]. Experimental data are fundamental for demonstrating the reliability of computer codes in simulating the behavior of a NPP during a postulated accident scenario: in general, this is a regulatory requirement [2].International efforts have been lavished to promote and organize activities aimed at increasing confidence in the validity and accuracy of analytical tools and demonstrating the competences of the involved institutions. Relevant examples of those activities are the ISP [3] under the aegis of the NEA/CSNI (the ISP-50 is currently ongoing and the draft report of the blind phase has been issued [4]), the ICSP sponsored by IAEA (e.g. the ICSP on MASLWR is currently ended [5]), but also analytical exercises carried out and documented in the framework of international groups connected with experimental programs in test facilities (e.g. Refs. [5], [6] and [8]).

1.1. Objectives of the research

The performed research activity is aimed at contributing to the assessment of TH-SYS codes in their application to issues related to the safety analysis of nuclear technology, in particular for the predictive analysis of complex transient two-phase flow and heat transfer conditions as expected to occur in Light Water Reactors (LWR) under accident and off-normal conditions. In this frame, this research is designed to approach new challenges and future needs in nuclear thermal-hydraulics which might arise from the simultaneous modelling of multi-dimensional effects which are always present in the full-size plant during an accident scenario. The fulfillment of this aspect will require the development of new strategies for the validation of 3-D prediction capability using experimental data that coming from

integral and separate effect tests carried out following an integrated approach (namely executed in a complementary way). In this way it is possible to reproduce at the scaled level the broad spectrum of phenomena featuring the specific accidental transient (system and component level) as well as to assess the TH-SYS codes toward a best estimate thermal hydraulic modeling.

1.2. Framework

The research has been carried out in the framework of the OECD/NEA CSNI PKL-2, http://www.nea.fr/jointproj/pkl.html, (2008-2012) and has thus profited of the availability of large experimental databases as well as of the connection to a wide number of internationally recognized experts in the fields of nuclear reactor safety and thermal-hydraulic and code development and assessment. The project is aimed at studying selected accident scenarios at system level, understanding the thermal hydraulic phenomena and processes occurring in pressurized water reactor design as well as validating and improving complex thermal-hydraulic system codes used in safety analysis. The experimental program consists of eight tests (G series), carried out in PKL-III facility by AREVA NP in Erlangen (Germany). It represents the scaled down layout of a 1300-MW PWR NPP (KWU-Siemens, Philippsburg NPP unit 2).

1.3. Description of the performed activity

The activity performed for fulfilling the objectives of the research is outlined in

Figure 1. The steps below were executed to fulfill the following objectives:

- acquisition of expertise in the thermal hydraulic field, taking advantage from the participation in international activities;
- investigation of issue related to the use of TH-SYS codes and related methodologies;
- development of a methodology and related tools for accident analysis in PWR systems;
- qualification activities to support the reliability of the analyses;
- application of the methodology for predicting the phenomenology expected to occur during a MSLB scenario simulated in PKL-III/ROCOM test facilities.

The work is the result of the following TH-SYS code-related activities carried out within the San Piero a Grado Research Group (GRNSPG) of University of Pisa:

- TH-SYS code analyses for various purposes such as code assessment against integral and separate effect tests and investigation of the code numerical scheme capabilities through numerical tests;
- supporting nuclear reactor safety studies, etc.;
- participation in international meetings, workshops and events, being in contact with several internationally recognized experts.

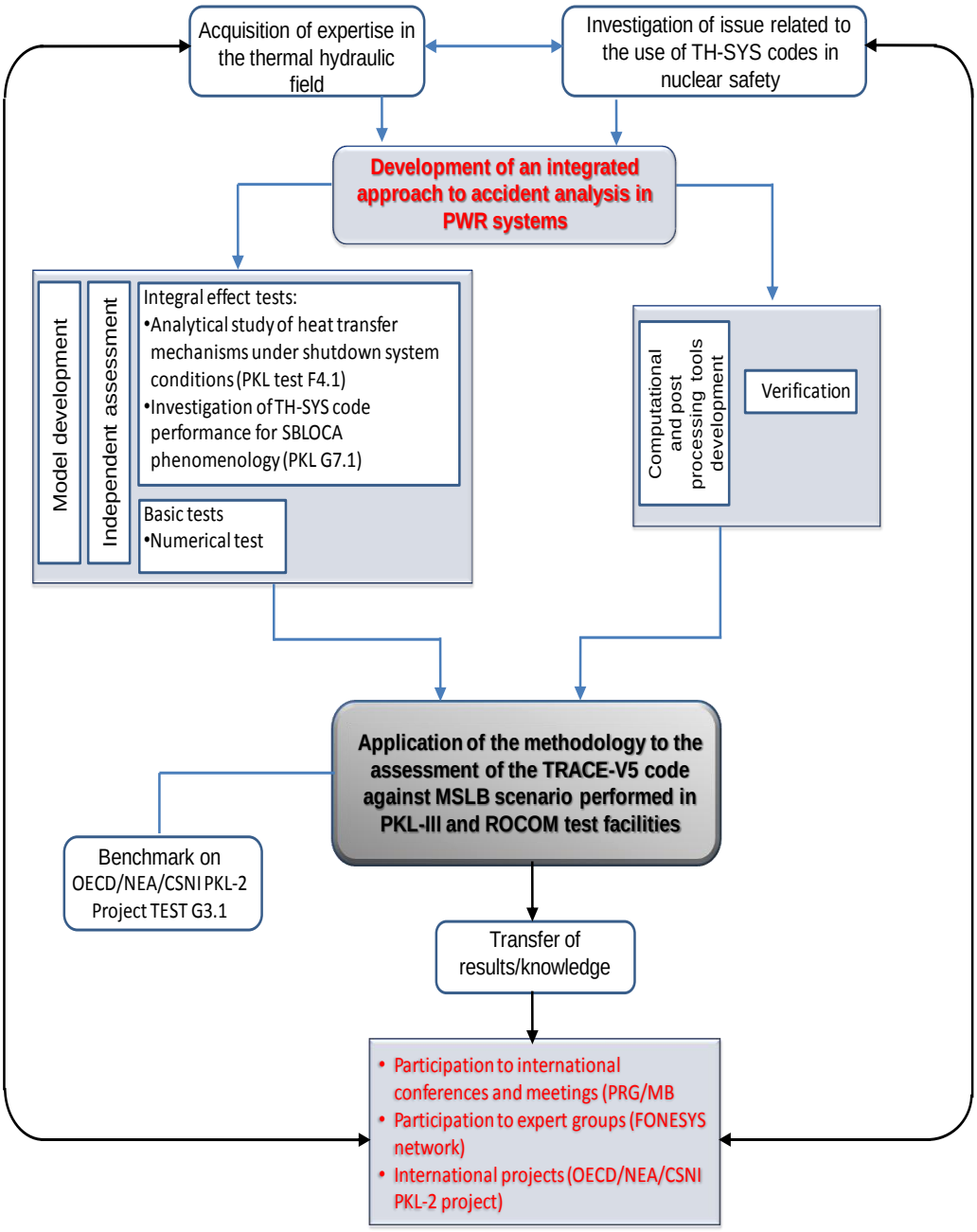

Figure 1 – Flow chard of PhD performed research activity

1.4. Structure of the document

The thesis is divided in seven chapters and five appendixes.

The **Introduction** contains the background information and the objective of the activity.

Chapter 2 describes the framework in which the methodology developed in this research, namely the best estimate deterministic safety approach.

Chapter 3 presents historical overview and the current state-of-the-art in the field of thermal-hydraulic numerical simulation related to nuclear technology and nuclear safety, with emphasis on various issues of TH-SYS codes.

Chapter 4 contains the description of the independent assessment approach for the TRACE-V5 code and nodalization assessment against experimental data from two PKL-III tests. The experimental facility is described, and the results obtained from the experiments are presented. In addition a basic numerical test has been selected to test the numerical characteristics of the algorithm implemented in the TRACE-V5 code.

Chapter 5 outlines the integrated analytical methodology to accident analysis in PWR systems.

Chapter 6 contains the results of the application of the integrated methodology for predicting the phenomenology characterizing the MSLB scenario throughout the comparison of the computational modelling results with the experimental results of the PKL-III/ROCOM complementary test (PKL test G3.1 and ROCOM test 1.1, 1.2 and 2.2)

Chapter 7 finally presents conclusions from the performed research activity.

2 DETERMINISTIC SAFETY ANALYSIS AND BEST ESTIMATE APPROACH

2.1. Framework

Thermal hydraulic safety (THS) assessment represents the most relevant issue in the design and licensing of NPPs ensuring the acceptability of SM. The two main branches through which develops the THS process, are the deterministic safety analysis (DSA) and the probabilistic safety (PSA) analysis. The framework in which is developed the research activity is linked with DSA, the purpose of which is to address plant behavior under specific predetermined operational states and accident conditions. In regard to this objective the PWR thermal hydraulic safety evaluation and assessment, is closely related the development of more sophisticated analytical tools able to predict the time-space thermal-hydraulic conditions throughout the reactor coolant system.

Historically the emergency core cooling systems (ECCS) against LOCA scenario was one of the major topics of safety assessment for light water reactors established with the publication of the 'Interim Acceptance Criteria (see [9]). This had as outcome the assessment of the thermal hydraulic safety analysis performed through the use of analytical and experimental methods, which in turn have resulted in various safety analysis codes and experimental facilities. Several integral and separate effect test facilities have been built and operated since 1960s (see Figure 2 in which is represented the spectrum of test facilities vs scale) aiming to provide useful information and experimental data on the thermal hydraulic behavior LWR under accident conditions and on the reliability of the TH-SYS code in performing accident analysis.

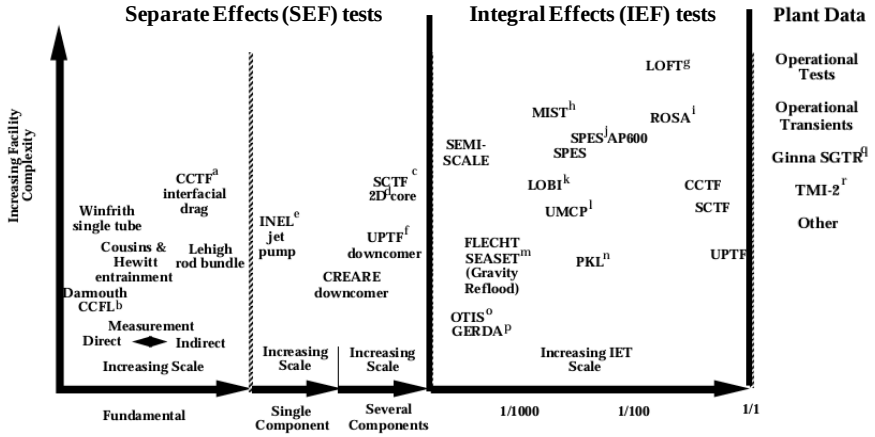

Figure 2 – Spectrum of SET, CET and IET facilities[1].

[1] Figure is illustrative and is not intended to include all SET, CET, and IET facilities

2.2. Deterministic safety analysis

Deterministic safety analysis is an important tool for confirming the adequacy and efficiency of provisions within the defense in depth concept for the safety of nuclear power plants (NPPs) [9]. Two different methodologies has been adopted to assess the deterministic thermal hydraulic safety analysis, namely the conservative approach and the best estimate approach. The concept of conservative methods was introduced in the early days of safety analysis to cover uncertainties that prevailed in the 1970s due to the limited capability of modelling and the limited knowledge of physical phenomena, and to simplify the thermal hydraulic analysis. The results obtained by this approach may be misleading (unrealistic behavior predicted, order of events changed) and level of conservatism is unknown. Therefore, there has been a move away from over-conservatism in safety analysis towards the application of so-called best estimate methodologies.

2.2.1. Conservative approach

The conservative approach has traditionally been used for the licensing analyses, being part of a NPP's commissioning activities and has to be submitted to and approved by the regulatory authority. In a traditional conservative analysis, both the assumed plant conditions and the physical models used are set conservatively. The reasoning is that such an approach would demonstrate that the calculated safety parameters are within the acceptance criteria and would ensure that no other transient of that category would exceed the acceptance criteria. However, in those analyses the safety margins obtained are expected to be conservatively large, as certain TH phenomena as well as certain plant and system features are not credited. Besides, it should be noted that the conservative approach does not provide any indications as to the true safety margins nor does it provide a true simulation of a specified scenario. For example, the assumption of a high core power level may lead to high levels of steam–water mixture in the core in the case of a postulated small break loss of coolant accident. Consequently, the calculated peak cladding temperature may not be conservative. As another example, the assumption that reduced interfacial shear between water and steam may lead to higher cladding temperatures in the upper core region, is conservative. However, this conservative assumption will lead to an optimistic estimate for the refilling/reflooding time, as it will appear that more water remains in the primary cooling system than is actually the case. In cases where a realistic analysis could demonstrate that important safety issues may be being masked, the conservative licensing calculations should be accompanied by a best estimate analysis, without

a)	Cylindrical Core Test Facility.	f)	Upper-Plenum Test Facility.	k)	Loop for Blowdown Investigation.	p)	Geradrohr Dampferzeuger Anlage.
b)	Counter current flow limitation.	g)	Loss of Fluid Test.	l)	University of Maryland, College Park.	q)	Steam-generator tube rupture.
c)	Slab Core Test Facility.	h)	Multiloop Integral Test Facility.	m)	Full Length Emergency Cooling Heat Transfer-Separate Effects And Systems Effects Test.	r)	Three Mile Island, Unit 2.
d)	Two dimensional.	i)	Rig of Safety Assessment.	n)	Primarkreislaufe.		
e)	Idaho National Engineering Laboratory.	j)	Simulatore PWR per Esperienze di Sicurezza.	o)	Once-Through Integral Systems.		

an evaluation of the uncertainties, to ensure that important safety issues are not being concealed by the conservative analysis [10].

2.2.2. Best estimate approach

The best estimate approach is the actual trend of the NPP deterministic analysis [11]. The concept of best estimate is generally applied to the codes used in the analysis. However the best estimate approach concept has a broader meaning. It applies to the general framework of the analysis, and it involves not only the codes, but the kind of analyses to be performed, the approach to realize the models to be realized for the analyses, the input data including boundary and initial conditions also. The best estimate approach is not only connected with a calculation performed with a best estimate code. The result of the analysis is a best estimate evaluation, if all the aspects of the analysis (input data, systems models, results) are best estimate, in addition to the codes. As a consequence, the use of a best estimate code, assuming not best estimate data or systems model cannot be considered a best estimate analysis.

In the BE analyses, the TH phenomena are simulated as accurately as possible (according to present knowledge) and the safety margins obtained more closely reflect the real margins in the plant. This type of analyses also provides more realistic simulations of the NPP behavior during the course of the transient scenarios and can consequently reveal detailed system information that can be relevant for the understanding of TH phenomena interaction. If BE analyses are used for licensing purposes, they must be accompanied by uncertainty analyses to quantify the uncertainty of calculated parameters. The uncertainty includes contributions from simplifications introduced both into the governing equations and to the constitutive relationships and models, but also from using such models outside their original ranges of validity.

3 STATE OF THE ART IN THE APPLICATION OF TH-SYS CODES TO NRS

3.1. History and current status of TH-SYS codes

The need to support safety analyses in nuclear technology has begun to be increasingly important in the past 40 years in relation to the efforts in predicting the behavior of two phase flow in complex systems. Therefore, several Thermal Hydraulic SYStem (TH-SYS) codes have been developed for simulating nuclear reactor in normal operation and in accidental transients. These codes started to be developed since the end of the 1960's as a response to the requirements, or knowledge targets, put by the Regulatory Body in the United States, US Atomic Energy Commission (US AEC), presently US Nuclear Regulatory Commission (US NRC). This promote a wide variety of research aimed at the evaluation of safety margins and focusing on the estimation of the maximum temperature on the surface of fuel rods following large break loss of coolant accidents (LB-LOCA). *Appendix K* to paragraph *10 CFR-50.46* followed in 1974 [12]. The publication of the *Interim Acceptance Criteria for ECCS* [13] shall be taken as the starting date for system thermal hydraulic.

The first generation of these codes was developed by the United States safety authority, which sponsored the work until late '60s. They used uniform flow and thermal conditions and were referred to as homogeneous models. The next generation codes has recognized the importance of dealing with gas-liquid flow patterns and exchanges at the gas-liquid interface because of the non-thermal and non-mechanical equilibrium of the flow conditions. This has led to the development of system codes based on two phase flow models that solve a greater number of balance equations than the homogeneous models (six instead of three), with higher degree of complexity. To have a clear picture of the complexity which characterizes the TH-SYS codes, it is necessary to describe the approach on which the two phase models used are based into the current codes.

At least two essential different methods are used to model the two phase flow. The first of these is based on the Hamilton's variational principle[2] which allows to derive

[2] The Hamilton's principle states that the governing equations for the two phase flow are derivable by the application of variational procedure given by:

$$\delta \int_{t_1}^{t_2} (T - V)\, dt + \int_{t_1}^{t_2} \delta W dt = 0$$

where δ represents the variation over an appropriate space of functions, T and V are the kinetic and the potential energies, δW is the virtual work, and t_1 and t_2 are two arbitrary times. A variational formulation has an advantage in that if is it desired to include certain effect (for example the virtual mass), that effect would be included consistently in the mass momentum and kinetic energy equations. In continuum mechanics the use of the Hamilton's principle is straightforward in a Lagrangian description, namely it is formulated for material volume. Eleurian description can be used to develop a variational principle for

the governing equations by the minimization of an appropriate Lagrangian [15], [16], [17]. This approach leads to the systems of balance laws for each phase whose interaction is governed by the terms prescribed by the Lagrangian substance. The second approach, used in the present generation of codes, is based on a homogenization technique, namely a macroscopic description of the Navier-Stokes equations for liquid and vapor, using time and volume averaged values for all state and flow parameters. Such averaging procedures lead to a two-fluid model of two-phase flow, in which both phases are treated as interpenetrating continua. These averaging methods allow to focus on some macroscopic phenomena of interest while discarding all the microscopic details of the flows in order to reduce the CPU efforts. In fact the resulting averaged equations and the interfacial jump conditions form a mathematical model that is much simpler than the original formulation (local instantaneous conservation equations), but the information lost in the averaging process have to be supplied in the form of auxiliary relationships. These relationships are of two kinds: the first one concerns with interfacial and wall transfer of mass, heat and momentum, the second deals with the inter-phase distribution of the dependent variables.

In order to understand the process leading to the basic structure of the averaged two phase balance equations, we present a hierarchy of steps, named *Bestion's Hierarchy* (see Figure 3) [18] which describes the levels of approximation that filter the complexity of the physical reality and lead to the domain of the simulated reality. The successive steps leading to the simplified model of the governing equations consist in multiplying the local instantaneous balance equations by fluid-solid characteristic functions (in the frame of a porous 3-D modeling), by phase characteristic functions (in the frame of the two-fluid model), or field-characteristic functions (in the frame of the multi-field model) that characterize the presence of phase k at a given time t and location **x**. The last two levels of approximation of the hierarchical approach to derive a usable form of the two phase partial differential balance equations are spatial and time averaging processes.

Time averaging allows filtering all fluctuations due to turbulence and to the two-phase intermittency (succession of liquid and gas phases at a given point). The time scale of the averaging is supposed to be larger than the largest scale due to turbulence and to the two-phase intermittency and smaller than the time scale of variation of the averaged flow parameters during transients.

Let $\Phi(\boldsymbol{x}, t)$ be any quantity, than the time average of the field Φ is defined by:

$$\bar{\Phi}(\mathbf{x},t) = \frac{1}{\Delta T}\int_{t-\Delta T/2}^{t+\Delta T/2} \Phi(\mathbf{x},t)\, dt \qquad (1)$$

$$\Phi = \bar{\Phi} + \Phi'$$

To take in account that time averaging of the flow parameter Φ is used for each phase k we introduce the characteristic functions α_k, which represent the

---

two phase flow with the introduction of additional constraints (represented by the continuity equations for the two phase) throughout the use of Lagrangian multipliers, in this respect see Geurst [16].

probability of occurrence of the phase k at a given point in the time and space domain, accordingly the time average of the field Φ for the phase k become:

$$\bar{\Phi}_k(\mathbf{x},t) = \frac{1}{\alpha_k \Delta T} \int_{t-\Delta T/2}^{t+\Delta T/2} \chi_k \Phi(\mathbf{x},t)\, dt \qquad (2)$$

Where

$$\alpha_k = \bar{\chi}_k \qquad (3)$$

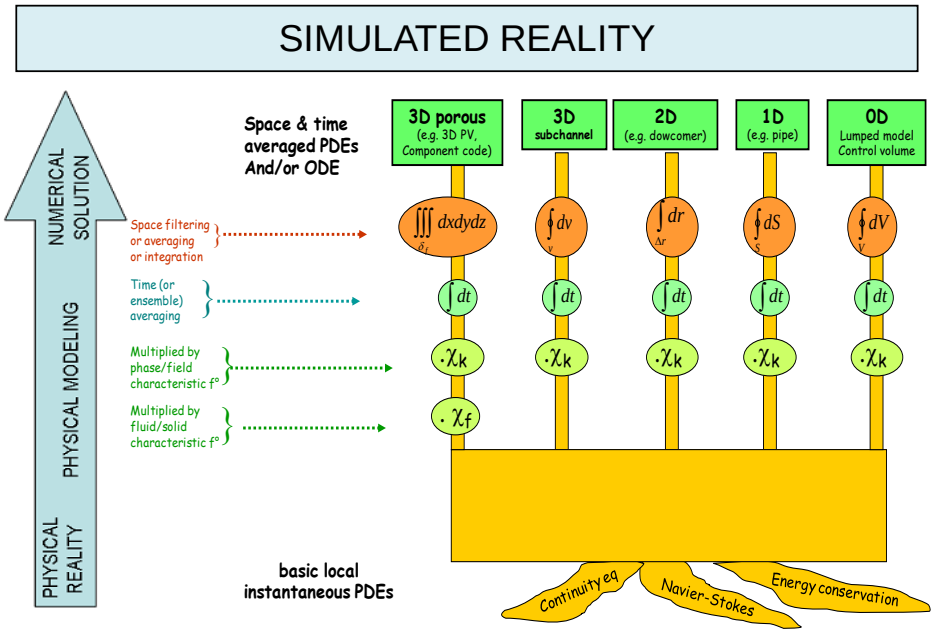

Figure 3 – The successive steps for establishing and solving thermal-hydraulic equations.

The space averaging, carried out using averaging operators and the Gauss and Leibniz rules ([15] and [19]), may be either a volume averaging used in the control volume context or in 3-D Pressure Vessel Modules in the frame of a porous body approach or a cross section averaging used in 1-D modules (for pipes, ducts, channels) or an averaging over one space dimension (e.g. for a 2-D modeling of an annular down-comer the equations are averaged over the radial dimension from Pressure Vessel wall to the core barrel).

The space averaging is also very helpful in two phase flows as it allows to reduce the complexity of the topological distribution of phases and the dynamics of the boundary among the phases. In fact with reference to the volume averaging, this leads to a sort of filtering over a sub-grid scale. Therefore effects of small scale processes on macroscopic evolution can be taken into account by appropriate closure relations.

As a result of the spatial/time averaging of the local instantaneous phase equations, the “macroscopic” balance equations of the two-fluid model can be formulated for each phase (k=l,g). The general form of governing equations (see [20 and [21]) is:

$$\frac{\partial(\alpha_k\rho_k)}{\partial t}+\nabla\cdot(\alpha_k\rho_k\mathbf{v}_k)=\Gamma_k$$

$$\frac{\partial(\alpha_k\rho_k\mathbf{v}_k)}{\partial t}+\nabla\cdot(\alpha_k\rho_k\mathbf{v}_k\mathbf{v}_k)+\alpha_k\nabla p_k+\left(p_k-p^{\text{int}}\right)\nabla\alpha_k-$$

$$-\nabla\cdot\left(\alpha_k\bar{\bar{\mathbf{T}}}_k\right)=\mathbf{F}_k^{\text{int}}+\Gamma_k\mathbf{v}^{\text{int}}+\mathbf{F}_k^{ext} \qquad (4)$$

$$\frac{\partial\left[\alpha_k\rho_k\left(u_k+1/2\,\mathbf{v}_k^2\right)\right]}{\partial t}+\nabla\cdot\left[\alpha_k\rho_k\mathbf{v}_k\left(h_k+1/2\,\mathbf{v}_k^2\right)\right]+p^{\text{int}}\frac{\partial(\alpha_k)}{\partial t}-$$

$$-\nabla\cdot\left(\alpha_k\bar{\bar{\mathbf{T}}}_k\cdot\mathbf{v}_k\right)+\nabla\cdot(\alpha_k\mathbf{q}_k)=Q_k^{\text{int}}+\Gamma_k\left(h_k+1/2\,\mathbf{v}_k^2\right)^{\text{int}}+\mathbf{F}_k^{\text{int}}\cdot\mathbf{v}^{\text{int}}+Q_k^{ext}$$

The left-hand sides of the equations (4) represent the advection or Euler part of the flow equations. The right-hand side terms include diffusive effects due to bulk heat conduction $\boldsymbol{q}_k$, the molecular and/or equivalent turbulent viscosity tensor $\bar{\bar{T}}_k$ and related energy dissipation, interfacial source terms due to mass, momentum and energy transfer $\Gamma_k, F_k^{int}, Q_k^{int}$ at the interface, as well as body forces (gravity) $\boldsymbol{F}_k^{ext}$ and external heat sources due to instantaneous fission power generation and fission product decay Q_k^{ext}.

So as to ensure the conservation of the same quantity for the two phase system it is necessary to impose jump conditions throughout the interface (see Eq. (5)). As the system of equations (4) also the balance equations throughout the discontinuity represented by the interface are written in local-instantaneous form and subject to the same averaging procedure.

$$\sum_{k=1}^{2}\Gamma_k=0$$

$$\sum_{k=1}^{2}\mathbf{F}_k^{\text{int}}=0 \qquad (5)$$

$$\sum_{k=1}^{2}\left[Q_k+\Gamma_k\left(h_k+1/2\,\mathbf{v}_k^2\right)\right]^{\text{int}}=0$$

All the current TH-SYS codes make use of balance equations referable to the system (4)[3] derived starting from the local instantaneous formulation and applying the hierarchical method[4] (*Bestion's Hierarchy*).

The major difficulty in applying the two-fluid approach arises from the fact that, even when the balance equations are complemented by the state equations for the two phases and by additional correlations for the right-hand side coupling terms, the resulting set of relationships contains more unknown dependent variables than the number of available equations. The most common strategy for the system of equations closure is to assume a local pressure equilibrium among the two fluids. Phasic pressure differences arising from the curvature of the liquid–vapor interface (surface tension effects) in different flow regimes are thereby neglected. The single pressure formulation has been used in nearly all current systems code. In the French and German codes, CATHARE and ATHLET, is present a model for computing the effect of the pressure difference between the bulk of the phase *k* and interface *int* (see [22] and [23]). An additional statement that simplify the model for two phase flow is based on the assumption of exclusively algebraic functions of the flow and state parameters of the two phases for the source terms of the balance equations.

During the evolution process of computer codes, different system computer codes were generated to deal with different events or different characteristics of the complex system (see Figure 4). Some of this scope customizing still prevails in the industry today, but the number of variations has been reduced in recent years by employing a modular construction for system computer codes. This allows subsystems and components to be excluded when they have a minor role and/or to focus on the most essential phenomena.

The applications of these analytical tools in the framework of safety and licensing process is mainly due to the impracticability of executing full-scale safety related experiments and the absence of simplified scaling criteria for the important physical processes (occurring during the scenarios of interest) which would allow a direct transfer of results from small scale test facilities to the nuclear power plant. The main objective of developing the present generation of system codes was to

---

[3] At present, almost none of the thermal hydraulic codes include the simulation of molecular and turbulent transfer. Except in the following TH-SYS codes, that are: RELAP5-3D, MARS (Korean TH-SYS code) and CATHARE codes.

[4] It is important to known that in the derivations of the macroscopic balance equations used in the current generation of TH-SYS use is made of the following simplifying assumption:

$$\langle fg \rangle \cong \langle f \rangle \langle g \rangle$$

Obviously this hypothesis does not take into account the correlation of the two variables in the control volume. Indeed, by the definition of covariance follows:

$$\langle fg \rangle - \langle f \rangle \langle g \rangle = \mathrm{cov}(f, g)$$

In the majority of circumstances which involve transient two phase flow in the nuclear technology the above assumption can be used with good approximation.

replace the *evaluation model* (EM) approach which includes the definition of a limited number of worst case scenarios in combination with conservative assumption by *best-estimate* (BE) methodologies. The best-estimate approach aims to provide a detailed realistic description of postulated accident scenarios based on best-available modelling methodologies and numerical solution strategies which have been sufficiently verified against experimental data from differently scaled separate effects and integral test facilities.

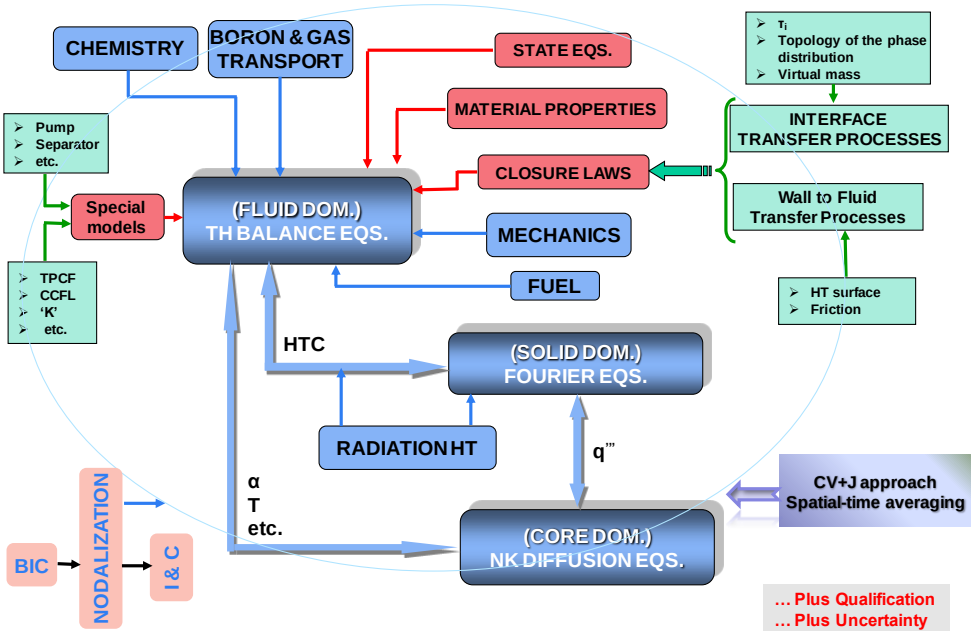

Figure 4 – Attributes and feature requested for a TH-SYS code

Although the capabilities of current computational tools and methods are able to address the safety issues, some weaknesses were identified. The physical modelling is limited by the capabilities of the averaged two-fluid six equation model and there is a lack of appropriate modelling of small scale three-dimensional phenomena. The present numerical schemes are robust and efficient but not accurate enough. At the beginning of nineties several workshops on Transient Thermal-Hydraulic and Neutronic Code Requirements to analyze the state of art of the present TH-SYS were organized by OECD/CSNI (Aix en Provence, 1992 [24], Annapolis, 1996 [25], Barcelona, 2000 [26]). The aim of these workshops was to identify the main inherent limitations of the current system code mainly evident in the simulation of the following process and phenomena:

- counter flows;
- critical flows;
- stratification in large volumes of water;
- three-dimensional flows.

All of these drawbacks are due to the approximations assumed in the complex two-phase processes simulation and to the typical assumptions used in the numerical

methods. The assessment of new generation codes must be developed considering the following items: physical simulation and numerical methodology. These two items lie within the V&V framework, which is a crucial part in the code development process.

Physical simulation points out the requirement to raise the level of accuracy of the models implemented in the current TH-SYS codes in order to be able to capture the relevant, multi-dimensional and interface phenomena. This means overcoming the algebraic empirical approaches of the two fluid models present in the formulation of the closure laws, which describe the interface and wall-to-fluid transfer processes. The degree of empiricism can be reduced by identifying new concept with respect to the physical modeling.

From the numerical methodology point of view a suitable numerical solution method is needed to solve all the equations that constitute a TH-SYS code, because the numerical solution method affects the result of any calculation. The lack of convergence comes from the use of ill-posed non-hyperbolic system of equations which can results in unstable problems in some system code. The equations require meshes large enough to prevent instability through numerical diffusion. When decreasing the mesh size, numerical diffusion is decreased and the unstable nature of equation is revealed. Hence there is the need of qualitative requirements for the numerical methods as the robustness, the stability and the non-diffusivity of the solution. Another requisite of the numerical methods is the calculation speed consistent with the available computing power.

TH-SYS codes, in the framework of BE approaches, are expected to play an important role for the safety assessment of LWRs with standard or evolutionary designs. It is evident that each model or code represents an approximation of the real system or plant. The final use of these codes will therefore largely depend on the progress in quantifying the uncertainty associated with the prediction of the plant behaviour.

3.2. Assessment strategy: Verification and validation (V&V)

As discussed above the TH-SYS codes require many assumptions, approximations, and a very large number of closure laws. Therefore, their use in the framework of nuclear safety analysis needs to an assessment process to ensure their capacity to simulate transient scenarios with a sufficient degree of reliability and accuracy. The two relevant aspects that have been identified for the assessment strategy are: the *Verification* and the *Validation* (V&V) (see Figure 4).

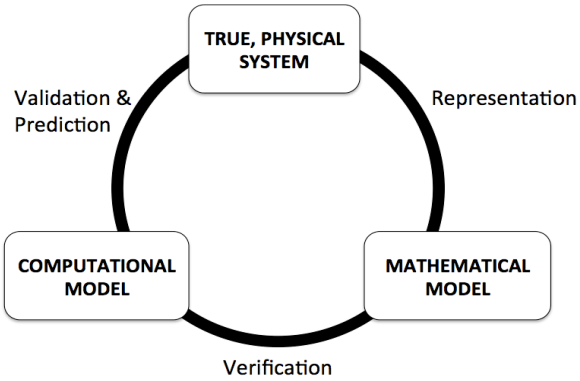

Figure 5 – Flow diagram for verification and validation of a system code [27].

Verification and validation are a crucial part in a code development and assessment processes. Verification is a process to assess the code correctness and numerical accuracy of the solution to a given mathematical model defined by a system of partial differential or integral equations which are derived from the physical reality (see [28]). In other words, verification is performed to demonstrate whether the equations are correctly solved by the code. In the case of the validation process, the aim is to quantify the accuracy of the model through comparisons of experimental data with simulation outcomes from the computational model. Verification activities can be clearly addressed to TH-SYS code development process. Precisely the verification activities are needed to demonstrate the correct working of the mathematical model, the source code in terms of software quality engineering and solution algorithms, respectively. The schematic for the verification process of a system code is shown in Figure 5.

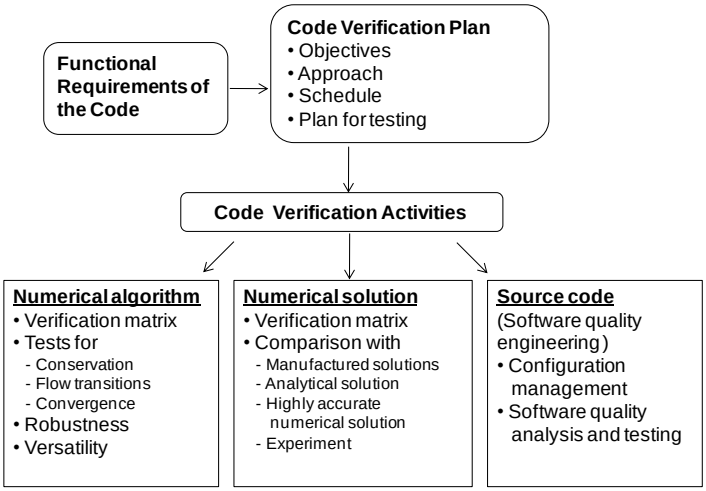

Figure 6 – Flow diagram for verification of a system code.

The validation process is oriented in assessing the adequacy of the physical models on which is based the code (see Figure 7). Physical models include some first principles laws which do not require any validation and many closure relationships which are simplified descriptions of the flow processes and which require a validation. The reality of interest of the system codes is the modelling of the reactor cooling circuits, or test facility. The system of balance equations which describe the fluid dynamics behavior of the two phase flow in the domain of interest (NPP, ITF, SETF) are written in the TH-SYS codes with some degree of approximation related to space and time averaging. Averaging process is equivalent to low-pass filtering to eliminate high-frequency fluctuations (see section § 3.1 and Figure 2). In averaging, information about the details of fluctuations is lost in return for simplified and tractable properties and equations. Although fluctuation details are lost as a result of averaging, their statistical properties and their effects on the averaged balance equations can be accounted for. For exemple in the case of single phase turbulent flow the time averaging of the balance equation determines a lose of information about time fluctuations, but it is possible to include their effects on average momentum and energy equations by introducing eddy viscosity and heat transfer eddy diffusivity, or by using a turbulent transport model (such as the k-ε model). These additional models and correlations are often empirical and therefore, need of a validation activities. These activities are performed through the establishment of *Validation Matrices* which allow the testing of the physical models and the code suitability and accuracy against a wide and complete set of basic, separate effects and integral tests.

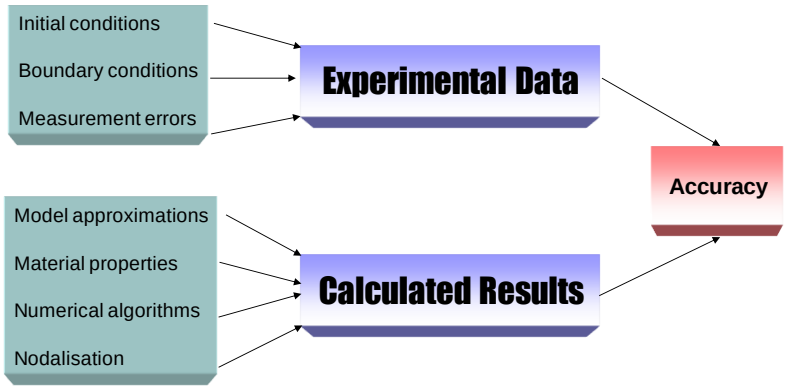

Figure 7 – Flow diagram for validation of a system code

3.3. Needs and challenges in nuclear thermal hydraulics

The status of the nuclear thermal-hydraulics regarding the physical modeling and the numerical methods used in the present TH-SYS codes, points out the fact that although the codes today show to be able of delivering fairly reliable safety evaluations for a broad spectrum of accident scenarios, they might not be adequate for future needs. Such future needs might arise from:

- Re-licensing of older plants with regard to life-time extension using best-estimate plus uncertainty (BEPU) licensing procedures,
- Design and safety analysis of Advanced Light Water Reactors (ALWR) or Generation IV reactors relying largely on passive safety systems characterized by low pressure low flow transients, two-phase natural circulation or strong coupling of the behaviour in primary coolant system and containments,
- Simulation of 3-D phenomena that occur in the primary system and in the containment such as for exemple the boron or cold water dilution in the primary system, mixing of various gases (steam, air, hydrogen) in the containment, stratification of containment pools, etc
- Evaluation of the Critical Heat Fux (CHF),
- Identifying processes suitable for demonstrating codes assessment against scaling in the frame of V&V [29].

The fulfillment of these needs represent a challenge for the system thermal hydraulics and will require the improvement of the two phase flow modelling and the prediction capability of the numerical schemes of the current generation of TH-SYS codes. Some possible improvements may come answering to the following key topics which are still open issues in the framework of the system thermal hydraulics, namely [30]:

- virtual mass and interfacial pressure terms in the frame of hyperbolicity;
- statements about mesh convergence;
- CHF benchmark, with the goal to evaluate the differences between six-equation 1D models in different codes;
- comparison *drift flux – six equations – multi-filed models*;
- transport of Interfacial Area plus Turbulence models: experiments and development;
- 3-field equations: experimental basis and theory;
- extension of system codes' capabilities for super-critical water, gas, sodium and lead-bismuth reactors.

The first two topics deal with the mathematical form and the numerical solution of the basic two phase flow equations. The role of virtual mass and interfacial pressure terms is of particular concern since the presence of these terms is such as to make the system of governing equation hyperbolic. The hyperbolicity is open issue in the framework of the development of system codes for predicting multiphase thermal hydraulics in nuclear reactor's transient and accident regimes, because of ill-posedness[5] nature of some of the model's equations. The necessity

[5] The notion of well-posedness was introduced by Hadamard in his analysis of the nature of mathematical modelling. According to Hadamard's classification, well-posedness requires the existence and uniqueness of the solution of the model and that the solution depends in continuous fashion on the initial and boundary data (see [31] and [32]). This requisite is induced by the fact that any model is bound to contain approximations and errors, be they in the initial or boundary conditions, or in the equations themselves. In order for the model predictions to be meaningful, it is necessary to ensure that a small perturbation in the data should give rise to a small variation of the solution at any point of the domain at a finite distance from the boundaries. For systems of partial differential equations, continuous dependence on the data is intimately related to hyperbolicity of the equations, as the solution of the initial value problem for non-hyperbolic systems fails to depend continuously on the initial conditions.

of hyperbolic two fluid model, characterized by the existence of only real eigenvalues, is connected with the physical aspect that any transient flow process might be seen as a response to perturbations manifesting them-selves in wave propagation phenomena but also whit the mathematical aspect that hyperbolic models do not suffer from high wave-number instabilities (as do their non-hyperbolic counter-part). Moreover the experience in applying models, which are ill-posed, has shown that in most applications stable solutions can be obtained since the present numerical techniques used in some system codes provide a sufficiently large damping mechanism but at the expense of large artificial diffusion or viscosity effects. Therefore, if the stability only depends on numerical diffusion, instability may occur when the mesh size is small enough to reduce the stabilizing effects of numerical diffusion. This implies that codes which use ill-posed equations cannot do mesh convergence tests with very small mesh size. In turn the existence of a hyperbolic system of equations is the key to the robust numerical treatment of the two fluid model; in fact it is an essential condition for the application advanced new low-diffusive numerical methods which make explicit use of the eigenstructure of the flow equations (like Riemann Solver or Flux Vector Splitting techniques). The problem to have a model of the balance equations which is either well-posed or ill-posed has been extensively (and controversially) discussed in the past with respect to the accuracy of the numerical solution and to the presence of unbounded numerical oscillations. There is not jet a common strategy dealing with this issue, accordingly it is necessary to provide guidelines to approach to this open issue also because it is of paramount importance in the frame of the safety concern of the nuclear power plants.

Another important aspect concerns the analysis of the level of accuracy of the closure models implemented in the current TH-SYS codes with particular regard to CHF correlations. The CHF is a very important limit in the safety analysis of nuclear reactors. Indeed the occurrence of CHF condition causes a drastic reduction of heat transfer coefficient and sometimes involves a physical failure of the heated surface. Therefore, it is crucial to assess the accuracy of these models and to try to highlight the lack of understanding of the various physical processes governing the critical heat flux in such a wide range of flow parameters.

In the framework of the physical modelling of the present thermal-hydraulic system code, a comparative analysis of various two phase flow modelling approaches, ranging from drift flux, six-equation up to the multi-field models, are important topics regarding the domain of applicability of these models taking in account that all kind of thermal and mechanical non equilibrium may exist in the spectrum of reactor accidental transients. For example sub-cooled liquid with direct contact condensation after ECCS injection have to be modelled. Superheated vapor has to be modelled mainly when Post-CHF heat transfer occurs in the core. Meta-stable superheated liquid and sub-cooled vapour exist in flashing flows with a small relaxation time constant (of the order of 10^{-3} second). Models with two mass balance equations plus two energy balance equations can model all these situations. Mechanical non equilibrium is also encountered in most situations with possible weak coupling between phases. Using only one momentum equation with a drift flux algebraic equation is sufficient for many situations, particularly when the coupling between phases is rather strong. Two momentum equations are necessary in other cases particularly when inertial forces play a role in the slip

ratio. Droplets created in the core during a reflooding are entrained by steam but do not reach the equilibrium slip velocity before leaving the core due to high inertia. Flashing or highly condensation flows need of two momentum equations because of phase changing effects and acceleration are not negligible. Better capabilities are also found for stratified flows by writing two momentum equations, which allows representing wave propagation phenomena. Multi-field models are expected to have better capabilities for annular-dispersed flows or stratified-dispersed flows but a higher CPU cost and a lack of experimental data for validation temporarily disqualified them.

In the frame of understanding of the interface processes a key topic is represented by the modeling of interfacial area. The averaging process of the local instantaneous balance equations for the individual phases, as mentioned earlier, has as outcome to lose information on the local flow conditions which have to be provided in the form of source terms describing the local phenomena of transfer (mass, momentum and energy) on the interface and in the vicinity of the wall. The interfacial transport processes are assumed to be algebraic functions of the interfacial area concentration (interfacial area per unit volume) a^{int} and the driving force X_k representing the deviations from the mechanical and thermal equilibrium between the phases: e.g. the local phase velocities (slip) or the difference between the phase temperatures and the equilibrium temperature,

$$\sigma_k^{\text{int}} = C_k a^{\text{int}} X_k \tag{6}$$

The transfer parameter C_k is usually fitted from the condition of best agreement with experimental data or for providing *reasonable* values of the obtained deviations from thermal and mechanical equilibrium. As indicated in equation (6) the key parameter for the interfacial transfer process is the interfacial area concentration which strongly depends on the local spatial phase distribution. Since the balance equations give no information on the two-phase flow structure, additional modeling is required to provide at least an approximate value for the interfacial area concentration. In the current nuclear reactor system analysis codes and in many practical two-phase flow analyses, the interfacial area concentration is calculated by flow regime dependent correlations that do not represent the changes in interfacial structure dynamically. The flow regime transition criteria are developed for fully developed steady-state two-phase flow conditions and are not capable of describing the evolution of interfacial structure. It is clear that the lack of proper mechanistic models for the interfacial area concentration may limit the thermal-hydraulic analysis of nuclear reactors and other engineering systems. Then the description of the flow regime in a gas liquid flow cannot ignore the need on having an adequate description of the topological distribution of the phases based on dynamical evaluation of interfacial structure of the system. Several shortcomings were identified by Mortensen (1995) and Kelly (1997) (see [21], [33], [34] and [35]) related to the flow regime based static approach, and they can be summarized as follows:

- Since the flow regime transition criteria are algebraic relations for steady-state fully developed flows, they reflect neither the true dynamic nature of changes in the interfacial structure, nor the gradual regime transition.

- The method based on the flow-regime transition criteria is a two-step method that requires flow configuration transition criteria and interfacial area correlations for each flow configuration. The compound errors from the transition criteria and interfacial area correlations can be very significant.
- The existing flow regime dependent correlations and criteria are valid in limited parameter ranges for certain operational conditions. Often the geometrical scale effects are not taken into account correctly. When applied to high-to-low pressure steam-water transients these models may cause significant discrepancies, artificial discontinuities and numerical instabilities.

Basically, the interfacial area transport model consists of a balance equation for interfacial area concentration given by (see [20], [36] and [37]):

$$\frac{\partial}{\partial t}\left(a^{\text{int}}\right)+\nabla\cdot\left(a^{\text{int}}\left\langle\mathbf{v}^{\text{int}}\right\rangle\right)=\sigma^{A}$$

$$\left\langle\mathbf{v}^{\text{int}}\right\rangle=\frac{1}{A_{\xi}^{\text{int}}}\int_{A_{\xi}^{\text{int}}}\mathbf{v}^{\text{int}}dA \qquad (7)$$

$$\sigma^{A}=\frac{1}{V_{\xi}^{\text{int}}}\int_{A_{\xi}^{\text{int}}}\left(\nabla\cdot\mathbf{v}^{\text{int}}\right)dA$$

The source term on the right hand side of the equation (7), σ^{A}, represents the effects of the interaction processes leading to the formation and disintegration of interfacial area that occur during either flow regime transitions or processes like particle (droplet or bubble) deformation; namely break-up and coalescences or distortions processes. The interfacial area transport model is very challenging but very important and attractive problem since it allows to describe the topology of the phases distribution as a dynamic time-dependent process and is expected also to provide a more physically-based prediction of flow regime transitions. However, in the frame of the averaging approaches, the crucial point is always the formulation of the corresponding source or sink terms σ^{A} and the interfacial velocity v^{int}. What is needed to understand the underlying physics that governs these processes would be a more fundamental characterization of the interface by parameters which are defined for any flow regime like for example the average curvature. Another possibility would be to treat the interface not just as a geometrical configuration rather than a separate phase with thermodynamic state parameters including surface tension. Also form the experimental point of view many efforts are needed to develop new instrumentations and advanced measurement techniques to identify accurate constitutive relations to solve two fluid models. So far, interfacial area transport models have been applied only to rather well structured flow regimes like mono-dispersed bubbly or droplet flows, as did Staedtke which implemented an interfacial area transport equation within the JRC Ispra code or as has been done in TRACE code in which was implemented one-group interfacial area transport equation [38].

The extension of system codes capabilities to support the simulation of Generation IV of nuclear reactors is particularly attractive in the context of safety related studies aimed at establishing the basic feasibility of the advanced reactors design, which include super-critical water, gas, sodium and lead-bismuth reactors. Therefore, the current generation of TH-SYS codes must include the extension to new fluids (Pb-Bi, CO_2, He, Na, NaK, Li-Pb) and new modeling features to model forced convection heat transfer in rod bundles in liquid metal, in super critical water (SCW) and in pebble bed but also to model pressure drop taking in account the effect of heated wall on the friction factor for SCW and so on.

Through the description of these fundamental aspects have been highlighted the needs and the challenges of the current thermal hydraulic simulation tools taking also into account that most codes have reached a level of development which is probably *saturated*.

3.4. Overview of EU projects connected to TH-SYS

There are important research projects and initiatives that have been carried out or are in progress in the area of TH-SYS:

- EUROFASTNET: Project (EU Project for future advances in sciences and technology for nuclear engineering thermal-hydraulics) started in September 2000 for 18-month duration and was led by CEA (France). The Project was aimed at discussing and identifying the needs for R&D activities to be carried out in the field of the thermal-hydraulics applied to nuclear reactor safety, design and economic operation issues.
- NURESIM: The Project aims at establishing the basis for the realization of a common European standard software platform for nuclear reactor simulations. The key objectives of the Project are the following:
    - the integration of advanced physical models in a shared and open software platform;
    - promoting and incorporating the latest advances in reactor and core physics, thermal-hydraulics, and coupled (multi-) physics modelling progress assessment by using deterministic and statistical sensitivity and uncertainty analyses, verification and benchmarking;
    - training, dissemination, best practice and quality assurance.
- ASTAR: Project (ASTAR: Advanced 3-D Two-Phase Flow Simulation Tool for Application to Reactor Safety) was launched in September 1999 to further develop, verify and assess 3-D modelling approaches and related new computational strategies which have the potential to substantially improve the numerical simulation of transient two-phase flow. The project consortium comprises leading European institutions in the field of nuclear thermal-hydraulics and related code development. These include CEA-Saclay (F), EDF-Chatou (F), GRS-Garching (D) JRC-Ispra (I) and PSI-Villigen (CH), as well as academia with special expertise in computational

fluid dynamics: Manchester Metropolitan University (UK) and the Von Karman Institute for Fluid Dynamics, Brussels (B).

- FONESYS: Project (Forum & Network of TH-SYS Codes in Nuclear Reactor Thermal-Hydraulics) was proposed by University of Pisa to promote the cooperation between code-developers and code users with the following main targets:
    - to highlight the capabilities and the shortcomings in both modeling and numerical fields, proposing an alternative approaches to overcome limitations of the current thermal hydraulic system codes;
    - to establish acceptable and recognized procedures and thresholds for V&V;
    - to promote the use of TH-SYS Codes and the application of the BEPU approaches.

  The forum comprises leading International institutions in the field of nuclear thermal-hydraulics and related code development. This includes GRNSPG/UNIPI (IT), VVT (FI), GRS (DE), CEA (FR), AREVA NP SAS (FR), KINS (KR) and KAERI (KR). Additionally, AECL (CA) and INL (US) participate with "observer" status.

- US NRC supporting the development of TH-SYS codes (e.g. TRACE) and running the related CAMP program, other than continuously evaluating new reactors and updating the licensing process (in this last case with a number of connections to TH).

- ATLAS, MARS and SPACE projects in Korea, that are an integrated approach to SYS TH, involving experiments, modeling, and numerical development.

4 METHODOLOGY FOR INDEPENDENT ASSESSMENT OF TH-SYS CODES

4.1. Overview of independent Assessment approach

The assessment of thermal hydraulic system codes is aimed at providing evidence that they can be used reliably and with sufficient accuracy within their ranges of applicability for realistic prediction of NPPs behavior during transients and off-normal conditions. Code assessment focuses on comparison between the results of code calculations and measured experimental data (or real plant data) (see Figure 8).

After the developmental assessment phase (performed by code developers, to assess and check the separate models and parts of the code), an *independent assessment* phase (performed by code users) can be identified as closure of the entire process.

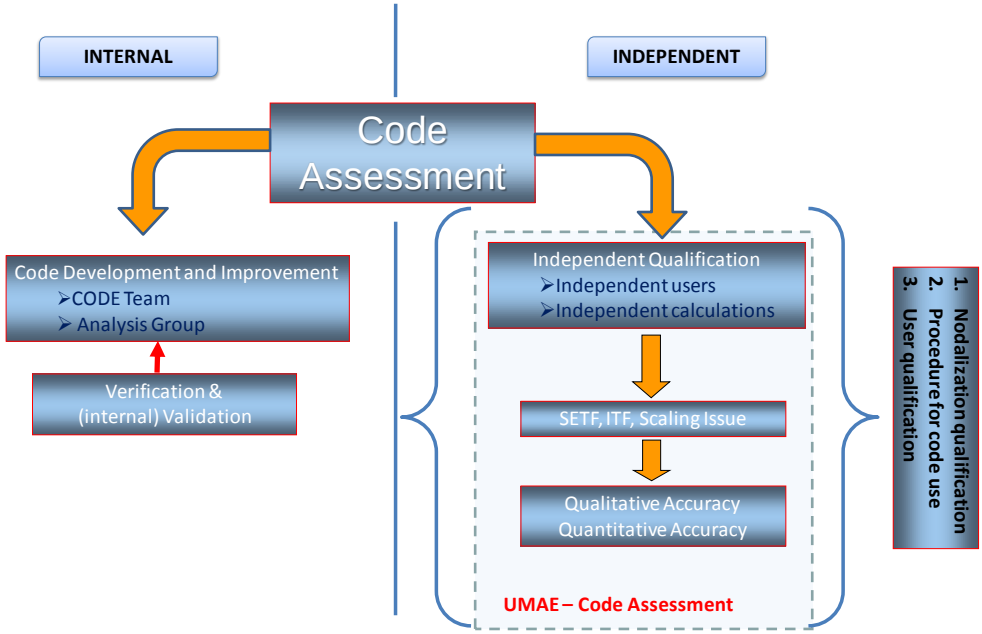

Figure 8 – Outline of the code assessment process

One of relevant needs for independent assessment comes from the domain of application of the concerned code that is nuclear reactor safety. Thus, the Defense-in-Depth principle applies and it justifies the additional effort to prove the validity of a tool utilized for the calculation of safety aspects of NPP (see [39]).

Prerequisites for an independent assessment of a code to be qualified are:

- selection of qualified experiments: this implies the selection of qualified facilities and qualified test design;
- qualified user
- nodalization qualification process;
    - qualitative and quantitative accuracy evaluation.

The selection of qualified experiments should consider (see [39]):

- design of the facility a scaling strategy based on identification of key phenomena and scaling of these phenomena,
- availability of well defined test facility design and test conditions (IC &BC).
- quality, quantity, and availability of the measurements with estimation of uncertainty.
- geometry representative of actual reactor.
- transient scenario representative of actual reactor scenario.

Regarding the user qualification process is performed through a training period aimed at producing qualified users being able to predict plant scenarios with state-of-the-art uncertainty. The user must be aware of physic models and limitations of the codes, and must have a good understanding of the major phenomena expected to occur during thermal hydraulic transients. Main topics of this could be:

- limits of applicability and capabilities of the code
- analysis of a separate effect test facility experiment (with nodalization set up by the user)
- analysis of an integral test facility experiment (with nodalization modified by the user).

The nodalization qualification process includes two main steps (see [40]):

a) on-steady-state qualification
b) on-transient qualification

The related activity of item (a) starts from the acquisition of the structural and operational ITF and SETF data and concludes when the nominal measured steady-state is reproduced. The latter item consists in fitting and testing the nodalization in time-dependent conditions reproducing the experimental transient performed in the involved facility (the selected one to quantify the investigated nodalization scheme). The Figure 9 describes the logical steps that characterize the nodalization qualification process.

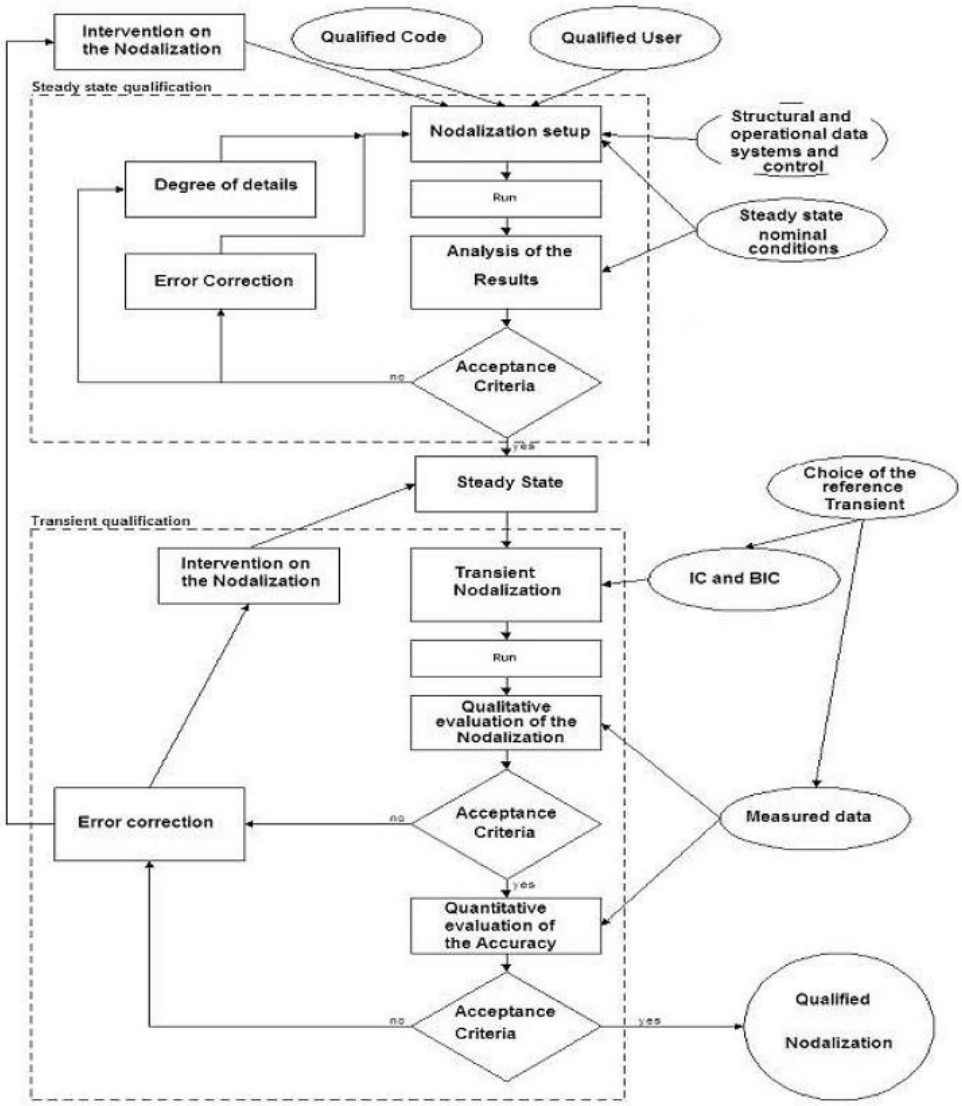

Figure 9 – Flow diagram of the nodalization process

4.1.1. Independent assessment matrix

The validation matrix, developed during the research activity, for the validation of the TRACE-V5 code includes the following type of tests:

- Basic tests
- Integral effect tests

The *basic tests*, sometimes referred to as fundamental tests, are used to validate the thermal hydraulic modeling on an idealized level. These problems usually

involve very simple geometries and may have an analytical solution. They do provide information on generic model and numerical schemes reliability used by the code. For example, a basic test may be the phase separation problem. This is an isothermal transient test case to investigate gravity-induced phase separation and related counter-current flow conditions. It tests the ability of the methods to predict counter-current flow conditions as exist in many reactor safety-related transients and the numerical stability of the scheme.

IETs model the reactor under accidental conditions with all system components and all interactions between them. IETs are reduced scale tests. The IET matrix suitable for the validation of best estimate thermal-hydraulic computer codes consists of phenomenological well founded experiments, for which comparison of the measured and calculated parameters allows the evaluation of the accuracy of the code predictions.

The selected experiments, for developing of the IAM based on the two typologies of tests listed above, are a gravity dominant experiment and two integral effect tests realized at PKL facility. The first one is a test in which the only source of momentum taking in account is the gravity. An example of this experiment is given by the water faucet problem aimed precisely to study the gravity effects on a vertical downward water jet flow. This problem has been extensively used to test numerical schemes in tracking volume fraction fronts (discontinuity waves). The reason of the choice of this numerical test is mainly due to investigate the stability of the discrete scheme and the effects of the artificial viscosity (that becomes really important for simulating the ROCOM tests) on the solution induced by the numerical method implemented in TRACE-V5 code (SETS method). The numerical analysis of PKL test F4.1 is used to demonstrate the capability of the code models to simulate correctly the transport of a scalar quantity, like the boron concentration, and the heat transfer mechanisms in natural circulation conditions (SPNC and TPNC) and RC mode. The qualification of the nodalization against heat transfer process in buoyancy driving flow conditions become relevant for simulating the PKL test G3.1, for which the simulation of the thermal energy exchange between the primary and the secondary system is one of the objectives of the experimental activity. Regarding the test G7.1 the analytical activity is aimed to demonstrate the adequacy of a given code to simulate the single and two phase critical flow phenomenon which features the SBLOCA scenario. Also for this test type the purpose is the assessment of the nodalization and code models (whit particular attention to the TRACE critical flow model) in order to evaluate the reliability of the TRACE scheme of PKL facility for simulating the test G3.1. The resulting assessment matrix is given in Table 1.

Table 1 – Independent assessment matrix

No	Test Type	Concerned NPP	Test	Concerned phenomenon or DBA	Notes
1	**Basic**		Numerical test	Gravity dominant test (water faucet problem)	Assessment of numerical scheme
2	**ITF**	**PWR**	PKL-III test F4.1 (RUN 1)	Inherent boron dilution phenomenon and heat transfer mechanisms under SNC, TPNC and RC modes	Key phenomenon for DBA Analysis
			PKL-III test G7.1	SBLOCA	Assessment of AM procedure

4.2. Assessment of the TRACE-V5 code against IETs

4.2.1. Description of the facility and experiment

4.2.1.1. PKL-III test facility description (configuration)

The PKL facility (see [41]) is a full height ITF (elevations scaled 1:1) (see Figure 10), that models the entire primary system and most of the secondary system (except turbine and condenser) of a 1300 MW PWR NPP. It has been used for extensive experimental investigations addressing the integral behavior of PWR NPP accident conditions (PKL is a German acronym for "Primary System"). Different test programs have been carried out with the PKL facility (see [42] and [43]).: PKL I and II test programs (1977 – 1986) focused on LB LOCA and SB LOCA and the PKL III test program (starting from 1986) focusing on the simulation of accident sequences, mainly on the BDBA and the issues related to the day-to-day operation of Siemens-built PWR.

The PKL facility is designed using the specific data of Philippsburg NPP unit 2. The scaling concepts are suitable for simulating the overall thermal-hydraulic behavior of the full-scale power plant. The main peculiarities of the facility are provided in Table 2, where they are compared with the main ITF representing a PWR system, including the VVER-1000.

The following features can be highlighted:

- full-scale hydrostatic head;
- power, volume, and cross-sectional area scaling factor of 1:145;
- full-scale frictional pressure loss for single-phase flow;
- simulation of all four loops;
- core and SG have full-scale rod and U-tube dimensions, spacers, heat storage capacity but the number of rods and tubes is scaled down;
- the first-priority objective is the simulation of phenomena compared to the consistent representation of the geometry, (e.g., in order to account for

important phenomena in the hot legs such as flow separation and countercurrent flow limitation (CCFL), the geometry of the hot legs is based on conservation of the Froude number and was finally designed on the basis of experiments at the full scale UPTF);
- the configuration of the RPV DC, modeled as two stand pipes connected to the lower plenum and as an annulus in the upper region, allows the frictional pressure losses preservation and a reasonable volume/surface ratio distortion;
- the operating pressure of the PKL facility is limited to 45 bar on the primary side and to 56 bar on the secondary side. This allows simulation over a wide temperature range (250°C to 50°C) that is particularly applicable to the cool-down procedures investigated.

The PKL test facility can be subdivided into RCS, SG SS, the interfacing systems on the primary and secondary side and the break. RCS comprises the vessel, the four loops (pipes, pumps and steam generators), and the pressurizer (PRZ) connected via the surge line to the loop #2.

The **vessel** includes the following parts:

- the **upper head** is a cylinder, full scale in height and 1:145 in volume. It contains the shaft of the RPV liquid level detector and in the bottom houses the top plate, the upper core support and the control rod guide assemblies.
- The **upper plenum** is full scale in height and scaled down in volume. The internals are simulated by means of seal-welded tube.
- The **upper head bypass** is modeled by four lines associated with the respective loops to enable detection of asymmetric flow phenomena in the RCS (e.g., single-loop operation).
- The **reactor core model** consists of 314 electrically heated fuel rods (diameter 10.75 mm and pitch 14.3 mm) and 26 control rod guide thimbles (diameter 13.6 mm). Three concentric zones can be heated independently and simulate a radially variable power profile. The maximum electrical power of the test bundle is 2512 kW distributed as follows: 504 kW in the inner zone (63 rods with 8 kW each one); 944 kW in the central zone (118 rods with 8 kW each one) and 1064 in the outer zone (133 rods with 8 kW each one). Thermocouples are located in the rod bundle for measuring the rod temperatures.
- The **reflector gap** is between the rod bundle vessel and the bundle wrapper (the barrel in the real plant). Following the reference plant, the flow resistance is designed in order to have 1% of the total primary side mass flow (with MCP in operation) through the reflector gap. In this zone there are also located 2 concentric 1.5 mm thick nickel sheets with the function to protect the rod bundle vessel against overheating (max allowable temperature is 300°C).
- The **lower plenum** contains the 314 extension tubes connected with the heated rods. The down-comer pipes are welded on the lower plenum bottom in diametrically opposite position. Two plates are located in this zone: the Fuel Assembly Bottom Fitting and the Flow Distribution Plate.

- The **down-comer** is modeled as an annulus in the upper region and continues as two stand pipes connected to the lower plenum. This configuration, as already mentioned above, permits symmetrical connection of the 4 CL to the RPV, preserves the frictional pressure losses and does not unacceptably distort the volume/surface ratio. The hydraulic diameter of the down-comer vessel is equal to the one of reactor. The down-comer pipes simulate the lower portion of the reactor down-comer and the diameter is equal to the hydraulic diameter of the annular down-comer in the prototype reactor.

The facility has four loops, each one constituted by a hot leg, a U-tube SG (primary side), a loop seal, a main circulation pump and a cold leg. The **hot legs** are designed taking into account the relevance of an accurate simulation of the two phase flow phenomena, in particular CCFL, in the hot leg piping as in the reactor. For this reason the hot leg has the scaled diameter in the part flanged to the upper plenum and then a concentric increase from 80.8 mm to 154 mm upstream the connection to the SG inlet plenum. The **cold legs** connect the SG to the MCP through a loop seal and the MCP to the DC vessel. The hydrostatic elevations of the loop seals are 1:1 compared to the prototype NPP. The cold legs have also nozzles located between the MCP and the DC vessel for the ECCS injection and two seats in CL 1 and 2 for the break simulation. The PKL **MCPs** are vertical single-stage centrifugal pumps, driven by variable-speed motors provided with anti-reverse rotation devices. The PKL **PRZ** has full height and it is connected through the surge line to the hot leg #2. The electrical heaters and the water spray are modeled in the water and steam plenum respectively. The four **SG (primary side)** of the PKL test facility are vertical U-tube bundle heat exchangers like in the prototype NPP. The scaling factor has been preserved by reducing the number of tubes: 28 tubes with outside diameter of 22 mm and wall thickness of 1.2 mm. Seven different lengths are modeled with the shortest and the longest tubes that have the same height of the reactor SG.

The **SG (secondary side)** comprises the tube bundle zone which constitutes the interface between the RCS and secondary side. Below the shortest tubes, there are seal-welded hollow fillers which allow to achieve the correct volumetric scaling of the SG secondary side. The DC model can be divided into three parts: the upper, located above the U-tube zone, is annular and contains the FW ring; the central, in the tube bundle zone, is modeled by two tubes outside of the SG housing; the lower has annular shape formed by a cylindrical shroud within the vessel. The flow distribution plate is attached to the bottom of the shroud. The uppermost part of the SG, the larger part of the SG vessel, models the steam plenum. The SG outlet nozzle has a restriction, like the prototype system, in order to reduce the blow-down rate in the MSLB events. Finally the moisture separator, the dryer and the perforate plate of the reactor SG are simulated with a perforate plate, with appropriate flow resistance, located below the SG outlet nozzle. The condensate, formed in this plate, returns to the SG DC through a funnel place in the uppermost part of the SG below the perforate plate. The main parameters, characterizing the SG secondary side of the PKL facility are reported in Table 3, which includes also the main data of relevant ITF representing PWR system at different scale.

The main **interfacing systems** have been also implemented in the PKL test facility in order to simulate the correspondent systems necessary for the prototype NPP operation.

Finally, connections to different primary and secondary side components are envisaged for the **break** simulation in order to test and optimize different system operating regimens and operational procedures during the SBLOCA events (see configuration of the facility for the test G7.1). Also the SGTR events are simulated by means of pipes with isolation valves connecting the SG primary side (tube bundle) to the SG secondary side at different elevations.

The measurement system for detecting the boron concentration during the transient scenario is shown in Figure 10. Two types of measures are available: the continuous measurement of boron concentration performed through COMBO devices described in [44] and the sample measures. For this analysis, only measures of the COMBO devices are considered and compared with the code results.

During the test F4.1 RUN 1 the initial heat transfer mechanism to the secondary side occurs through sub-cooled single phase natural circulation (SPNC). Following the stepwise reduction of the coolant in the primary side and the achievement of the saturation conditions, void volume starts to be produced in the upper head of the RPV (Reactor Pressure Vessel). Once the steam produced reached the test section outlet of the RPV, two phase natural circulation becomes established. The continuous reduction of coolant inventory during the test causes the interruption of liquid flow over the apexes of the steam generator U-tubes, with the resulting occurrence of phase separation and the stopping of natural circulation. Then heat transfer from the core to the steam generators takes place through operation in the reflux-condenser mode. Between the two phase natural circulation and the establishment of pure reflux condensation regime, large oscillations caused by U-tubes plugging (flooding) and plug carryover occur. This flow regime has been characterized as “siphon condensation” and it occurs during the test F4.1 RUN1 at mass inventories of the primary system around 65% and 65%-70% of the nominal value. The reduction of primary coolant was terminated soon after core uncovery, with pure RC conditions (i.e. when there was no more transport of water from the steam generator inlet to outlet side). After the coolant mass inventory reduction phase, the primary level was stepwise increased until the transport of borated water from steam generator inlet to outlet sides was re-established.

Table 2 – AREVA NP PKL III versus LOBI, SPES, BETHSY, LSTF facilities and KRSKO NPP: hardware data of steam generators

PARAMETERS	UNIT	PKL	LOBI	SPES	BETHSY	LSTF	KRSKO
Number of U-tubes (one SG)	--	28	il 24 bl 8	13	34	141	4674
SG primary side total volume	m^3	0.261	il 0.1213 * bl 0.0401	0.0493	0.2713	1.5132 1.5126	24.997
U-tubes volume	m^3	0.155	il 0.1033 bl 0.0341	0.0402	0.2011	0.8384	16.576 *
U-tubes total flow area	m^2	0.0084 5	il 0.0072 bl 0.0024	0.0024	0.0103	0.0425	1.036 *
U-tubes inner diameter	mm	19.6	il 19.6 bl 19.6	15.42	19.68	19.6	16.8
U-tubes outer diameter	mm	22	il 22 bl 22	17.46	22.22	25.4	--
U-tubes average length	m	18.34	il 14.265 bl 14.113	16.564	19.45	19.7	16 *
U-tubes max. height	m	10.31	il 7.163 bl 7.133	8.323	10.5	10.62	--
U-tube min. height	m	8.288	il 6.913 bl 6.883	8.153	9	9.156	--
U-tubes min l/d	--	845	il 711.32 bl 707.23	1084.5 6	928.76	971.30	952.3 **
U-tubes total inner surface	m^2	31.62	il 21.08 bl 6.952	10.431	40.88	171	4460
SG total height	m	14.011	il 12.382 bl 12.371	15.594	16.011	19.839	17.792 *
DC-riser heat transfer area	m^2	0	il 7.799 bl 5.434	0	0	2.737	82.14 *
DC diameter (d) or gap (g)	mm	80 (d) 2 pipes	il 12 (g) bl 6	43 (d) 2 pipes	43.1 (d) 4 pipes	97.1 (d) 4 pipes	557 (g) *
SG riser diameter	m	0.258	il 0.301 bl 0.201	0.173	0.326	0.694	--
SG U-tubes total HT area/ core active HT area	--	3.43	3.713	3.344	2.965	4.026	2.723
SG U-tubes total flow area/ITF volume	m^{-1}	0.0103	0.0148	0.0114	0.0105	0.0106	0.0124
SG U-tubes total vol./ITF vol.	--	0.189	0.2118	0.1932	0.3163	0.2108	0.3006 *

* Values obtained from nodalization
** U-tubes average l/d

Table 3 – AREVA NP PKL III versus LOBI, SPES, BETHSY, LSTF and PSB-VVER facilities: main scaling characteristics.

PARAMETERS	UNIT	PKL	LOBI	SPES	BETHSY	LSTF	PSB-VVER
Reference reactor or reactor	--	**S-PWR 4-loop**	**S-PWR 4 loops**	**W-PWR 3 loops**	**FRA-PWR 3 loops**	**W-PWR 4 loops**	**VVER-1000 v320**
Power of the reference reactor	MWth	3765	3900	2775	2775	3423	3000
Reported Kv	--	1/145	1/712	1/427	1/100	1/48	1/297
ITF number of loops	--	4	2	3	3	2	4
ITF nominal power	MWth	2.512	5.280	6.490	2.860	10.000	1.500
ITF volume (with PRZ)	m^3	3.282	0.648	0.624	2.88	7.952	1.349
ITF volume (without PRZ)	m^3	2.766	0.561	0.5286	2.473	6.805	1.090
Primary side fluid total mass ^	kg	-	436	423	1984	5404	827
Pressurizer nominal pressure ^	MPa	4.5 **	15.7	15.5	15.5	15.55	15.53
Inlet core mass flow rate ^	Kg/s	--	3.5	4.25 *	17.5 *	48.4	8.7 *
Outlet core temperature ^	K	--	589	589	588	589	584
SG secondary side volume	m^3	5.824	il 0.7307 bl 0.1648	1.163	1.952	4.842 4.742	--
SG secondary side total mass (^)	Kg	-	ll 325 bl 115	182, 183 185.5	780.6	2569.5	--
Secondary side operating pressure (^)	MPa	5.6 **	il 6.94 bl 6.91	6.94	6.80, 6.84 6.84	7.0	6.9
PS Heat Losses	kW	90 ^^	110	150	54.2	167	180

* Calculated value.
** Low pressure facility
(^) This data is referred to the SBLOCA counterpart test (see [45])
(^^) Heat losses in PRZ excluded

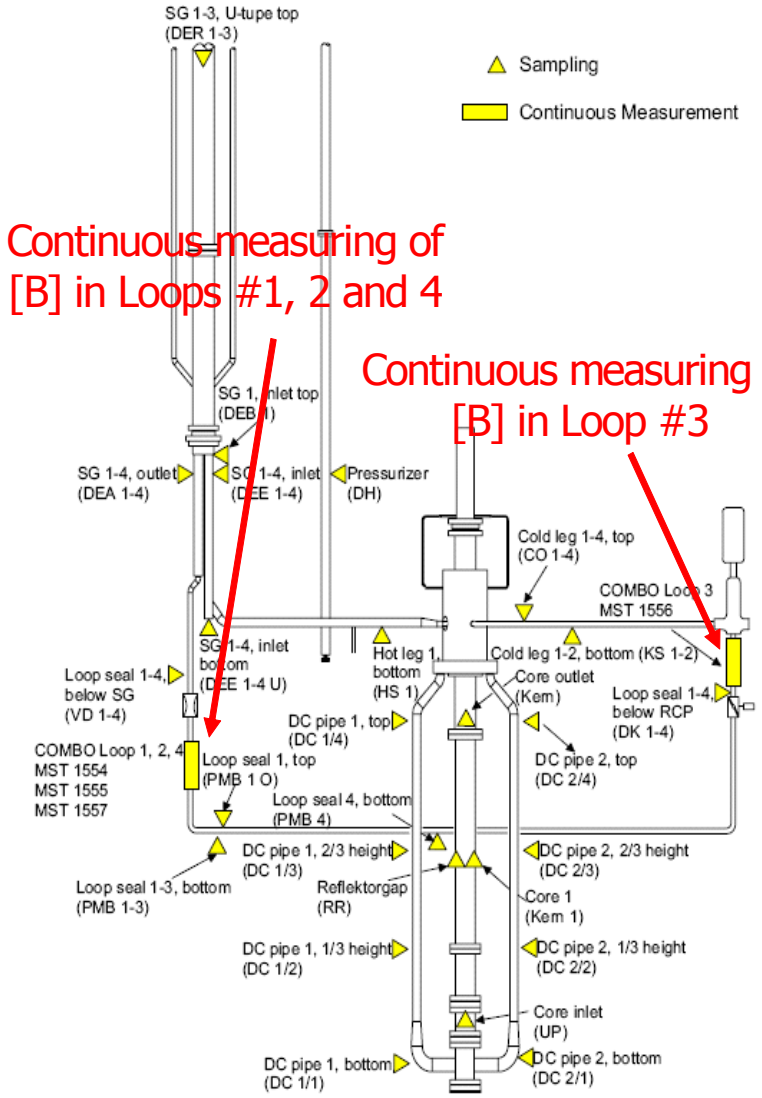

Figure 10 – PKL III experiment F4.1 RUN 1: boron concentration measurement instruments locations

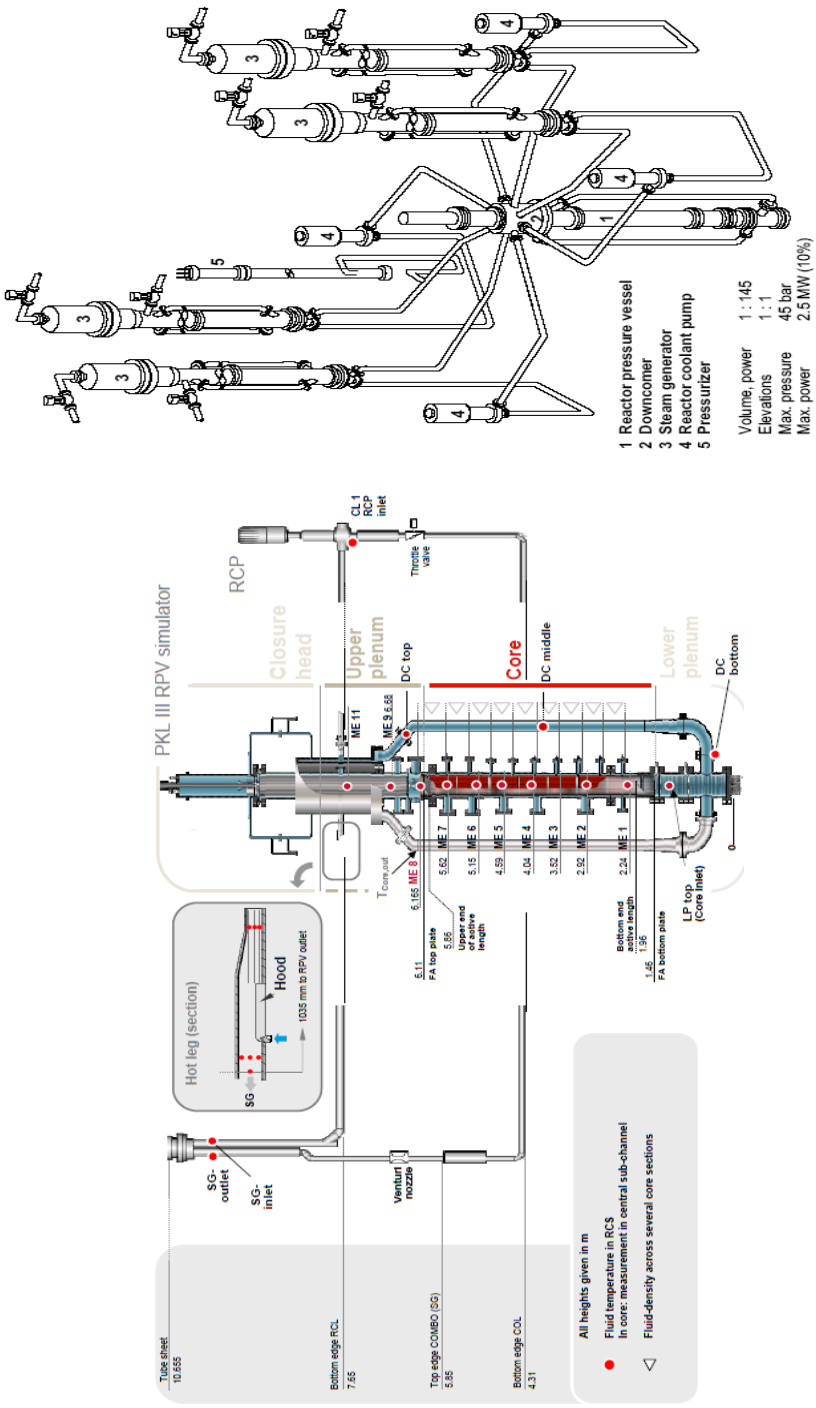

Figure 11 – PKL III test facility and RCS-dimensions

4.2.1.2. PKL-III test F4.1

4.2.1.2.1. Objectives of the test F4.1

The main objective of the Test F4.1 RUN 1 executed in PKL-III facility was to investigate the inherent boron dilution process due to the RC conditions as a function of the primary mass inventory. The parametric approach was carried out choosing as survey parameter the primary side mass inventory which was stepwise reduced and increased notably in order to investigate the behavior of the boron concentration at the steam generator (SG) outlet in the transition regime between two phase NC and RC conditions. The transition from the two phase NC (TPNC) to the RC conditions occurs when the systems is voided and as well, when it is refilled. The secondary pressure was increased during the reduction of the primary coolant mass inventory in such a way, that the primary system pressure was kept constant.

4.2.1.2.2. Outline of the test F4.1

During the test F4.1 RUN 1 the initial heat transfer mechanism to the secondary side occurs through sub-cooled single phase natural circulation (SPNC). Following the stepwise reduction of the coolant in the primary side and the achievement of the saturation conditions, void volume starts to be produced in the upper head of the RPV (Reactor Pressure Vessel). Once the steam produced reached the test section outlet of the RPV, two phase natural circulation becomes established. The continuous reduction of coolant inventory during the test cause the interruption of liquid flow over the apexes of the steam generator U-tubes, with the resulting occurrence of phase separation and the stopping of natural circulation. Then heat transfer from the core to the steam generators takes place through operation in the reflux-condenser mode. Between the two phase natural circulation and the establishment of pure reflux condensation regime, large oscillations caused by U-tubes plugging (flooding) and plug carryover occur. This flow regime has been characterized as “siphon condensation” and it occurs during the test F4.1 RUN1 at mass inventories of the primary system around 65% and 65%-70% of the nominal value. The reduction of primary coolant was terminated soon after core uncovery, with pure RC conditions (i.e. when there was no more transport of water from the steam generator inlet to outlet side). After the coolant mass inventory reduction phase, the primary level was stepwise increased until the transport of borated water from steam generator inlet to outlet sides was re-established.

On the basis of the different coolant circulation conditions sequence, the test can be subdivided in main phases and sub phases as listed in Table 6

The configuration of the facility is summarized in Table 5. Boundary conditions are reported in the Table 4 .The initial conditions of the test at the beginning of the conditioning phase are reported in Table 4 [46].

Figure 12 to Figure 14 are depicted the trends of the main parameters characterizing the experiment: primary and secondary pressures, primary mass inventory (without PRZ), average mass flow rates, boron concentration in the loop seals, core outlet coolant temperature and cladding temperature on the top of the core.

Table 4 – PKL III Test F4.1: relevant initial and boundary conditions

#	Conditions	Value	Note
1	General conditions of flow and heat transfer	--	Primary completely filled with water, heat transfer primary-secondary with subcooled NC
2	Coolant inventory	2475 kg	155 kg in PRZ
3	Boron concentration	2000 ppm	Homogeneous concentration
4	Core power (decay heat)	600 kW (1.8%)	
5	Primary side pressure	30.2 bar	
6	Coolant temperature a t core outlet	231 °C	
7	Sub-cooling at core outlet	4. °C	
8	Pressurizer fluid temperature	233-234 °C	
9	Pressurizer level (collapsed)	4.7 m	
10	Flow rate in loops	1.27 kg/s	Average value. RCP switched off: sub-cooled natural circulation in all the loops
11	Main steam pressure in SG secondary side	19.2 bar	
12	Main steam temperature in SG secondary side	210 °C	
13	Collapsed level in SG secondary side	12.2 m	
14	Feedwater temperature	118 °C	

Table 5 – PKL III facility configuration

#	System/component	Characteristics	Definition/value
1	Injection location	Lower part of DC tubes (two injection points)	Modified CVCS connection
2	Injected water boron concentration	2000 ppm	
3	Drainage location	Lower plenum of the RPV	
4	ECCS not available	--	--
6	Heat losses	RPV upper head 0.0 kW PRZ heaters 8.2 kW MCP-1 cooling about 10.5 kW MCP-2 cooling about 10.5 kW MCP-3 cooling about 10.5 kW MCP-4 cooling about 10.5 kW SG 1-4 bypass 12 kW	Estimated values from parameter time trends
7	Butterfly valve	Closed	Simulation of MCP hydraulic resistance

Table 6 – PKL III test F4.1 RUN 1: phenomenological analysis

#	Phase	Sub-Phase	Time span [s]	Note
0	Start of Test (SoT)	--	0 - 1000	
1	Conditioning Phase	Reaching of saturated conditions at core outlet / Single Phase natural circulation	1000 - 3390	
2	Drainage	Single Phase natural circulation	3390 - 6404	During 2nd drainage
3		Two phase natural circulation	6404 - 22000	Achievement of the peak mass flow rate between the 4th and the 5th drainage
4		Instability and siphon condensation	22000- 28660	
5		Reflux-condenser conditions	28660 - 42520	
6	Core uncovered	Core dry-out and minimal mass occurrence	42520 - 42580	
7	Filling up	Reflux-condenser conditions	42580 - 66670	
8		Instability and siphon condensation / Two phase natural circulation	66670-70230	
9				
10	End of Test (EoT)	--	70230	

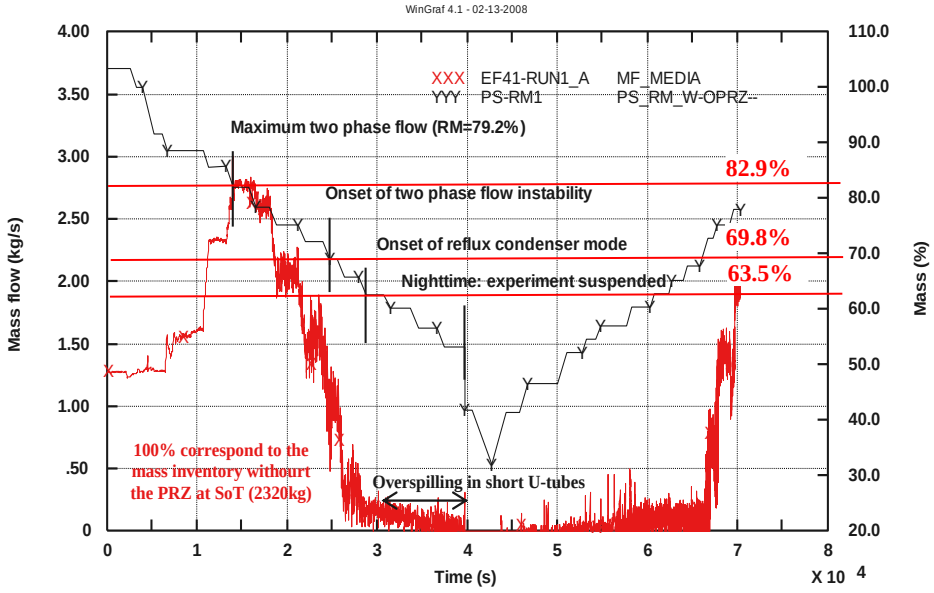

Figure 12 – PKL-III F4.1 RUN 1: measured trends of loop average mass flow rate and non-dimensional residual mass inventory

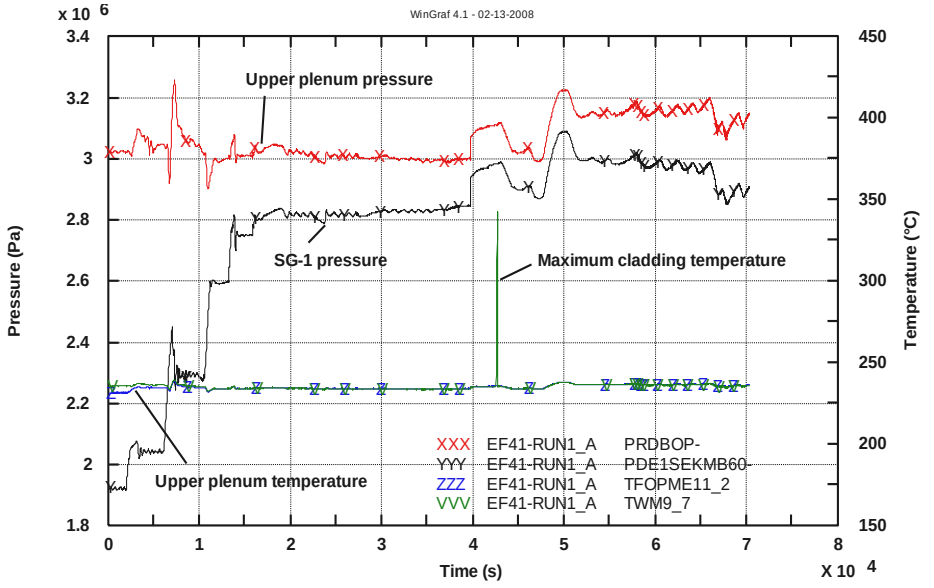

Figure 13 – PKL-III F4.1 RUN 1: measured trends of primary pressure, secondary side pressure, maximum rod surface temperature and core outlet fluid temperature.

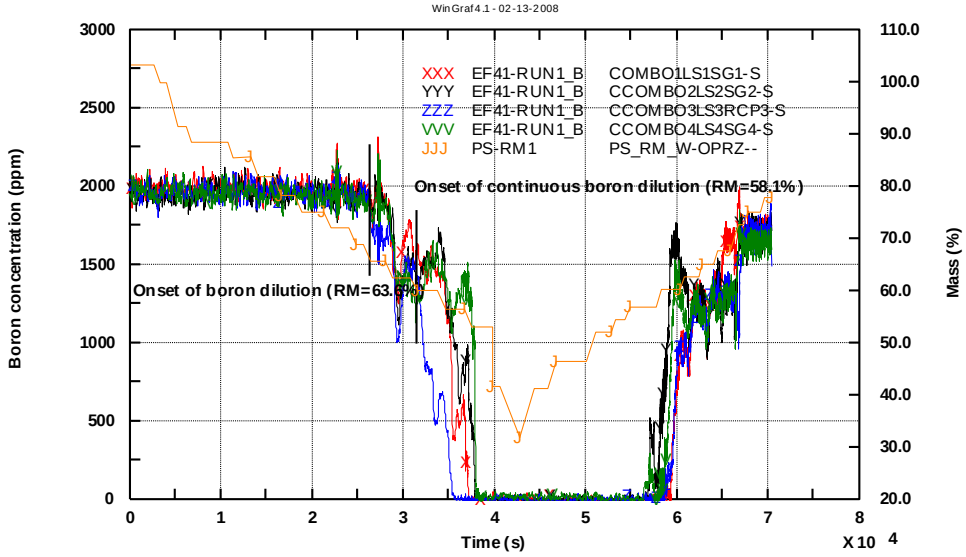

Figure 14 – PKL-III F4.1 RUN 1: measured trends of boron concentration in loop seal 1 to 4

4.2.1.3. PKL-III test G7.1

4.2.1.3.1. Objectives of the test G7.1

Background for the PKL G7.1 test is a hot leg SBLOCA (see [47]) scenario superposed by additional system failures (no high pressure safety injection, no automatic secondary-side cool down). The postulated additional system failures return a course of events that necessitates AM measures to prevent a core-melt scenario. Therefore, a secondary-side depressurization was employed as AM measure for restoration of the secondary side heat sink aiming for a fast reduction of the primary pressure. The reduction of the primary pressure down to ACC injection pressure then determines the transition to the low pressure phase with the LPSI active.

The main test objectives comprise questions on:

- the efficiency of the AM measures performed (SG de-pressurization);
- re-establishment of core cooling.

The test was also performed to assess:

- the plausibility/reliability of the CET measurement,
- the correlation between CET and PCT,

and to provide information on physical phenomena responsible for the CET performance.

Significant phenomena and effects to be investigated by the G7.1 test are:

- core uncovery due to loss of inventory (boil-off) with the formation of superheated steam as well;
- as the primary-side pressure behavior before and after occurrence of core uncover;
- effectiveness of a secondary-side depressurization and its influence on the primary pressure as well as the acc injection after the SG depressurization and its influence on the core cooling;
- relation between the PCT and CET during these processes;
- scaling effects between the PKL and ROSA/LSTF test facilities (the test is counterpart test).

4.2.1.3.2. Configuration of the facility, boundary and initial conditions of the experiment

The configuration of the facility (see Table 7) is summarized, as follows.

- The pressurizer heater is in operation to prevent displacement of water into PRZ and to compensate for heat losses (12 kW).
- The break device simulating the SBLOCA scenario (detailed descriptions of the break configuration is reported in Figure 15) is located in the HL 1. It simulates the 1.5% break by means of a nozzle with diameter of 0.0079 m equivalent to 0.7 m^2 in PWR.
- Four ACCs connected whit cold legs 1 to 4.
- Two LPIS connected whit cold legs 1 and 4. The mass flow injected in the primary system is defined by the experimentalists.
- Two MSRCV are located in the steam line of SG 1 and 3 and full open whit the nozzle diameter of 0.019 m for the depressurization of all SGs. The SGs 1 and 4 are connected via main steam header.
- RPV closure head trace heater in operation to compensate for heat losses.

The initial conditions of the test, summarized in Table 8 (see [47]) were achieved after a conditioning phase, which drives the test rig towards the thermal hydraulic conditions imposed at the start of the experiment. At the beginning of the conditioning phase the reactor coolant system was completely filled and sub-cooled natural circulation was present. The heat was removed symmetrically by all 4 SGs (connected via main steam header). The primary pressure was controlled by the secondary pressure (only MSRCVs of SGs 1 and 3 in are operation). All secondary sides were filled up to a level of 11.9 m see Table 8. The attainment of the RC conditions in the test facility at SoT was obtained throughout the temporary opening of the break in HL 1. After closing the break the SG secondary sides were activated again and then the primary-side pressure controlled at 45 bar by the secondary sides. During this part of the conditioning phase the secondary-side liquid levels were reduced to approx. 8 m by the SG blowdown system (according to the ROSA/LSTF test). After adjusting the liq-uid levels the SG secondary sides were isolated again and the test was started under stationary RC conditions.

4.2.1.3.3. Outline of the test G7.1

The baseline conditions for test G7.1 are established in a conditioning phase. The conditioning phase started with filled RCS and single phase natural circulation characterizes the flow pattern. The isolation of the secondary side determines the

increase of the pressure on PS (see Figure 16) and the consequent reduction of subcooling. The transition to the RC flow regime in the test ring is realized by opening the break located in the HL 1. After closing the break the primary pressure increases again until it reaches 4.5 MPa, whereupon the RCS is maintained under this condition through the activation of SGs secondary side (opening of MSRCVs of SGs 1 and 3).

The initiating event, which triggers the transient scenario, is due to the opening of the break device. Two relevant phases can be distinguished during the evolution of the experiment, plus specifying two sub-phases as follows:

- **Phase I (0 s – 1360 s)**: opening of the break to secondary side depressurization;
- **Phase II (1360 s – 5685 s)**: from the beginning of the secondary-side depressurization (CET > 368 °C) to end of the test, depressurization of the primary side;
- **Subphase II-a (1360 s – 1500 s)**: from the beginning of the secondary-side depressurization to the start of accumulator Injection;
- **Subphase II-b (1500 s – 1860 s)**: accumulator injection;
- **Subphase II-c (1860 s – 5865 s)**: ACC injection up to end of test; Starting of LPSI injection at approximately 2060 s after SoT (primary pressure < 7.7 bar).

The main results of the conditioning and test phases are depicted in Figure 16, Figure 17 and Figure 18. The imposed sequence of main events compared with the TRACE-V5 results are summarized in Table 11.

Table 7 – OECD/NEA/CSNI PKL-2 Project, Test G7 1: facility configuration

#	SYSTEM	SYMBOL	CHARACTERISTICS	STATUS	REMARKS
1	PRZ connection status	--	Loop #2	--	Initial level equal to 7.4 .
2	PRZ heater	--	--	In operation	Simulation of pressurizer heating and compensation for heat losses (12 kW)
3	UH – DC bypass	--	Orifice: Φ= 6.8 mm; L = 5mm	--	1.5 % of core flow rate with running RCPs
4	Break component	--	Connected with HL 1 Nozzle: Φ= 7.9 mm	--	Cold leg loops 1 to 4 at 8 bar
5	ECCS Accumulators	JNG	8 systems available	In operation	Cold legs of loops 1 to 4
6	ECCS HPIS	JND	4 trains connected with all CL and HL	Not operated	Flow rate of a HPIS pump regulated as in **Errore. L'origine riferimento non è stata trovata.**
7	ECCS LPIS	JNA	4 trains connected with all CL and HL	In operation	
8	MCP	--	4 MCP in operation	At rest	
9	MCP butterfly valves		4 butterfly valves	Closed	To simulate the hydraulic resistance of MCPs at rest
10	Volume Control System	KBA	--	Not operated	--
11	Residual Heat Removal System	JN(A)	--	Not operated	--
12	FW	LAB	--	Not operated	--
13	AFW /EFW	LAR	--	In operation	--
14	MSRCV		Connected to SGs 1 and 3 snd fully opened (nozzle, d = 19.2 mm per SG)		

Table 8 – OECD/NEA/CSNI PKL-2 Project, Test G7 1: relevant initial and boundary conditions *at start of both conditioning phase and test phase*

			Cond. Phase	Test Phase
#	QUANTITY	Unit	Y_{DESIGN}	Y_{DESIGN}
1	Core thermal power	kW	565	565
2	PRZ heaters thermal power	kW	12	12
3	Upper plenum pressure	MPa	4.16	
4	SG-1 exit (top of the SG)	MPa	2.49	4.37
5	SG-2 exit (top of the SG)	MPa	2.49	4.37
6	SG-3 exit (top of the SG)	MPa	2.49	4.37
7	SG-4 exit (top of the SG)	MPa	2.49	4.37
8	Core outlet (upper plenum)	°C	245	257
	Accumulators level	m	1.62	1.62
	Accumulators N2 volume	m^3	0.099	0.099
	Accumulators N2 temperature	°C	33	33
	Accumulators N2 pressure	MPa	2.26	2.26
9	SG-1 DC pipe	°C	224	256
10	SG-2 DC pipe	°C	224	256
11	SG-3 DC pipe	°C	224	256
12	SG-4 DC pipe	°C	224	256
13	PRZ level (collapsed)	m	3.2	0.8
14	SG-1,2,3,4 Riser	m	11.9	7.7
	Feed water temperature	°C	--	73

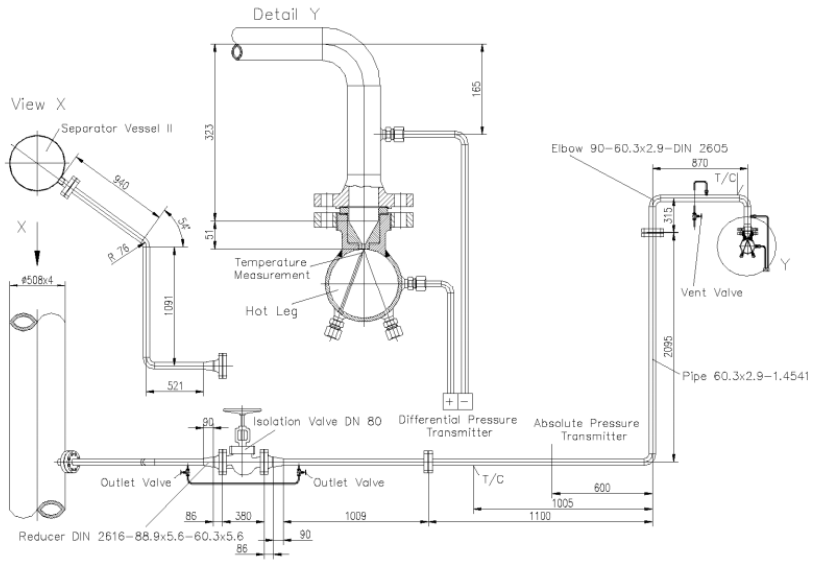

Figure 15 – Break line: hot leg 1 to separator vessel

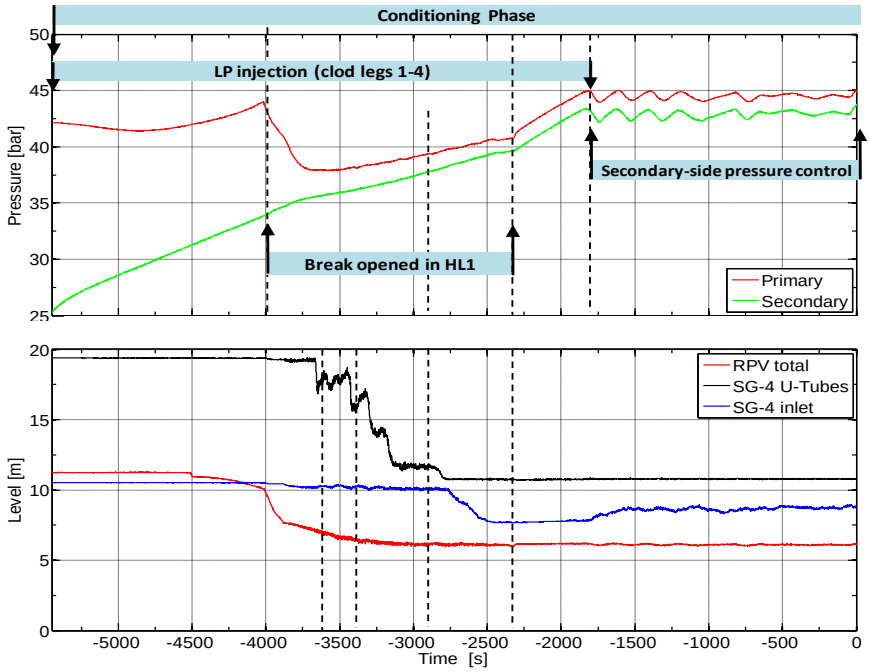

Figure 16 – PKL Test G7.1: pressure and liquid levels trends during the test phase conditioning phase

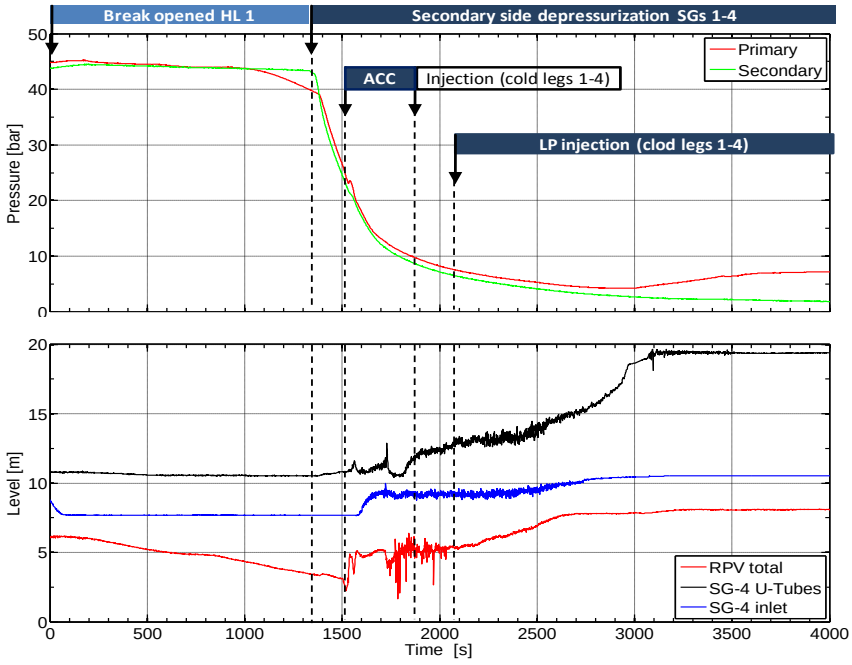

Figure 17 – PKL Test G7.1 test phase: pressure and liquid levels trends during the test phase

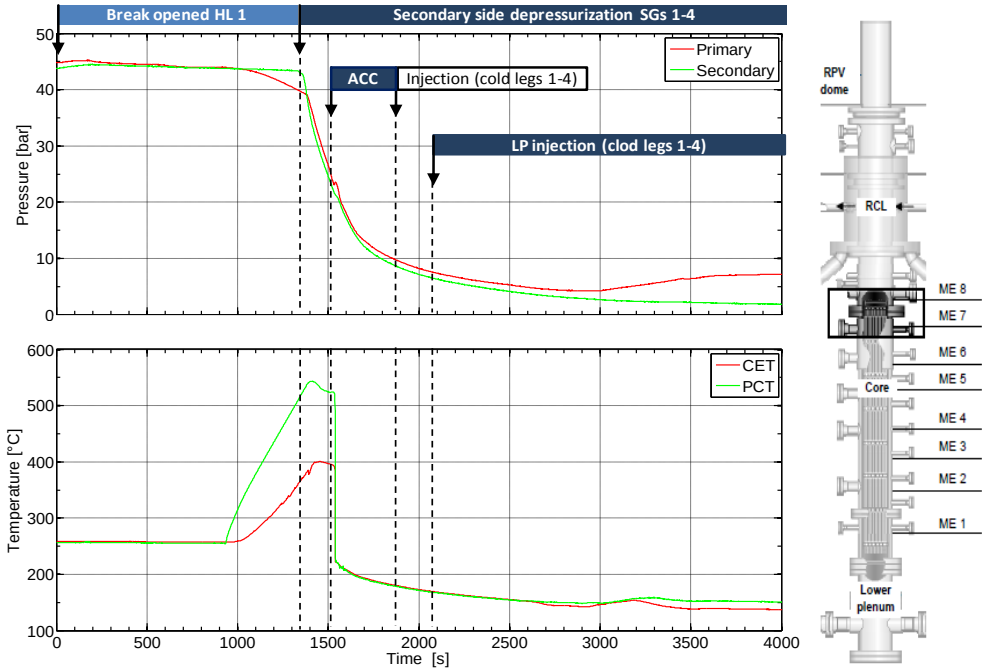

Figure 18 – PKL Test G7.1 test phase: pressure and peak cladding/core exit temperature trends during the test phase

4.2.2. TRACE-V5 nodalization development for PKL facility

4.2.2.1. Features of TRACE-V5 nodalization for simulating the test F4.1

The PKL TRACE model reproduces the geometry and the hydraulic configuration of the primary circuit as well as the secondary side of the experimental facility (see Figure 10 in which is reported the RCS and sketch of PKL-III IET). The rod bundle vessel (RBV) and the RPV down-comer are modelled through two 3-D vessel components (see Figure 14 for details od core nodalization). Each of the four loops on the primary side is modelled separately. Each loop includes a hot leg (HL), one U-tube that models the 28 U-tubes of one SG, a pump seal, a butterfly valve, a reactor cooling pump and a CL. On the secondary side, connected to the primary side via heat structures, the input deck includes three one dimensional components which simulate respectively the riser, the two down-comer pipes that are lamped in one equivalent tube and the steam dome. Flow path areas, elevations, heat structures and capacities have been taken into account from the PKL data base. The detailed description of the nodalization of the PKL is carried out in APPENDIX B.

4.2.2.2. Features of TRACE-V5 nodalization for simulating the test G7.1

The TRACE-V5 model of the RCS and secondary side of the test rig for simulating the experiment G7.1 is similar to that realized for numerical investigation of the test F4.1 (Figure 14). The main modifications and features of new model are:

- new initial and boundary conditions are implemented according with the specifications of the test;
- new logics is implemented for regulating the SG levels, the opening of the break and the opening of the valves that simulate the MSRCVs for the secondary side depressurization;
- Ramson-Trapp chocked flow model with choked-flow multiplier: 1.0 for liquid phase and 1.1 for two-phase;
- no CCFL model is activated;
- accumulators and connection lines with the cold legs are modeled (see Figure 40);
- simulation of break line according to AREVA information (see Figure 41and [47]).

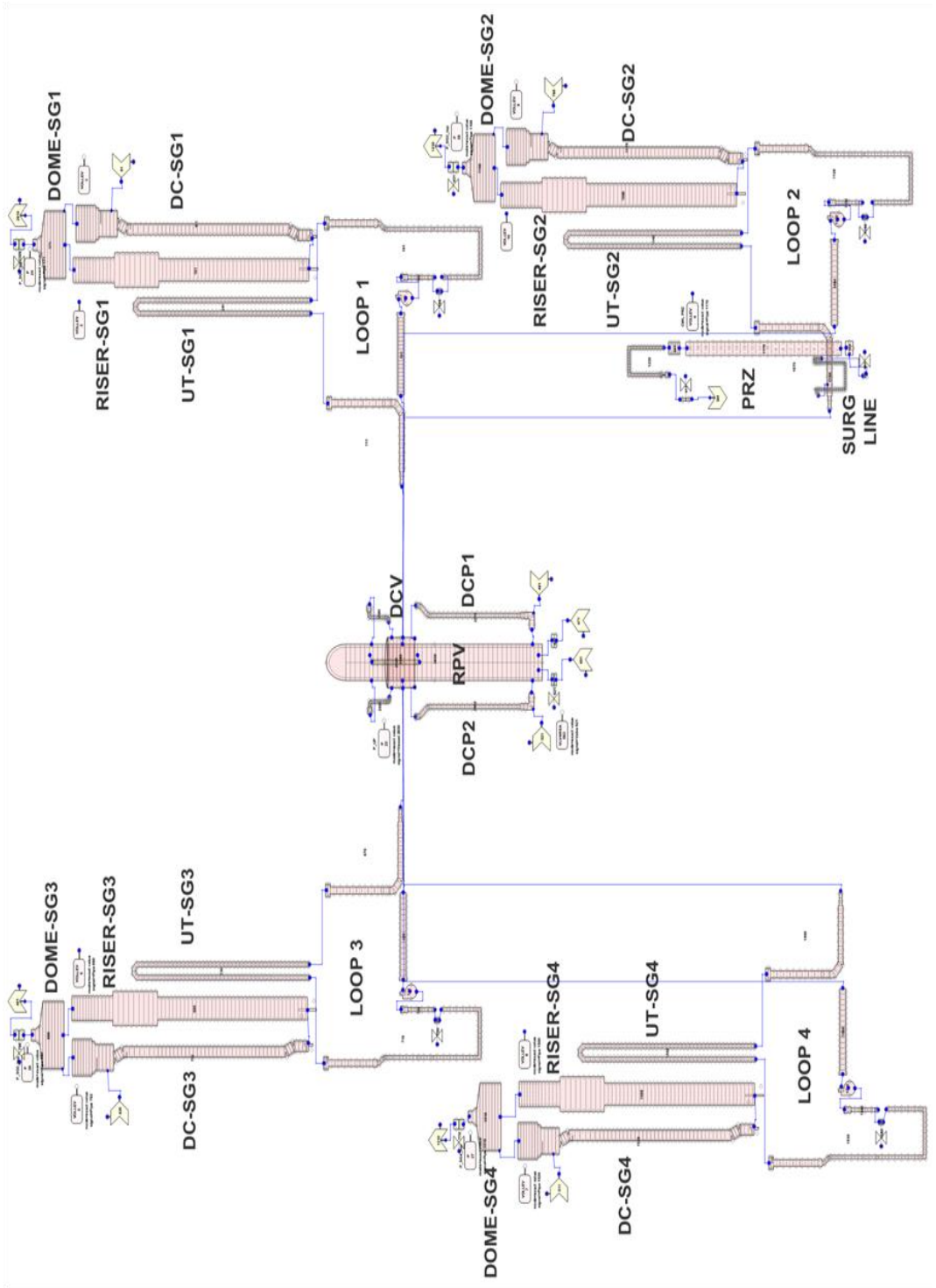

Figure 19 – TRACE-V5 nodalization of the PKL III integral test facility

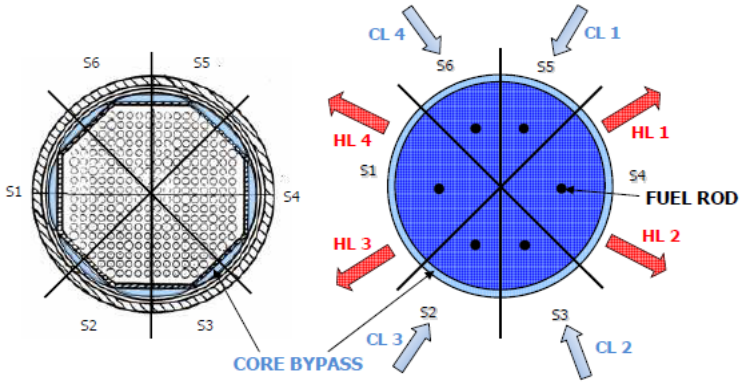

Figure 20 – Azimuthal and radial nodalization of the core region

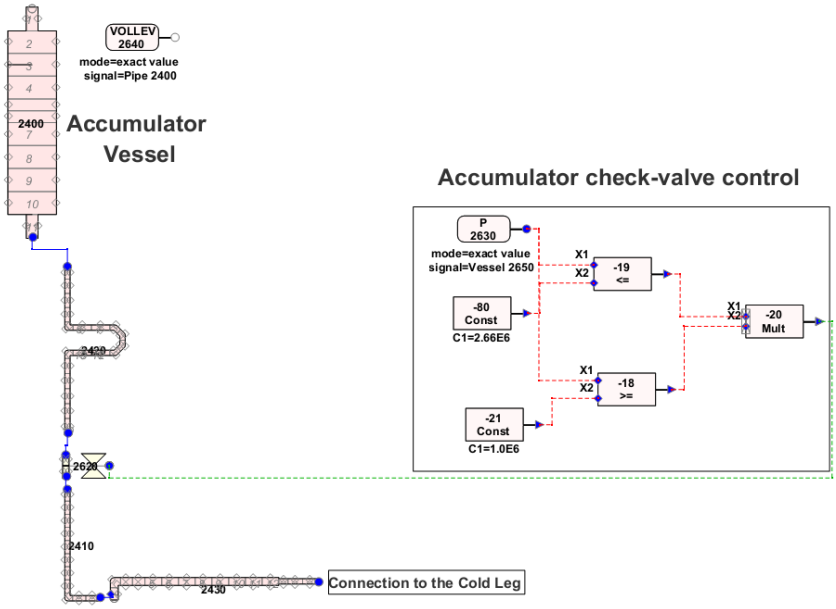

Figure 21 – TRACE-V5 Nodalization of the accumulator and cold leg connection

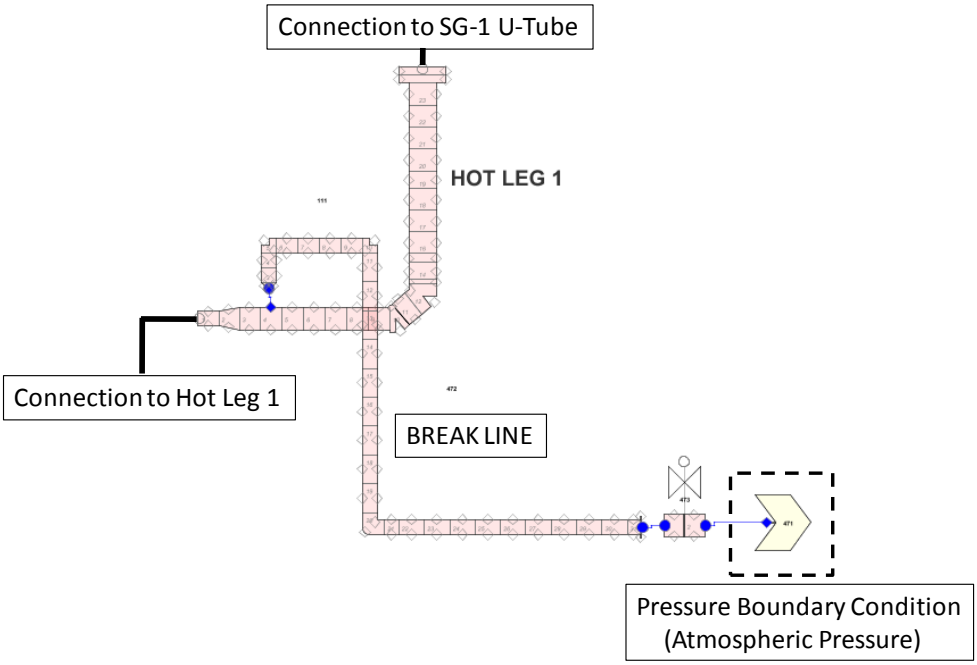

Figure 22 – TRACE-V5 Nodalization of the break line

4.2.3. Analytical study of heat transfer mechanisms under shutdown system conditions (PKL test F4.1)

4.2.3.1. Analysis of the post test results

The methodology applied for the simulation of F4.1 RUN 1 test consists in the following two steps, which synthesize the general procedure developed for the code assessment at University of Pisa [40]:

- The first step concerns the steady state evaluations of results (i.e. *steady state qualification level*). This phase includes the nodalization development step (e.g. the verification of volumes, heat transfer areas, elevations, pressure drops distribution, etc.) and the simulation of the nominal steady state conditions against acceptability thresholds.
- The second phase is focused on the evaluation of the capability of the reference results in order to reproduce the relevant thermal-hydraulic phenomena occurring during the transient (*transient qualification level*). At this level the code assessment is carried out by means of a qualitative and quantitative (through the application of the FFTBM) evaluation of the code results accuracy.

Concerning the first phase, the key operational parameters of the simulated system have been compared with the nominal steady state conditions reached by the experiment after 1000 s of null transient. The evaluation of the discrepancies between experimental data and the calculated values, reported in Table 2, is performed considering any error if the calculated value is inside the bands of the

measurement accuracy. If it is outside, it is calculated as difference between the calculated value and upper or lower limit of measured values.

The main objective of the simulation at the transient level concerns reproducibility of the relevant thermal-hydraulic phenomena and processes which occurs during the SB-LOCA boron dilution transient scenario, namely subcooled SPNC, TPNC , unstable TPNC or siphon condensation (SC) mode, transition to reflux condensation conditions, pure condensation conditions and transition from reflux condensation to TPNC ([44] [48] [49])

The test began (3390-6404 s) with the onset of subcooled natural circulation. Stepwise drainages are performed in order to obtain stable NC conditions in the loops between two consecutives steps. The drainage starts at 3390 s after the isolation of the PRZ (3200 s) reducing the primary mass inventory up to 88.5%. During this first phase of the test, TRACE parameters, such as coolant mass flow rates in the loops (from Figure 23 to Figure 26), pressure in primary and secondary side[6] (Figure 27 and Figure 28), liquid temperature at the core inlet (Figure 29) as well as collapsed level in core region (Figure 30) are stabilized to values similar to measures ones. Therefore, a correct coolant inventory (Figure 31) and thermal-hydraulic behavior is predicted by the code.

The transition to two phase NC mode occurs as a consequence of the onset of steam production at the test section outlet which flows through the hot leg in the U-tubes of the SGs. During this phase five drainages are performed in the facility. The PMI is reduced up to about 70% at the end of the phase. The secondary side pressure is increased for compensating the enhanced heat exchange in the SGs, due to the two phase flow NC condition (see Figure 32 and Figure 33 in which are depicted the differential temperature between inlet and outlet for SG-1 and SG-4).

In the TPNC regime both driving and resistant forces increase, but the driving force is prevalent (in the case of small decreases of mass inventories as happens in the F4.1 test). This implies an increase of the loop mass flow rate in the RCLs. The monotonous behavior ends when the maximum coolant flow rate is achieved for a PMI value corresponding to about 79%. Physically the maximum two phase flow rate is achieved when the static differential pressure between inlet and outlet of the SG is maximum. TRACE results for the simulation of the two phase natural circulation mode at the different coolant levels agree rather well with the temporal trends of the experimental values recorded during the F4.1 test. In fact the onset of the TPNC is well predicted in almost all the four loops, only the loop 2 shows a different behavior (from Figure 23 to Figure 26). The maximum value of the pressure drops through the SGs and the mass flow rate are predicted quite well (Figure 34 and Figure 34). The collapsed level in the test section at the core region during this transient phase is correctly calculated by the code (Figure 30)..

The SC-NC is characterized by the decreasing of NC driving forces, the small temperature difference across U-Tubes of steam generators and the occurrence of the Counter Current Flow Limiting Phenomenon (CCFL) at the entrance of U-tubes

[6] The secondary side pressure is imposed in the calculation while in the experiment is kept at the design values through the manual operation of the steam line valves. In Figure 21 is showed only the pressure trend of one SG, namely SG-1.

[50]. These conditions are responsible for the wide system oscillations. For specific values of the PMI, depending by the system layout and the pressure, the efficiency of the condensation heat transfer across U-tubes causes the release of almost all core thermal power in the ascending side of U-tubes. Liquid level builds up and is prevented to drain down by the steam-liquid mixture velocity at the tube entrance, i.e. the CCFL condition occurs. Therefore, liquid level rises in the U-tubes till reaching the top. During this period, the flow rate at core inlet is close to zero and core boil-off occurs. Once the liquid level reaches the upper bend of U-tubes, the siphon effect occurs and causes the emptying of the ascending side of U-tubes and the reestablishment of core inlet flow rate. A new cycle starts. The characteristic high oscillations in mass flow rate of this thermal-hydraulic regime are observed also in code results, but with higher amplitude than the experimental values. This is probably due to numerical instability induced by ill-posed mathematical nature of the two phase flow model in TRACE code (from Figure 23 to Figure 26)

The transition from TPNC to reflux condensation is characterized by constant decrease in mass flow rate in the RCLs, as the PMI is reduced until no more coolant is transfer from the inlet to the outlet of SGs. As observed from the test, the transition to pure RC mode takes place when the PMI reaches 60.5%, (28660s corresponding to 27660 s after SoT). During this part of the transient the decrease in boron concentration at SGs outlet becomes more evident in all the loops (Figure 36 Figure 37).

At low mass inventories of primary coolant, steam velocities in the upper part of the system including hot legs and steam generator entrance are low. Weak interactions occur at the steam-liquid interface and they are not enough to cause CCFL. In these conditions, the liquid that is condensed or entrained in the ascending side of the U-tubes may flow back to the hot leg and to the core. Stratified counter current steam and liquid flows occur simultaneously in the hot legs. Mass flow rate at the core inlet is close to zero and the core thermal power is removed through the steam condensation on the U-tubes walls. This led to a boron dilution of the cold legs of the primary system. The thermal-hydraulic phase described above illustrates the establishment of pure reflux condensation mode in the system (38660-42580 s). During this phase the calculated collapsed levels show an asymmetric trend, in fact the level of the single U-tube model of the loops 1 over predicts the behavior of the experimental value in the average U-tube in both ascended and descended side, as shown in Figure 38 and figure 40, whereas for loop 3 the collapsed level presents a correct qualitative behavior (Figure 39 and Figure 41). A similar asymmetric behavior (see Figure 42) is observed also for the loop seals levels (on descended side).

The transition from pure reflux-condensation to the two-phase natural circulation is predicted with TRACE to occur at the same primary coolant mass inventory as observed during the PKL experiment. The TRACE simulation results for this test phase are in agreement with the experimental data: the levels in various parts of the primary system agree well with the experimental data (see Figure 30 and from Figure 38 to Figure 43). The coolant circulation in the loops is predicted to be restored at similar flow rates, but the replenished boron concentration in loops

seals stabilizes at values lower than those observed in the experiment (Figure 36 and Figure 37).

Fast Fourier Transform Based Method (FFTBM) (see [51] and [52]), is used for the quantification of the code results accuracy. Table 8 summarizes the results obtained by the simulation for the overall transient. The table includes the detail of the parameters selected for the application of the FFTBM, the labels that identify the values of the accuracies and of the weighted frequencies. The selected parameters are 24. This is the minimum number relevant to describe the transient, considering both the peculiarities of the transient and the availability of experimental data. These parameters are then combined to give an overall view of calculation accuracy. The total average amplitude of the transient is the sum of all the average amplitudes with their “weights”. The “weight” of each contribution depends on the experimental accuracy, the relevance of the addressed parameter and a normalization component referring to the average amplitude evaluated for the primary side pressure. The reference results of the method are usually focused on three values: the averages amplitudes of the primary pressure and of the global (or total) response, consistently with the typical application of the method plus the coolant temperature at the affected SG outlet due to the peculiarity of the test. The detailed presentation of the method is given in APPENDIX E.

Table 9 – PKL III test F4.1 RUN 1, TRACE-V5p2: comparison between measured and calculated relevant initial and boundary conditions.

#	QUANTITY (*)	UNIT	DESIGN	TRACE-V5	ER.	ACCEPT. ER. (°)
						,
1	**PRIMARY CIRCUIT POWER BALANCE**					
1-1	Core thermal power	MWth	0.600	0.600	0.0 %	**2.0 %**
2	**SECONDARY CIRCUIT POWER BALANCE**					
2-1	SG-1, 2, 3, 4 power exchanged	MWth	--	0.420	--	**2.0 %**
3	**ABSOLUTE PRESSURE**					
3-1	PRZ pressure	bar	29.88	29.95	0.23%	**0.1 %**
3-2	Upper plenum pressure	bar	30.20	30.18	0.066%	
3-3	SG-1 exit pressure	bar	19.21	19.19	0.10%	
3-4	SG-1 exit pressure	bar	19.26	19.26	0%	
3-5	SG-1 exit pressure	bar	19.20	19.21	0.052%	
3-6	SG-1 exit pressure	bar	19.24	19.24	0%	
4	**FLUID TEMPERATURE**					
4-1	PRZ fluid temperature	°C	233-234	233.32	0.13-0.29 %(**)	**0.5 % (**)**
4-2	Core inlet temperature (lower plenum top)	°C	208.8	208.41	0.19%(**)	
4-3	Core outlet temperature (upper plenum)	°C	231.7	229.95	0.75%(**)	
4-4	Upper head temperature	°C	230.3	227.64	1.15%(**)	
5	**ROD SURFACE TEMPERATURE**					
5-1	Clad temperature at 2/3 of the core	°C	229.4	232.01	2.61	**10 °C**
5-2	Clad temperature at top of the core	°C	235.7	235.42	0.28	
7	**HEAT LOSSES**					
7-1	Heat losses primary side	kW	--	180.31		**10.0 %**
8	**LOCAL PRESSURE DROPS**					
8-1	Pressure drop	bar	--			**10.0 % (^)**
9	**MASS INVENTORY IN PRIMARY CIRCUIT**					
9-1	Primary circuit mass inventory (with PRZ)	kg	2475	2504.6	1.19%	**2.0 % (^^)**
9-2	PRZ and surge line mass inventory	kg	155	163.4	5.42%	
11	**FLOW RATES**					
11-1	CL 1 mass flow rate	kg/s	1.32	1.21	8.33%	**2.0 %**
11-2	CL 2 mass flow rate	kg/s	1.29	1.20	6.97%	
11-3	CL 3 mass flow rate	kg/s	1.26	1.19	5.55%	
11-4	CL 4 mass flow rate	kg/s	1.26	1.12	11.1%	
12	**BYPASS MASS FLOW RATES**					
12-1	Core bypass flow rate (+)	%	--	1.7	--	**10.0 %**
12-2	UH-DC bypass flow rate (+)	%	0.5	0.88	0.38 %	
13	**PRESSURIZER LEVEL (COLLAPSED)**					
13-1	PRZ collapsed level	m	4.69	4.67	0.02 m	**0.05 m**
14	**SECONDARY SIDE OR DOWN-COMER LEVEL**					
14-1	SGs level (collapsed)	m	12.2	12.07	0.13 m	**0.1 m (^^)**
15	**BORON CONCENTRATION**					
15-1	Boron concentration in primary system	ppm	2000	2000	0.0 %	**--**

(°) The % error is defined as the ratio $\frac{|\text{reference or measured value} - \text{calculated value}|}{\text{reference or measured value}} \cdot 100$

The "dimensional error" is the numerator of the above expression

(*) With reference to each of the quantities below, following a one hundred s "transient-steady-state" calculation, the solution must be stable with an inherent drift < 1% / 100 s

(**) And consistent with power error. The errors are calculated in K.

(^) Of the difference between maximum and minimum pressure in the loop

(^^) And consistent with other errors.

(+) This is a design data of the PKL III facility

Table 10 – PKL III test F4.1 RUN 1: summary of results obtained by application of FFTBM (reference calculation) – overall transient.

#	PARAMETER	TRACE5	
	Description	(0-4410s)	
		AA	WF
1	*UP pressure [MPa]*	0.128	0.0052
2	*SG #1 pressure-sec. side [MPa]*	0.038	0.0069
3	*Core inlet fluid temp. [K]*	0.518	0.0044
4	*Core outlet fluid temp. [K]*	0.038	0.0059
5	*Upper head fluid temp. [K]*	0.039	0.0063
6	*SG DC bottom fluid temp. [K].*	1.077	0.0012
7	*Heater rod temp. (midd. lev.) [K]*	0.074	0.0080
8	*Heater rod temp. (high lev.) [K]*	0.397	0.0058
9	*Primary side mass [kg]*	0.042	0.0085
10	*Core lev. [m]*	0.352	0.0099
11	*SG #1 DC lev. [m]*	0.177	0.0052
12	*PRZ lev. [m]*	0.451	0.0069
13	*LS #1 desc. side lev. [m]*	0.649	0.0044
14	*DP inlet outlet SG #4 [kPa]*	1.337	0.0059
15	*DP across DCV 1 inlet and RPV outlet 1 [kPa]*	2.974	0.0063
16	*Core power [kW]*	0.956	0.0012
17	*Mass flow rate loop #1 [kg/s]*	1.700	0.0080
18	*Mass flow rate loop #2 [kg/s]*	1.765	0.0058
19	*Mass flow rate loop #3 [kg/s]*	1.582	0.0126
20	*Mass flow rate loop #4 [kg/s]*	1.628	0.0117
21	*[B] concentration in LS #1 [-]*	0.988	0.0080
22	*[B] concentration in LS #2 [-]*	0.949	0.0084
23	*[B] concentration in LS #3 [-]*	0.930	0.0087
24	*[B] concentration in LS #4 [-]*	0.945	0.0082
TOTAL AVERAGE ACCURACY ***Total (24 parameters)***		**0.5**	**0.063**

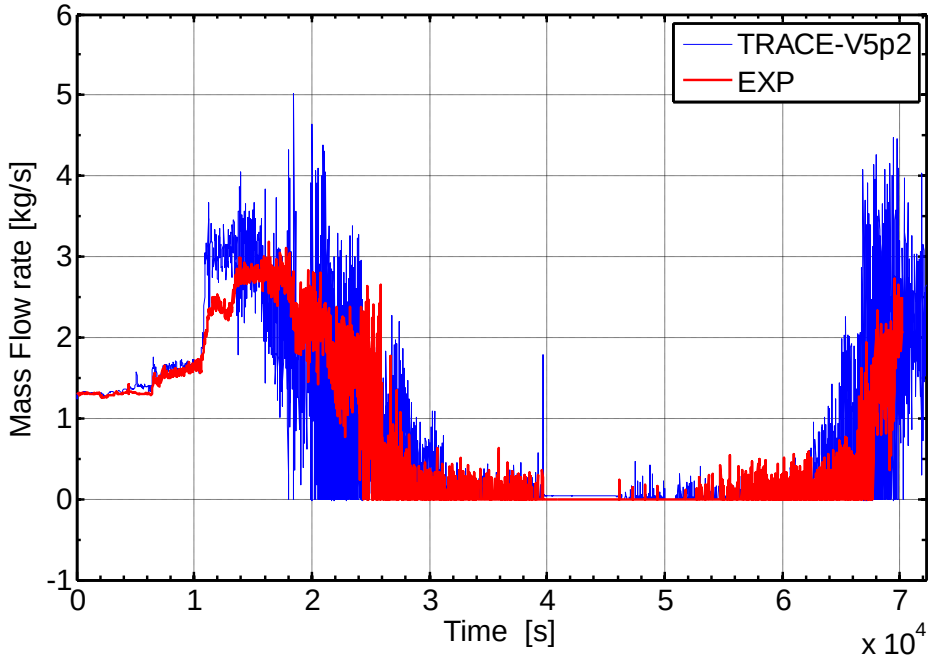

Figure 23 – PKL III test F4.1 RUN 1, posttest results: loop 1 SG outlet mass flow rate trends (0 – 70230 s)

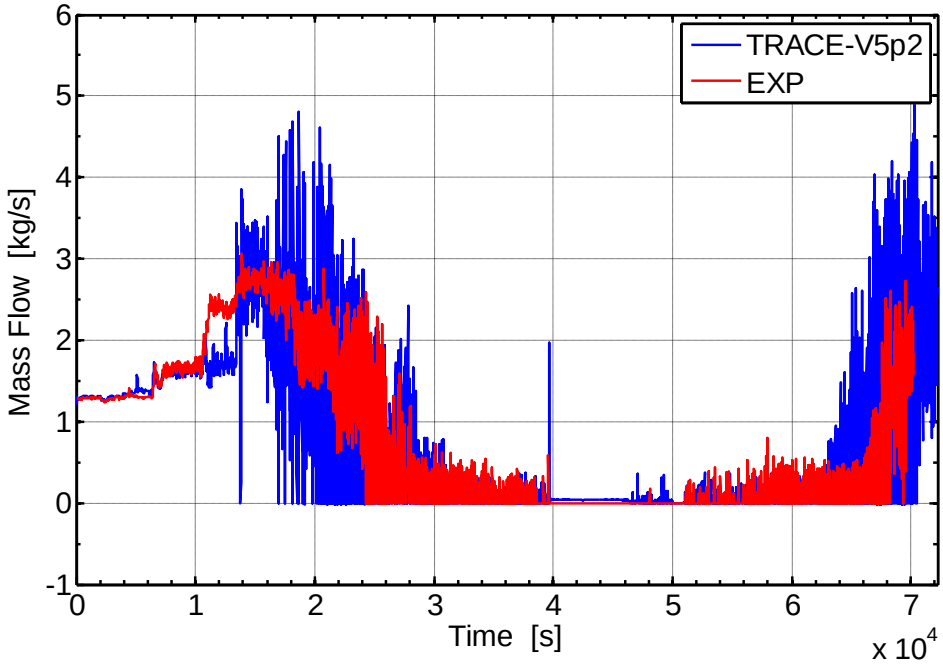

Figure 24 – PKL III test F4.1 RUN 1, posttest results: loop 2 SG outlet mass flow rate trends (0 – 70230 s)

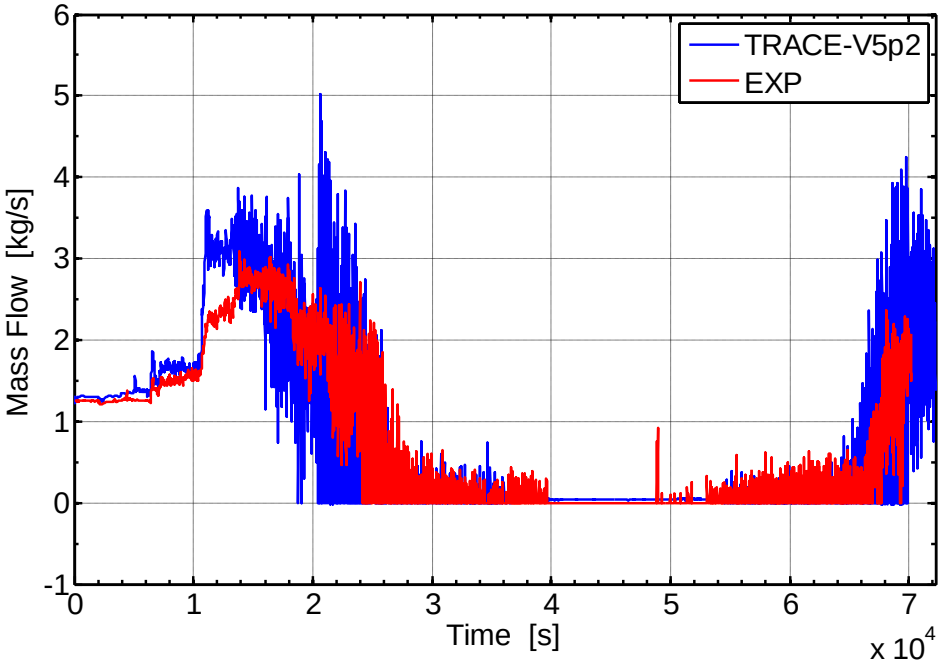

Figure 25 – PKL Test F4.1, posttest results: loop 3 SG outlet mass flow rate trends (0 – 70230 s)

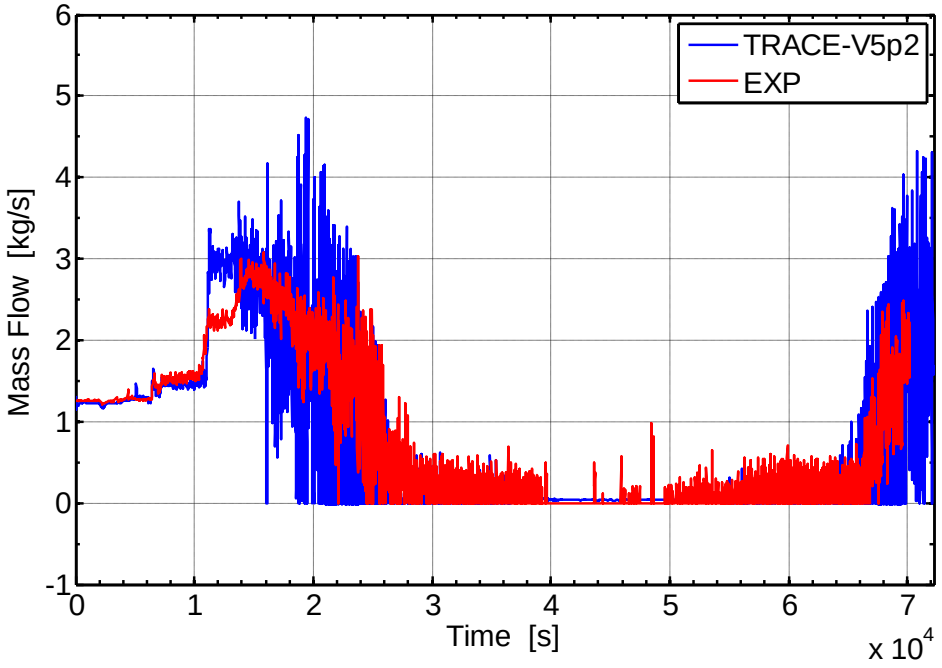

Figure 26 – PKL III test F4.1 RUN 1, posttest results: loop 4 SG outlet mass flow rate trends (0 – 70230 s)

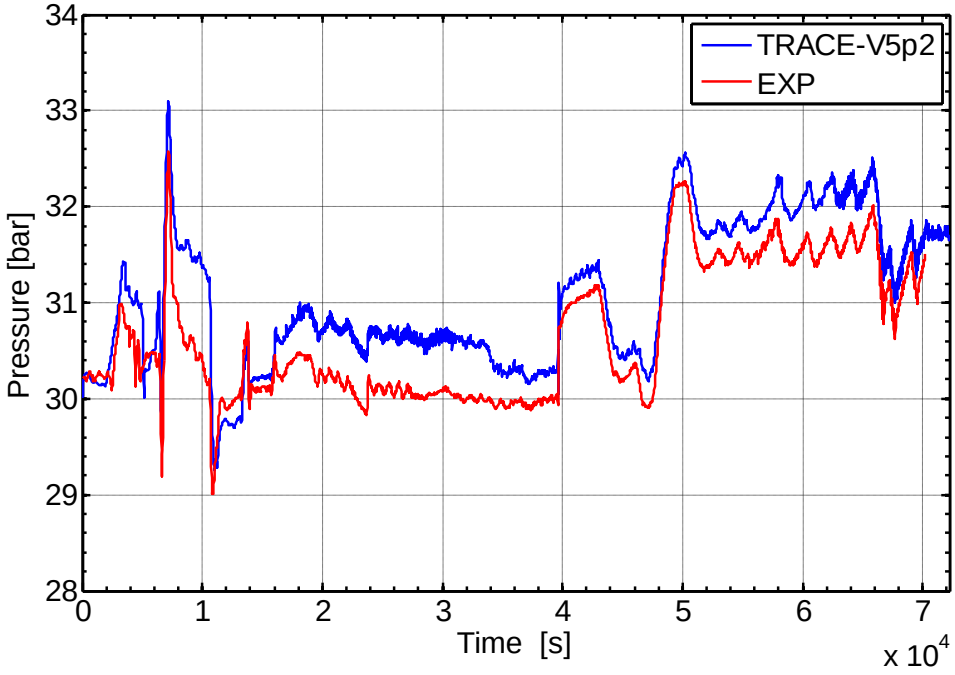

Figure 27 – PKL III test F4.1 RUN 1, posttest results: UP pressure trends

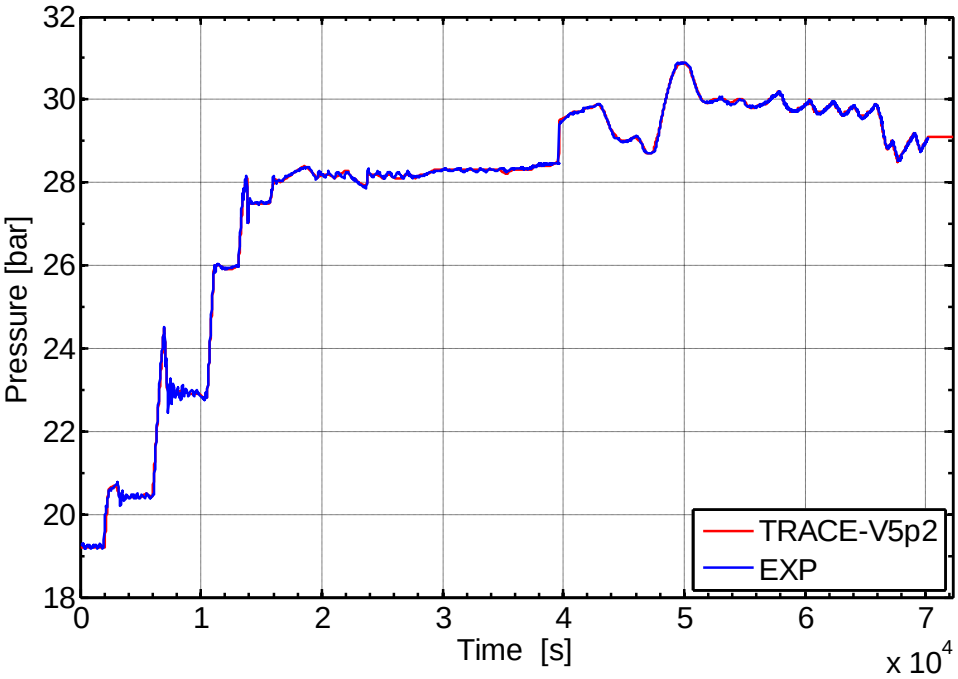

Figure 28 – PKL Test F4.1, posttest results: SG-1 pressure trends

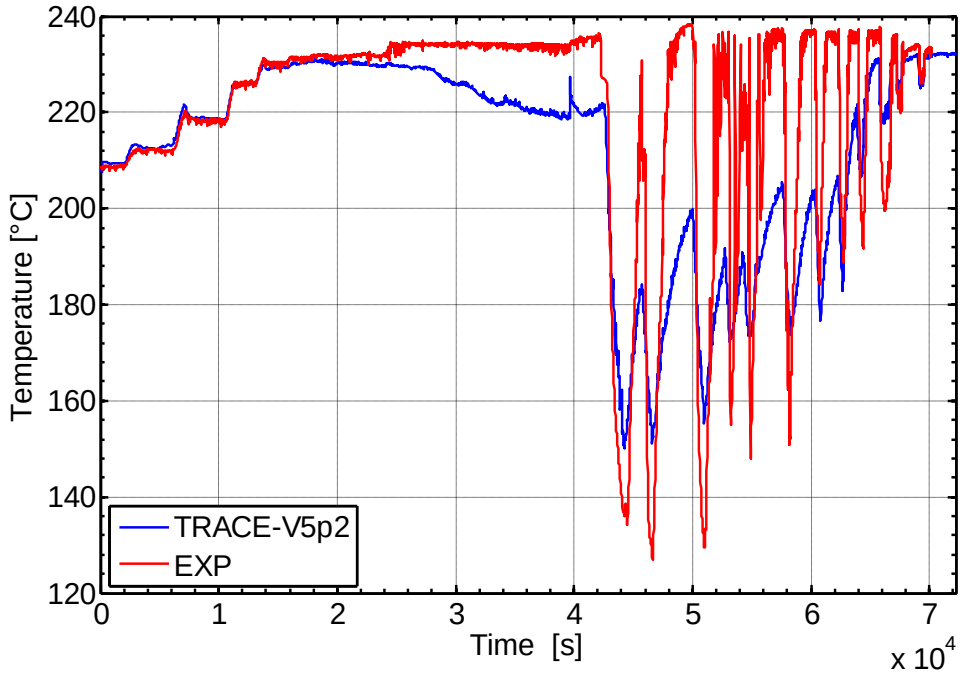

Figure 29 – PKL III test F4.1 RUN 1, posttest results: LP coolant temperature trends

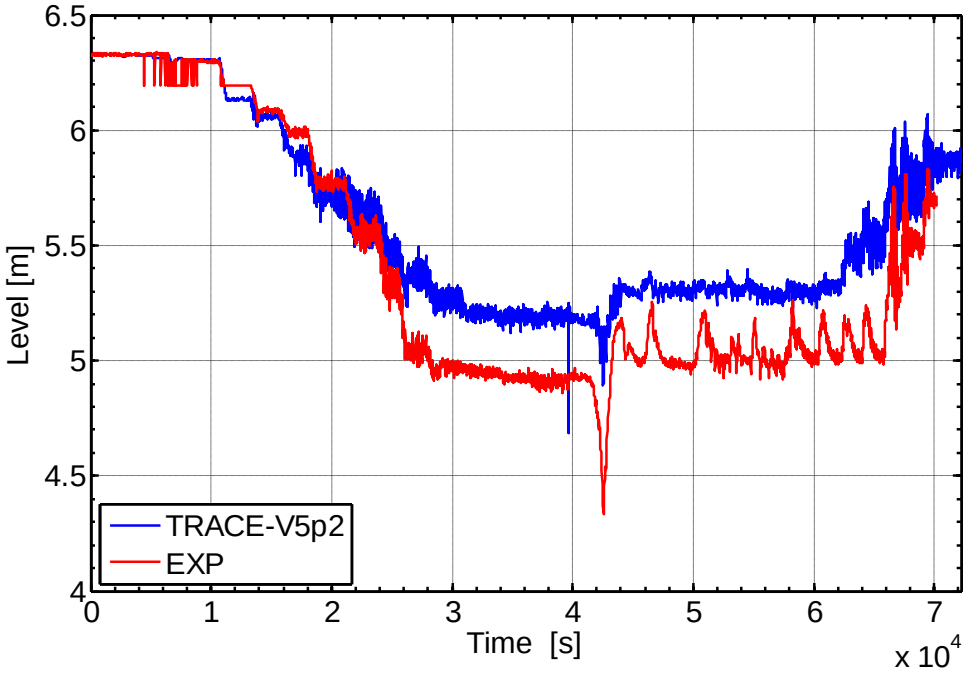

Figure 30 – PKL III test F4.1 RUN 1, posttest results: core collapsed level

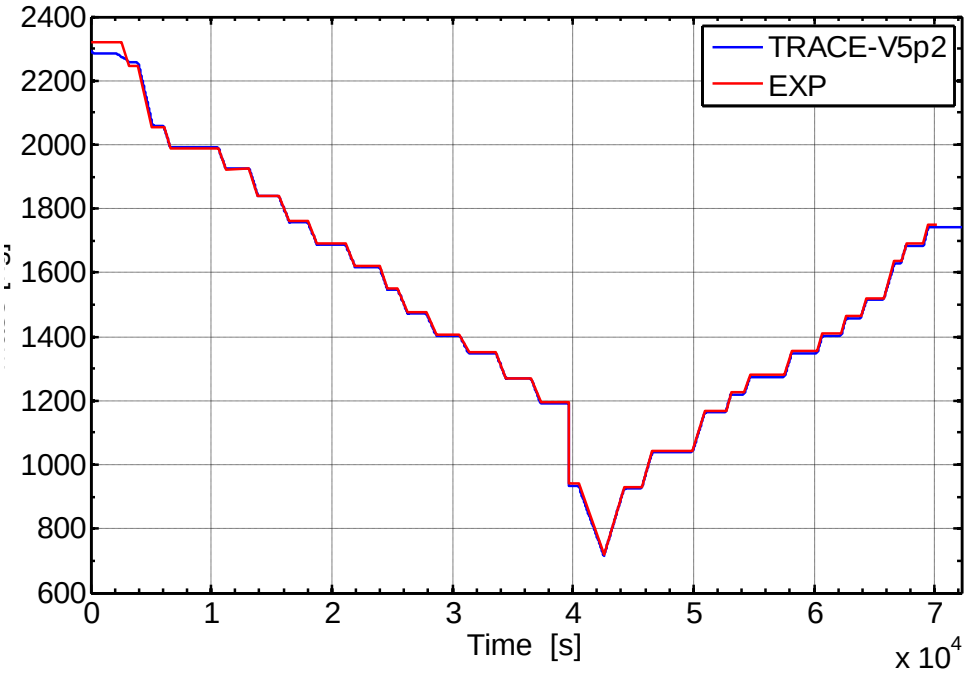

Figure 31 – PKL III test F4.1 RUN 1, posttest results: primary side total mass (without PRZ)

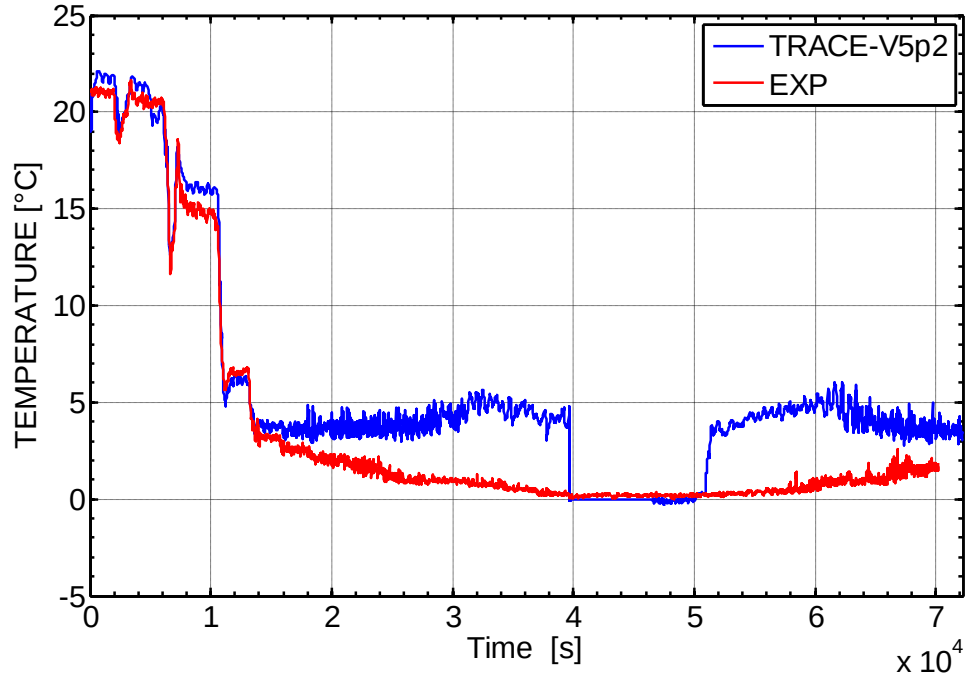

Figure 32 – PKL III test F4.1 RUN 1, posttest results: differential temperature SG-1 inlet/outlet

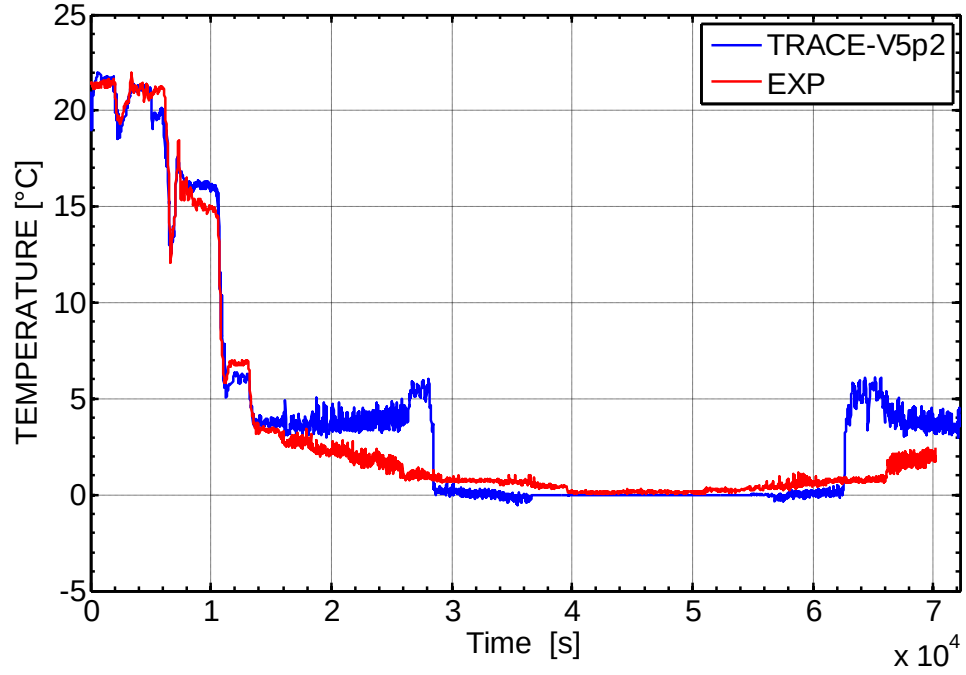

Figure 33 – PKL III test F4.1 RUN 1, posttest results: differential temperature SG-4 inlet/outlet

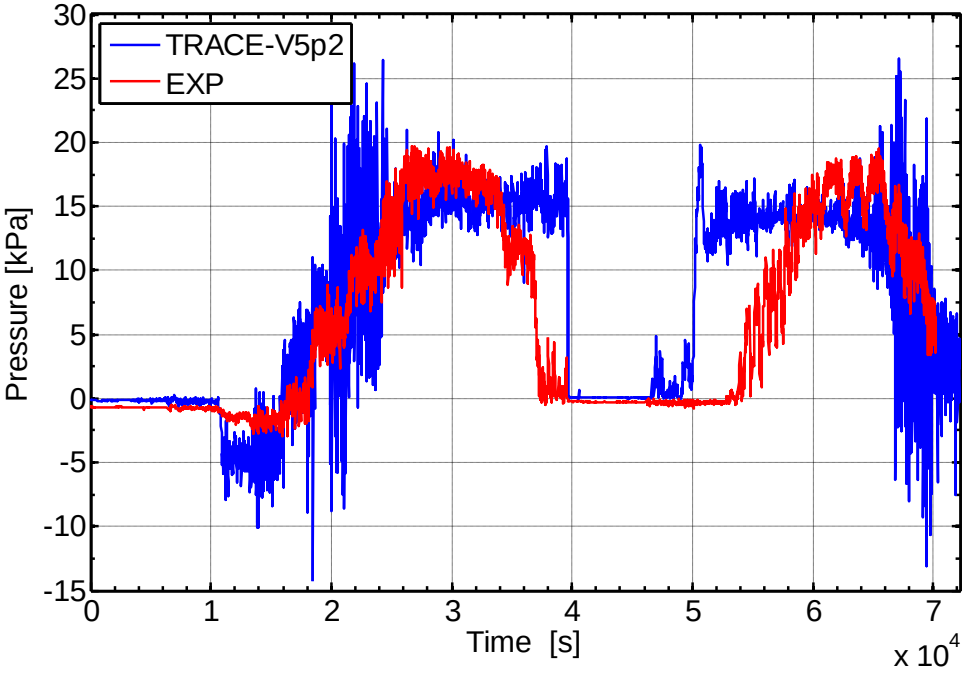

Figure 34 – PKL III test F4.1 RUN 1, posttest results: DP inlet outlet SG-1 primary side

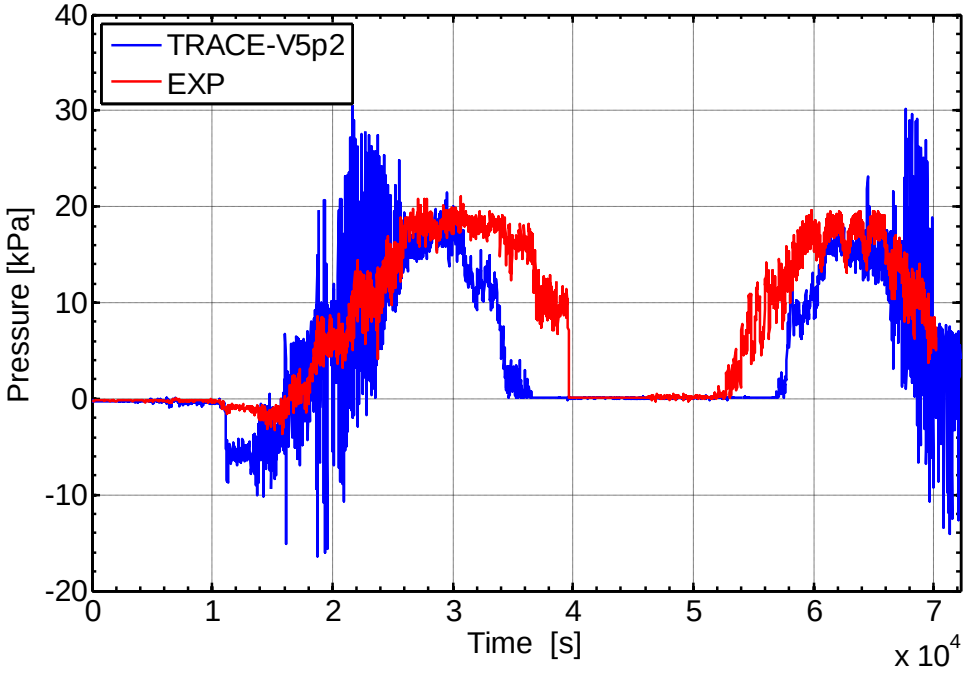

Figure 35 – PKL III test F4.1 RUN 1, posttest results: DP inlet outlet SG-4 primary side

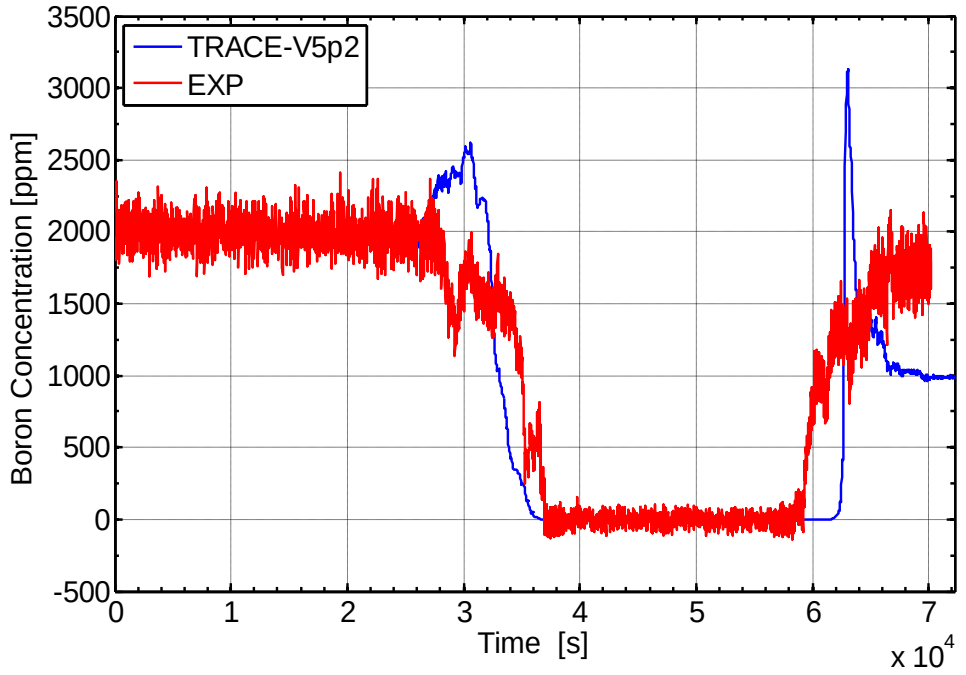

Figure 36 – PKL III test F4.1 RUN 1, posttest results: boron concentration in CL-1

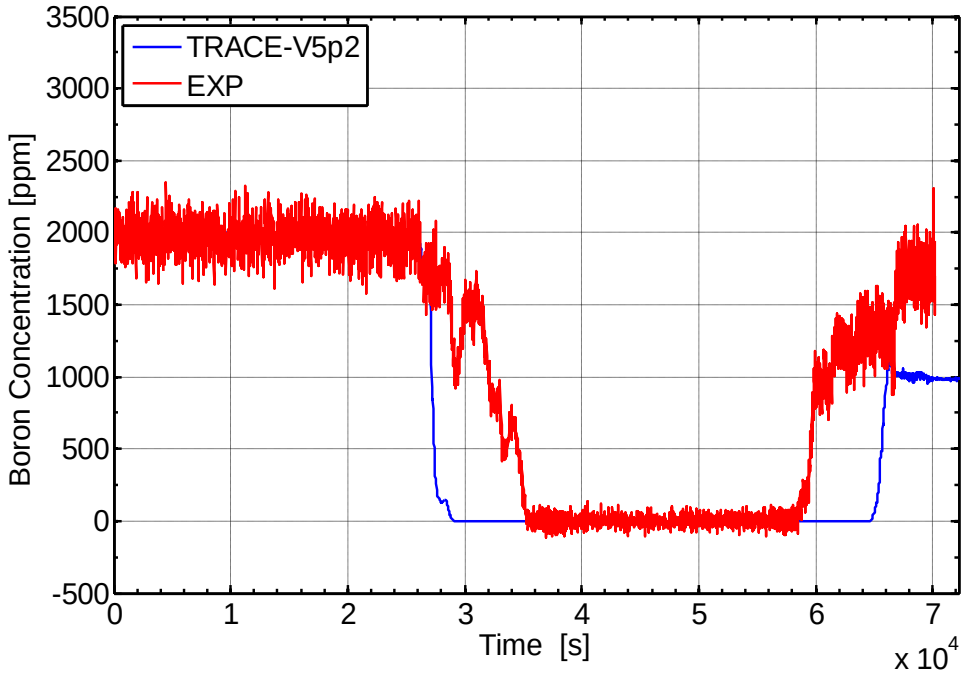

Figure 37 – PKL III test F4.1 RUN 1, posttest results: boron concentration in CL-3

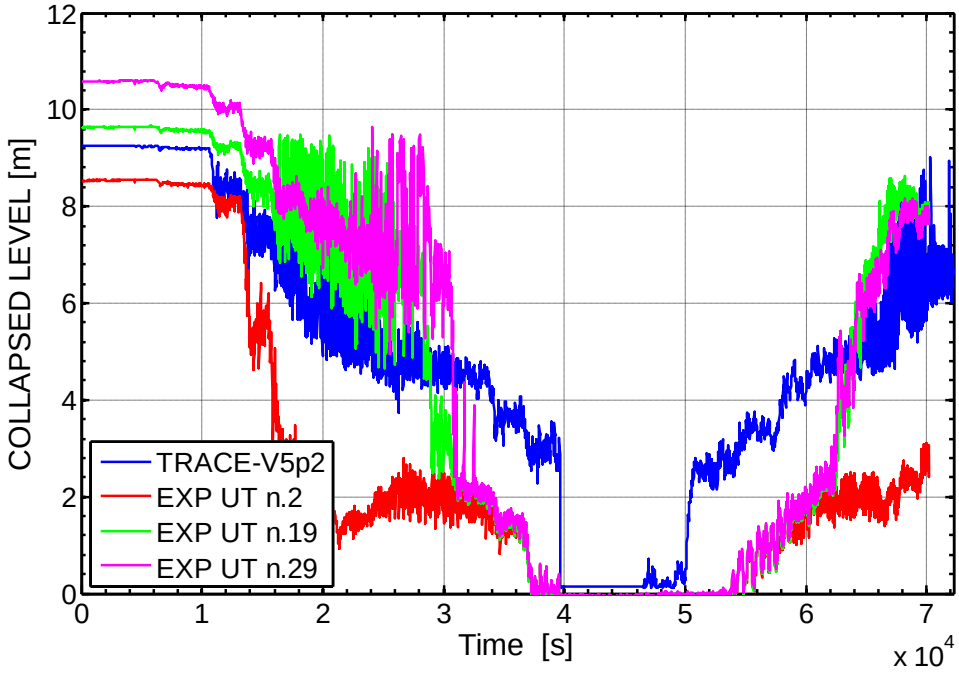

Figure 38 – PKL III test F4.1 RUN 1, posttest results: SG -1 U-tube ascending side collapsed levels

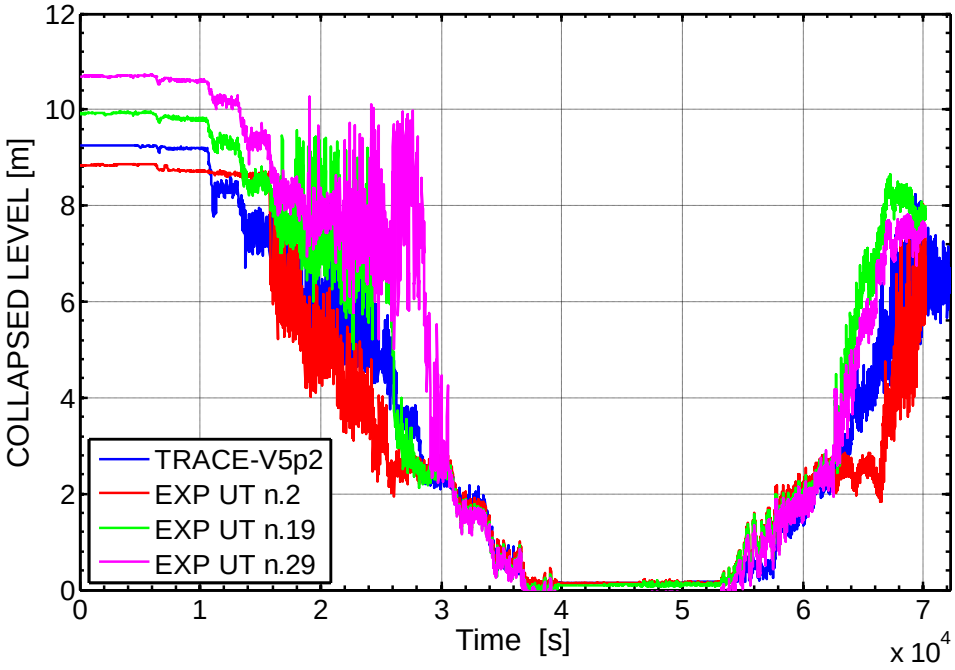

Figure 39 – PKL III test F4.1 RUN 1, posttest results: SG -3 U-tube ascending side collapsed levels

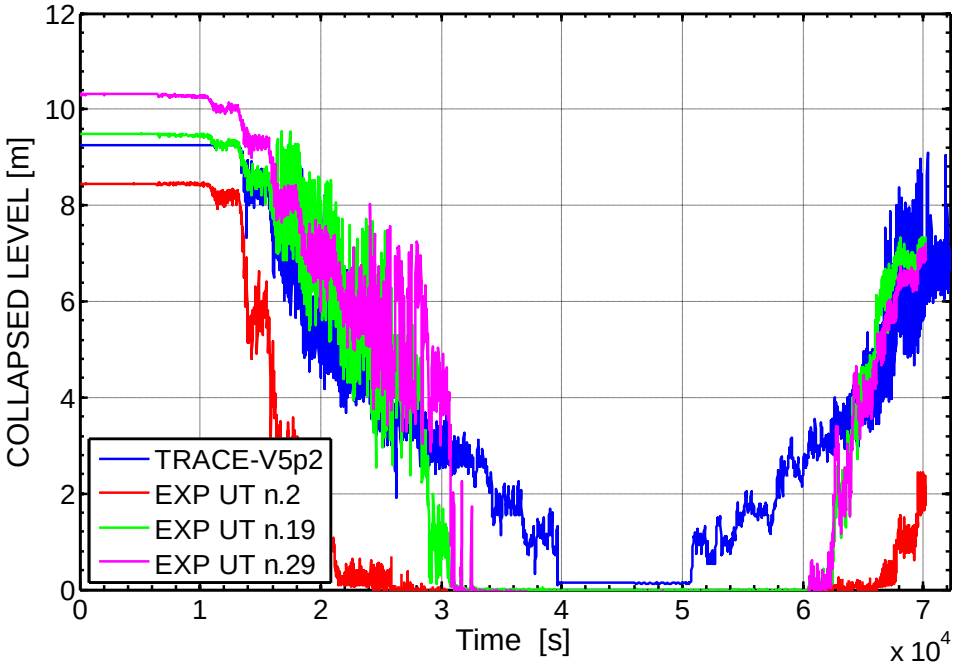

Figure 40 – PKL III test F4.1 RUN 1, posttest results: SG -1 U-tube descending side collapsed levels

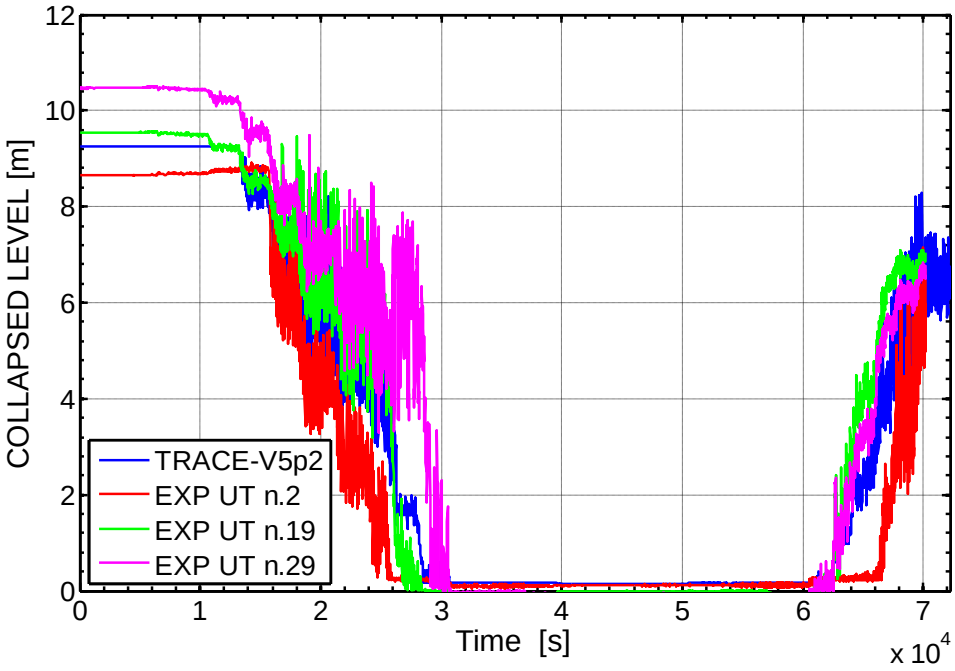

Figure 41 – PKL III test F4.1 RUN 1, posttest results: SG -3 U-tube descending side collapsed levels

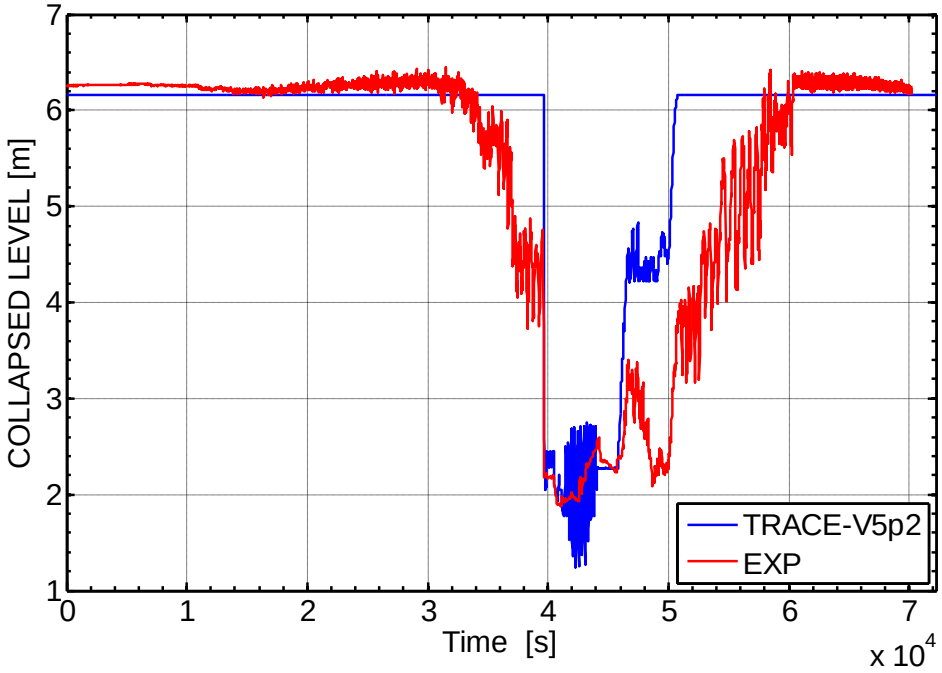

Figure 42 – PKL III test F4.1 RUN 1, posttest results: loop seal 1 descending side collapsed level

4.2.4. Investigation of TH-SYS code performance for SBLOCA phenomenology (PKL test G7.1)

4.2.4.1. Analysis of the post test results

The analysis of the TRACE results is carried out fulfilling the two steps of the qualification process outlined in the section § 4.1.

The results concerning the steady state analysis are reported in Table 12, in which are compared only the analytical and experimental conditions reached at the beginning of the test phase (achieved at the end of the conditioning phase).

The evaluation of the TRACE capabilities in capturing all relevant phenomena that occur during the test phase is obtained analyzing the test results and comparing them with the code predictions at the qualitative level first and then quantifying the error using FFTBM, which provides an estimation of the goodness of calculations.

The qualitative analysis is performed following the chronology of the phenomenological windows in which is subdivided the test.

Phase I (0 s – 1360 s)

At the beginning of the test the heat transfer mechanism responsible for transporting the core power to the secondary side heat sinks occurred in symmetric way (with all 4 SGs isolated) under stationary RC operating conditions.

In the instants immediately after the opening of the break, the hot-side coolant swell level reached into the SG inlet chambers and the break flow was in two phase saturated choked regime. The transition to only steam discharge, as soon as the swell level decreased down to the hot legs, occurred rapidly. The break flow rate was well reproduced by the TRACE simulation (see Figure 43) during this period but the initial swelling level into the vertical part of the HL 1 immediately after the break opening, was not predicted by the code (see Figure 44).

The course of events occurring during the evolution of the transient up to 250 s are characterized by RC condition that partially was responsible for removing of the steam emerging from the core. After 250 s from the SoT, no heat was removed by the secondary side as a result of the balance between the increase in enthalpy due to the generation of steam in the core and the enthalpy discharged through the break (see Figure 45 and Figure 46 in which are represented the differential temperature throughout SG-1 and 4). Under this condition the experimental primary and the secondary side pressures evolved constantly and almost parallel. The simulation showed the same trend confirming a well prediction of the phenomena that occurred during the first part of the phase I of the test (see Figure 47).

Around 940 s the core region toke place a progressive decrease of the collapsed level due to a consequent lowering of level from the hot leg to the core upper edge (i.e. replicated height of fuel element upper tie plate) (see figures from Figure 54 to Figure 55). During the occurrence of core heat-up phenomenon, predicted by TRACE beforehand, the CET started to raise with a response delay around 50 s respect to the increase of the PCT. The simulation shows an unstable increase of the CET because of same liquid remains there (void fraction is around 0.98), whilst

the PCT started to increase whit a delay of approximately 70 s compared whit the experimental cladding temperature (see figures from Figure 59 to Figure 61).

Following the start of core heat-up the heat transfer from the overheated steam to structures in its flow path caused the heat up of un-heated structures above the active length of the core and upper core structures. This process determined reduction of the steam flow from the RPV. As result of the imbalance between the core emerging from the RPV and the break flow, the primary pressure started to decrease slowly. Consequently the primary pressure fell short of the secondary pressure around 1000 s after SoT. The same behavior has been reproduced also in the simulation (see Figure 48).

Phase II (1360 s – 5685 s)

Subphase II-a (1360 s – 1860 s)

The secondary side depressurization was triggered by the condition of reaching the temperature set point imposed on the core exit temperature, namely $CET \geq 368\,°C$. The measured and calculated main steam flow rates and the secondary-side liquid levels in SGs 1 and 4 are depicted from Figure 49 to Figure 52)

The secondary-side depressurization simulated by the code is well reproduced (see Figure 48) but the starting time point of this process is delayed because of the calculated CET reached the set point approximately at 1405 s (after the SoT) with a delay of 40 s compared to the experimental value (see Figure 59 and Figure 60). The fast secondary-side depressurization has the effect of intensifying the heat exchange on the secondary side, which in turn is accompanied by intense condensation in the U-tubes. This phenomenon is responsible of the depressurization on the primary pressure. Optimal heat removed in the U-tubes by means of reflux-condensation conditions with film-condensation across the entire heat transfer area assured a close coupling of the primary pressure to the secondary that is also well predicted by the code (see Figure 47). The TRACE code underestimate the heat exchange in the SG 1, whilst in SG 4 during the secondary side depressurization is well reproduced (see Figure 45 and Figure 46).

As soon as a stable and intense heat removal to secondary side is established, a distinct differential pressure became apparent between RPV inlet and outlet as well as in the computational model (Figure 53). The increase of the pressure drop through the RPV causes the dislocation of coolant from the downcomer into the core region. Displacement of coolant in concurrence with expansion of the swell level in the core determines the onset of the partial core quenching. This phenomenon is also visible in the core level obtained by the TRACE code (see Figure 55). Despite the intense heat transfer in the U-tubes and the fast primary-side pressure reduction no CCFL with displacement of water from RPV to SGs occurred in the experiment.

Subphase II-b (1500 s – 1860 s)

At 1500 s after SoT the primary pressure had decreased to 26.6 bar, and the accumulator (ACC) injection was started in all 4 cold legs. This condition is reached in the calculation at 1533 s after the SoT. As a result of the cold ECC being injected into the cold legs (see Figure 62 in which the calculated and experimental ECC total mass flow rates are compared), dislocations of the coolant

inventories of the loop seals and RPV took place. The high condensation induced by the injection of cold water throughout the ECCs nozzles in the cold legs caused an inversion of the differential pressure between RPV inlet/outlet. The lowering of the pressure on the cold side had the effect of coolant redistribution in the RCS. Namely in the core got dislocated towards the downcomer on one hand, and the coolant in the loop seals got dislocated towards the RCP on the other hand (see Figure 55 and Figure 56). In the SG side of the individual loop seals a clearing phenomenon occurred as well in the TRACE results (see Figure 57 and Figure 58) with the consequence of steam flowing towards the RPV. This reestablished a pressure balance between the pressures of the hot and cold sides. By rebalance of the pressures a coolant re-dislocation in the RPV in concurrence with the injected ECC caused the increased supply of the core region with ECC. The code reproduced qualitatively well this thermal hydraulic behavior in the core region as well in the loop seals (see Figure 55, Figure 57 and Figure 58). At 1860 s after SoT, the ECC injections had been stopped at a pressure of 1 MPa, as specified in the experiment.

Subphase II-c (1500 s – 5865 s)

After the primary pressure decreased to 7.7 bar at approx. 2060 s after SoT the LPSI was started in all 4 cold legs (see Figure 63). By activation of the LPSI the RCS was filled continuously and achieved subcooled state at 2620 s after SoT. After 3000 s after SoT, the RCS is completely filled and non-simultaneous onset of natural circulation in the individual loops. During this phase the calculated mass flow rate in all four loops exhibit strong oscillations compared to the experiment.

The quantitative evaluation of the accuracy of the test G7.1 has been performed as for the F4.1 applying the FFT algorithm. The outcome of the analysis is summarized in Table 13. The results are in good agreement with qualitative considerations drawn from the observation of the corresponding curves

Table 11 – PKL III Test G7 1, posttest results: resulting sequence of main events

#	EVENT DESCRIPTION	EXP TIME(s)/SET POINT	TRACE-V5	Note
1	Start of transient: break opening in HL #1	0	0	Imposed
2	Begin of core uncovery	940	810	
3	Fall of the primary pressure above secondary side pressure	1000	767	
4	SG bypass heater reduction initiated according to the secondary side depressurization	1250	NA	
5	Secondary side depressurization of all 4 SGs at CET = 368 °C	1360/ CET = 368 °C	1405/ CET = 368 °C	Imposed set point
6	Start of ACC injection into	1500/P_{ps} =	1533/P_{ps} =	Imposed

	cold legs 1 to 4	26.6 bar	26.6 bar	set point
7	Stop of ACC injection	1860/ P_{ps} = 10 bar	1949// P_{ps} = 10 bar	
8	LPIS start	2060/ P_{ps} = 7.7 bar	2170// P_{ps} = 7.7 bar	
9	PRZ heater switched off	3380	680	
10	End of the test	5685	5685	

Table 12 – PKL Test G7.1 posttest: steady state results

#	QUANTITY	ID	UNIT	EXP. VALUE	CALC	ACCEPT. ER. (°)
1	**PRIMARY CIRCUIT POWER BALANCE**					
1-1	Core thermal power	PELGESAMTIZ+MZ +AZ	kWth	565	565	0
1-2	PRZ heaters thermal power	PELDHBYPASSH	kWth	2.9	2.9	0
2	**SECONDARY CIRCUIT POWER BALANCE**					
2-1	SG-1 power exchanged	--	kWth		85.0	
2-2	SG-2 power exchanged	--	kWth		82.5	
2-3	SG-3 power exchanged	--	kWth		88.4	
2-4	SG-4 power exchanged	--	kWth		88.8	
3	**ABSOLUTE PRESSURE**					
3-1	PRZ pressure (top of the PRZ)	PDHMB50	bar	44.6	44.9	0.6
3-2	Upper plenum pressure	PRDBOP	bar	44.9	45.2	0.6
3-3	SG-1 exit pressure (top of the SG)	PDE1SEKMB60	bar	43.7	43.5	0.4
3-4	SG-2 exit pressure (top of the SG)	PDE2SEK	bar	43.8	43.6	0.5
3-5	SG-3 exit pressure (top of the SG)	PDE3SEK	bar	43.7	43.5	0.3
3-6	SG-4 exit pressure (top of the SG)	PDE4SEK	bar	43.8	43.6	0.5
4	**COOLANT TEMPERATURE**					
4-1	Core inlet temperature (lower plenum top)	TFLPOBEN	°C	255	241	
4-2	Core outlet temperature (upper plenum)	TFOPME11- (1-4)	°C	257	258	
4-3	Upper head temperature	TFDKME (17.2-19)	°C	257	258	
5	**MASS INVENTORY IN PRIMARY CIRCUIT**					
5-1	Prim. mass inventory (without PRZ and ACCs)	--	kg	--	927	
6	**MASS FLOW RATES REACTOR COOLANT SYSTEMS**					
6-1	CL 1 mass flow rate	FDE1AUS-WR	kg/s	0.0322	0.023	
6-2	CL 2 mass flow rate	FDE2AUS-WR	kg/s	0.0272	0.0274	
6-3	CL 3 mass flow rate	FDE3AUS-WR	kg/s	0.0301	0.0299	
6-4	CL 4 mass flow rate	FDE4AUS-WR	kg/s	0.0318	0.0281	
7	**BYPASS MASS FLOW RATES**					

7-1	Core bypass flow rate	--	kg/s	--	--	
7.2	UH-DC bypass flow rate	--	kg/s	--	--	
8	**PRESSURIZER LEVEL**					
8-1	Pressurizer level (collapsed)	HJEF10CL001	m	0.73	0.879	0.15 m
9	**SECONDARY SIDE LEVEL**					
9-1	SG-1 level (collapsed)	HDE1SEKSTGRM-GES	m	7.58	7.73	0.14 m
9-2	SG-2,3,4 level (collapsed)	HDE(2-4)SEKSTGRM-GES	m	7.72/7.75/7.73	7.71/7.65/7.65	0.011/0.09/0.07 m

Table 13 – PKL Test G7.1 posttest: summary of results obtained by application of FFTBM (reference calculation): (0 ─ 3300 s)

#	PARAMETER	TRACE5	
	Description	**(0 ─ 3300 s)**	
		AA	**WF**
1	*UP pressure [bar]*	0.0608	0.0443
2	*Core inlet fluid temperature [°C]*	0.6197	0.0284
3	*Core exit fluid temperature [°C]*	0.4656	0.0653
4	*Upper head fluid temperature*	0.0985	0.0375
5	*Heater rod temp. (middle level) [°C]*	0.1883	0.0462
6	*Heater rod temp. (high level) [°C]*	0.5453	0.0588
7	*Integral break flow rate [kg]*	0.1597	0.0472
8	*Break flow rate [kg/s]*	1.1257	0.1391
9	*Core level [m]*	0.5346	0.0801
10	*SG-1 Riser level [m]*	0.4258	0.0555
11	*SG-4 Riser level [m]*	0.4307	0.0506
12	*Loop seal 1 descending side level [m]*	0.8869	0.1013
13	*Loop seal 1 ascending side level [m]*	0.7799	0.1823
14	*Hot leg 1 horizontal part level [m]*	1.1250	0.1091
15	*DP inlet-outlet RPV [bar]*	1.2080	0.1212
16	*DP inlet-outlet SG 2 [bar]*	1.4814	0.0726
17	*Core power [kW]*	0.0652	0.0746
18	*SG-1 pressure - secondary side [bar]*	0.0673	0.0268
TOTAL AVERAGE ACCURACY ***Total (18 parameters)***		**0.46**	**0.061**

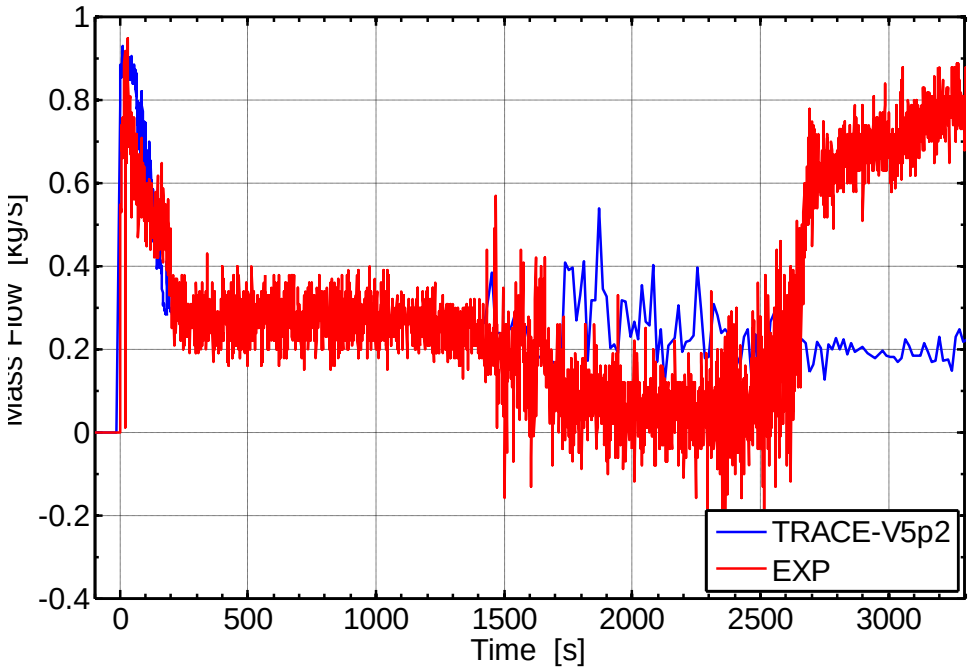

Figure 43 – PKL Test G7.1, posttest results: hot leg 1 break mass flow rate

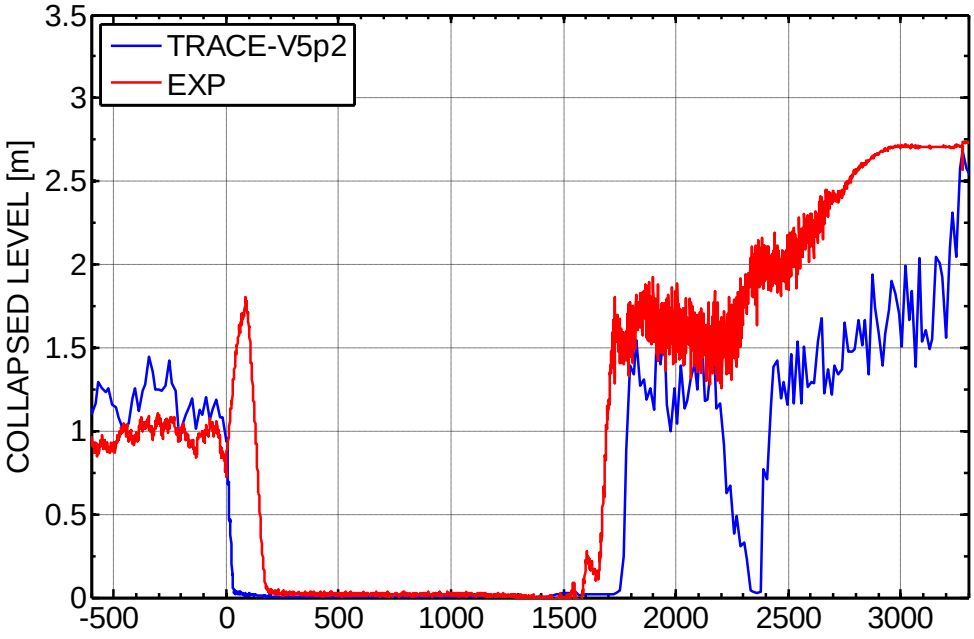

Figure 44 – PKL Test G7.1, posttest results: hot leg 1 collapsed level (vertical) (-600 – 3300 s)

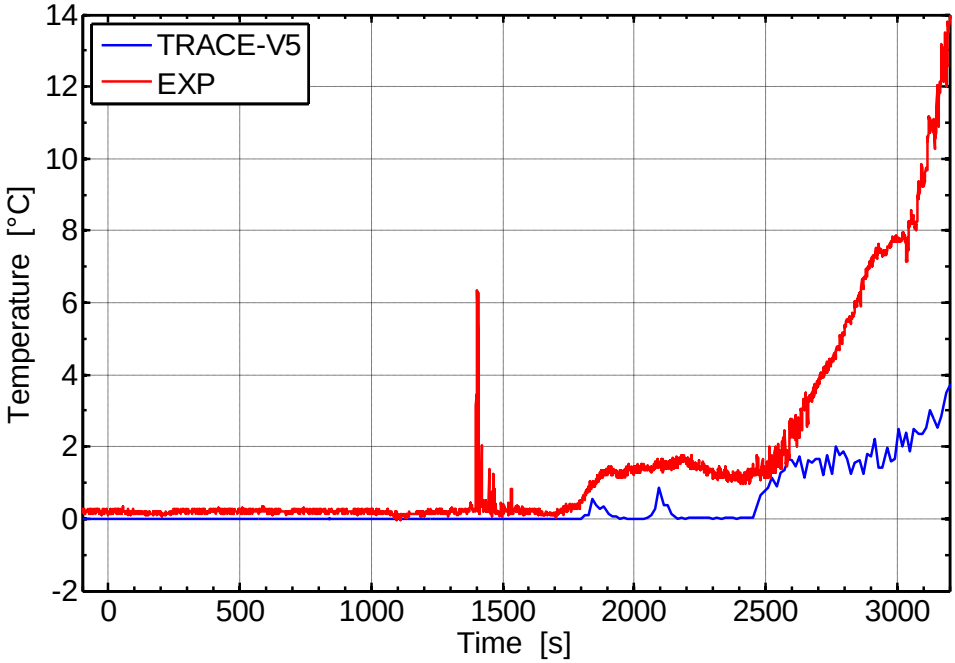

Figure 45 – PKL Test G7.1, posttest results: differential temperature SG 1 inlet/outlet

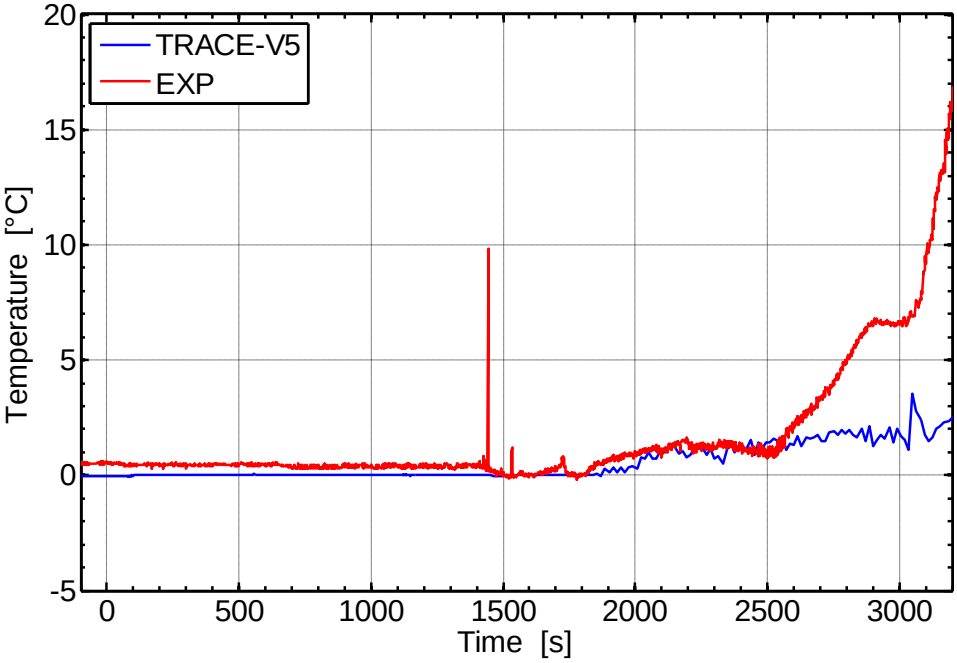

Figure 46 – PKL Test G7.1 , posttest results: differential temperature SG 4 inlet/outlet

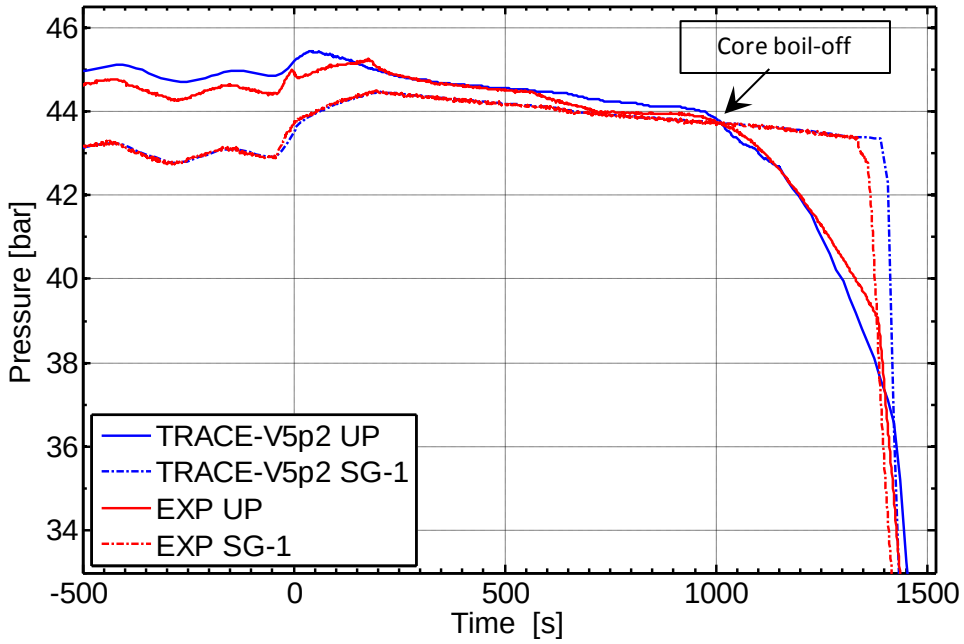

Figure 47 – PKL Test G7.1, posttest results: UP and SG-1 pressure trends (-500 – 1550 s)

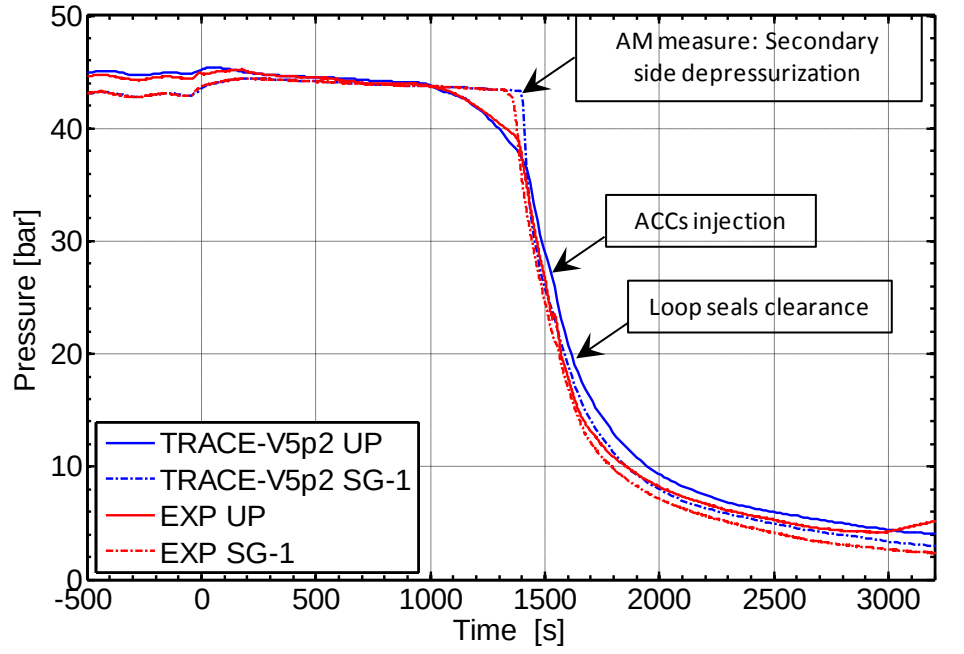

Figure 48 – PKL Test G7.1, posttest results: UP and SG-1 pressure trends (-500 – 3300 s)

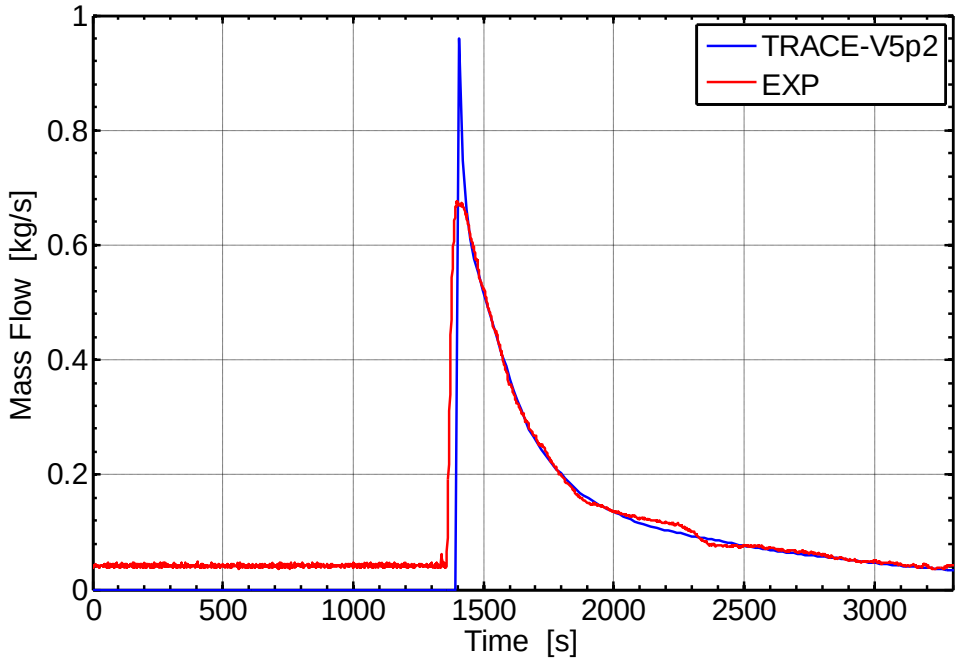

Figure 49 – PKL Test G7.1, posttest results: MSL 1 nozzle mass flow rate trends (secondary side depressurization)

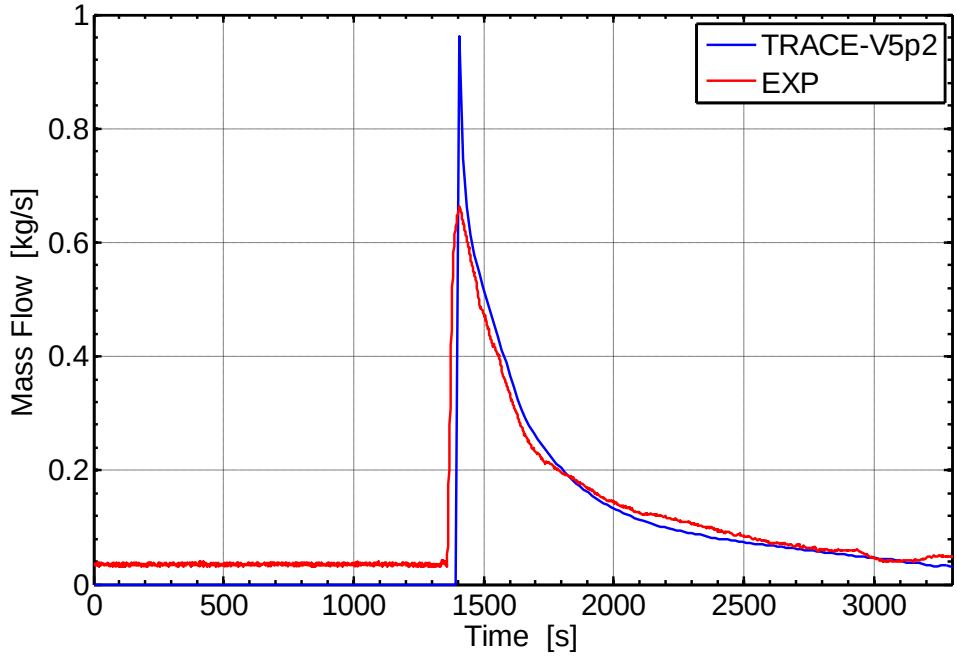

Figure 50 – PKL Test G7.1, posttest results: MSL 3 nozzle mass flow rate trends (secondary side depressurization)

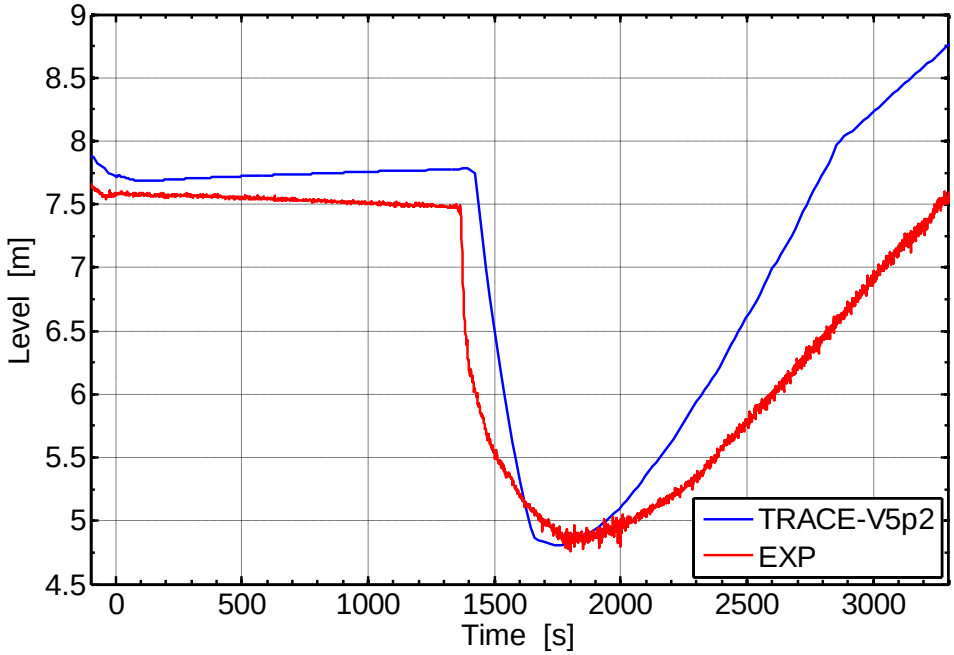

Figure 51 – PKL Test G7.1, posttest results: SG-1 riser collapsed level (-100 – 3300 s)

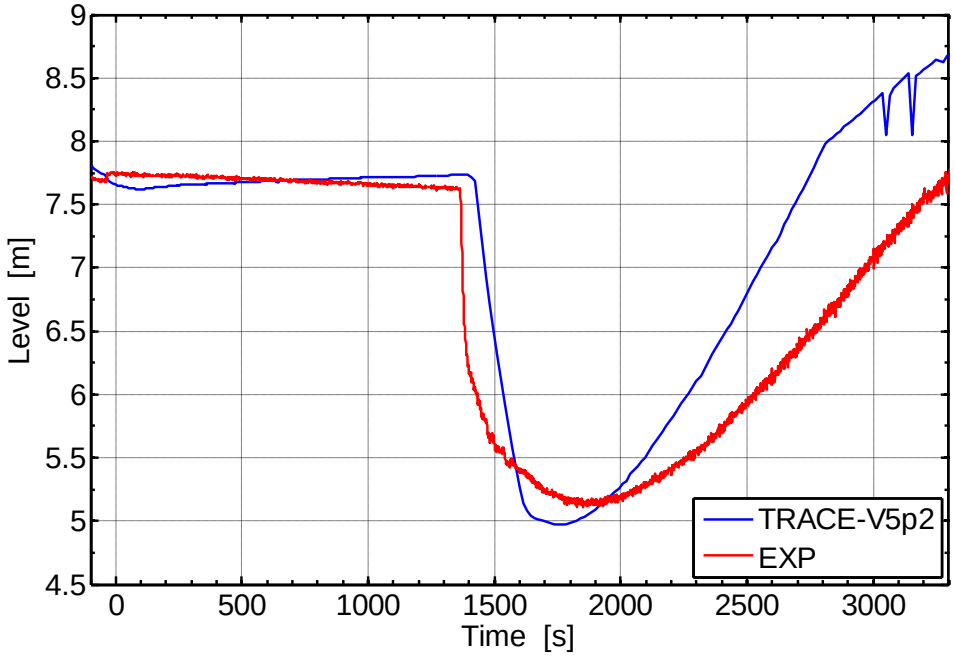

Figure 52 – PKL Test G7.1, posttest results: SG-1 riser collapsed level (-100 – 3300 s)

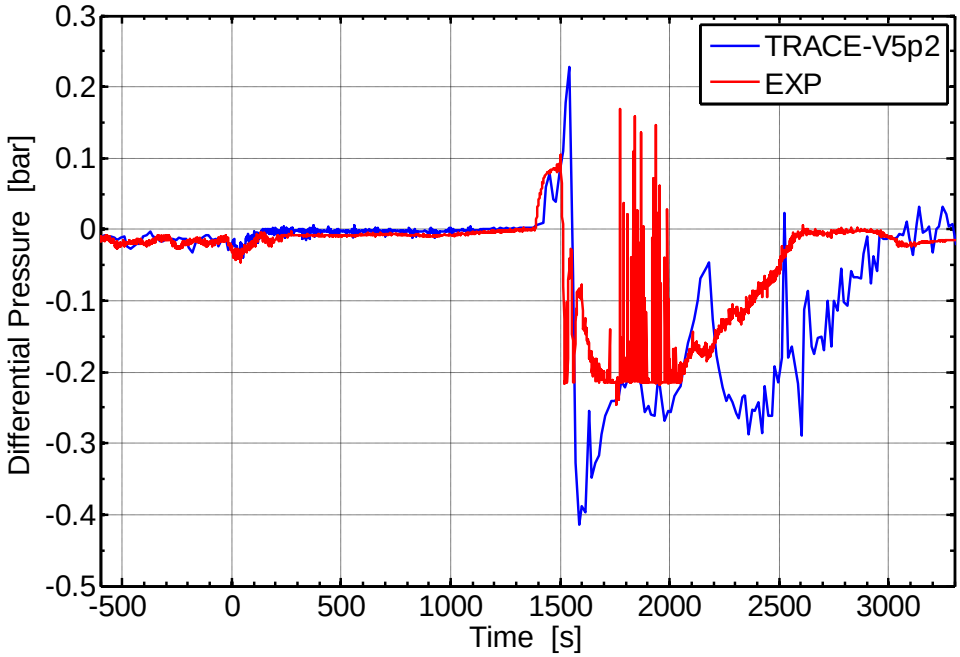

Figure 53 – PKL Test G7.1, posttest results: DP DC vessel inlet /RPV outlet (*-600 – 3300 s)*

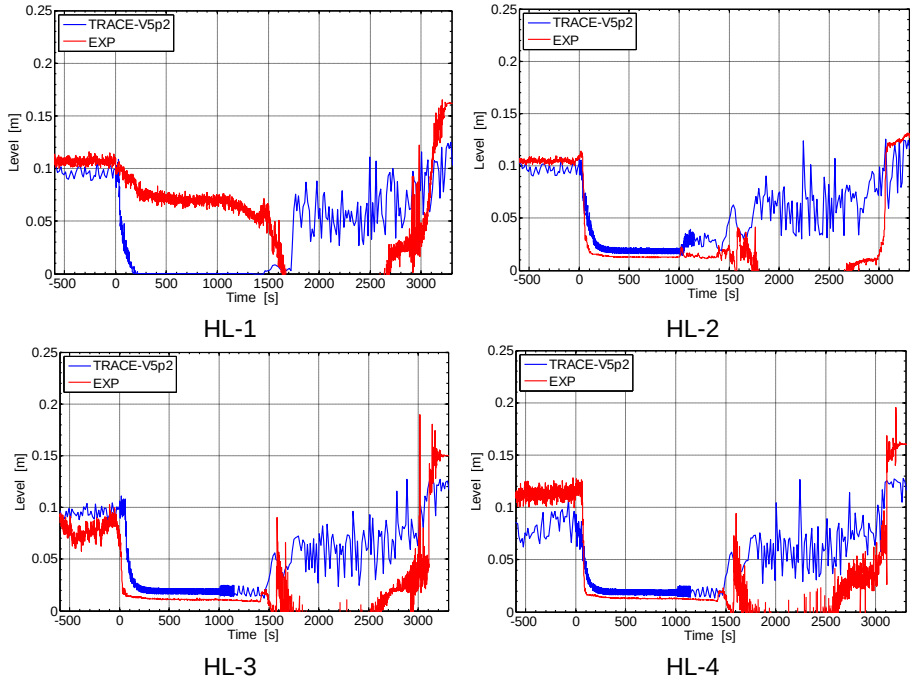

Figure 54 – PKL Test G7.1, posttest results: hot legs collapsed level (horizontal) (-600 – 3300 s)

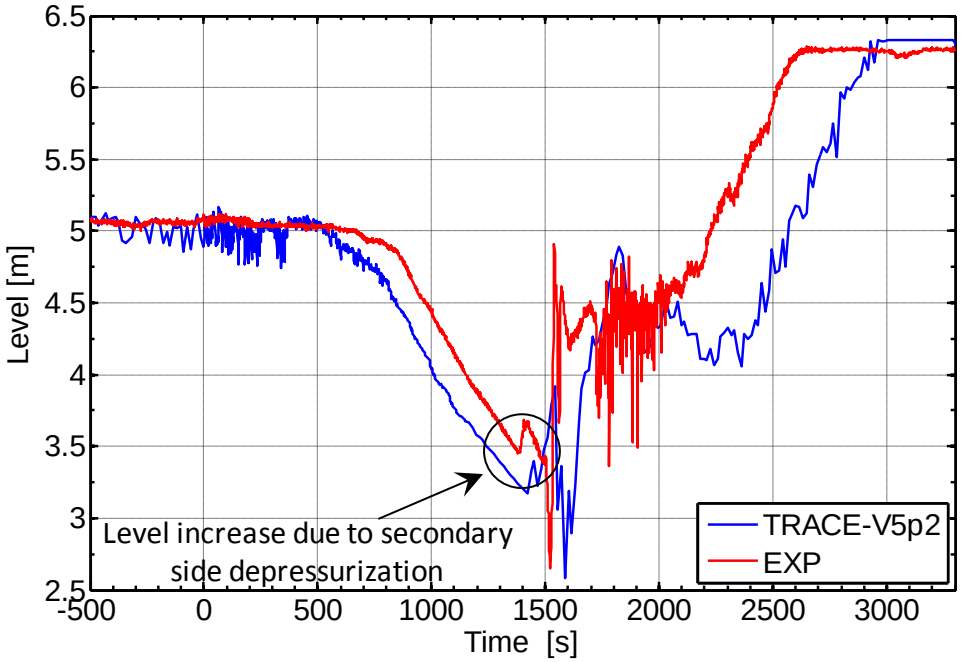

Figure 55 – PKL Test G7.1, posttest results: core collapsed level (-600 – 3300 s)

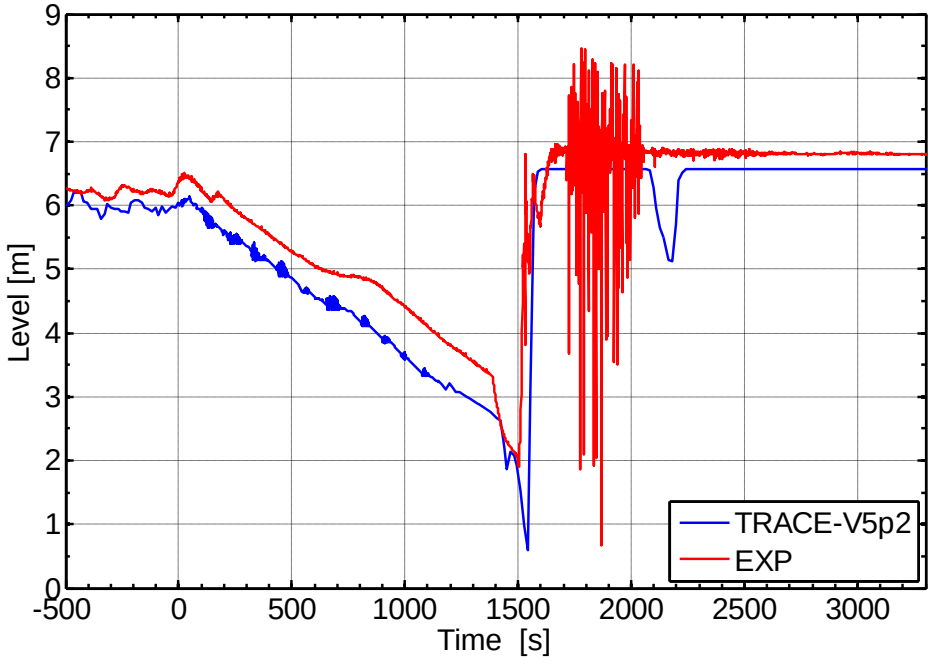

Figure 56 – PKL Test G7.1, posttest results: DC pipe collapsed level (-600 – 3300 s)

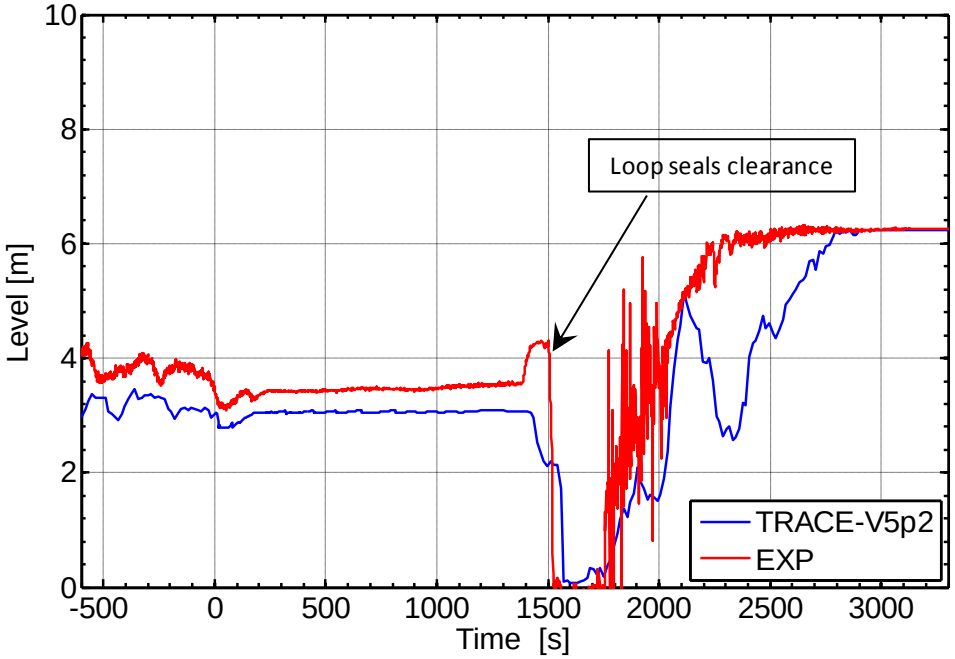

Figure 57 – PKL Test G7.1, posttest results: loop seal 1 SG side collapsed level

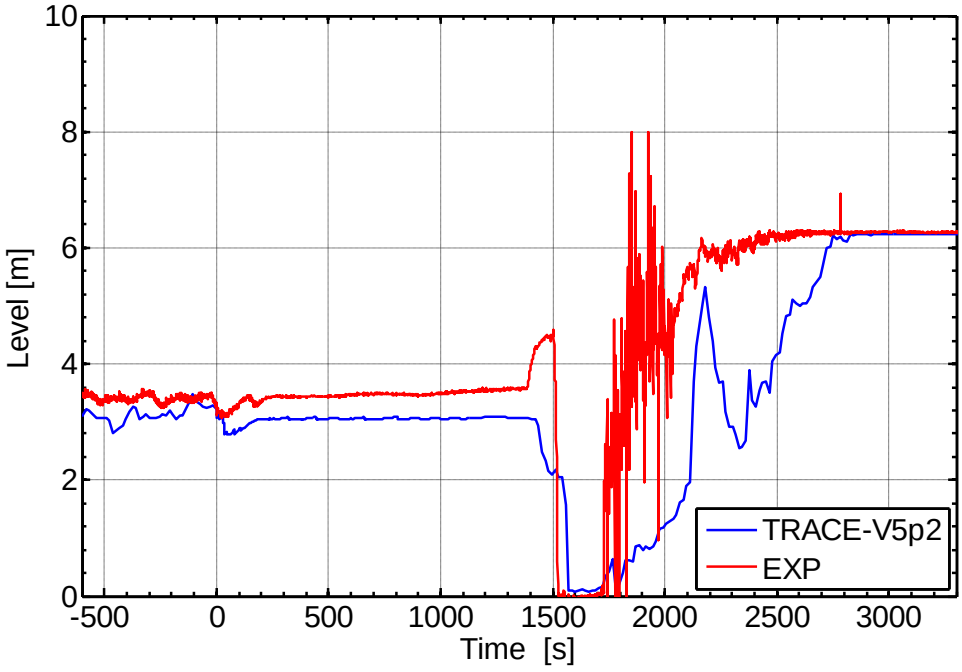

Figure 58 – PKL Test G7.1, posttest results: loop seal 4 SG side collapsed level

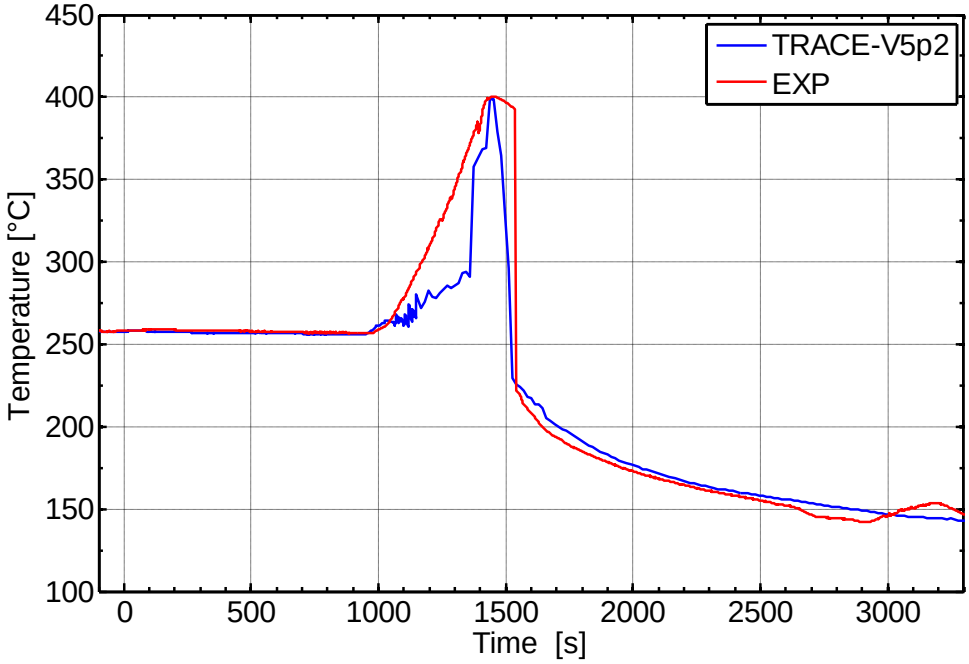

Figure 59 – PKL Test G7.1, posttest results: CET trends

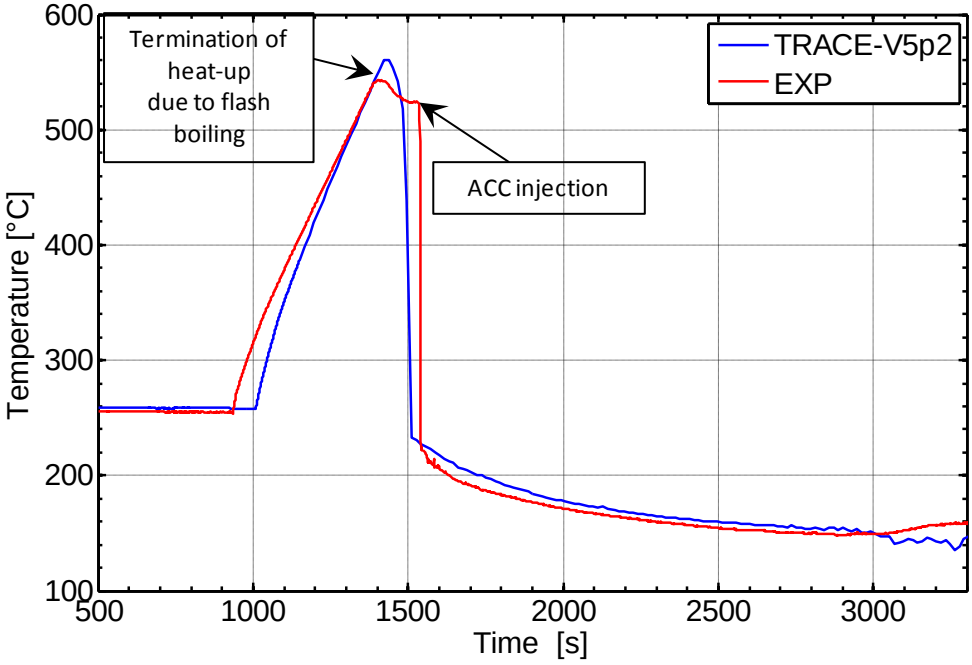

Figure 60 – PKL Test G7.1, posttest results: PCT trends (500 – 3300 s)

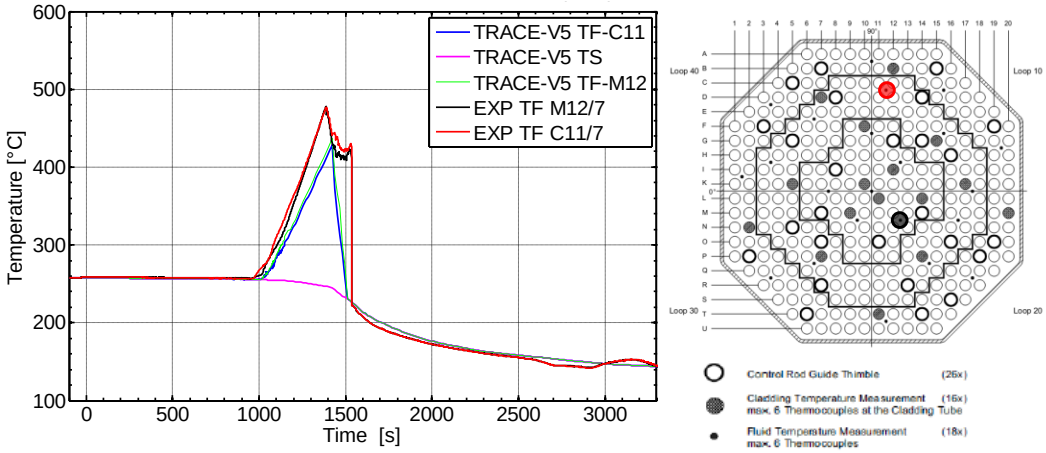

Figure 61 – PKL Test G7.1, posttest results: Core fluid temperature trends in subchannels at core level ME7

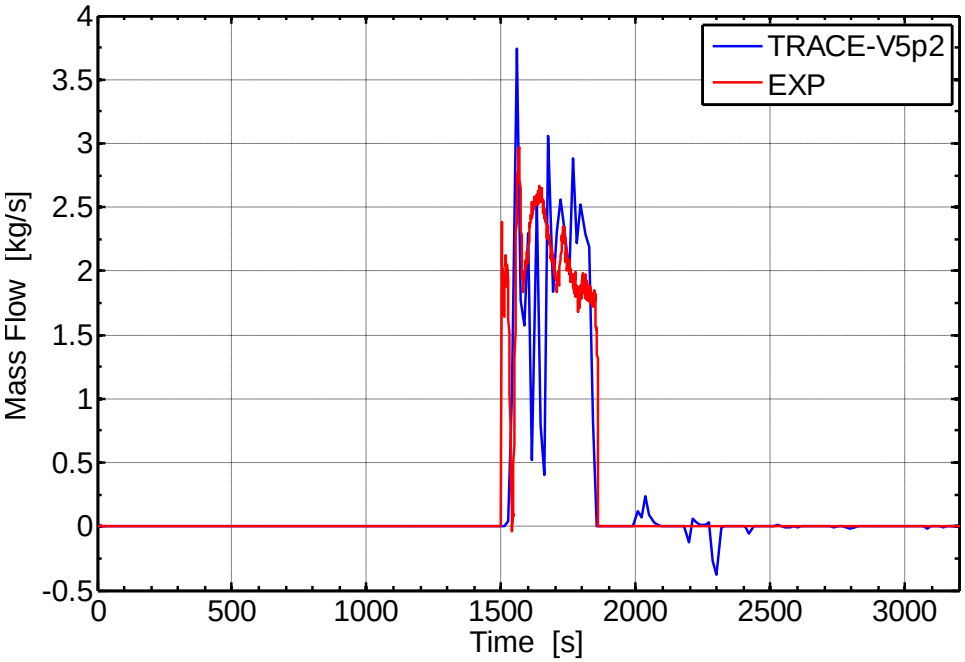

Figure 62 – PKL Test G7.1, posttest results: total mass flow rate injected by ACCs in CL-1 – CL-4

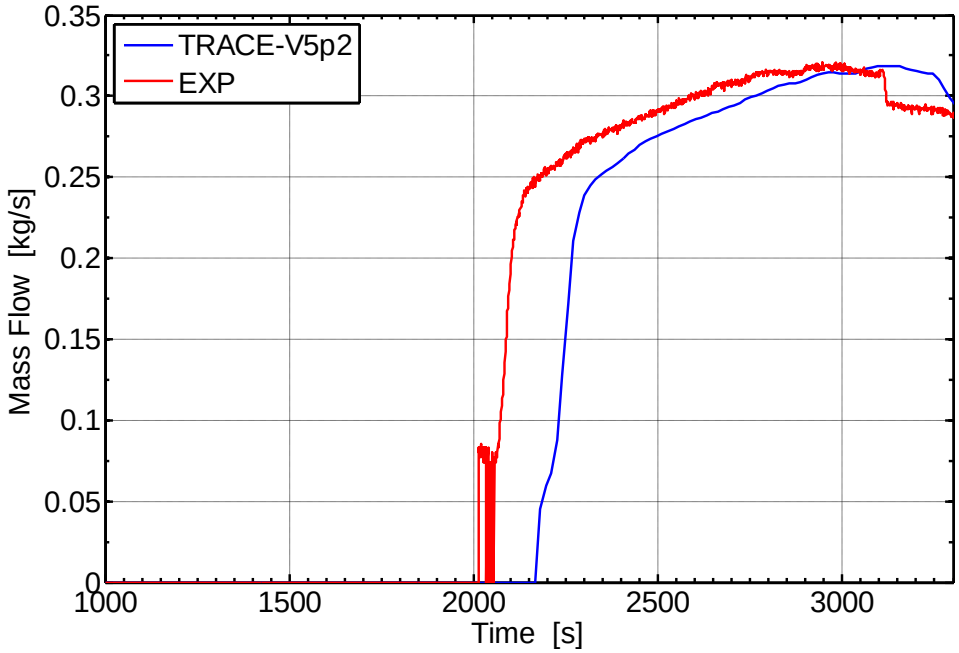

Figure 63 – PKL Test G7.1, posttest results: total mass flow rate injected by LPISs in CL-1 - CL-4

4.3. Gravity dominant test: water faucet problem

The basic test problem chosen to investigate the property of the numerical scheme (stability, convergence and the effects of the artificial viscosity on the numerical solution) implemented in TRACE-V5 code, namely the SETS method (see [53] e [54]), is the water faucet problem proposed by Ransom as a test for numerical methods for the two-fluid model (see [55]). In this problem the gravity plays the role of dominant force that drives the dynamics of the fluid flow generating a sharp discontinuity in the volume fraction profile (contact discontinuity) that propagate through the fluid domain. The algorithm must therefore be able to resolve a discontinuity whilst maintaining stability in the other fluid fields. Taking in account that the of two fluid model equations of two phase thermal hydraulics, solved by TRACE-V5, are ill-posed, i.e. the system of balance equations is not-hyperbolic, the solution of the water faucet problem could be instable, manifesting waves characterized by increasing amplitude over the time, and not converge. The cause of this is connected with the lack of *physical regularization* terms, like interfacial pressure and virtual mass force able to rendering all eigenvalues real and making the two-fluid model hyperbolic. An approach is to leverage on the properties of discrete models to remedy the difficulties imposed by the ill-posed mathematical formulation. This is the chief idea on which is based the *numerical regularization* [56]. The important element of the numerical regularization is represented by the presence of numerical diffusion. His feature is extensively utilized in all TH-SYS

codes, as well in TRACE code, to achieve a robust numerical treatment at the price of the solution accuracy. Numerical diffusion masks ill-posedness of two-fluid model, in turn limiting numerical diffusion by grid refinement causes the ill-posed nature of the solution to reveal itself, usually as a large dispersion error. Therefore, a rationale is suggested to use discretization fine enough to minimize numerical diffusion yet large enough to keep the solution stable. In this section, the value of such approach is put under scrutiny.

The objective of this problem is to test the stability and the convergence of the numerical solution method. The diffusive character of the numerical method is also tested since a discontinuity in the void fraction is propagated through the solution space.

4.3.1. Description of the water faucet problem

The water faucet problem represents a conceptual test consisting of a liquid stream entering a vertical solution space (a vertical pipe 12 m in length and 1 m in diameter) at the top and falling under the action of gravity as schematically shown in Figure 63. Initially, the tube is filled with a uniform column of water entering in the simulation domain at a velocity of 10 m/s surrounded by stagnant vapor, such that the vapor volume fraction is 0.2. The thermodynamic properties of the system at the initial state are assumed constant at values appropriate for air–water mixture and are 50 °C for the temperature and 10^5 Pa for the pressure. The boundary conditions for vapor phase are a fixed pressure at the exit of the solution space with the top closed to the vapor flow. .The initial and boundary conditions are summarized in Table 13.

The physical phenomenon reproduced in this benchmark problem is the acceleration of the liquid column under the action of gravity, which causes a narrowing of the jet and the propagation of a void wave downwards and out of the domain (steady state). In fact the increasing of the liquid velocity because of the gravity had, leads to a contraction of the cross section area, i.e. a decreasing void profile down the pipe. Therefore, there is a decoupling of the motion of the liquid and the gas, which requires the use of a two-fluid model.

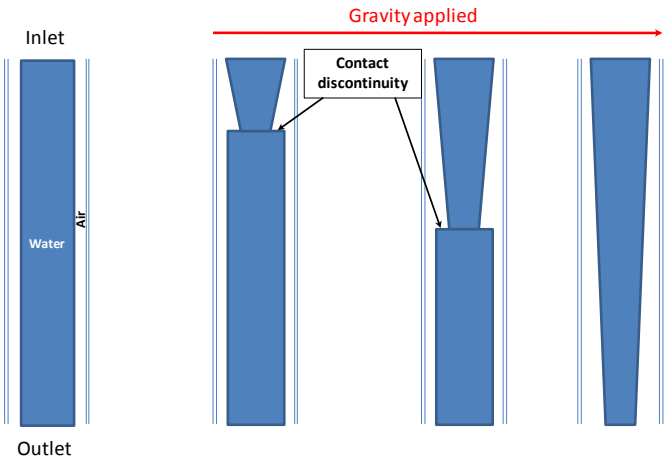

Figure 64 – Schematic of the time evolution of liquid Column

The main assumptions of the problem are:

- both wall friction and interphase friction are omitted;
- the liquid-vapor interface is assumed to be uniform and circular in cross section;
- No virtual mass effect needs to be considered;
- all interfacial dynamics associated with surface tension force are neglected;
- the model is assumed to be one-dimensional so that transverse momentum effects are negligible.
- the phasic pressures are assumed equal at each axial location.

Table 14 – BICs for the water faucet problem

BOUNDARY CONDITIONS		INITIAL CONDITIONS	
Inlet		Temperature (°C)	50
Temperature (°C)	50	Pressure (Pa)	10^5
Vapor velocity (m/s)	0	Vapor velocity (m/s)	0
Liquid velocity (m/s)	10	Liquid velocity (m/s)	10
Void fraction	0.2	Void fraction	0.2
Outlet			
Pressure (Pa)	10^5		

GEOMETRY DESCRIPTION	
Vertical tube	
Length (m)	12
Diameter (m)	1

4.3.2. Analytical solution

Under the assumptions made for this problem, the momentum balance equation for the liquid phase contains nonzero terms for the temporal and spatial acceleration and body force. The resulting equation is:

$$\frac{\partial v_l}{\partial t} + v_l \frac{\partial v_l}{\partial x} = g \tag{8}$$

The associated differential equation for the void fraction is established from continuity considerations for the liquid phase (incompressible hypothesis) and is:

$$\frac{\partial (1-\alpha)}{\partial t} - v_l \frac{\partial \alpha}{\partial x} + (1-\alpha)\frac{\partial v_l}{\partial x} = 0 \tag{9}$$

The solution for the liquid velocity and volume fraction response can be obtained in closed form since Equation (9) is a single hyperbolic partial differential equation having real characteristics. The characteristic curves are defined by:

$$dx = v_l dt \tag{10}$$

The equation (10) represent the path of a liquid particle, and along this path, equation (8) can be integrated directly to obtain the following expression for the liquid velocity:

$$v_l = v_{l0} + g\left(t - t_0\right) \tag{11}$$

V_{l0} is the initial or boundary velocity corresponding to the point x_0, at the time t_0. The corresponding length coordinate along the particle path is obtained by integration of Equation (10) and using the liquid velocity relation (11) giving the following relation:

$$x = x_0 + v_{l0}\left(t - t_0\right) + \frac{1}{2} g\left(t - t_0\right)^2 \tag{12}$$

Using the solution for the velocity, Equation (9) can be integrated to obtain the solution for the liquid fraction along the characteristic curve. In this case two possible solutions are obtained. The first applies if the initial point of the characteristic curve lies on the $t_0 = 0$ (initial value) curve and is:

$$\alpha = \alpha_0 \tag{13}$$

The second corresponds to cases where the initial point on the characteristic curve lies on the $x_0 = 0$ boundary. In this case the liquid volume fraction, using the Equation (12) to eliminate $(t-t_0)$ is given by:

$$\alpha = 1 - \frac{\left(1-\alpha_0\right) v_{l0}}{\sqrt{v_{l0}^2 + 2g\left(x - x_0\right)}} \tag{14}$$

whilst the velocity profile is given by:

$$v_l = \sqrt{v_{l0}^2 + 2g\left(x - x_0\right)} \tag{15}$$

To summarize, combining relations (11) to (15), it is obtained the following transient solution for the void fraction and liquid velocity:

$$\alpha = \begin{cases} 1 - \dfrac{\left(1-\alpha_0\right) v_{l0}}{\sqrt{v_{l0}^2 + 2g\left(x - x_0\right)}} & if \;\; x \le x_0 + v_{l0} t + \dfrac{1}{2} g t^2 \\ \alpha_0 & otherwise \end{cases} \tag{16}$$

$$v_l = \begin{cases} \sqrt{v_{l0}^2 + 2g\left(x - x_0\right)} & if \;\; x \le x_0 + v_{l0}t + \frac{1}{2}gt^2 \\ v_{l0} + gt & otherwise \end{cases} \tag{17}$$

The analytical solution is depicted in Figure 64

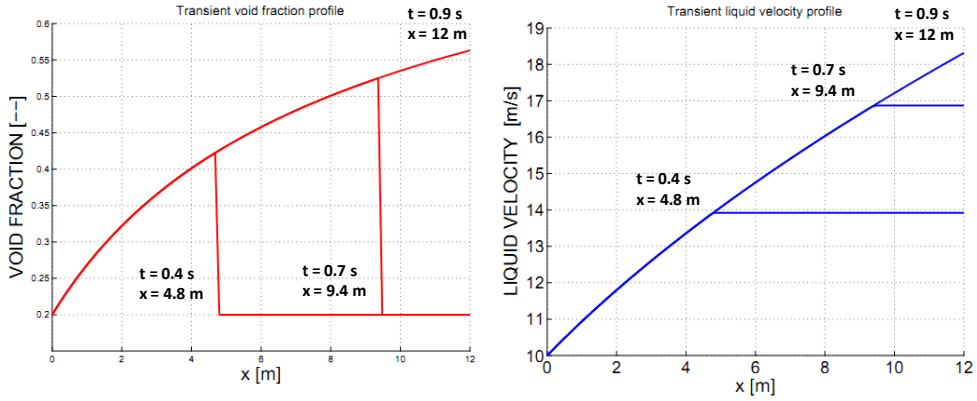

Figure 65 – analytical solution: void fraction and liquid velocity trends

4.3.3. Numerical solution

The input model (see [57]) is shown in Figure 66 ,it is composed by a pipe component that simulates the computational domain whilst the boundary conditions are introduced into TRACE-V5 nodalization through FILL and BREAK components that reproduced respectively the inlet and outlet flow condition of the test problem. The following two modifications to TRACE-V5 are made to run the faucet problem:

- interface drag was reduced to a small value (10^{-10});
- the interphase heat transfer coefficient was reduced to a small value (10^{-10}).

The TRACE-V5 numerical scheme tested for simulating the water faucet problem is the SETS method. This numerical method is based on a staggered grid/donor cell approach with a partial implicit time integration to eliminate the material Courant stability limit condition, namely a semi-implicit step (*basic step*) is used only as an intermediate result, followed by a *stabilizer step* to provide conservation of mass and energy for the two separated phases.

For the nodalization study, a coarse discretization of the computational domain is adopted first, that is 24 cells with a node size equal to 0.5 having a time step of 0.01 s. Data were collected on the void fraction and the velocity across the pipe at 0.4, 0.7 and 0.9 s (time at which the discontinuity wave has left the solution space). For this case numerical solutions are excessively diffusive (smoothing of the gradient of the solution) as they are obtained on very coarse grids (see Figure 66). The accuracy of prediction increases with in case of consecutive grid refinement going from 100 to 384 meshes ($\Delta x = 0.12,\ \Delta x = 0.03125$) (see Figure 67, Figure 68 and Figure 70). In fact calculated data show a continuous convergence towards

the analytical solution, trying to capture the discontinuity, but for the case of highest number of mesh cells the non monotonic character of the numerical scheme is reveled manifesting by means of unbounded growth waves (high wave numbers) and dispersion error become relevant. This last aspect is clearly visible in Figure 68 in which is plotted the numerical solution obtained with 500 mesh cells and time step equal to 0.01 s.

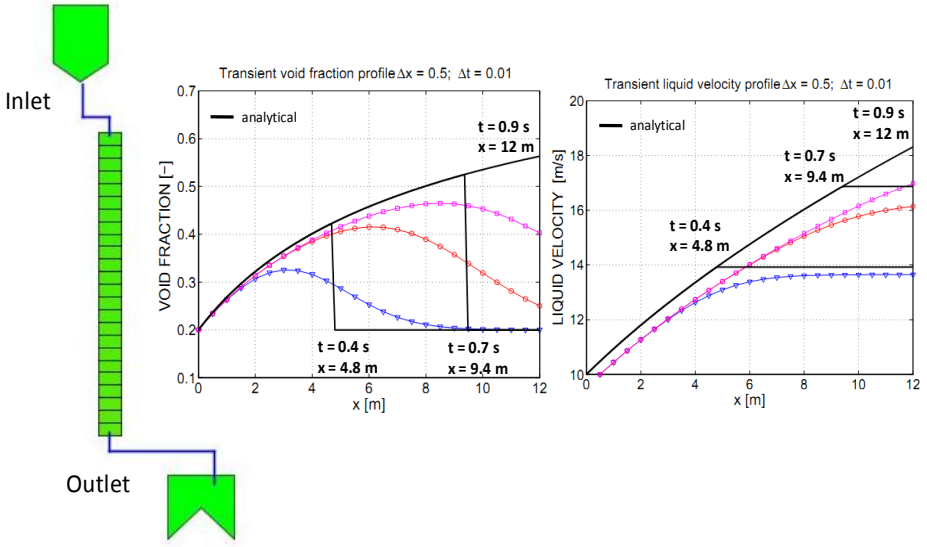

Figure 66 – numerical simulation of the discontinuity wave propagation and velocity profile at three different time points

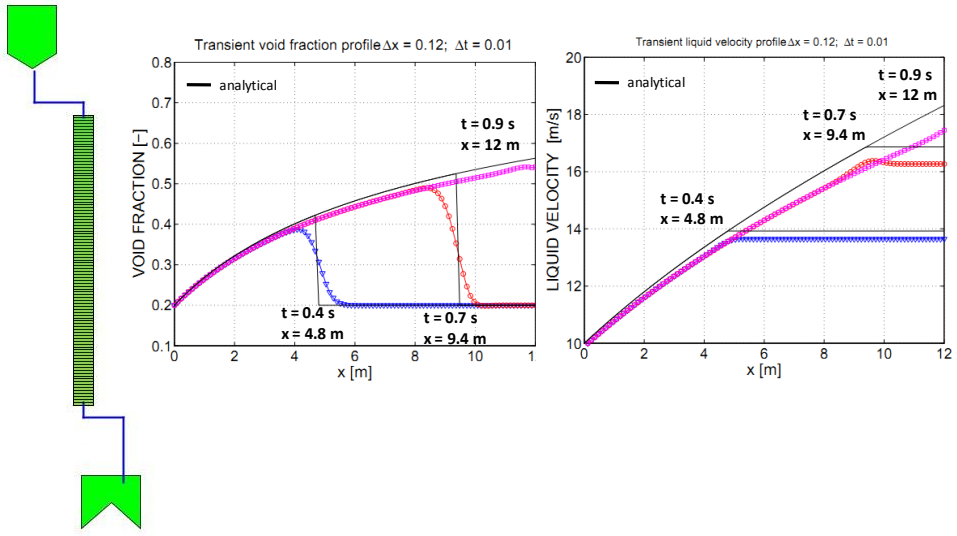

Figure 67 – numerical simulation of the discontinuity wave propagation and velocity profile in the case of grid refinement (100 cells)

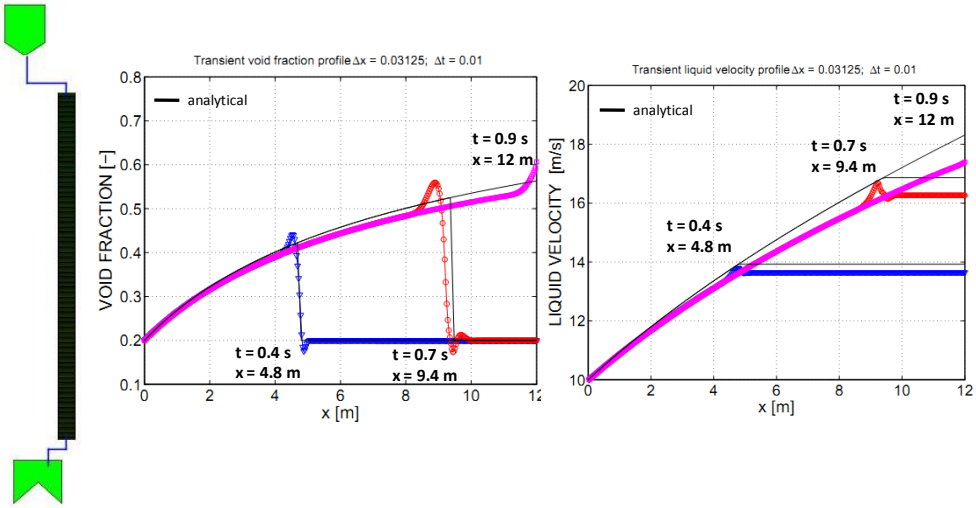

Figure 68 – numerical simulation of the discontinuity wave propagation and velocity profile in the case of grid refinement (384 cells)

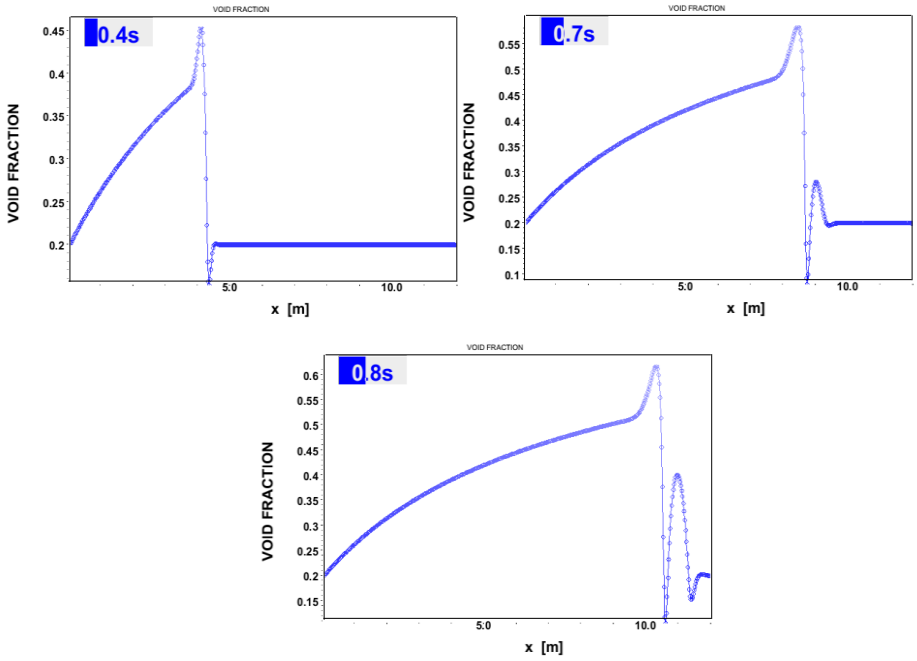

Figure 69 – effects of the grid refinement (500 cells) on the numerical error (dispersion error, high wave number oscillations)

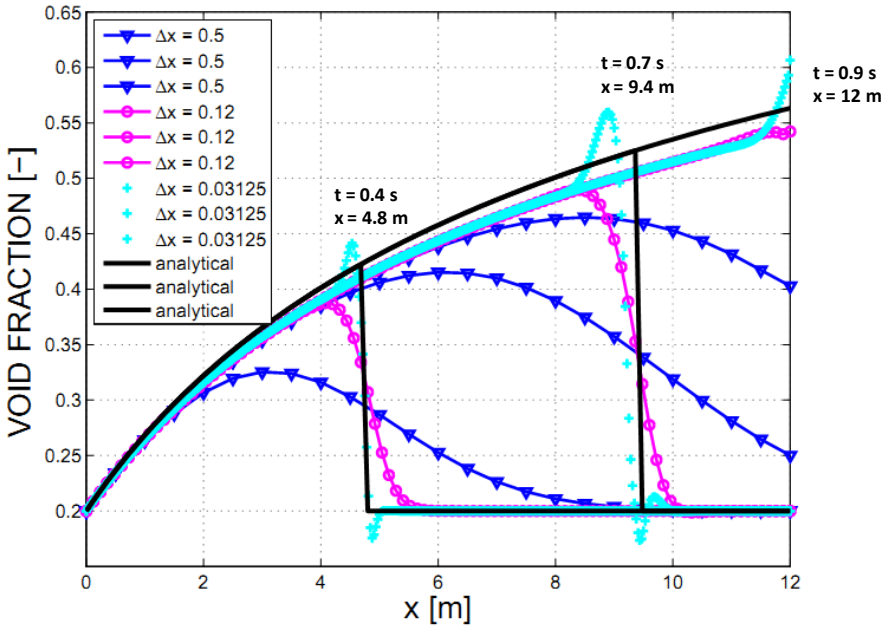

Figure 70 – void fraction distribution at different time: comparison of analytical solution with TRACE-V5 results

4.4. Outcomes of the independent assessment process

The present chapter presented and discussed the results obtained by the independent assessment process performed by means of the simulations of two integral effect tests in order to evaluate the capabilities of the code and nodalization scheme (of the PKL facility) in reproducing the relevant thermal-hydraulic phenomena which occur during the different stages of the two transients. The outcomes get by this analysis were important for the qualification of the nodalization used for the application of the integrated approach to safety analysis of PWR systems (see chapter 5 for the description of the methodology)

In particular the main flow regimes of the NC test F4.1 RUN1 are predicted with good accuracy by the code; namely

- single-phase natural circulation;
- (stable) two phase natural circulation;
- siphon condensation or (unstable two phase natural circulation);
- the reflux condensation mode, including,
    - RC with intermittent boron transport,
    - Mere RC with interruption of transport phenomena.
- The results of the FFTBM demonstrate good average accuracy

Specific outcomes from the post test analyses of the F4.1 RUN1 test are highlighted below:

- The interruption and the restart of the NC are correctly predicted.
- The variation range of the primary system mass inventory for the occurrence of single phase natural circulation, the two phase natural circulation and the reflux condensation has been properly predicted.
- The mass flow rate observed during unstable two phase natural circulation shows high amplitude oscillations. The reasons for this behavior could be connected whit the mathematical aspect of the TRACE model's equations that are non-hyperbolic and therefore suffer from high wave-number instabilities.
- The evolution of the boron concentration in loop seals is correctly predicted (both qualitatively and quantitatively) during the drainage phase and qualitatively during the refilling phase.

Regarding the post test calculations of test G7.1, they presented a good agreement with the experiments in terms of system behavior (i.e. thermal hydraulic phenomena and processes which characterize the test) and the CET temperature could be adequately modelled as long as saturated or superheated steam prevailed in the upper plenum region. Most difficulties, encountered to correctly simulate the system behavior evolution during the condition phase, were related to the modelling of the break flow related phenomena (choked flow, single and two phase) which strongly influence the thermal hydraulic behavior of the primary system during this phase (non experimental data for the break mass flow rate are supplied during the CPh) , whilst in the test phase liquid entrainment and vapor pull-through through the break become significant. The saturated two phase critical flow is well predicted by the code at the beginning of the test phase. Another important aspect was the importance of correctly modelling the time delay at which superheating appeared in the CET location after core uncovery started. This might be relevant if Emergency Operating Procedure (EOP) actions are to be based on the appearance of superheating at the top of the core. When core uncovery starts, steam is superheated in the core and flows towards the CET location. In the way to the measurement, the steam is cooled down by the heat structures and might become saturated again. In addition, it takes some time for the superheated steam to reach the CET measurement. Therefore a delay between the initial start of the core uncovery and the first appearance of superheating in the CET location is expected. In the calculation this delay was not reproduced by the code/nodalization. The correct simulation of the Reactor Pressure Vessel (RPV) bypasses was essential to correctly model the downcomer and core levels evolution. The local pressures at the top of the DC and in the UP define the difference between the DC and core levels. This pressure difference depends on different aspects of the model; however, one very influential parameter is the pressure loss in the bypass lines connected to these regions.

The other important test included in the independent assessment matrix, is a basic numerical test, which has been chosen to assess the performance of the SETS numerical scheme, implemented in TRACE-V5 code, regarding the numerical diffusion. The aim is to show how much false diffusion the numerical method introduces when simulating a particular flow pattern, such as that characterizing the water faucet problem. The effect of the numerical diffusion is highlighted showing the distortion of the discontinuity wave as it is transported across the

simulation domain. The comparison of the degree of distortion, thus, provides qualitative information about the performance of the method.

The main reason in using this test problem is connected whit the fact that for complex methods, such as the SETS method, the task of obtaining a simple formula becomes much more difficult compared to the case of relatively simple numerical schemes, e.g. explicit and implicit upwind, for which a mathematical expression for calculating the diffusion coefficient is available. In addition, for the complex flow patterns and component nodalization schemes and configurations usually employed in simulations with TH-SYS codes, a formula to obtain the overall numerical diffusion may not be available.

5 DEVELOPMENT OF AN INTEGRATED APPROACH FOR ACCIDENT ANALYSIS AND CODE QUALIFICATION (TRACE CODE)

The purpose of this chapter is to describe the main steps involved in the development of an integrated analytical methodology based on the use of reliable experimental database that covers all relevant thermal hydraulic phenomena occurring during a selected accident scenario in a PWR system aimed at TH-SYS code assessment. The methodology takes cue from the UMAE approach. The philosophy behind this methodology is the assessment of the uncertainty through the extrapolation of accuracy that can be quantified by comparing the code predictions against a series of experimental test results carried out in ITF (which gives the method its *integral character*), as well as in SETF (see [58], [59] and [60]). The data coming from both integral and the separate effects experiments are used following a parallel procedure, that is: determine the accuracy of a broad spectrum of parameters which characterize the transient scenario in a integral way (at the system level) and after comparing the accuracy computed using the same number of parameters but taking in account only a single phenomenon simulated through separate effect tests (component level analysis). The two typologies of experiments are not performed in combination, but independently reproducing the same phenomenon at system level and at the component level. Such an approach restricts the evaluation of the accuracy to a single physical aspect. Therefore, this cannot give a measure of the suitability and ability of the code physical models and numerical solution procedure to capture all the relevant phenomena expected to occur during the transient under investigation. The IA aims to circumvent this weakness in the UMAE methodology trying to quantifying the code accuracy through the use of experiments performed in a complementary way. These kinds of tests combine the features of both system and component test rigs without losing links and mutual influences between the various phenomena occurring during the accident scenario.

5.1. Outline of the methodology

The starting point of the methodology is to select a qualified TH-SYS code that is utilized to predict the scenario of interest. The code selected for the present analysis is the TRACE-V5 code that was subjected to an independent assessment as discussed in the previous chapter. The next phase concerns the definition of a specific behavior scenario important for PWR system safety. Once the specific scenario has been identified, the methodology is oriented to define the relevant phenomena and processes that drive the system response.

After the definition of all phenomena and interactions during the selected scenario, a corresponding process for establishing a test matrix is developed. The construction of the test matrix is carried out identifying a set of tests performed in integral and separate effects tests facilities achieved in a complementary way, in

the sense that the results of the integral effect test provide the initial and boundary conditions for separate effects tests.

ITF are designed to simulate the overall behavior of the prototype, whilst separate effect experiments performed in SETF have the purpose to study “separable” physical processes similar to those expected in nuclear power plants typical conditions or to characterize the behavior of a single component: examples for separate effect test activity are those correlated to the fuel bundle heat transfer characterization, the downcomer countercurrent flow behavior, the evaluation of pumps performance.

The need to interface experiments executed at different scale in test rigs having different targets (arise from the complex two phase flow behavior within a PWR system. In fact in a prototype system (PWR), as it undergoes to an accident event, the thermal hydraulic of two phase flow patterns are observed to occur at three phenomenological levels: local level processes (e.g. interfacial processes, namely heat mass and momentum interactions between the two phases), component level processes (e.g. liquid levels within a component, mixing in the RPV) and system level processes (e.g. oscillation, loop to loop asymmetries, natural circulation). An integral test carried out in an integral test facility which is designed to follow the time preserving scaling philosophy combined with a direct proportional scaling of energy sources and sinks (power/volume = constant) provide data on thermal hydraulics regimes of the two phase flow which are predominantly *one-dimensional*. Therefore, to investigate such phenomena which occur at the component level having a multi-dimensional nature, tests carried out in a separate effect simulator are needed. These tests can be realized in an independent way, investigating the relevant thermal-hydraulic phenomena/processes assumed to occur in NPP in transient conditions without taking in account the physical interaction between the different phenomenological levels, or in a complementary way, interfacing parameters between ITF, as results and SETF as initial and boundary conditions. This approach is well defined breaking down the relevant phenomenological aspects, during a transient, in different physical parts and indentifying the key parameters from which depend on. In this way is possible to highlight how the different levels (system and components) are coupled physically. For exemple selecting as postulated transient scenario a main steam line break event, a relevant aspect concerns RPV integrity under consideration of pressurized thermal shock (PTS) due to the discharge of cold water in the RPV downcomer. This is important above all when the cooling of the primary coolant is intensified by injection of emergency cooling water into the cold leg at high primary-side pressure. The important thermal hydraulic parameters of interest for the PTS phenomenon are the RCS pressure and heat flux from the vessel wall to downcomer fluid. The heat flux is defined by elementary parameters, that is: flow velocity, flow and wall temperature gradient. In turn the downcomer fluid velocity is upstream dependent on the thickness of the stratified zone in the cold leg, of the ECCS mass flow rate and of the emergency cooling water temperature. These parameters are initial and boundary conditions supplied from the ITF to the SETF, as it is shown in the Figure 71

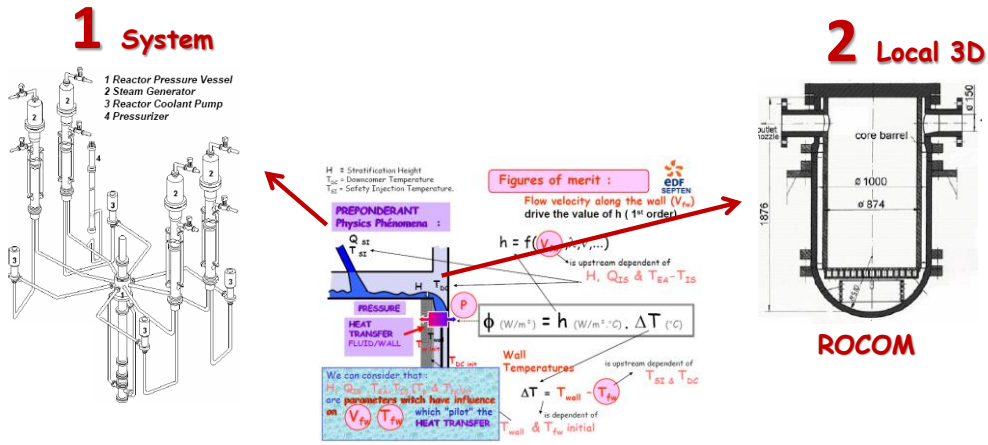

Figure 71 – Phenomenology of the PTS: breaking down the phenomena identification and separation in different phenomenological levels (system and component/local)

The integration between the two kinds of tests must be obtained in consistent way; namely the transfer of the results from the ITF to the SETF in the form of initial and boundary conditions of measured parameters, is obtained throughout scaling considerations between the ITF and the prototype and the prototype and SETF, and thermal hydraulic similarity consideration during the data transfer.

The prediction of the phenomenology of the postulated incident is achieved through the use of a validated nodalization (computational model of the facilities) capable of simulating all key phenomena with acceptable agreement to experimentally generated data by the complementary tests performed in the scaled facilities (separate effects and integral facilities). The acceptability of the code results requires the solution of two main issues:

- the first one deals with the definition of the accuracy in the prediction of the scenario of the tests carried out in scaled facilities;
- the second is related to the definition of the uncertainty of the behavior of the full scale NPP.

The last issue is not part of the methodology. The integrated approach focuses primarily on the quantification of the discrepancies between experimental data and calculated results, interfacing tests on different scales and phenomenological levels.

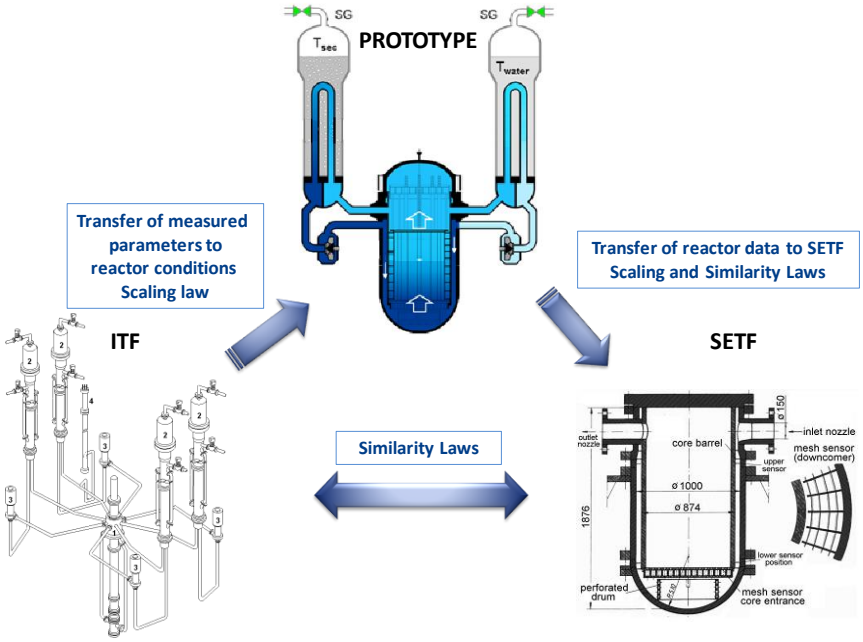

Figure 72 – Scaling strategy to perform complementary test

5.2. Selection of the accident scenario: Main Steam Line Break (MSLB)

The selected accident scenario for the application of the methodology is the MSLB, for its relevance in the frame of the PWR safety and for the existence of experimental data sets available for the code assessment.

The main steam line break accident is one of the severe abnormal transients that might occur in a NPP. The study of this transient is required in the Chapter 15 of the Final Safety Analysis Report (FSAR) of a nuclear power plant. In general, the concerns of the MSLB accident are the possible return to power condition, high local power peaking which might damage fuel rods and the occurrence of pressurized thermal shock generated by cooldown of the RPV wall, as a consequence of both, the rapid depressurization of the secondary circuit and the cold water emergency (ECC) injection into the cold leg during the transient.

The MSLB is an accident event initiated by the structural failure of the main secondary circuit resulting in a fast depressurization of the secondary loop working fluid that is accelerated out of the break point by the high pressure difference between the secondary system (6.9 MPa) and the containment (0.1 MPa). The velocity of the single phase gas media, which is much higher than that during normal operation, produces an enhancement of the heat transfer from the primary loop to the secondary system. In fact looking to the heat transfer coefficient of the steam generator which can be determined from the Nusselt number relation:

$$Nu = c\,\mathrm{Re}^{a}\,\mathrm{Pr}^{b} \tag{18}$$

where

$$Nu = \frac{hD}{k} \tag{19}$$

$$\mathrm{Re} = \frac{\rho v D}{\mu} \tag{20}$$

(21)

c

as the fluid velocity, v, increases, the heat transfer coefficient, also increases and this in turn enhances the heat flux as shown by the Newton's law (see Eq 22).

$$q'' = h \cdot \Delta T \tag{22}$$

Accordingly the thermal energy removed from the primary coolant system results much higher compared to that under normal operation. This situation is called *excess heat removal* in a main steam line break accident. The thermal hydraulic consequence of the excess heat removal is the fast cooldown of the core inlet coolant temperature. This induces a shrinking of the primary mass inventory and hence a depressurization of the primary system. The low steam generator pressure results in reactor scram, and the reduction of core power generation increases the rate of primary coolant inventory shrinkage. This process will continue until the steam blowdown out of the rupture steam pipe is reduced or terminated.

An important characteristic of the MSLB accident is the asymmetric thermal hydraulic behavior. Taking in account that a typical PWR has three or four steam generators, the coolant temperature of the affected loop will be lower than that of the intact loops. Therefore, the temperature distribution in the downcomer and in the core inlet will not be uniform.

The relevant aspects during the transient, related to the low coolant temperature as consequence of the excess heat removal, concern the recriticality and the RPV integrity under consideration of pressurized thermal shock (PTS).

The fuel temperature reactivity coefficient (Doppler effect) and the moderator temperature reactivity coefficient during most of core life are negative, whilst the moderator density reactivity coefficient is positive. Because of the decrease of the coolant temperature, that decreases the fuel rod temperature, all the three reactivity coefficients result in positive reactivity additions to the core. The scram response to the transient adds negative reactivity to the core to compensate the positive reactivity addition resulted from the accident. However, at high burnups the magnitude of the possible positive reactivity addition resulting from the cooldown of the reactor coolant system following an MSLB accident is large, and may even offset the negative reactivity addition due to scram. As a result, recriticality and an unintentional power generation could occur. This is the so called return to power of the MSLB accident. the return to power condition may result in high local power peaking, and fuel rod damage will be possible.

The fast cooldown of the primary system and the injection of emergency cooling water at relatively high primary side pressure, which play an important role in the mitigation of an MSLB accident, raise the possibility of pressurized thermal shock event. The concern is that the cooling will bring a substantial portion of the vessel to a temperature where a brittle fracture may occur. The thermal stratification of the cold leg flow can provoke the growth of a cold plume in the PWR downcomer. The pressure vessel in contact with the cold plume suffers a fast cooling at high pressure. This in turn can affect the structural integrity of the PWR vessel.

5.3. Phenomena identification

The key phenomena/processes which characterize the transient scenario of interest, namely the MSLB, have been identified making use of the list of phenomena (related to PWR) proposed by experts from the CSNI (see [1]). In the identification procedure, the scenario is subdivided in phenomenological time periods, so called "*Phenomenological Windows*", in order to establish a temporal ranking of the key phenomena involved that are distinctive of the class of transients (for exemple break flow). The peculiarity of each transient is in turn identified by the definition of the *relevant thermal hydraulic aspects* that are characteristic for the given transient scenario (these are events or phenomena consequent to the physical process, for example sub-cooled blow-down, occurrence of loop seal clearing time windows, residual mass inventory at time of dryout, etc.) In order to use the identified phenomena and RTA for the code assessment purpose, they must be well characterized from the experimental point of view. Therefore, phenomena/processes have to be connected with the experiments carried out in both integral test facilities and separate effect test facilities. Of course, for the objectives of the IA the two types of tests have to be integrated in order to perform the overall physical phenomenology occurring in each component and in each Ph.W. during the postulated accident scenario.

The key phenomena/processes relevant for the MSLB transient scenario are listed in Table 15 and Table 16.

Table 15 – Key phenomena/processes relevant for the MSLB. (part 1 of 2)

#	RELEVANT PHENOMENON/PROCESS
1	***Asymmetric loop behavior***
2	***RPV CORE reactivity feedback***
3	***RPV CORE 3D power distribution***
4	***RPV heat transfer in CORE covered (including DNB)***
5	***Behaviour of coolant within a buoyancy driven flow***
6	***RPV UH void formation and condensation***

Table 16 – Key phenomena/processes relevant for the MSLB (part 2 of 2)

#	RELEVANT PHENOMENON/PROCESS
7	***RPV UH coolant flow paths (including 3D flow paths)***
8	***PRZ thermo-hydraulics: depressurization, evaporation condensation***
9	***Natural circulation (single phase)***
10	***SG primary side: heat transfer***
11	***SG secondary side: heat transfer***
12	***SG secondary side: depressurization***
13	***SG secondary side: mixture level***
14	***SG secondary side: void distribution***
15	***SG secondary side: liquid entrainment***
16	***SG secondary side: break (critical) flow***
17	***Structural heat and heat losses***
18	***1 phase pump behavior***
19	***ECC injection leading to stratification flows***
20	***Turbulent mixing due to convection and buoyancy***
21	***Formation of 3D patterns (azimuthal sectors and transition region in axial direction) leading to a stratification in the downcomer***
22	***Mixing in the cold leg until the RPV inlet***
23	***Flow development (flow splitting, flow reversal)***
24	***3D temperature distribution in the inlet nozzle, downcomer and core inlet plane***

5.4. ITF and SETF for the selected scenario

The selection of the experimental rigs (ITF and SETF) with reference to the selected transient scenario is done on the basis of existence of experiments conducted under conditions of interest for the application of the methodology, taking into account the relevance of the tests with regard to the reactor conditions (including the range of parameters) and to the scaling value of the measured experimental data.

In the framework of the OECD-PKL 2 test program, complementary experiments on MSLB have been performed at two different phenomenological levels, namely at the system level using the PKL-III integral test facility and at component level using the ROCOM separate effect test facility. Backdrop of these tests was a 0.1A (non-isolable) main steam line break that arises under hot stand-by conditions. The main goal of these tests is to provide a reliable experimental data sets for the validation of TH-SYS codes in regard to the recriticality and PTS. Therefore, it is necessary to assess the scaling value of the measured experimental data and the possibility to transfer the main outcomes to the scale of a PWR. This step has been taking in as far as the general phenomena occurring in the PKL-III MSLB

experiment are concerned: the single phase natural circulation, heat transfer under asymmetric conditions, fast cooldown and mixing processes. In fact due to the design features (four loop configuration, geodetic elevations in 1:1 KONVOI scale, pressure losses in the primary circuit overall and in the individual components correspond to those in a KONVOI PWR) the PKL test facility is well suitable to simulate the thermal hydraulic phenomena of a MSLB (see section § 4.2.1.1. and [61]).

It should be noted that the depressurization rate of the affected steam generator during main steam line break test may differ at the scale of NPP (this is due to the fact that the masses of the metallic structures are not well scaled). This may lead to different minimum coolant temperature and the time of its occurrence in the affected loop of the primary side, which in turn can affect the reactivity effects and re-criticality phenomena at the scale of a PWR. In addition, the geometrical configuration of the downcomer in the PKL facility notably limits the transferability of measured data for further analysis of PTS. Therefore, the issue is addressed by complementary experimental tests in ROCOM facility with initial and boundary conditions provided from PKL test G3.1 (see Figure 73). Yet, the scaling issue for each of the facilities has to be taken into account in this one-way coupling (i.e. PKL to ROCOM data transfer, without feedback) process. As a consequence, the outcomes from these tests are qualitatively applicable, but tests results should be transferred to PWR scale with caution, even though both PKL and ROCOM test facilities are well-scaled with respect to physical phenomena.

The density differences between the different coolants in the facility (reactor) play an important role for the phenomena in these tests (see chapter 6 in which shall discussed the PKL test G3.1 and the ROCOM tests in detail). The Froude number is the main dimensionless similarity number, which can be used to characterize buoyant single-phase flows. The Froude number represents the ratio of inertia and gravitational forces. The influence of the inertia in flowing media is characterized by the density, the influence of the gravity by the density difference. That means that the density difference between injected and ambient water is the key parameter in determining characteristics of the Froude number. The boundary conditions should be selected in such a way that the Froude number in the ROCOM experiment is identical to the Froude number under reactor conditions. In the current experiments the similarity of the Froude number was achieved by using the same density differences under reactor (PKL) conditions and scaling the velocity determined for reactor conditions down by a factor of $\sqrt{5}$ (see [61]).

The combination of the PKL and the ROCOM experiments cover all the thermal hydraulic phenomena relevant for the MSLB (see Table 15 and Table 16). The final goal will be to make accurate prediction for PWR systems with regard to recriticality and PTS for relevant scenarios by using systems code that have been assessed on the basis of complementary tests for plant calculations with PWR geometry and PWR initial and boundary conditions.

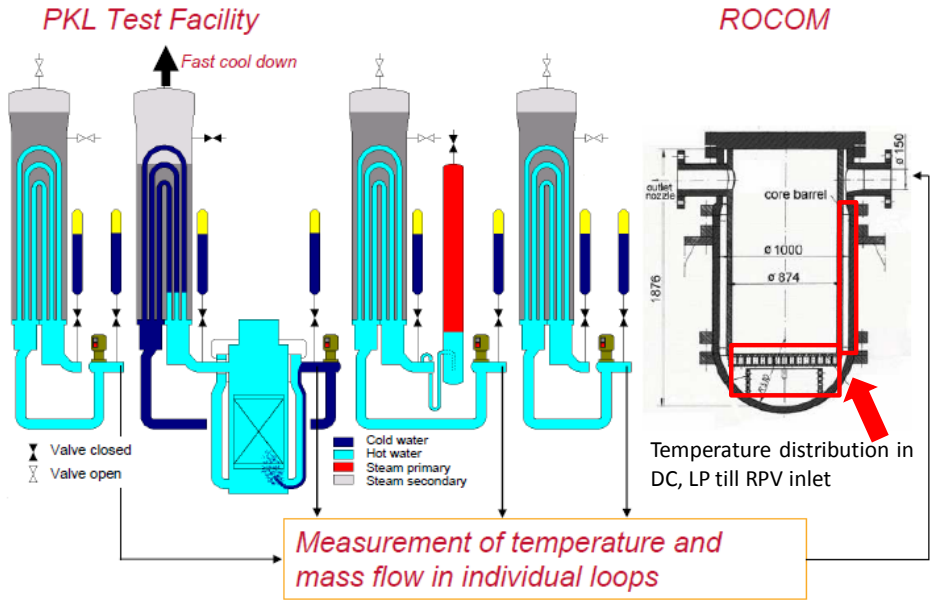

Figure 73 – Complementary test: initial and boundary conditions provided to SET rig (ROCOM) from IET facility (PKL)

5.5. Establishing of the test matrix

Valuation matrix related to MSLB with the objective of allowing a selection of tests suitable for code assessment has been established. This matrix has been developed on the basis on that developed originally by the CSNI for PWR systems (see [1] and [62]). The cross reference matrix comprises the key phenomena/processes which are expected to occur during the transient, test type, and both integral and separate effect test facilities. This is done to feature the system response and the experimental reproducibility of the key phenomena at different phenomenological levels by the two typologies of test rigs, In addition to these categories; integrated tests facilities are listed in the validation matrix (see Table 17). Integrated tests facilities means combination of test rigs to achieve complementary tests. The aim is to focus the capability of complementary tests to simulate all effects caused by the accident scenario in a "*pseudo-simultaneous*" way. In this acceptation simultaneous don't means realization of two tests in real time, but its meaning is tied to the use of the thermal hydraulic parameters of one test facility refers to particular instants (relevant for the transient) and transferred to the other facility. This gives a character of temporal continuity, and therefore, of simultaneity to the transfer of information between the two test facilities.

The relationships between the different categories create a cross reference matrix. These relationships are:

- *phenomenon versus test type* indicate which phenomena are occurring in which test types,
- *test facility versus phenomenon* which indicate the suitability of the test facilities for code validation of the different phenomena,
- *test type versus test facility* indicates which test types are performed in which test facilities.

Among the integral system test facilities the category PWR is included under test facilities. The analysis of accidents in actual nuclear power plants is potentially valuable with reference to scaling and simulation problems.

The relationship phenomenon versus test type is rated at one of three levels:

- occurring: which means that the particular phenomenon is occurring in that kind of test (plus sign in the matrix);
- partially occurring: only some aspects of the phenomenon are occurring (open circle in the matrix);
- not occurring (dash in the matrix).

The relationship test facility versus phenomenon is rated at one of three levels:

- suitable for code assessment: a facility is designed in such a way as to simulate the phenomenon assumed to occur in the plant and it is sufficiently instrumented to reveal the phenomenon (plus sign in the matrix);
- limited suitability: the same as above with problems due to imperfect scaling or insufficient instrumentation (open circle in the matrix);
- not suitable: obvious meaning, taking into account the two previous items (dash in the matrix).

The relationship test type versus facility is rated at one of three levels:

- performed: the test type is useful for code assessment purposes (plus sign in the matrix);
- performed but of limited use: this kind of test has been performed in the facility, but has limited usefulness for code assessment purposes, due to poor scaling or lack of instrumentation (open circle in the matrix);
- not performed (blank).

The process of the selection of the experiments, for which comparison of measured and calculated parameters form a basis for establishing the accuracy of test calculation results, has been conducted considering that:

- the tests selected must clearly exhibit all relevant thermal hydraulic phenomena/processes expected to occur during the postulated accident;
- the quality and completeness of experimental data
- challenge to system codes

5.6. Accuracy evaluation for complementary tests

For completing the steps which make up the integrated approach, aimed at system code validation, it is required to measure the discrepancies among corresponding time trends or point value. This results in evaluating the accuracy of the computational model obtained by comparing its responses with experimentally measured responses. The evaluation of the code accuracy is carried out following a similar approach to the one adopted in the UMAE (see [60] and [63]), which requires the accomplishment of the two steps listed below:

- demonstration of the acceptability of the code results at qualitative level;
- demonstration of the acceptability of the code results at quantitative level.

Concerning the qualitative accuracy this implies a systematic comparison between measured and calculated data and the user assigning subjective (as far as possible, objective) judgment marks. The comparison activity is based on the following procedures:

- comparison between corresponding time trends of selected variables;
- comparison between the resulting sequence of main events; the same events must be appear in the experimental and calculated data base resulting time differences must be acceptable to the user (subjective judgment);
- comparison between the experimental and computed key phenomena that distinguishes;
- comparative analysis of the parameters characterizing the RTA.

In this context, the evaluation of the RTA is provided, based on (subjective/qualitative) engineering judgments, as:

- Excellent ("E" mark): code predicts the parameter or the phenomenon qualitatively and quantitatively. Calculation remains within the foreseeable or envisaged experimental data uncertainty band.
- Reasonable ("R" mark): code predicts the parameter or the phenomenon qualitatively but not quantitatively. Calculation lies outside the experimental data uncertainty band totally or in part but shows correct behavior and trends.
- Minimal ("M" mark): the parameter or the phenomenon is not predicted; however, the overall behavior is not affected (subjective evaluation) and the reason for the misprediction is understood (sensitivity analysis reveal necessary to this aim);
- Unqualified ("U" mark): the code does not predict the parameter and the reason is not understood (Unqualified - calculation result does not show correct trend and behavior, reasons are unknown and unpredictable).

A positive overall qualitative judgment is achieved if "U" mark is not present. In this way is possible operate a first classification about the calculation quality. This phase of the accuracy evaluation is a necessary prerequisite to the application of the quantitative analysis.

The quantification of the code accuracy, which represents the second level in the evaluation of the accuracy of the computational simulation, is achieved making use

of an integral approach. This method is based on the application of the FFT in order to transform the time trends discrepancies among code results and experimental data in the frequency domain.

The simplest quantitative formulation of the accuracy of a given calculation is obtained by the difference function:

$$\Delta g(t) = g_{calc}(t) - g_{\exp}(t) \tag{23}$$

The integral approach have the characteristic to condensate the information provided by instantaneous trend of a given time function (Δg) in a single value. This value is taking as indexes for quantifying accuracy. The tool used for the application of the method, as mentioned above, is the FFTBM which is a well established tool to evaluate the accuracy of the system code applications. It is applied to a set of time dependent scalar quantities that typify the thermal hydraulic phenomena occurring during the transient scenario (such as primary and secondary pressure, pressure drops, coolant and cladding temperatures, flow rates, etc.) and for each of them provides quantification of the discrepancy between code prediction and experimental data throughout the definition of two values which are characteristic of each calculation: a *dimensionless average amplitude* and a *weighted frequency* (see Eq. 24) .

$$AA = \frac{\sum_{n=0}^{2^m} \left|\Delta\tilde{g}(f_n)\right|}{\sum_{n=0}^{2^m} \left|\tilde{g}_{\exp}(f_n)\right|} \qquad WF = \frac{\sum_{n=0}^{2^m} \left|\Delta\tilde{g}(f_n)\right| \cdot f_n}{\sum_{n=0}^{2^m} \left|\Delta\tilde{g}(f_n)\right|} \tag{24}$$

Where $\Delta\tilde{g}(f_n) = \tilde{g}_{exp}(f_n) - \tilde{g}_{calc}(f_n)$ is the error function evaluated in the frequency domain (f). Furthermore, each of such scalar quantities is assigned a weighting factor to account for their importance and reliability relevance, and then all average amplitudes are averaged with proper weighting to obtain a single figure of merit that characterizes the overall discrepancy and therefore the code performances. A detailed description of the FFTBM is given in APPENDIX E.

Finally, the suitability of code in predicting the results of the complementary tests is obtained splitting the quantification of the accuracy in two phases. The first phase concern the evaluation of the accuracy in a integral sense that is assess the code results at the system level (analysis of the overall thermal hydraulic response of the PWR system) against experimental data of the integral test performed in PKL-III facility. The second phase is oriented to measure the code discrepancies focusing the attention to the component level phenomena identified in the PWR system during the accident scenario under investigation and not experimental captured by the integral test. This last phase is connected, from the experimental point of view, with the tests carried out in the ROCOM test facility. In this way it is possible to cover experimentally the overall spectrum of phenomena expected to occur during the MSLB transient and assess the computational results using the same code (TRACE-V5 TH-SYS code) to simulate both tests: integral and separate effects tests.

Table 17 – Cross reference matrix for MSLB in PWR systems

CROSS REFERENCE MATRIX FOR MAIN STEAM LINE BREAK		Test Type[1]	Test Facility and Volumetric Scaling			Integrated test facilities
			System Tests		Separate tests	Complementary Tests
Phenomenon versus test type + occurring o partially occurring - not occurring **Test facility versus phenomenon** + suitable for code assessment o limited suitability - not suitable **Test type versus test facility** + performed o performed but of limited use - not performed or planned		Main Steam Line Break	PWR 1 : 1 (KONVOI)	PKL-III 1: 145	ROCOM 1:5	PKL-III/ROCOM
PHENOMENA	*Asymmetric loop behavior*	+	+	+	-	+
	RPV CORE reactivity feedback	+	+	-	-	-
	RPV CORE 3D power distribution	+	+	-	-	-
	RPV heat transfer in CORE covered (including DNB)	+	o	+	-	+
	Behaviour of coolant within a buoyancy driven flow	+	+	-	+	+
	RPV UH void formation and condensation	o	o	o	-	o
	RPV UH coolant flow paths (including 3D flow paths)	o	o	o	-	o
	PRZ thermo-hydraulics: depressurization, evaporation condensation	+	+	+	-	+
	Natural circulation (single phase)	+	+	+	-	+
	SG primary side: heat transfer	+	+	+	-	+
	SG secondary side: heat transfer	+	+	+	-	+
	SG secondary side: depressurization	+	+	+	-	+
	SG secondary side: mixture level	o	+	o	-	o
	SG secondary side: void distribution	o	o	o	-	o
	SG secondary side: liquid entrainment	o	o	o	-	o
	SG secondary side: break (critical) flow	+	+	+	-	+
	Structural heat and heat losses	+	+	+	-	+
	1 phase pump behavior	+	+	+	-	+
	ECC injection leading to stratification flows	o	o	o	o	o
	Turbulent mixing due to convection and buoyancy	+	-	-	+	+
	Formation of 3D patterns (azimuthal sectors and transition region in axial direction) leading to a stratification in the downcomer	o	-	-	o	o
	Mixing in the cold leg until the RPV inlet	+	-	-	+	+
	Flow development (flow splitting, flow reversal)	+	+	-	+	+
	3D temperature distribution in the inlet nozzle, downcomer and core inlet plane	+	-	o	+	+
Test Facility	**PWR (KONVOI)**	-				
	PKL-III/ROCOM	+				

(1) Test type is referred to the complementary test PKL-III/ROCOM

(2) The phenomenon may be relevant for the transient scenario depending upon the selected boundary and initial conditions.

6 APPLICATION OF IA TO PKL-2/ROCOM EXPERIMENTS

The integrated analytical methodology has been applied to the test G3.1 which is the third test of an experimental campaign, consisting of eight tests (G series) carried out in integral test facility PKL-III in the framework of the OECD/NEA CSNI PKL-2 (2008-2012). This test has been selected also by the program review group and the management board (PRG/MB) for performing an analytical activity among the Project participants (see [64]).

The test G3.1 is fast cooldown transient, namely a main steam line break. The design of the experiment involves two phases: the first based on the 0.1A break in the main steam line as initiating event and the second consisting in the emergency core cooling system injections by means of the high pressure injection system connected with the cold legs 1 and 4. During the Phase I, focus is given to the recriticality and pressurized thermal shock aspects. The second phase of the test addresses the effects of the injections in cold legs on the single phase natural circulation in the loops, when the pressurized safety valve is operated as well as the effects of the pressurized thermal shock phenomenon on the RPV integrity due to the introduction of cold water in the RPV downcomer. Therefore, in order to overpass the limitations of PKL facility (which is oriented to PWR system behavior) in reproducing three dimensional phenomena, a separate effect facility (i.e. ROCOM) is then operated based on the PKL results for investigating these aspects.

The analytical activity is divided into two phases. The first phase deals with the validation of the TRACE-V5 code performances in simulating the transient thermal hydraulic phenomena that occur in the reactor coolant system (RCS) (PKL test G3.1). The second phase concerns the assessment of the code capabilities to predict the 3-D thermal hydraulic flow conditions that are established in the vessel during the accident scenario (ROCOM complementary tests).

6.1. PKL-2 Project PKL-III Test G3.1

6.1.1. Objectives of Test G3.1

The subject of the test G3.1 is a main steam line break in one SG. The purpose of this test is to investigate the transient behavior resulting from the break. Of particular interest were the effects of the main steam line break on the primary side system conditions during the boiling-off phase of the affected SG and the subsequent primary-side injection from two safety injection pumps.

The main objectives of the Test G3.1 are (see [65]):

- to investigate PTS and recriticality aspects;
- to obtain experimental data for validation of thermal-hydraulic codes applied to main steam line break scenario (the main phenomena /processes investigated are reported in section and in Table 17;
- to provide the boundary condition for a SETF experiment (ROCOM), focused on mixing in downcomer and lower plenum.

6.1.2. Configuration of the facility, boundary and initial conditions of the experiment

The configuration of the facility (see Table 18) is summarized, as follows.

- The pressurizer is connected to the HL of loop 2.
- The break device is located in the main steam line 1. It simulates the 0.1A break by means of a nozzle with diameter of 29 mm and L/D equal to 12.
- Two HPIS connected with cold legs 1 and 4. The mass flow injected in the primary system is defined by the experimentalists. Deviations from the specified values are due to the pump characteristic, which is unknown.

The initial conditions of the test (see Table 19) are achieved with the core power corresponding to the hot shut down conditions at the reference power plant, taking into account the heat losses of the facility. The primary pressure is maintained at 4.2 MPa, with the secondary side pressure at about 3.5 MPa. The heaters in the PRZ are active in order to compensate the heat losses of the component. The MCP are operated at 2500 rpm, which corresponds to a mass flow rate of 34 kg/s in each loop. This is approximately the scaled down nominal mass flow rate of a KWU Siemens NPP. The coolant temperature at core outlet is about 7 °C subcooled. The test starts with the SG isolated (i.e. main steam isolation valve closed). Due to this, the energy in the primary system rises during the conditioning phase (i.e. primary coolant temperature increase of 12 °C/h).

The secondary side levels of the intact SG are kept at the nominal value (about 12.3 m) on the contrary to the affected SG-1 where the level is lower (i.e. about 9 m). This difference is due to the design of the experiment and the break characterization as outlined (in the section § 6.1.2.1). Indeed, only single phase (critical) flow was planned during the SG blowdown (see [66]). Due to the lower level, the natural circulation in the affected SG results interrupted, therefore coolant temperature stratification is observed in the downcomer.

These quasi steady state conditions are reached during the conditioning phase. The experimental data provides 440 s (see [65]) of parameters trends before the start of the transient. More detailed information is reported from [65].

6.1.2.1. PKL Test G3.1 break component and characterization

The break component is installed in the steam line of the steam generator 1 (see Figure 77). Characterization tests were executed in order to optimize the procedure for conducting the experiment. The boundary and initial condition (Table 19) of two tests, called T8 and T9, as well as the main parameter trends were provided. In both cases, the primary system is inactive and only the steam generator 1 is operated.

6.1.3. Outline of the PKL-III G3.1 experiment

The initiating event is the 0.1A rupture in main steam line of SG-1. Two relevant phases can be distinguished, plus specifying three sub-phases as follows:

- **Phase I (0s – 1130s)**: SG-1 depressurization and primary system overcooling, from the SoT up to HPIS injection;

- **Phase II (1030s – 4400s)**: primary system filling, from HPIS injection up to the EoT;
- **Subphase II-a (1130s – 1420s)**: PRZ filling, from HPIS injection up to first PRZ safety valve opening;
- **Subphase II-b (1420s – 1840s)**: primary system depressurization by means of PRZ SV vapor flow, from first up to second PRZ safety valve opening;
- **Subphase II-c (1840s – 4400s)**: primary system solid and PRZ SV liquid flow, from second PRZ safety valve opening up to the EoT.

The imposed and the resulting sequence of main events are summarized in Table 20 and table 21.

Phase I (0s – 1130s)

As soon as the break opening occurs, the SG-1 pressure starts to decrease (Figure 83), causing the evaporation of the coolant and, therefore, the enhancement of the heat exchange between primary and secondary systems. Single phase critical flow, with a maximum of 2.06 kg/s at 10 s form SoT, is measured at the break (Figure 87). The SG-1 collapsed level drops quickly below 5 m after 25 s (Figure 87). The intact SG, corresponding to the loops 2, 3 and 4, are isolated (Figure 83).

The loss of AC power is also assumed with the initiating event, thus the MCP start coasting down with the time trends depicted in Figure 82. The pressurizer heaters are also switched off. From about 50 s and on, and therefore before the MCP are at rest, the mass flow rate in loop 1 is larger than in the other loops (see Figure 86). Once the MCPs are stopped, the butterfly valves close in order to simulate correctly the pressure drop across the MCPs.

The primary coolant temperature and, as a consequence, the pressure decrease due to the heat exchange in the loop of the affected SG (Figure 85). Also the PRZ level smoothly drops because of the coolant density increase (see Figure 83).

No perfect loop to loop mixing is observed: the temperature in loop 1 at SG 1 inlet is lower than in the other loops (see Figure 85). The PRZ empting is also visible: during the first 230 s, cold water from the PRZ surge line enters in the hot leg of loop 2 then, hot water coming from the PRZ vessel is detected at the SG-2 U-tubes entrance.

The minimum coolant temperature in the RCS at SG 1 outlet (153 °C) is reached at about 525 s, whereas it is observed at core inlet at 780 s (Figure 85)., when the affected SG is almost emptied (see Figure 87). From this time on, the mass flow rate in loop 1 reaches approximately the value of 1.2 kg/s, which is higher than in the other loops and remains almost unperturbed up to the end of the phase (see Figure 86).

Once the heat sink is lost, the energy of the primary system slowly increases again (see Figure 83 and Figure 85). At 1030, the HPIS pumps, connected with loops 1 and 4, are switched on and the phase I of the experiment is terminated.

Phase II (1030s – 4400s)

Subphase II-a (1030s – 1420s)

The injection of cold water from HPIS (see Figure 88) causes the filling up of the primary system thus, the primary pressure and PRZ level increase, as depicted in see Figure 83. Coolant temperature stratification is observed in PRZ vessel (see Figure 84), as well as in cold leg 1 and 4 (see [65])

The coolant temperature in loop 1 at SG outlet rises, whereas the average coolant temperature in the system slightly decreases (see Figure 83). The measures of the mass flow rate in the loops demonstrate a smooth oscillatory reduction in loop 1, until about 0.9 kg/s at 1400 s and analogous increase in the other loops (see Figure 84).

At 1420 s the primary pressure reaches the set point for PRZ safety valve opening, when the PRZ level is about 8.5 m.

Subphase II-b (1420s – 1840s)

When the PRZ SV opens (4.2 MPa), the mass flow of the HPIS rises because the primary pressure drops. The PRZ safety valve is controlled on the basis of the pressure drop in the discharge line. The signal for the valve closure occurs when the primary pressure is about 4.05 MPa but it remains partially open with steam flowing through. The primary pressure continues to descend until the cushion of steam in the PRZ top disappears (1820 s). Then, it rises with a rate of 0.05 MPa/s up to 4.7 MPa. As consequence of this the HPIS mass flow rate decreases rapidly (see Figure 88).

During this phase the mass flow rate in the loops remains unperturbed (see Figure 86).

Subphase II-c (1840s – 4400s)

The water is discharged through the PRZ SV, which opens on high primary pressure signal. The valve is then regulated in order to maintain the pressure of the system at about 4.15 MPa. The pressure (measured in the upper head) is controlled with a PI-controller (K_P=0.501 and K_I=2.661) (see [67]). During this phase the pressure of the primary system (see Figure 83), the mass flow discharged, the mass flow injected by the HPIS (see Figure 88), and the opening of the valve oscillate (see also Ref. [65]). The coolant in primary system is cooled down very slowly. The mass flow rate in the loops remain unperturbed (see Figure 86) with the loop 1 having larger mass flow rate than the other loops.

At 4400 s, the experiment ends with the coolant temperature in primary side equal to 210 °C and the pressure stabilized at 4.15 MPa.

6.1.4. Selected parameters for code assessment

954 parameters are measured in the test G3.1. These data are suitable both for the analysis of the experiment as well as for the code assessment. Among these, more than 60 parameters are selected for the analysis of the computational results. The requested parameters and their positions in the facility are available in Figure 74, Figure 75, Figure 76, Figure 77 and Figure 78.

Table 18 – OECD/NEA/CSNI PKL-2 Project, Test G3.1: facility configuration.

#	SYSTEM	SYMBOL	CHARACTERISTICS	STATUS	REMARKS
1	PRZ connection status	--	Loop #2	--	Initial level equal to 7.4 .
2	PRZ safety valve	--	Nozzle: Φ= 3.9 mm; L = 5 mm	Active	Part of the PRZ control system including also the spray system (not operated)
3	UH – DC bypass	--	Orifice: Φ= 3.9 mm; L = 5 mm	--	--
4	Break component	--	Connected with main steam line 1. Nozzle: Φ= 29 mm; L = 350 mm.	--	--
5	ECCS Accumulators	JNG	8 systems available	Not operated	--
6	ECCS HPIS	JND	4 trains connected with all CL and HL	2 trains active: CL-1 and -4	Flow rate of a HPIS pump regulated as in [66] (Table 6)
7	ECCS LPIS	JNA	4 trains connected with all CL and HL	Not operated	--
8	MCP	--	4 MCP in operation	Active	MCP operated at 2500rpm corresponding to 34 kg/s per loop MCP coastdown relative rotation vs. time in Figure 82
9	Volume Control System	KBA	--	Not operated	--
10	Residual Heat Removal System	JN(A)	--	Not operated	--
11	FW	LAB	--	Not operated	--
12	AFW /EFW	LAR	--	Not operated	--

Table 19 – OECD/NEA/CSNI PKL-2 Project, Test G3.1: relevant initial and boundary conditions.

#	QUANTITY	ID	Unit	Y_{DESIGN}	Y_{EXP}
1	Core thermal power	PEL INNERE ZONE NEU PEL MITTLERE ZONE N PEL AEUSSERE ZONE N	kW	260	52.39 97.30 110.91
2	PRZ heaters thermal power	PEL DH STUETZHEIZ PEL RDBSTUETZHEIZ PEL DH BYPASSH	kW	12	0.01 1.07 11.89
3	Upper plenum pressure	P RDB OP	MPa	4.2	4.21
4	SG-1 exit (top of the SG)	P DE1 SEK MB 50	MPa	3.5	3.50
5	SG-2 exit (top of the SG)	P DE2SEK	MPa	3.5	3.51
6	SG-3 exit (top of the SG)	P DE3 SEK	MPa	3.5	3.51
7	SG-4 exit (top of the SG)	P DE4 SEK	MPa	3.5	3.52
8	Core outlet (upper plenum)	TF OP ME11/1 TF OP ME11/2 TF OP ME11/3 TF OP ME11/4	℃	246	244.5 243.5 243.3 243.4
9	SG-1 DC pipe bottom	TFDE1DC(1-2)UN-SEK	℃	200	202-194

	(top)			(210)	(220-210)
10	SG-2 DC pipe bottom (top)	TFDE2DC(1-2)UN-SEK	℃	240	237-240 (237-238)
11	SG-3 DC pipe bottom (top)	TFDE3DC(1-2)UN-SEK	℃	240	243-238 (238-239)
12	SG-4 DC pipe bottom (top)	TFDE4DC(1-2)UN-SEK	℃	240	241-241 (241-241)
13	Loop mass flow rate	F DE1 AUS-WR F DE2 AUS-WR F DE3 AUS-WR F DE4 AUS-WR	kg/s	34	33.7 33.7 33.6 33.5
14	PRZ level (collapsed)	H JEF 10 CL 001	m	7.4	7.44
15	SG-1 DC (Riser)	H DE1SEKSTGRM/GES (H JEA 10 CL851)	m	8.8 (9.2)	8.83 (9.22)
16	SG-2,3,4 DC (Riser)	H DE2-4SEKSTGRM.UN (H JEA 20-40 CL851)	m	12.3 (12.3) 12.3 (12.2) 12.5 (12.2)	12.3 (12.3) 12.3 (12.2) 12.5 (12.2)

Table 20 – OECD/NEA/CSNI PKL-2 Project, Test G3.1:

#	IMPOSED EVENT DESCRIPTION	SYSTEM	SIGNAL (TIME OR SET POINT)	REMARKS
1	0.1A BRK opening in steam line 1	Break component	0 s	--
2	PRZ heaters turned off	PRZ heaters	0 s	
3	Trip of the MCP and coast-down	MCP	0 s	Coast-down in Figure 82
4	Butterfly valve closed	Butterfly valve	210 s	Pressure drop simulation of the MCP at rest
5	ECCS HPIS injection	2 HPIS systems	1130 s	mass flow per loop equal to 0.20 kg/s
6	ECCS HPIS injection reduction	2 HPIS systems	2150 s	mass flow per loop equal to 0.14 kg/s
7	First PRZ safety valve actuation	PRZ SV	Opening: 4.2 MPa Closure: 4.05 MPa	Small leakage occurred at PRZ SV closure
8	Second PRZ SV actuation	PRZ SV	Opening: 4.7 MPa	--
9	End of the transient	--	Conditions: • Primary pressure 4.2 MPa • Coolant temperature 210 °C	

Table 21 – OECD/NEA/CSNI PKL-2 Project, Test G3.1: phenomenological windows and resulting sequence of main events (part 1 of 2)

Ph.W.	DESCRIPTION & PHENOMENA/PROCESSES	TIME SPAN [S]	EVENT	EXP [s]	Note
I	SG-1 depressurization and primary system overcooling: – **PRZ thermo-hydraulics (depressurization, evaporation, condensation)** – **natural circulation (single phase)** – **heat transfer in intact and affected SG** – **break (critical) flow** – **SG (affected) depressurization, mixture level, void distribution, liquid entrainment** – **heat transfer in core covered** – **structural heat and heat losses**	**0 – 1030**	*SoT (break opening) in SG #1 steam line*	**0**	Imposed
			Heaters in SG#1 switched off	**0**	Imposed
			Trip of the MCP and coastdown	**0**	Imposed
			PRZ heaters switched off	**0**	Imposed
			Stop of FW#1 pumps	**0**	Imposed
			Butterfly valves closure	**210**	Imposed
			MCPs completed stopped	**210**	Imposed
			SG-1 lev. lower than < 8.0m	**6.4**	
			SG-1 lev. lower than < 5.0m	**32**	
			SG-1 lev. lower than < 2.5m	**393**	
			SG-1 lev. lower than < 1.0m	**579**	
			SG-1 lev. lower than < 0.1m (emptied)	**828**	
			SG-1 pressure lower than <3.0MPa	**10.4**	
			SG-1 pressure lower than <2.0MPa	**47**	
			SG-1 pressure lower than <1.0MPa	**164**	
			SG-1 pressure lower than <0.5MPa	**435**	
			Min. coolant temp. in CL#1 SG outlet	**525-565**	
			Min. coolant temp. in at RPV inlet	**600**	
			Min. core inlet temperature due to SG#1 cooldown	**780-840**	
			Min. PRZ level	**819**	

Table 22 – OECD/NEA/CSNI PKL-2 Project, Test G3.1: phenomenological windows and resulting sequence of main events (part 2 of 2)

Ph.W.	DESCRIPTION & PHENOMENA/PROCESSES	TIME SPAN [S]	EVENT	EXP [s]	Note
II-a	PRZ filling: – **PRZ thermo-hydraulics (pressurization, condensation, stratification)** – **natural circulation (single phase)** – **stratification (horizontal) in CL 1 and 4 during ECCS injection** – **heat transfer in core covered** – **structural heat and heat losses**	**1030-1420**	*HPIS activated in loop #1 and 4 (0.2kg/s)*	**1030**	Imposed
			Min. mass flow rate in loop 2 to 4	**1060**	
			Mass flow rate in affected loop stopped	**--**	
II-b	Primary system depressurization by means of PRZ SV vapor flow: – **as II-a, except for:** – **PRZ thermo-hydraulics (depressurization, stratification)** – **mass flow through the PRZ SV (steam)**	**1420-1840**	*PRZ safety valve opening*	**1420**	Steam discharged
			PRZ safety valve closure (small leakage)	**1470**	
II-c	Primary system solid and PRZ SV liquid flow: – **as II-a, except for:** – **PRZ thermo-hydraulics (pressurization, stratification)** – **mass flow through the PRZ SV (liquid)**	**1840-4400**	*PRZ safety valve second opening*	**1840**	Water discharged
			HPIS injection reduced to 0.14kg/s	**2150**	Imposed
			End of calculation	**4410**	$P_{prim-side}$=4.2MPa $T_{core\ outlet}$=210°C

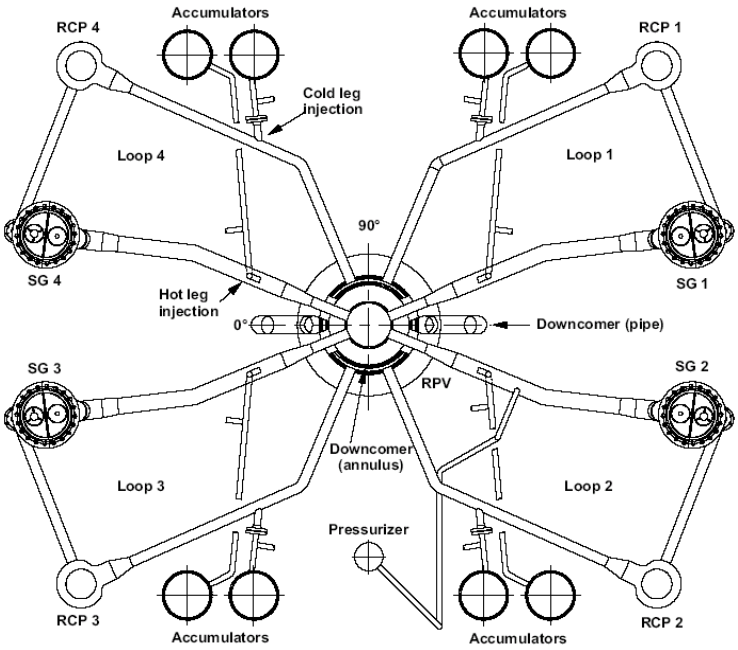

Figure 74 – AREVA NP PKL-III facility: elevations.

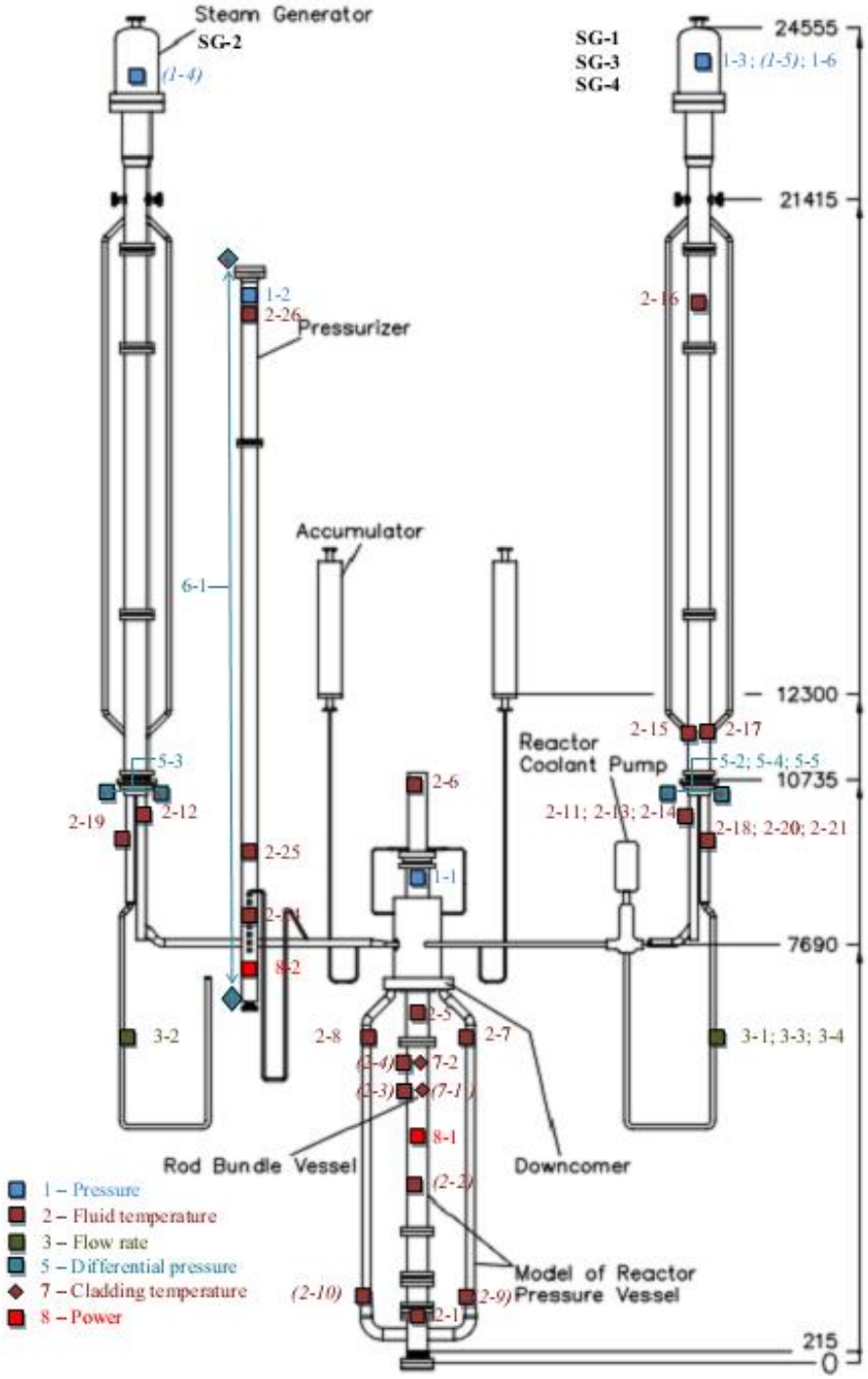

Figure 75 – AREVA NP PKL-III facility: elevations.

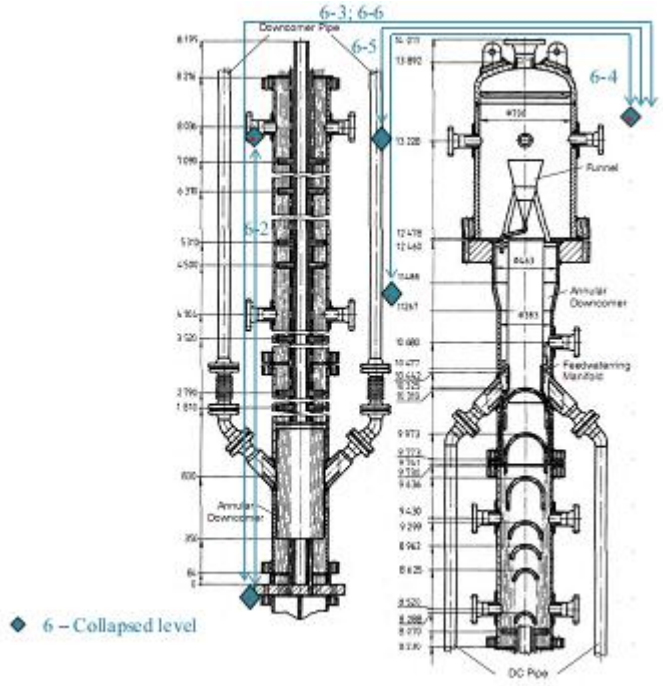

Figure 76 – AREVA NP PKL-III facility: steam generator

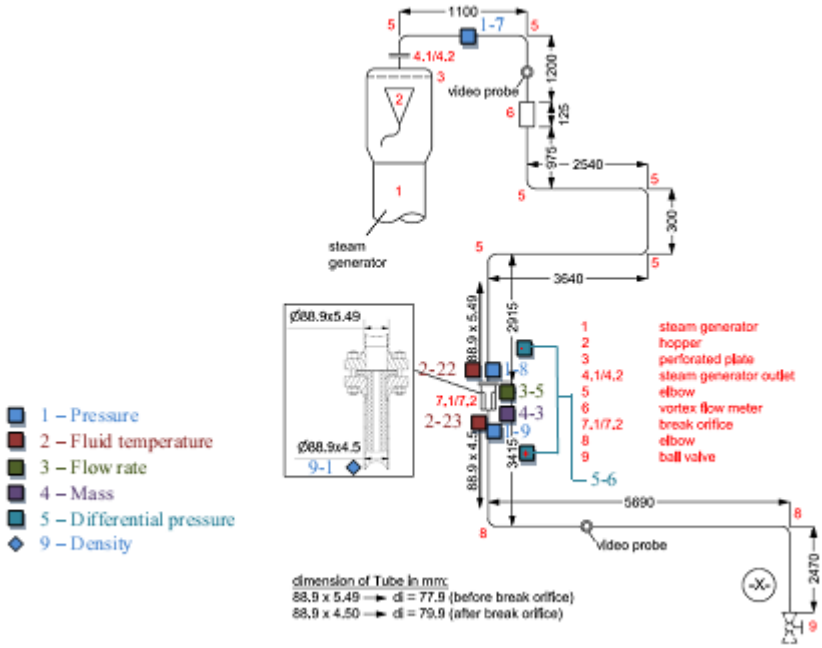

Figure 77 – AREVA NP PKL-III facility: Test G3.1 steam line break device.

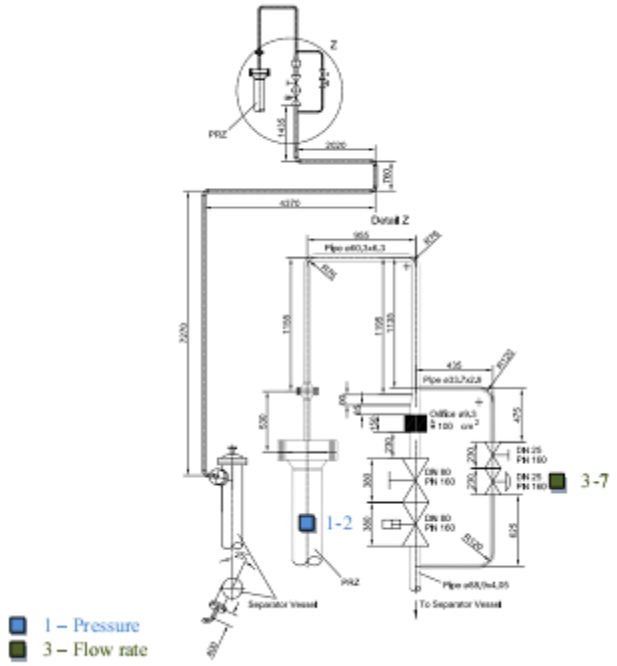

Figure 78 – AREVA NP PKL-III facility: pressurizer relief line

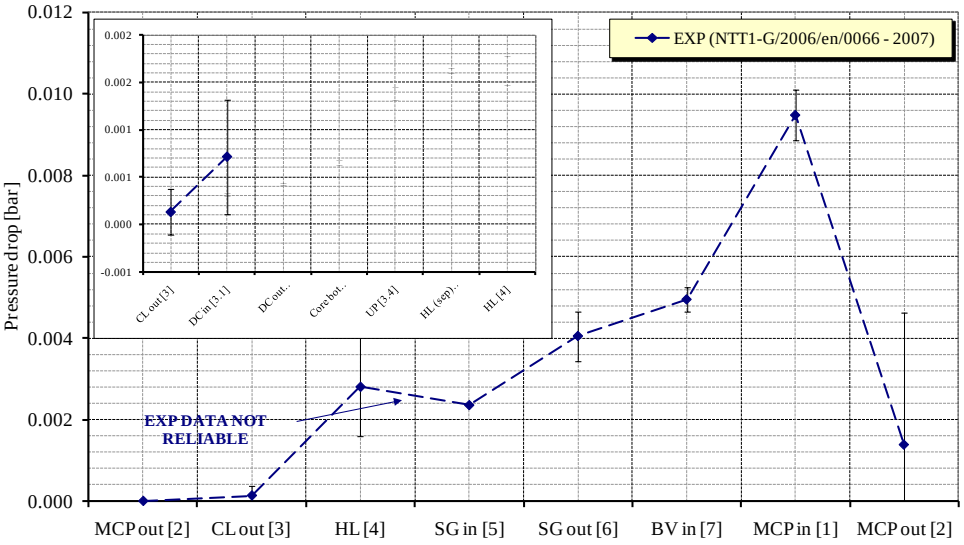

Figure 79 – PKL-III pressure drop characterization: DP vs. length at mass flow rate equal to 0.8 kg/s

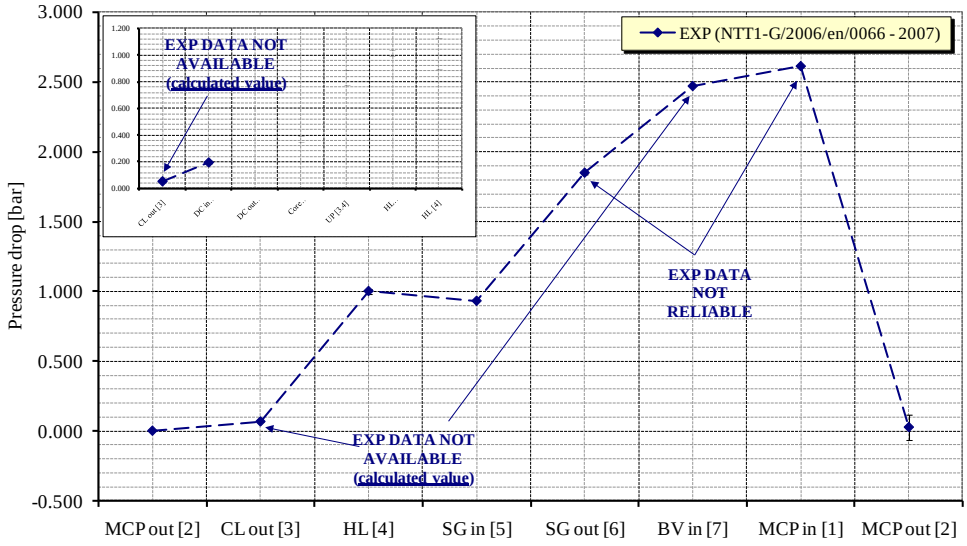

Figure 80 – AREVA NP PKL-III facility characterization: DP vs. length at mass flow rate equal to 25 kg/s

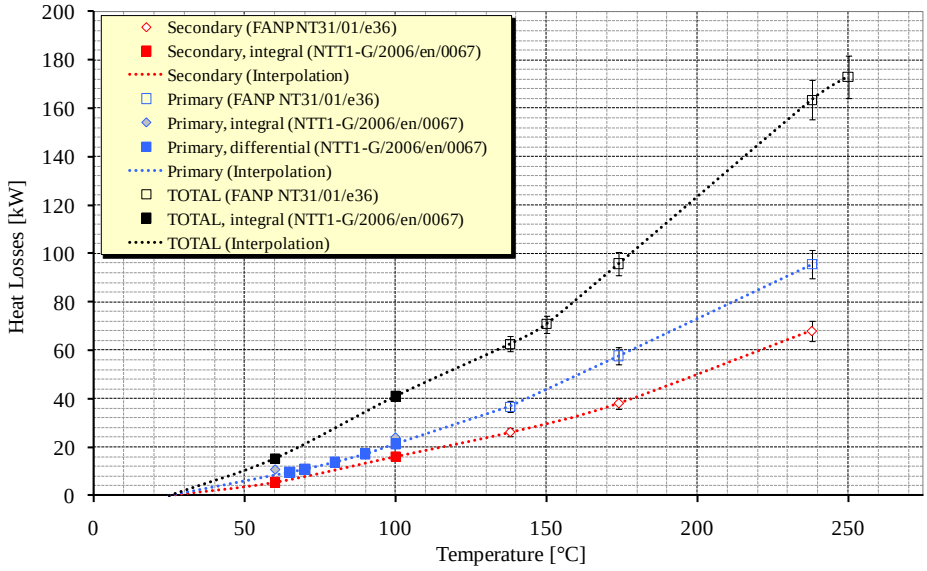

Figure 81 – AREVA NP PKL-III facility characterization: heat losses vs. temperature

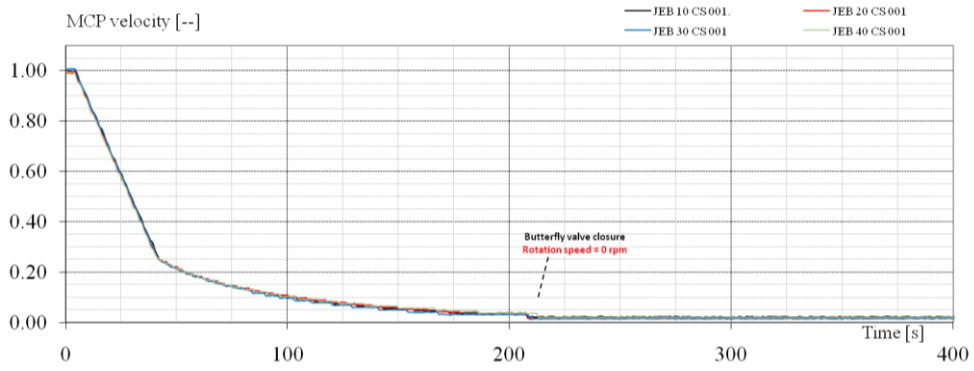

Figure 82 – OECD/NEA/CSNI PKL-2 Project Test G3.1: boundary conditions: MCP coastdown dimensionless velocity vs. time

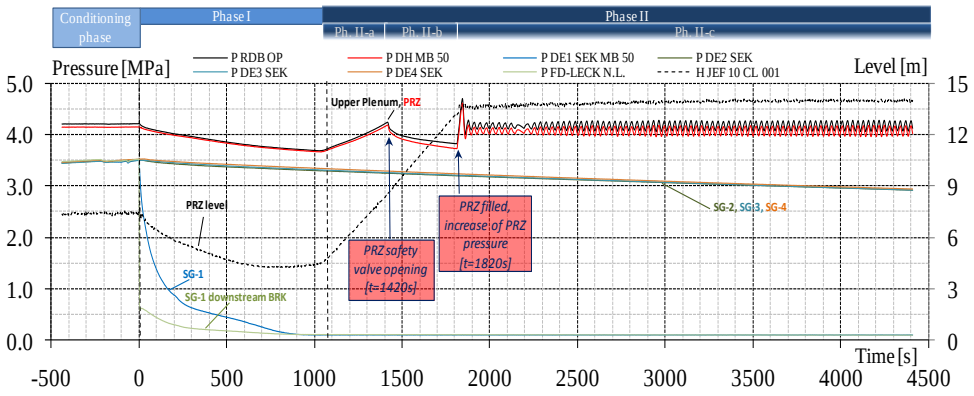

Figure 83 – OECD/NEA/CSNI PKL-2 Project Test G3.1: pressures in PRZ, UP, SGs, BRK line downstream the orifice and PRZ level.

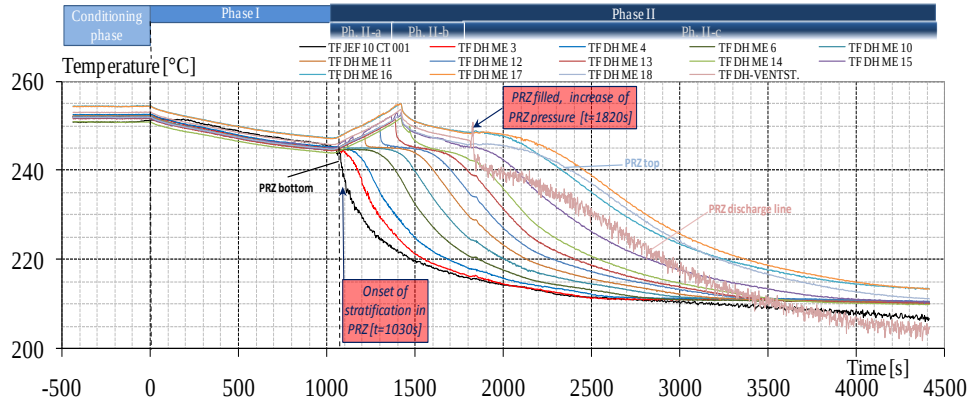

Figure 84 – OECD/NEA/CSNI PKL-2 Project Test G3.1: coolant temperatures in PRZ.

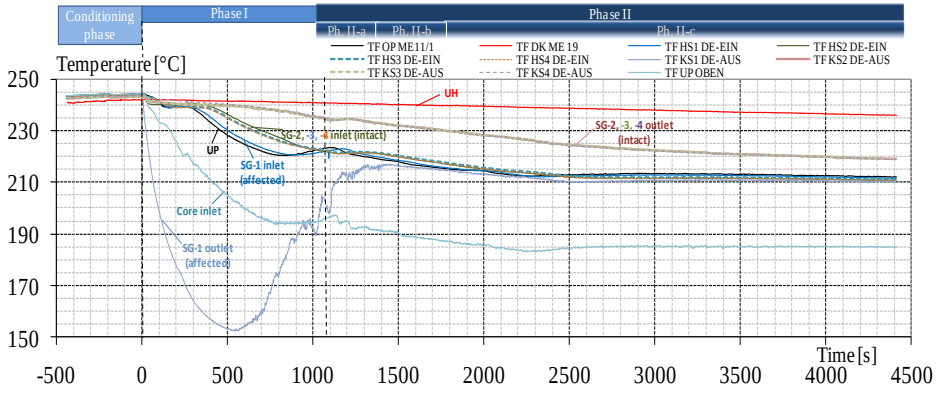

Figure 85 – OECD/NEA/CSNI PKL-2 Project Test G3.1: coolant temperatures in RPV and RCS.

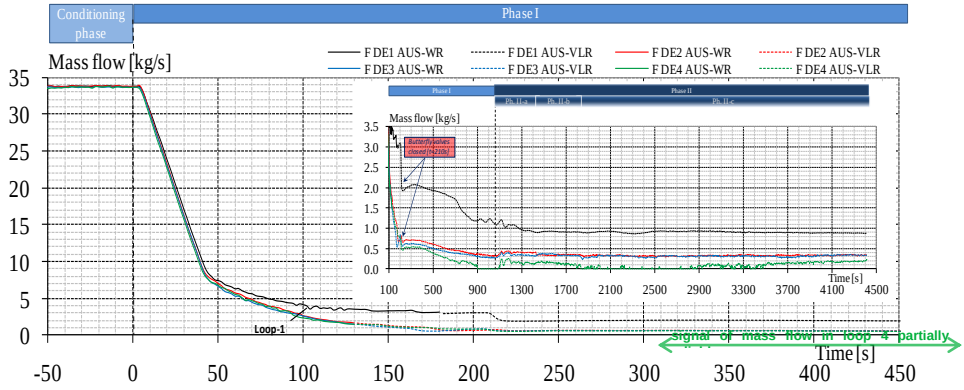

Figure 86 – OECD/NEA/CSNI PKL-2 Project Test G3.1mass flow rates in the loops.

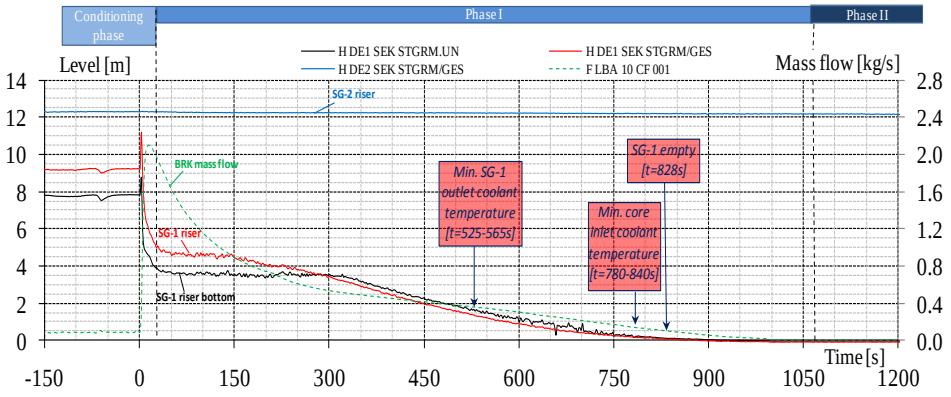

Figure 87 – OECD/NEA/CSNI PKL-2 Project Test G3.1: levels in SG-1, SG-2 and BRK mass flow rate.

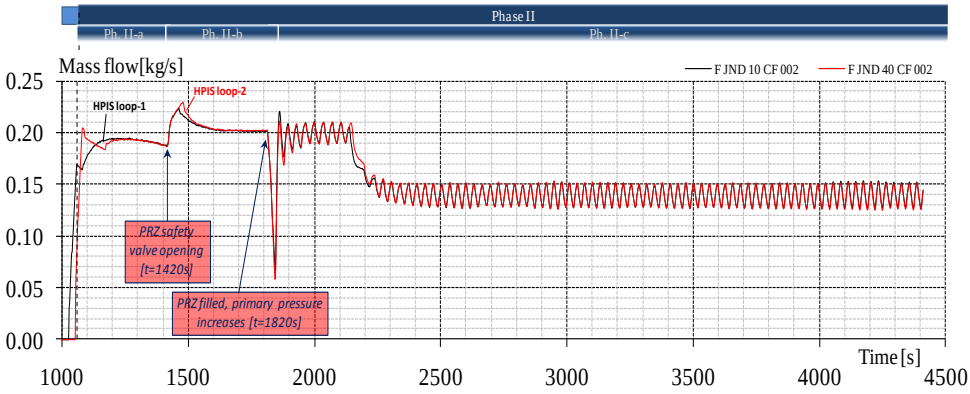

Figure 88 – OECD/NEA/CSNI PKL-2 Project Test G3.1: mass flow rates injected by HPIS in CL-1 and CL-4

6.2. Adopted nodalization for simulating the PKL-III G3.1 test

The PKL facility input deck set up using TRACE-V5 code is described in detail in APPENDIX B. The main features of the nodalization for simulating the test G3.1 deals with the modeling of the steam line and the break orifice, and the simulation of the relief valve. The nodalization of the main steam line, shown in Figure 89, is composed by a pipe component, with the characteristic to preserve the distance from the break systems to affected steam generator (SG 1), and a valve component, that models the orifice. The characterization of the PRZ relief valve behavior is obtained by means a simple trip procedure, shown in Figure 90, , in which we require that the valve open when the pressure in the UP of the 3D vessel component exceed the two pressure set points. These set points represent the two conditions for the opening of the relief valve. In order to realize this control system it is need to utilize three valves: two of these valves are connected in series, in turn connected in parallel with the third.

Ramson-Trapp choked flow model (see [67] and [68]) is activated to simulate the single phase critical flow condition at the throat of the break nozzle.

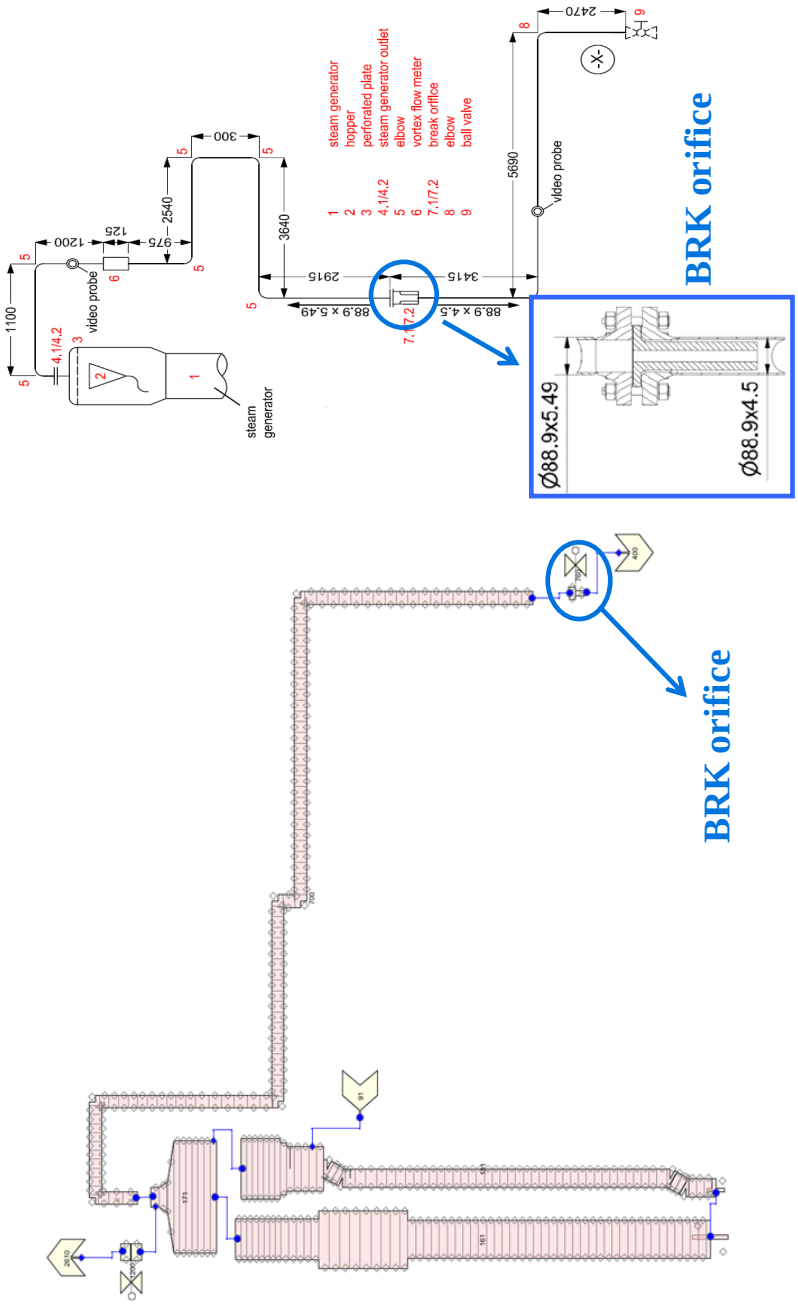

Figure 89 – TRACE model of the main steam line and break orifice

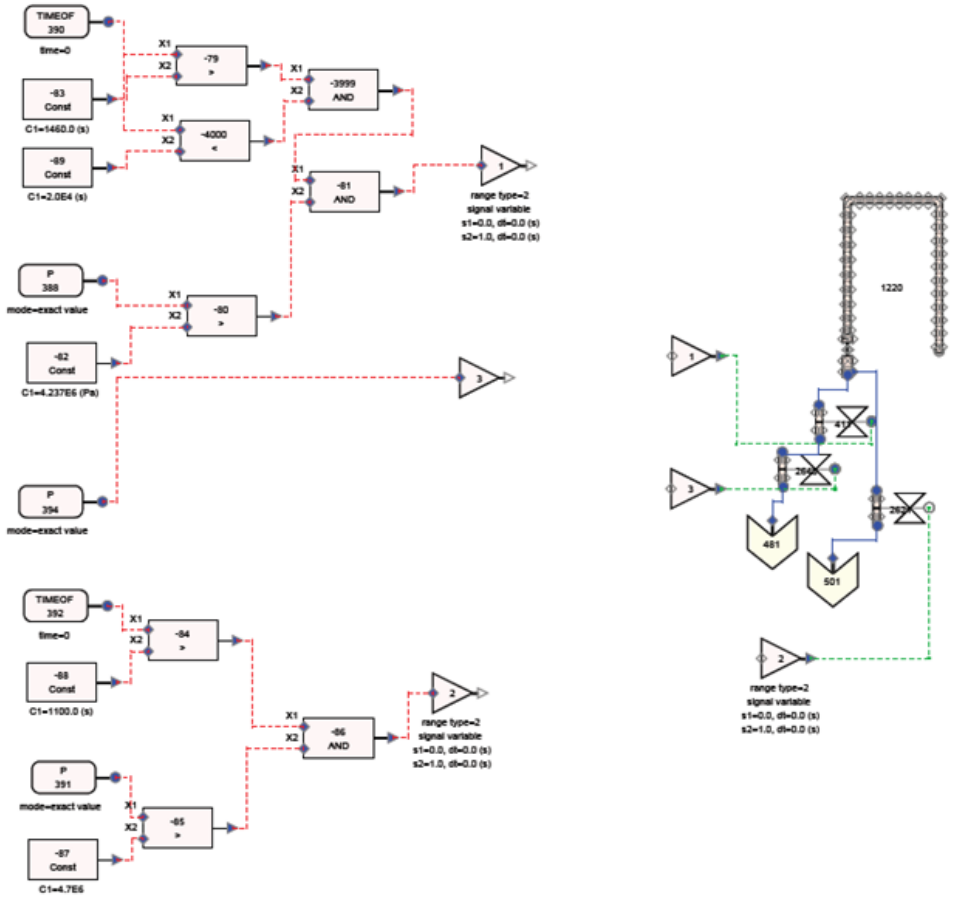

Figure 90 – TRACE model of the relief valve and control systems

6.3. Analysis of the post-test calculation results

6.3.1. Evaluation of steady state results

The nodalization qualification at steady state level is based on the fulfillment of two tasks:

1. the verification and evaluation of the geometrical fidelity of the model developed;
2. the capability of the analytical model to achieve stable steady state with the correct initial conditions as in the experiment.

The first consists (see APPENDIX B) in a systematic comparison between the quantities (i.e. volumes, surfaces, lengths, etc.), which demonstrate the adequacy of the model in representing the real system. The second item above is the properly defined steady state qualification (see also [40]). This step requires the comparisons between experimental measures (or, as in this case, with the design quantities) and the calculated results at the beginning of the transient.

The selection of the key parameters (see Table 23, Table 24 and Table 25) represents the relevant quantities for evaluating the steady state conditions. The tables report the following quantities: the experimental measurements, the codes results including the errors referred to the design data of the test, and the acceptable errors, according with [40]. In the tables, the ID of the measurements are also included for sake of completeness. In principle, the errors should consider the accuracy of the measurement gauges.

Figure 91 provides the pressure drops along the primary system. The experimental data are available across the MCP, thus representing the overall pressure drop across the RPV and RCS. The measures in other positions are not reported because their values are outside of the measurement range of the gauges.

The initial conditions of the test are achieved in “quasi” steady state. According with the specifications of the test, the energy balance of the facility causes an increase of the primary coolant temperature with a rate equal to 12 °C/h. Indeed, the secondary system (all SG) is isolated by means of the closure of the steam isolation valves. The feed water system is off and the natural circulation occurs in three out of four SG. The affected SG, having lower collapsed level, has the circulation between the riser and the downcomer interrupted, thus resulting in stratified conditions in the downcomer with lower coolant temperature in the bottom.

Table 23 – PKL Test G3.1 posttest: steady state results (part 1 of 3)

#	QUANTITY	ID	Unit	Y_{DESIGN}	Y_{EXP}	TRACE-V5 Y_{calc} (Er)[£]	Acc. ε °°
1	**PRIMARY CIRCUIT POWER BALANCE**						**2 %**
1-1	Core thermal power	PEL INNERE ZONE NEU PEL MITTLERE ZONE N PEL AEUSSERE ZONE N	kW	260	52.39 97.30 110.91	259.9 (0.0%)	
1-2	PRZ heaters thermal power	PEL DH STUETZHEIZ PEL RDBSTUETZHEIZ PEL DH BYPASSH	kW	12	0.01 1.07 11.89	--	
2	**SECONDARY CIRCUIT POWER BALANCE**						**2 %**
2-1	SG-1 power exchanged		kW	NA	NA	48	
2-2	SG-2 power exchanged		kW	NA	NA	44.16	
2-3	SG-3 power exchanged		kW	NA	NA	41.64	
2-4	SG-4 power exchanged		kW	NA	NA	42.47	
3	**ABSOLUTE PRESSURE**						**0.1 %**
3-1	PRZ (top of the PRZ)	P DH MB 50	MPa	4.2	4.15	4.11 (1.0%)	
3-2	Upper plenum pressure	P RDB OP	MPa	4.2	4.21	4.21 (0.0%)	
3-3	SG-1 exit (top of the SG)	P DE1 SEK MB 50	MPa	3.5	3.50	3.52 (0.6%)	
3-4	SG-2 exit (top of the SG)	P DE2SEK	MPa	3.5	3.51	3.51 (0.0%)	
3-5	SG-3 exit (top of the SG)	P DE3 SEK	MPa	3.5	3.51	3.50 (0.3%)	
3-6	SG-4 exit (top of the SG)	P DE4 SEK	MPa	3.5	3.52	3.50 (0.6%)	
4	**COOLANT TEMPERATURE**						**0.5 %**
4-1	Core inlet (lower plenum top)		°C	NA	244.1	243.94 (0.1%)	
4-2	Core outlet (upper plenum)		°C	246	244.5 243.5 243.3 243.4	244.07 (0.2%)(&)	
4-3	Core outlet (upper plenum)	TF OP ME11/1 TF OP ME11/2 TF OP ME11/3 TF OP ME11/4	°C	246	244.5 243.5 243.3 243.4	244.07 (0.2%)[(&)]	
4-4	Upper head	TF DK ME 17/2 TF DK ME 19	°C	--	241.5 241.7	243.12 (0.6%)[(&)]	
4-5	SG-1 DC pipe bottom (top)	TFDE1DC(1-2)UN-SEK	°C	200 (210)	202-194 (220-210)	209.5 (3.7%)[(&)]	
4-6	SG-2 DC pipe bottom	TFDE2DC(1-2)UN-SEK	°C	240	237-240 (237-238)	239.1 (0.4%)[(&)]	
4-7	SG-3 DC pipe bottom	TFDE3DC(1-2)UN-SEK	°C	240	243-238 (238-239)	235.6 (1.0%)[(&)]	
4-8	SG-4 DC pipe bottom	TFDE4DC(1-2)UN-SEK	°C	240	241-241 (241-241)	236.0 (2.1%)[(&)]	

Table 24 – PKL Test G3.1 posttest: steady state results (part 2 of 3)

#	QUANTITY	ID	Unit	Y_{DESIGN}	Y_{EXP}	TRACE-V5 Y_{calc} (Er)[£]	Acc. ε °°
5	**ROD SURFACE TEMPERATURE**						**2 %**
5-1	Max clad temp. / Height with ref. to BAF	TW I12/7 TW K10/6 TW M9/7 TW T11/7	°C/m	NA	241.9 242.7 242.3 242.2	244.48 / 5.58 (1.78°C)[(&)]	
6	**PUMP VELOCITY**						**2 %**
6-1	MCP-1		rpm	2500	*2523*	2500 (0.0%)	
6-2	MCP-2		rpm	2500	*2496*	2500 (0.0%)	
6-3	MCP-3		rpm	2500	*2537*	2500 (0.0%)	
6-4	MCP-4		rpm	2500	*2512*	2500 (0.0%)	
7	**HEAT LOSSES (@ nominal steady state conditions)**						**0.1 %**
7-1	RPV vessel (@ nominal steady state)		kW	5.0	--	46.22	
7-2	LOOPs (@ nominal steady state)		kW	6.0	--	27.61	
7-3	MCP (@ nominal steady state)		kW	6.0	--	13.56	
7-4	PRZ and surge line (@ nominal steady state)		kW	25.0	--	1.98	
7-5	SG secondary side (@ nominal steady state)		kW	9.0	--	54.14	
8	**MASS INVENTORY IN PRIMARY CIRCUIT**						**0.5 %**
8-1	PMI (with PRZ and without ACCs)		kg	NA	*NA*	2443	
9	**FLOW RATES**						**0.5 %**
10-1	CL 1 mass flow rate	F DE1 AUS-WR	kg/s	34	*33.7*	33.41 (0.87%)	
10-2	CL 2 mass flow rate	F DE2 AUS-WR	kg/s	34	*33.7*	33.42 (0.84%)	
10-3	CL 3 mass flow rate	F DE3 AUS-WR	kg/s	34	*33.6*	33.36 (0.72%)	
10-4	CL 4 mass flow rate	F DE4 AUS-WR	kg/s	34	*33.5*	33.44 (0.18%)	

Table 25 – PKL Test G3.1 posttest: steady state results (part 3 of 3)

#	QUANTITY	ID	Unit	Y_{DESIGN}	Y_{EXP}	TRACE-V5 Y_{calc} (Er)[£]	Acc. ε °°
11	**BYPASS MASS FLOW RATES**						**2 %**
11-1	Core bypass	--	kg/s	--	--	1.25	
11-2	DC-UH bypass	--	kg/s	--	--	0.63	
12	**PRESSURIZER LEVEL**						**2 %**
12-1	PRZ level (collapsed)	H JEF 10 CL 001	m	7.4	--	7.48 (0.08m)	
13	**SECONDARY SIDE COLLAPSED LEVEL**						**0.1 %**
13-1	SG-1 DC (Riser)	H DE1SEKSTGRM/GES (H JEA 10 CL851)	m	8.8 (9.2)	*8.83* *(9.22)*	8.87 (0.04m) (9.21 (-0.01m))	
13-2	SG-2,3,4 DC (Riser)	H DE2-4SEKSTGRM.UN (H JEA 20-40 CL851)	m	12.3 (12.3) 12.3 (12.2) 12.5 (12.2)	*12.3 (12.3)* *12.3 (12.2)* *12.5 (12.2)*	12.4 (0.1m) 12.3 (0.1m) 12.3 (0.1m)	
14	**SPECIFIC G3.1**						**0.5 %**
14-1	Coolant temperature increase @ core outlet		°C/h			12	

(£) The % error is defined as the ratio |*reference design value– calculated value*|/*reference design value*. The "dimensional error" is the numerator of the above expression. The error is evaluated against the Y_{DESIGN} data

(££) Including FW lines.

(£££) Heat loss has been corrected to achieve the appropriate heat-up rate of 12 K/h.

(*) Heaters in PRZ not active. Heat losses not simulated in order to achieve the energy balance in the PRZ.

(°°) The "acceptable error" is defined according with [40]

(°°°) The code model does not take into account for the heat losses in the PRZ

(^) Regulated on the basis of the SG level and the steam flow.

(^^) And consistent with other errors.

(^^^) And consistent with power error. The errors are calculated in °C.

(*) Not installed.

(**) Steam line and feed water system closed.

(***) Value is obtained by 10.8 kW (heaters them self) + 2kW directly released to the coolant

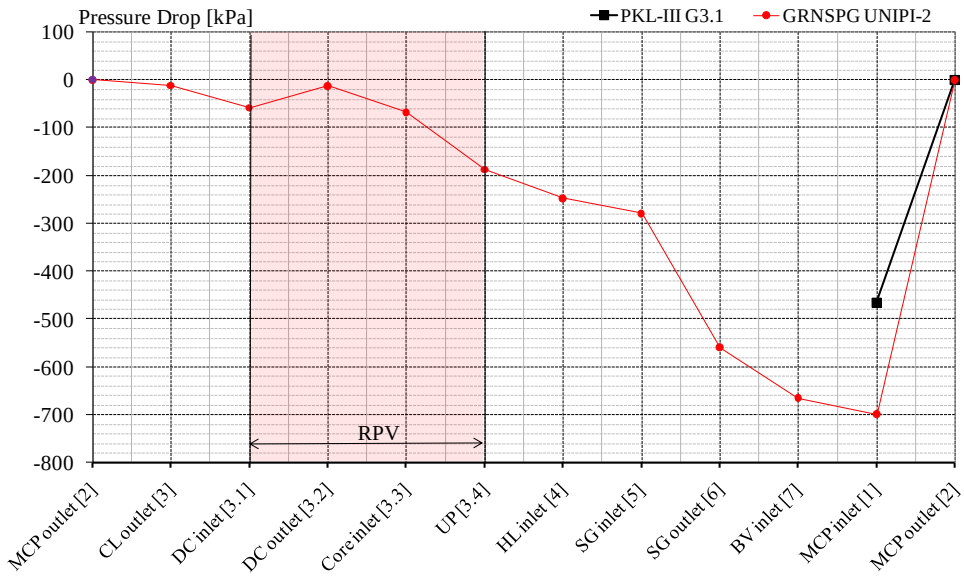

Figure 91 – PKL Test G3.1: primary system pressure drop vs. length

6.3.2. Comparison and evaluation of reference results

The comparisons between the experimental data and the calculated results are carried out with the objective of verifying if the code simulations are capable to reproduce the relevant thermal-hydraulic phenomena, processes and to provide a reliable estimation of the parameters relevant for safety analysis. A comprehensive comparison between measured and calculated trends or values is performed, including the following steps:

- qualitative evaluation (section § 6.3.1) of the results by making:
  - the comparisons between the resulting sequence of main events, section § 6.3.1.1,
  - the comparisons between experimental and calculated time trends on the basis of the selected variables, section § 6.3.1.26.3.2.1.2, and
  - the qualitative evaluation of calculations accuracies on the basis of the Relevant Thermal-hydraulic Aspects (RTA), see section § 6.3.1.3;
- quantitative accuracy evaluation by using the FFTBM, section § 6.3.2.

6.3.2.1. Qualitative accuracy evaluation

6.3.2.1.1. Table of resulting sequence of main events

Table 26 reports the list of the relevant events and the timing of their occurrences. These timings are compared with the corresponding values observed in the experiment. The considerations on the results are summarized hereafter.

- The SG-1 level is reasonably well simulated by the code. In fact the calculated level has good accuracy of the timing.
- The code predict correctly the depressurization of the affected steam generator.
- The minimum PRZ level occurrence is well calculated by code.
- The occurrence of the minimum coolant temperature at SG outlet and at core inlet is well predicted by TRACE-V5 code.
- An anticipated PRZ valve opening in the simulation is observed, which is connected with the phenomena occurring in the PRZ during the filling up besides the heat losses.
- The pressurizer filling and the start of water discharge through the PRZ safety valve is predicted reasonably well by TRACE-V5 code.

6.3.2.1.2. Selected time trends

For the qualitative analysis, 20 parameters are selected on the basis of the consideration that these time trends are evaluated as the minimum number of quantities that fully describe the experimental scenario and the code performances.

The analytical behavior of the primary pressure is shown in Figure 92. The simulation is qualitatively well predicted during the first phenomenological phase (occurrence of the main steam line break). In the temporal window that goes from the activation of the HPIS to the opening of the PRZ-safety (1030s to 1420s), the pressurization of the primary system simulated by the code is in agreement with the experimental pressure trend. Once the set point of the PRZ safety valve opening is reached (steam released), the pressure decrease part of the calculated upper plenum pressure trend is mainly affected by the different operation of the safety valve with respect to the experiment (have not been supply enough information on the geometrical characteristics of the valve). In fact the incorrect setting of the flow area fraction of the PRZ relief valve in the TRACE model causes a greater energy release the effect of which is reaching of the minimum value of the UP pressure (when the PRZ is completely filled with water) lower than the experimental value. The blowdown of the SG-1 is well predicted by the code simulation (see Figure 93). The trend of the pressure in the intact SG (see Figure 94 in which is depicted the pressure trend in the SG 4) is driven by the set up of the heat losses in the secondary side and the heat exchange between primary and secondary systems of the corresponding loops.

The coolant temperature in the lower plenum is qualitatively well predicted (see Figure 95). The calculated minimum core inlet temperature is in a range of ±10 °C, besides the occurrence of core inlet temperature, during the Phase I of the test, is delayed in the simulation with respect to the experiment. The quantitative discrepancies among the analytical parameter and the experimental datum are a consequence of the energy imbalance between the core power, heat losses and the primary to secondary heat exchange. This is particularly evident in last phase of the transient (between 2500 s and the EoT) in which the experimental datum is approximately constant, while the calculated value decreases progressively. considerations are applied to the trends of the coolant temperature in upper plenum (see Figure 96).

A relevant parameter, whose correct simulation is one of the objectives of the test, is represented by the CL coolant temperature at SG-1 outlet. Indeed, it is connected with the depressurization of the affected SG, the primary to secondary heat exchange, and drives the natural circulation in the loop. The posttest calculation provides satisfactory prediction of the parameter trend (see Figure 97). The CL coolant temperature at SG-4 outlet (Figure 98) is mainly well represented by the code but showing slightly faster cool-down rate compared to the experimental trend.

Figure 100, Figure 101, Figure 102 and Figure 103 show the calculated mass flow rates in the loops compared with the experimental data. From the beginning of the transient up to about 160 s the mass flow rate is mainly driven by the MCP rotation. The coastdown is provided in the specifications as boundary condition and it is set up correctly. As soon as the MCPs are stopped, the single phase NC (natural circulation) drives the mass flow in the primary system. It derives from the balance between driving and resistant forces. Driving forces are the result of fluid density differences occurring between descending side of U-tubes and DC vessel (“cold side”) and core zone and ascending side of U-tubes (“hot side”). Resistant forces are due to irreversible friction pressure drops along the entire loop. The simulations provide good predictions of the NC in the affected loop (Figure 100). Finally, the prediction of the NC by the code in the intact loops shows a qualitatively agreement with the experimental data (Figure 101, Figure 102 and Figure 103).

The mass flow rate throughout the break (in the SG1) during the break discharge phenomenon is simulated by the TRACE-V5 code using the single-phase vapor choked flow model based on isentropic expansion of an ideal gas. To account for any geometry effects, the TRACE-V5 choked-flow model allows the user to input two different coefficients in order to achieve the correct fluid flow through the break, namely subcooled multiplier and two-phase multiplier ([71]). These values are gain factors applied to the respective equations depending on the regime at the throat of the break. In the case of MSLB, single-phase vapor flows throughout the break. Therefore, when addressing this kind of scenario using TRACE-V5, there is no coefficient to adjust the choked flow under single-phase vapor. The two coefficients available in TRACE-V5 were tuned for the presented transient using the value 1.0 for liquid phase and 1.1 (which are the same values used for simulating the test G7.1). In general, the parameter trend is well simulated by the code. The code overestimates the maximum break mass flow rate; afterwards the mass flow is underestimated during the first phase of the break discharge, with the result of an overestimation of the affected SG collapsed level.

The evaluation of the integral break mass flow rate is reported in Figure 111. This parameter is not directly measured but calculated by means of integrating the experimental break mass flow rate. The comparisons of the analytical result with the experiment shows that TRACE-V5 code underestimate the integral break flow in the first phase of the transient (mainly due to the initial mass flow rate spike) and is underestimate, but quite reasonably predicted, during the overall transient.

The parameters depicted in figures from Figure 105 to Figure 107 are the pressure drops across the RPV, the SG-1 and 4 primary side. The measurements of the pressure drop in the primary system are not reliable for about 40 s from SoT because the signal exceeds the upper limit of the measurement range. Then,

following the MCP coast down, the mass flow rate in the primary system decreases and reaches the values at which the experimental data are meaningful for the comparisons.

The RPV pressure drop is well predicted in the simulation, but, as a consequence of non correct setting of energy loss coefficient (user effect) in RPV, a constant spread is observed in the computational trend. The pressure drop across the SG U-tubes (primary side) is rather well predicted by the computational model in the affected and the intact loops with some differences with respect to the experimental data observed in the Phase I of the transient.

The comparison between experimental and TRACE results of the PRZ, SG-1 and SG-2 riser level trends are shown in Figure 108 , Figure 109 and in Figure 110. The PRZ level is driven by the primary system cooldown during the first phase and by the ECCS injection during the second phase. The simulation is consistent with the experimental result. Regarding the level in the affected SG the results show a qualitative agreement with the experiment.

The calculated cladding temperature trend in Figure 112 is compared with the experimental value at the elevation where the maximum temperature is recorded. No DNB conditions are met; therefore the cladding temperature is driven by the forced convective heat transfer regime and the coolant temperature.

6.3.2.1.3. Qualitative accuracy evaluation of the RTA

The qualitative accuracy evaluation is based upon a procedure consisting in the identification of phenomena and RTA (see [70]).It essentially derives from a visual observation of the experimental and predicted trends discussed section

The related results are reported in Table 27, Table 28 and Table 29. The parameters characterizing the RTA (i.e., SVP = Single Valued Parameter, TSE = parameter belonging to the Time Sequence of Events, IPA= Integral Parameter and NDP = Non Dimensional Parameter) are used for evaluating the accuracy of the code simulations form a qualitative point of view.

6.3.3. Quantitative accuracy evaluation by the Fast Fourier Transform Based Method

The so called Fast Fourier Transform Based Method (see [71]) is used for the quantification of the accuracy of the code results. This tool gives an accuracy coefficient (AA) and a weighted frequency (WF) for each variable and for the overall transient. Roughly, the value assumed by AA represents the error in the calculation of the considered variable. The WF factor provides information whether the calculated discrepancies, between the measured and calculated trends, are more important at low frequencies (small value of WF) or high frequencies (large value of WF). In this last case, it can be stated that the discrepancies come from various kinds of noise and so it is less important.

Table 30 and Table 31 summarize the results for the Phase I and the overall transient. The tables include the detail of the parameters selected for the application of the FFTBM, the labels that identify the parameters in the experimental database, the values of the accuracy and of the weighted frequency

for the code run. In Figure 113 and Figure 114 the results of the total average amplitude compared in the framework of the benchmark activity are depicted.

There are 23 selected parameters. They are selected as the minimum number necessary to describe the transient, considering both the peculiarities of the transient and the availability of the experimental data as well. These parameters are then combined to give an overall picture of the accuracy of a given calculation. The total average amplitude of the transient is the result of the sum of all the average amplitudes with their "weights".

The "weight" of each contribution is dependent by the experimental accuracy, the relevance of the addressed parameter, and a component of normalization with reference to the average amplitude evaluated for the primary side pressure. The figure of merit of the method is usually consists of three values: the average amplitudes of the 1) primary pressure and of the 2) global (or total) response, consistently with the typical application of the method, plus the 3) coolant temperature at the affected SG outlet, due to the peculiarity of the test.

Table 26 – PKL Test G3.1, posttest results: resulting sequence of main events.

#	EVENT DESCRIPTION	EXP (sec)	TRACE-V5	Note
1	Start of transient (break opening) in SG #1 steam line	0	0	Imposed
2	Heaters in SG#1 switched off	0	0	Imposed
3	Trip of the MCP and coastdown	0	0	Imposed
4	PRZ heaters switched off	0	0	Imposed
5	Butterfly valves closure	210	210	Imposed
6	MCPs completed stopped	210	210	Imposed
7	Affected SG level lower than < 8.0m	6.4	9	
8	Affected SG level lower than < 5.0m	32	175	
9	Affected SG level lower than < 2.5m	393	422	
10	Affected SG level lower than < 1.0m	579	612	
11	Affected SG level lower than < 0.1m (emptied)	828	819	
12	Affected SG pressure lower than <3.0MPa	10.4	10	
13	Affected SG pressure lower than <2.0MPa	47	49	
14	Affected SG pressure lower than <1.0MPa	164	177	
15	Affected SG pressure lower than <0.5MPa	435	404	
16	Minimum PRZ level	819	806	
17	Minimum mass flow rate in loop 2 to 4	1060	NA	
18	Minimum coolant temperature in CL#1 (Phase 1)	525-565	608	
19	Minimum core inlet temperature (Phase 1)	780-840	867	
20	HPIS activated in loop #1 and 4 (0.2kg/s)	1030	1030	Imposed
21	Maximum temperature difference across SG #1 (Phase 1)	380-420	369	
22	PRZ safety valve 1st opening (steam released)	1420	1378	Steam discharged
23	Water released through the PRZ safety valve	1840	1887	
24	End of calculation	4410	4410	

Table 27 – PKL Test G3.1, posttest results: qualitative accuracy evaluation on the basis of RTA (part 1 of 3)

#	PARAMETER	TYPE	UNIT	EXP	TRACE-V5	
					Value	J
1	**RTA: BREAK FLOW RATE BEHAVIOR**					
1-1	MAX BRK mass flow rate	SVP	kg/s	2.06	2.48	R
1-2	MAX DP across the orifice	SVP	kPa	2520	3429	M
1-3	Integral BRK flow rate at P_{SG1}=3.0MPa	IPA	kg	31	21	R
1-4	Integral BRK flow rate at P_{SG1}=2.0MPa	IPA	kg	108	97	E
1-5	Integral BRK flow rate at P_{SG1}=1.0MPa	IPA	kg	245	423	M
1-6	Integral BRK flow rate at end of transient	IPA	kg	522	475	R
*1-7**	BRK flowrate (P_{SG1}=2.0MPa) / MAX BRK flow rate	*NDP*	--	*0.81*	*0.64*	*R*
*1-8**	BRK flowrate (P_{SG1}=1.0MPa) / MAX BRK flow rate	*NDP*	--	*0.41*	*0.28*	*M*
1-9	Time of BRK mass flow lower than 0.15 kg/s	TSE	s	768	784	E
*1-10**	Time of BRK mass flow rate ends (MF<0.01 kg/s)	*TSE*	*s*	*993*	*908*	*E*
2	**RTA: PRZ BEHAVIOR**					
2-1	Minimum PRZ level	SVP	m	4.24	4.09	E
2-2	PRZ level when ECCS is activated	SVP	m	4.47	4.33	E
2-3	PRZ level when safety valve is opened	SVP	m	8.56	7.92	R
*2-4**	*Mass flow rate through the SV at EoT*	*SVP*	*kg/s*	--	*0.26*	--
2-5	PRZ pressure (t of min PRZ lev) / PRZ pressure (t=0s)	NDP	--	0.88	0.90	E
2-6	PRZ pressure (t =1000s) / PRZ pressure (t=0s)	NDP	--	0.88	0.89	E
2-7	Time of safety valve opening	TSE	s	1420	1378	E
2-8	Time of MIN PRZ level	TSE	s	819	806	E

Table 28 – PKL Test G3.1, posttest results: qualitative accuracy evaluation on the basis of RTA (part 2 of 3)

#	PARAMETER	TYPE	UNIT	EXP	TRACE-V5	
					Value	J
3	**RTA: AFFECTED SG-1 BEHAVIOR**					
3-1	SG-1 pressure (t=10s) / SG-1 pressure (t=0s)	NDP	--	0.86	0.81	E
3-2	SG-1 pressure (t=50s) / SG-1 pressure (t=0s)	NDP	--	0.56	0.51	E
3-3	SG-1 pressure (t=100s) / SG-1 pressure (t=0s)	NDP	--	0.39	0.34	R
3-4	SG-1 pressure (t=200s) / SG-1 pressure (t=0s)	NDP	--	0.25	0.21	R
3-5	Time when SG-1 level equal to 8.0m	TSE	s	6.4	9	R
3-6	Time when SG-1 level equal to 5.0m	TSE	s	32	175	M
3-7	Time when SG-1 level equal to 2.5m	TSE	s	393	422	E
3-8	Time of SG-1 emptying (Lev<0.1m)	TSE	s	828	819	E
4	**RTA: NC BEHAVIOR**					
4-1	Mass flow rate in loop #1 (t=210s)	SVP	kg/s	2.52	2.43	E
4-2	Mass flow rate in loop #4 (t=210s)	SVP	kg/s	0.66	0.97	R
4-3	MAX mass flow rate in loop #1 (210s<t<1000s)	SVP	kg/s	2.07	2.42	R
4-4	MAX mass flow rate in loop #4 (210s<t<1000s)	SVP	kg/s	0.54	0.97	M
*4-5**	*Time when MAX mass flow rate in loop #1 occurs (210s<t<1000s)*	*TSE*	*s*	*210s 320s (4)*	*210*	*E*
*4-6**	*Time when MAX mass flow rate in loop #4 occurs (210s<t<1000s)*	*TSE*	*s*	*210s 320s (5)*	*210*	*E*
*4-7**	*ΔT across SG-1 when MAX mass flow rate in loop #1 occurs (210s<t<1000s)*	*SVP*	*°C*	*63 76 (6)*	*67*	*E*
*4-8**	*ΔT across SG-4 when MAX mass flow rate in loop #4 occurs (210s<t<1000s)*	*SVP*	*°C*	*-2.8 -2.1 (6)*	*-3.6*	*R*
5	**RTA: PRIMARY TO SECONDARY HEAT EXCHANGE**					
5-1	MAX ΔT between SG-1 out – SG-1 inlet	SVP	°C	78.4	82.0	E
5-2*	*Time MAX ΔT across SG-1 occurs (Phase 1)*	*TSE*	*s*	*380 - 420*	*369*	*E*

Table 29 – PKL Test G3.1, posttest results: qualitative accuracy evaluation on the basis of RTA (part 3 of 3)

#	PARAMETER	TYPE	UNIT	EXP	TRACE-V5	
					Value	J
6	**RTA: ECCS BEHAVIOR**					
6-1	Total integral ECCS flow rate when PRZ safety valve is opened	IPA	kg	123.7	123.93	E
6-2	Total integral ECCS flow rate at end of transient ($T_{core\ out}$=213°C)	IPA	kg	937.6	1068	R
7	**RTA: UNAFFECTED SG BEHAVIOR (SG4)**					
7-1	SG-4 pressure (t=10s) / SG-4 pressure (t=0s)	NDP	--	1.00	1.0	E
7-2	SG-4 pressure (t=100s) / SG-4 pressure (t=0s)	NDP	--	0.99	0.996	E
7-3	SG-4 pressure (t=210s) / SG-4 pressure (t=0s)	NDP	--	0.98	0.99	E
7-4	SG-4 pressure (t=1000s) / SG-4 pressure (t=0s)	NDP	--	0.95	0.96	E
7-5	SG-4 pressure (t=EoT) / SG-4 pressure (t=0s)	NDP	--	0.84	0.85	E

1) Reported value corresponds to the experimental peak at around 15 seconds
2) MAX BRK value = 5.6 kg/s derived from the submitted PSI results
3) MAX BRK value = 15.5 kg/s derived from the submitted UPC results
4) The maximum mass flow rate between 210 and 1000s is 2.58 at 210s form SoT. A second local maximum occurs at 320 s (2.12kg/s) with the butterfly valve fully closed.
5) The maximum mass flow rate between 210 and 1000s is 0.66 at 210s form SoT. A second local maximum occurs at 320 s (0.58kg/s) with the butterfly valve fully closed.
6) The first vale is referred to 210 s and the second to 320 s

* Added in the new revision of the output specifications

** Canceled in the new revision of the output specifications

*** Transient affected by imperfect set up of the boundary and initial conditions

Table 30 – PKL Test G3.1, posttest results: summary of results obtained by application of FFTBM – from 0 up to 1030 s

#	PARAMETER		TRACE-V5	
	Description	ID	(0-1030s)	
			AA	WF
1	*UP pressure*	*P RDB OP*	0.011	0.097
2	*PRZ pressure*	*P DH MB 50*	0.013	0.127
3	*SG-1 pressure*	*P DE1 SEK MB 50*	0.048	0.045
4	*SG-4 pressure*	*P DE4 SEK*	0.032	0.113
5	*LP coolant (liquid) temp.*	*TF UP OBEN*	0.065	0.105
6	*UP coolant (liquid) temp.*	*TF OP ME11/1*	0.063	0.101
7	*UH coolant (liquid) temp.*	*TF DK ME 19*	0.089	0.124
8	*PRZ coolant (liquid) temp. (at 1.716m)*	*TF DH ME 3*	0.006	0.106
9	*SG 1 outlet coolant (liquid) temp.*	*TF KS1 DE-AUS*	0.143	0.09
10	*SG 3 outlet coolant (liquid) temp.*	*TF KS2 DE-AUS*	0.034	0.121
11	*SG 1 outlet mass flow*	*F DE1 AUS WR – VR –VLR*	0.030	0.084
12	*SG 2 outlet mass flow*	*F DE4 AUS WR –VR –VLR*	0.028	0.066
13	*Steam line 1 BRK nozzle*	*F LBA 10 CF 001*	0.331	0.092
14	*Integral BRK flow rate*	--	0.036	0.08
15	*DC RPV inlet 1 / outlet 1*	*DP RDB EIN/AUS-1*	0.552	0.114
16	*DP inlet-outlet SG 1 (BL)*	*DP DE1 E/A*	2.214	0.155
17	*DP inlet-outlet SG 4 (IL)*	*DP DE4 E/A*	1.666	0.164
18	*DP across BRK device*	*DP FD-LECK DE10*	0.407	0.135
19	*PRZ collapsed level*	*H JEF 10 CL 001*	0.081	0.136
20	*SG-1 riser collapsed level*	*H DE1 SEK STGRM/GES*	0.187	0.096
21	*SG-1 DC collapsed level*	*H JEA 10 CL 851*	0.242	0.101
22	*SG-2 riser collapsed level*	*H DE2 SEK STGRM/GES*	0.046	0.083
23	*Hottest cladding temp.*	*TW K10/6*	0.045	0.068
TOTAL AVERAGE ACCURACY		***Total (23 parameters)***	**0.129**	**0.103**

Table 31 – PKL Test G3.1, posttest results: summary of results obtained by application of FFTBM – overall transient

#	PARAMETER		TRACE-V5	
	Description	ID	(0-4410s)	
			AA	WF
1	*UP pressure*	*P RDB OP*	**0.317**	**0.035**
2	*PRZ pressure*	*P DH MB 50*	**0.322**	**0.033**
3	*SG-1 pressure*	*P DE1 SEK MB 50*	0.053	0.033
4	*SG-4 pressure*	*P DE4 SEK*	0.033	0.062
5	*LP coolant (liquid) temp.*	*TF UP OBEN*	0.147	0.056
6	*UP coolant (liquid) temp.*	*TF OP ME11/1*	0.142	0.057
7	*UH coolant (liquid) temp.*	*TF DK ME 19*	0.436	0.054
8	*PRZ coolant (liquid) temp. (at 1.716m)*	*TF DH ME 3*	0.119	0.056
9	*SG 1 outlet coolant (liquid) temp.*	*TF KS1 DE-AUS*	0.171	0.053
10	*SG 3 outlet coolant (liquid) temp.*	*TF KS2 DE-AUS*	0.107	0.053
11	*SG 1 outlet mass flow*	*F DE1 AUS WR – VR –VLR*	0.033	0.066
12	*SG 2 outlet mass flow*	*F DE4 AUS WR – VR –VLR*	0.033	0.048
13	*Steam line 1 BRK nozzle*	*F LBA 10 CF 001*	0.322	0.073
14	*Integral BRK flow rate*	*--*	0.036	0.032
15	*DC RPV inlet 1 / outlet 1*	*DP RDB EIN/AUS-1*	0.482	0.058
16	*DP inlet-outlet SG 1 (BL)*	*DP DE1 E/A*	1.736	0.078
17	*DP inlet-outlet SG 4 (IL)*	*DP DE4 E/A*	1.610	0.084
18	*DP across BRK device*	*DP FD-LECK DE10*	0.421	0.081
19	*PRZ collapsed level*	*H JEF 10 CL 001*	0.096	0.078
20	*SG-1 riser collapsed level*	*H DE1 SEK STGRM/GES*	0.201	0.079
21	*SG-1 DC collapsed level*	*H JEA 10 CL 851*	0.249	0.081
22	*SG-2 riser collapsed level*	*H DE2 SEK STGRM/GES*	0.104	0.049
23	*Hottest cladding temp.*	*TW K10/6*	0.114	0.06
TOTAL AVERAGE ACCURACY		***Total (23 parameters)***	**0.226**	**0.054**

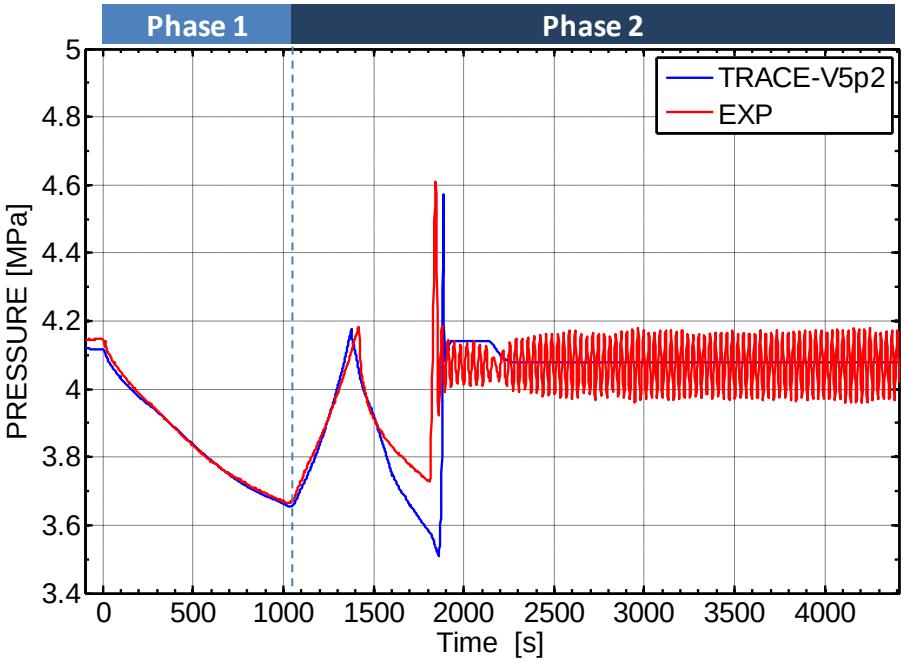

Figure 92 – PKL Test G3.1, posttest results: PRZ pressure trends

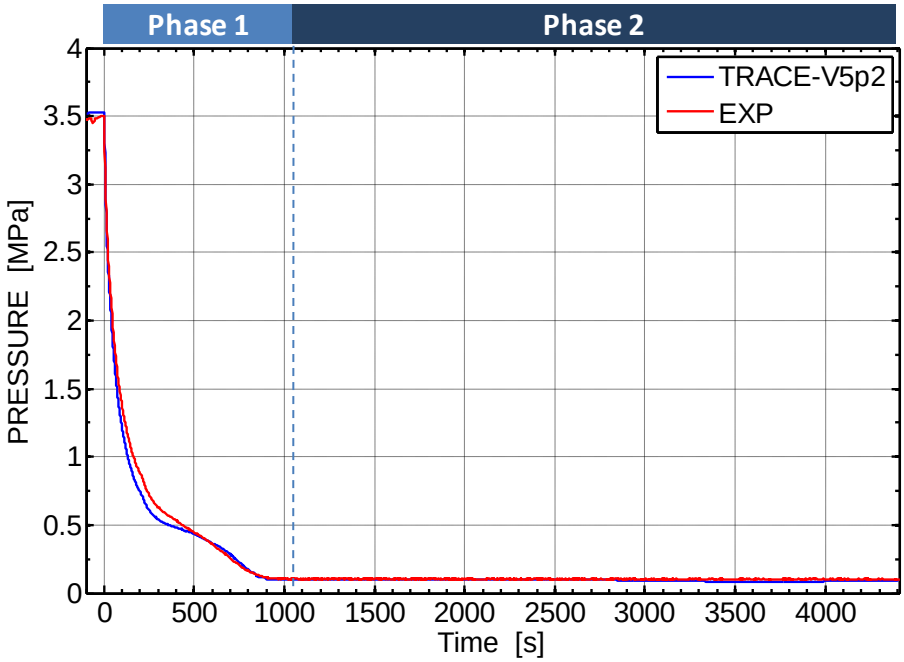

Figure 93 – PKL Test G3.1, posttest results: SG-1 pressure trends

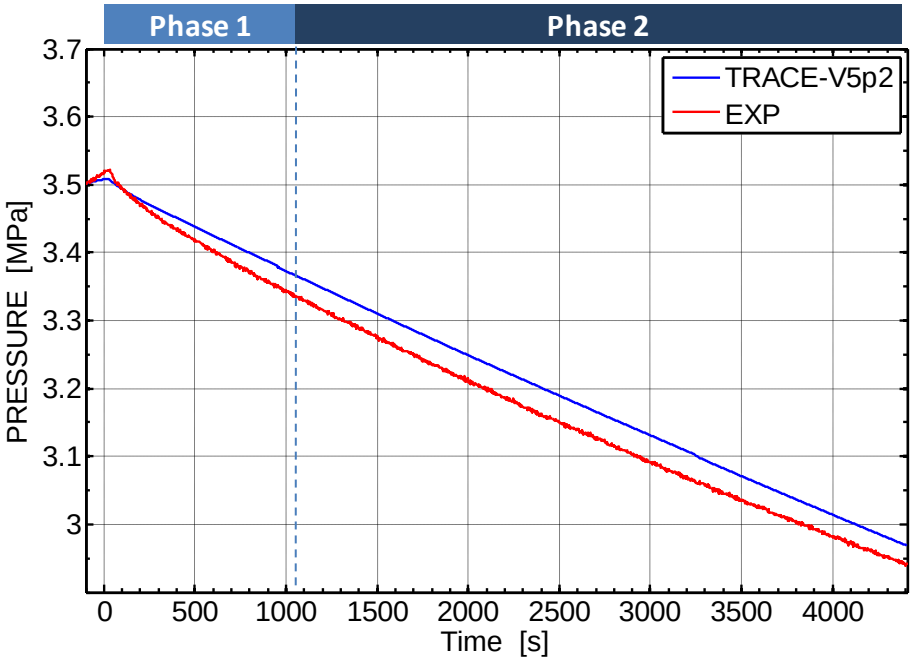

Figure 94 – PKL Test G3.1, posttest results: SG-4 pressure trends

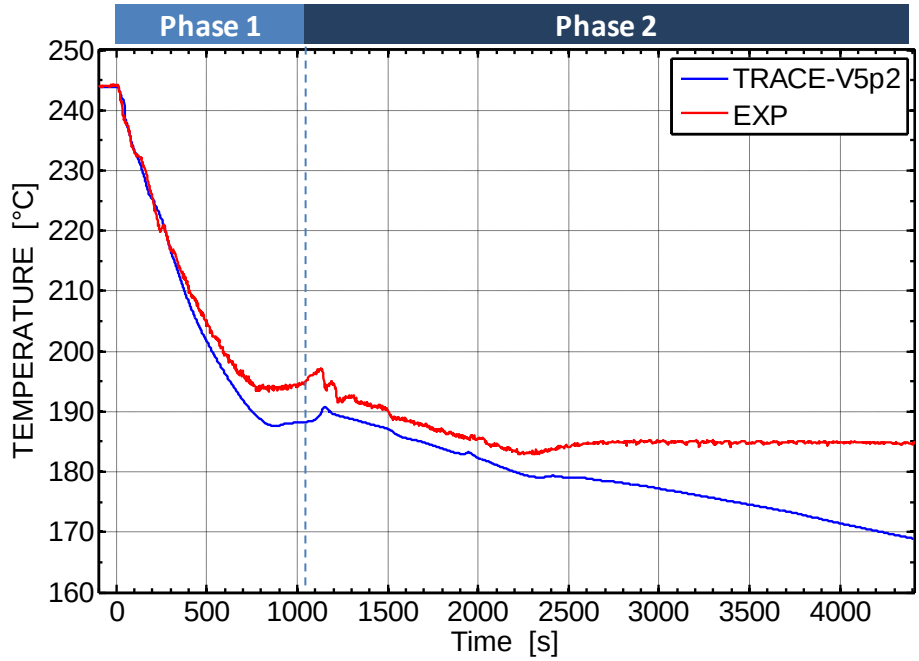

Figure 95 – PKL Test G3.1, posttest results: LP coolant temperature trends

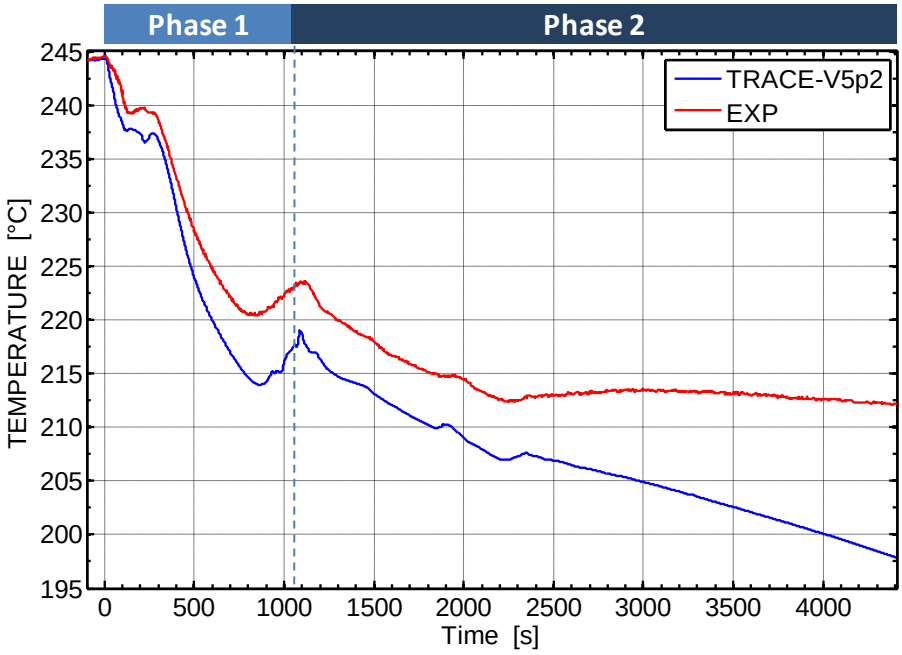

Figure 96 – PKL Test G3.1, posttest results: UP coolant temperature trends

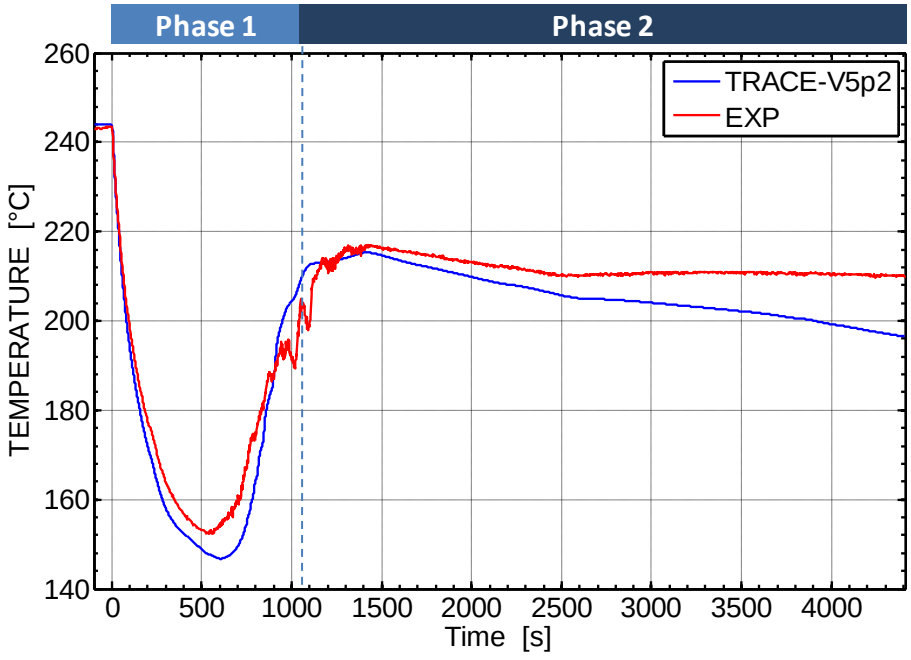

Figure 97 – PKL Test G3.1, posttest results: CL 1 SG outlet coolant temperature trends

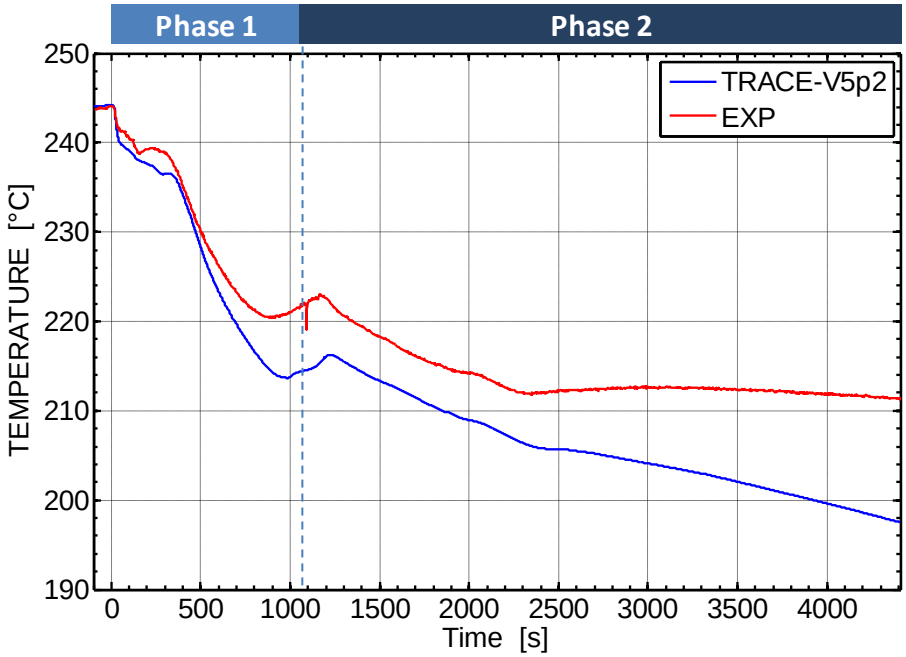

Figure 98 – PKL Test G3.1, posttest results: CL 4 SG outlet coolant temperature trends

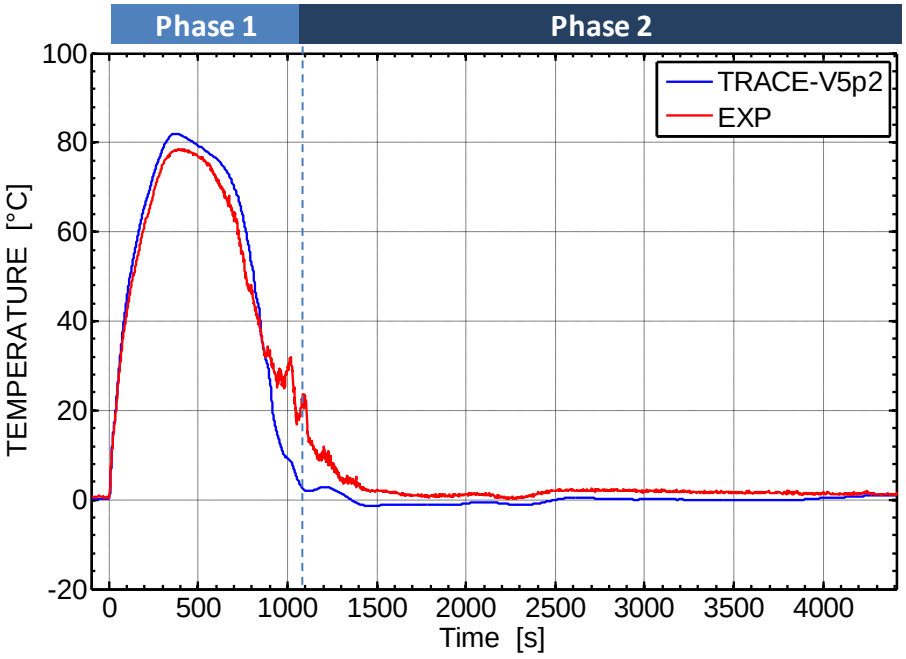

Figure 99 – PKL Test G3.1, posttest results: differential temperature SG 1 inlet/outlet

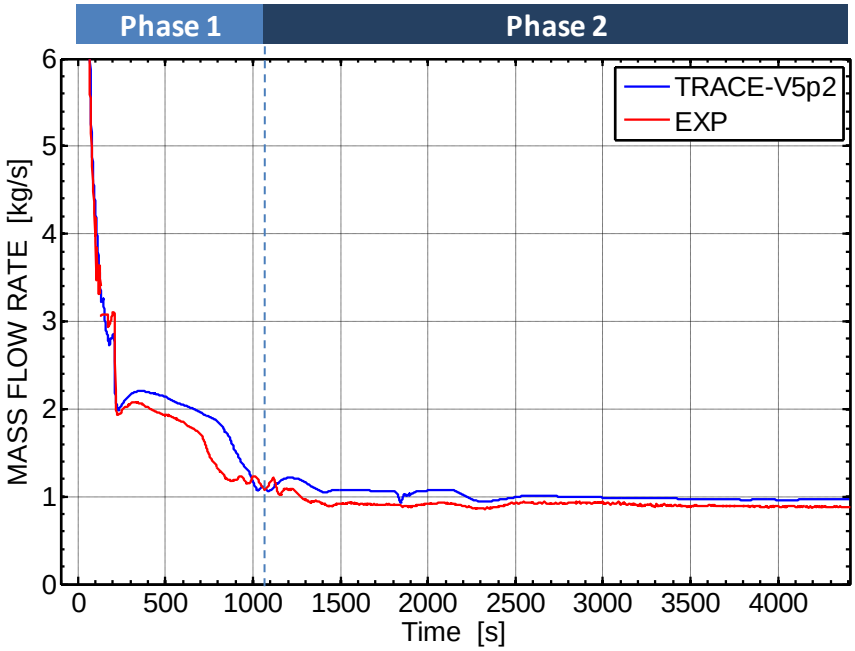

Figure 100 – PKL Test G3.1, posttest results: loop 1 SG outlet mass flow rate trends (-100 – 4410 s)

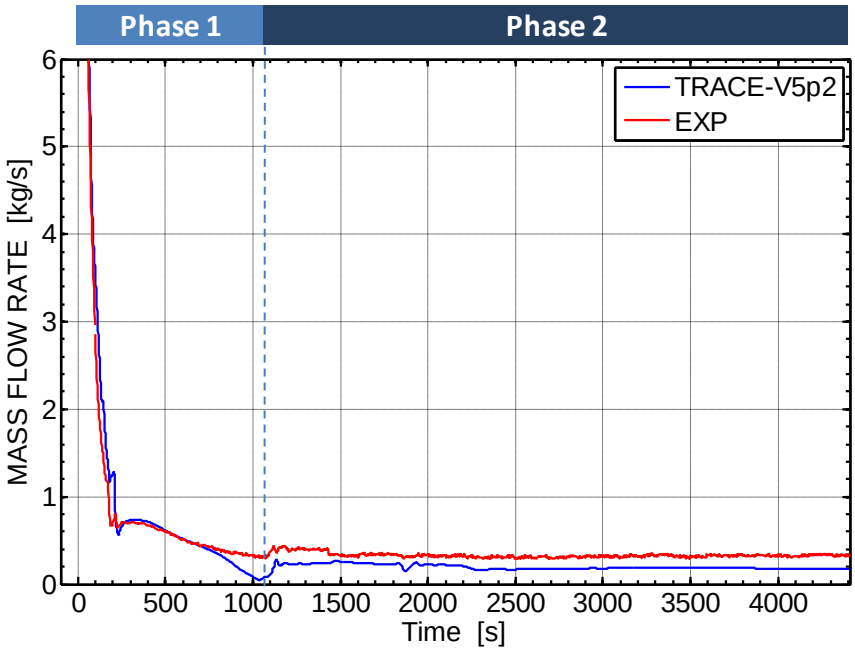

Figure 101 – PKL Test G3.1, posttest results: loop 2 SG outlet mass flow rate trends (-100 – 4410 s)

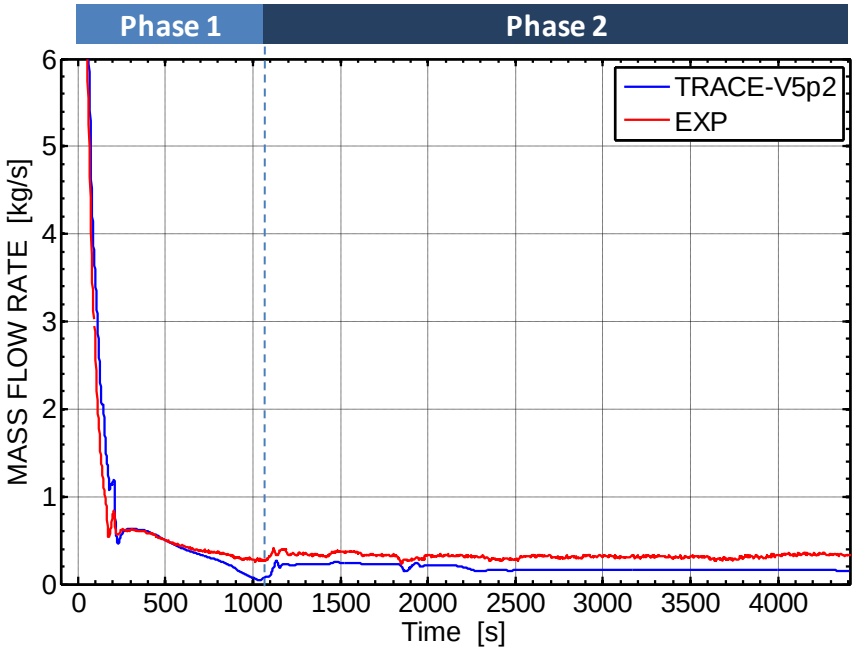

Figure 102 – PKL Test G3.1, posttest results: loop 3 SG outlet mass flow rate trends (-100 – 4410 s)

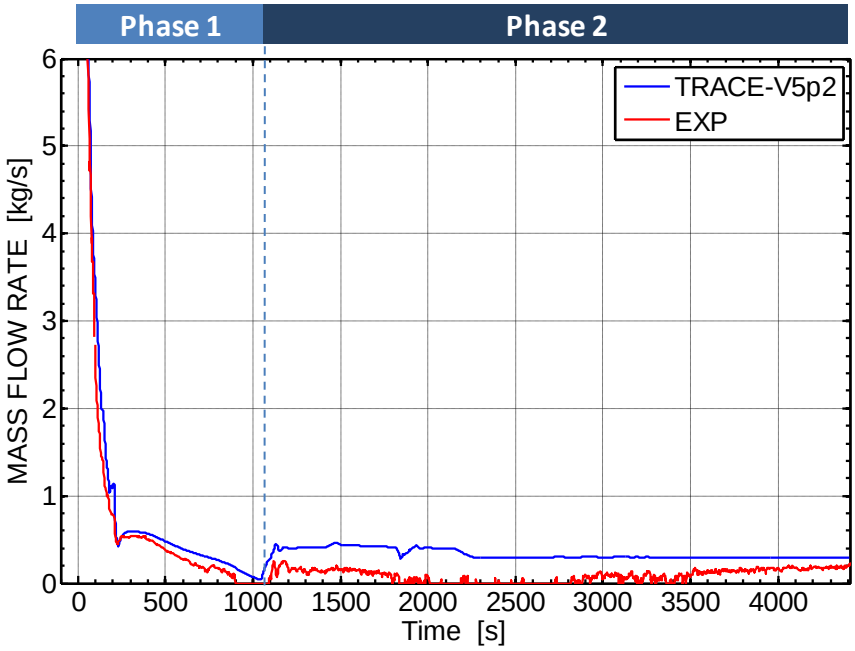

Figure 103 – PKL Test G3.1, posttest results: loop 4 SG outlet mass flow rate trends (-100 – 4410 s)

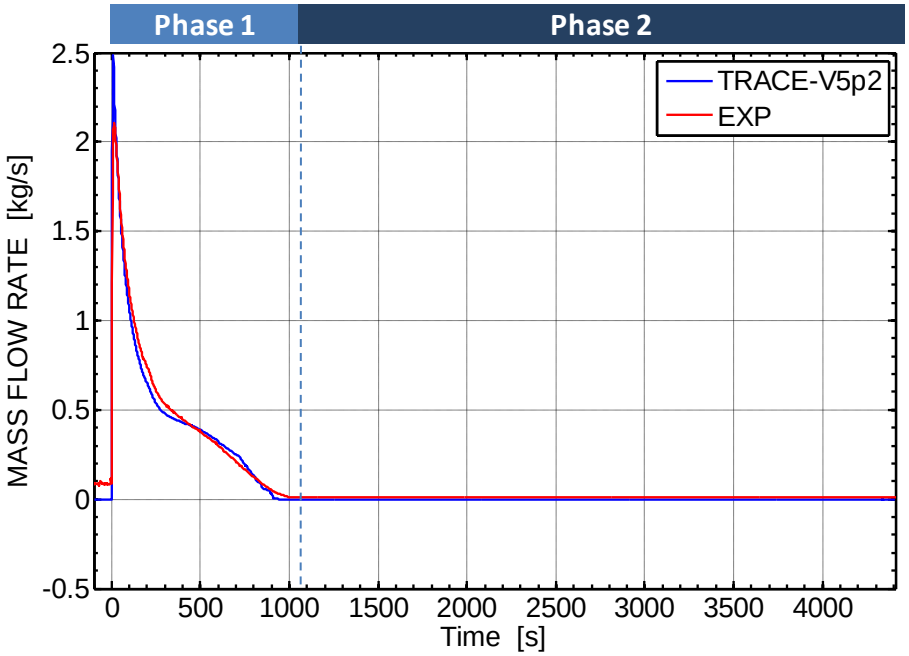

Figure 104 – PKL Test G3.1, posttest results: MSL 1 BRK nozzle mass flow rate trends (-100 – 4410 s)

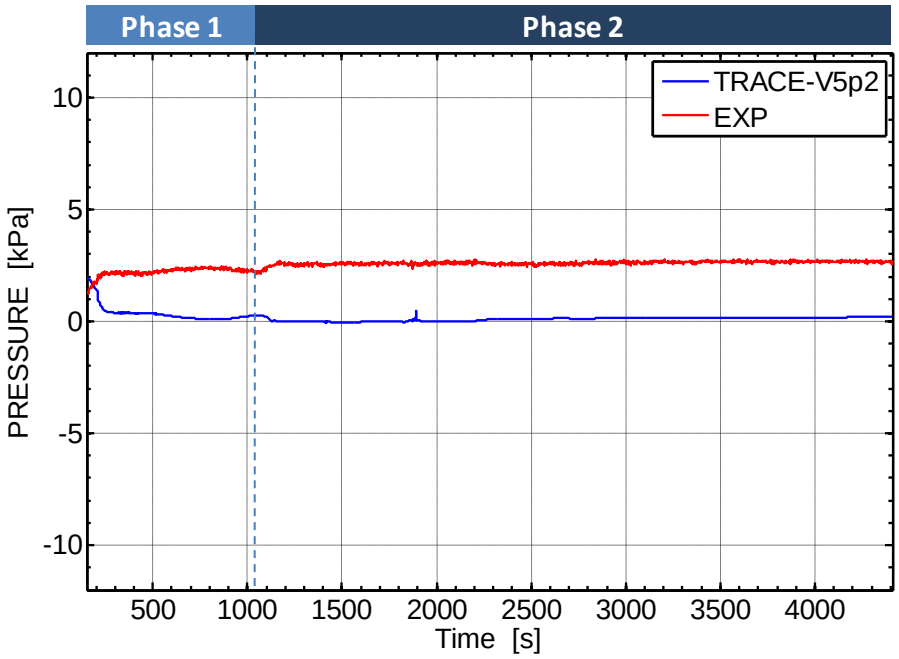

Figure 105 – PKL Test G3.1, posttest results: DP DC vessel inlet /RPV outlet (100 – 4410 s)

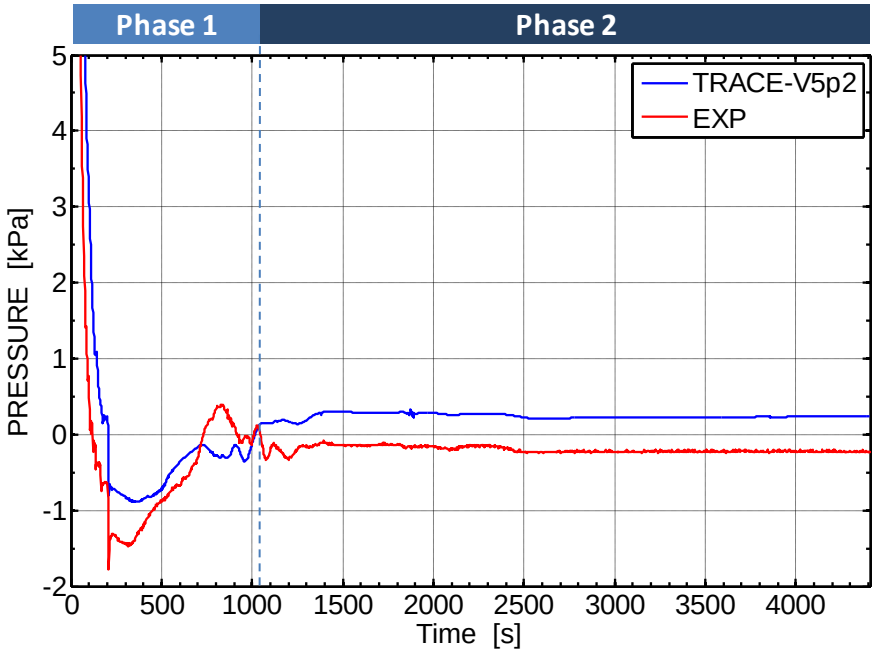

Figure 106 – PKL Test G3.1, posttest results: DP inlet/outlet SG 1 (0 – 4410 s)

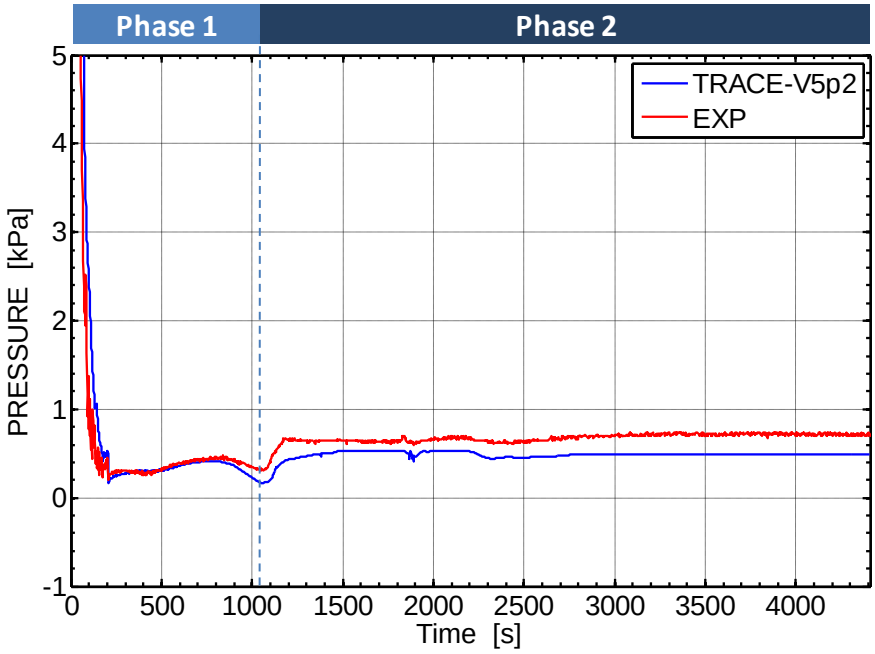

Figure 107 – PKL Test G3.1, posttest results: DP inlet/outlet SG 4 (0 – 4410 s)

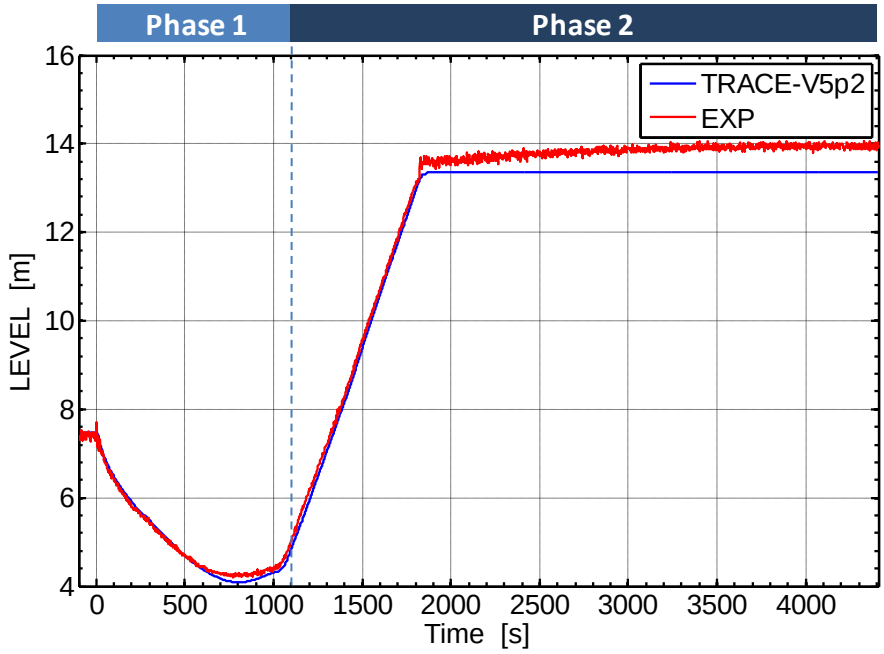

Figure 108 – PKL Test G3.1, posttest results: PRZ collapsed level (-100 – 4410)

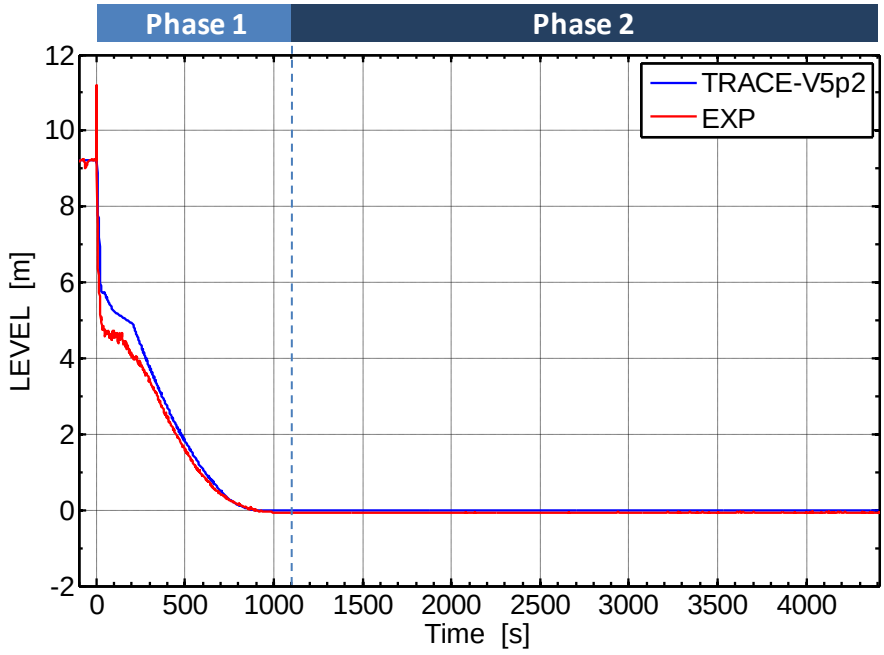

Figure 109 – PKL Test G3.1, posttest results: SG-1 riser collapsed level (-100 – 4410)

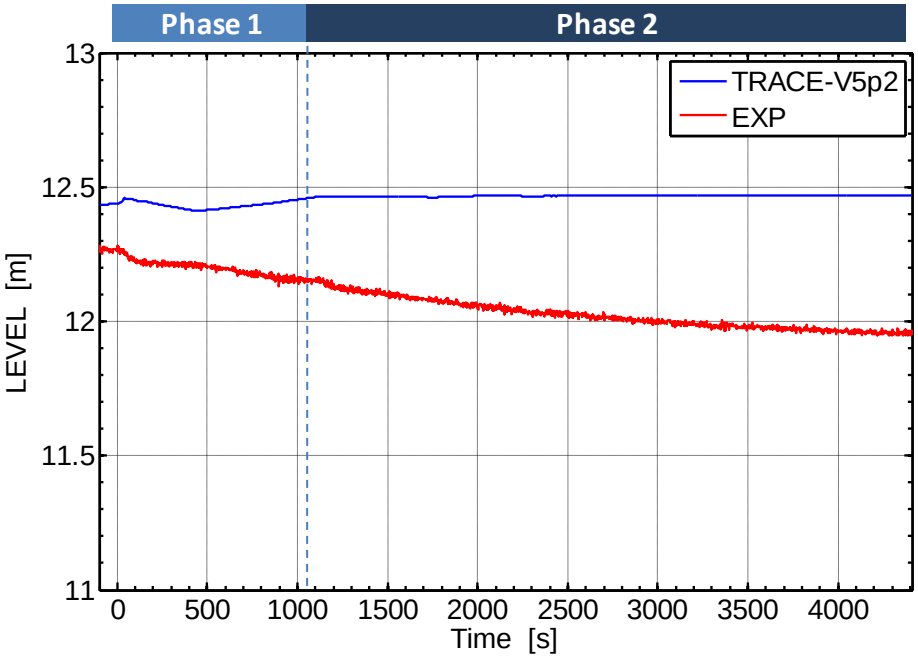

Figure 110 – PKL Test G3.1, posttest results: SG-2 riser collapsed level (-100 – 4410)

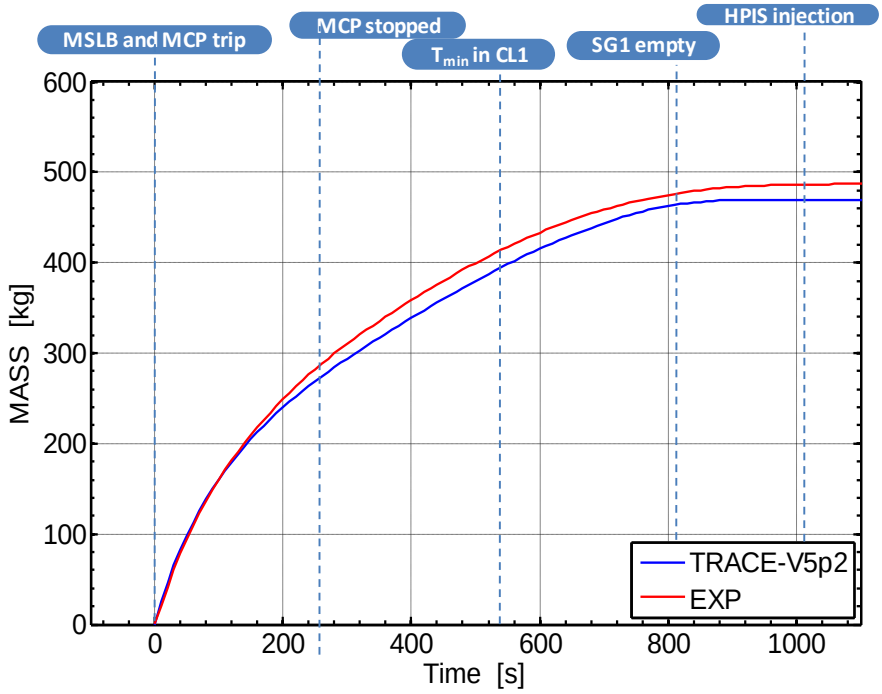

Figure 111 – PKL Test G3.1, posttest results: integral BRK mass flow trends (-100 – 1100 s).

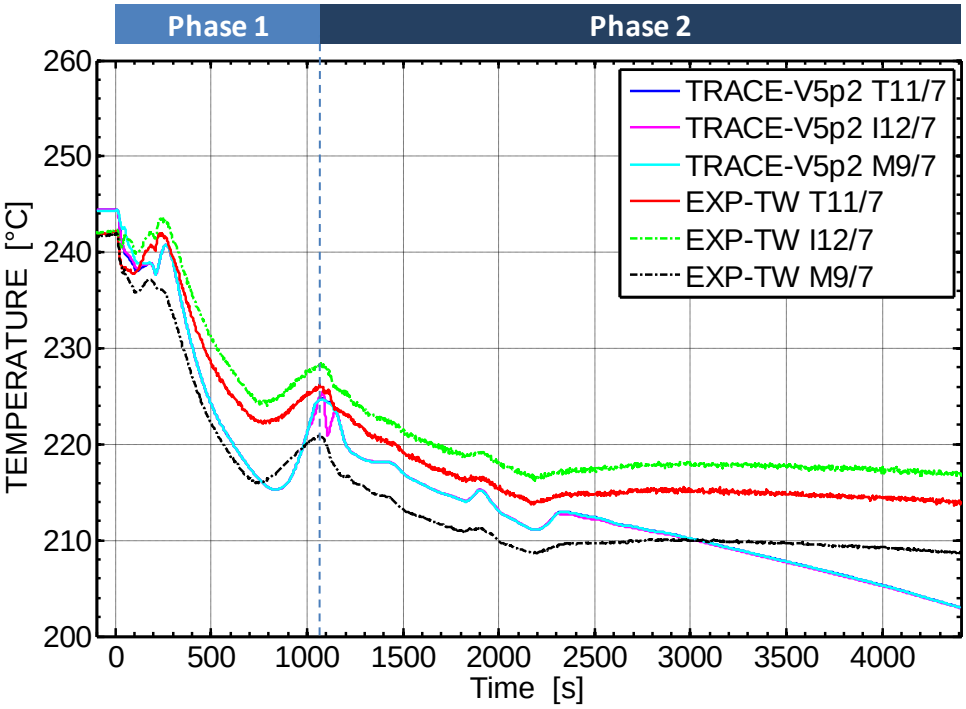

Figure 112 – PKL Test G3.1, posttest results: hottest cladding temperature at 5.62m from RPV bottom (-100 – 4500 s).

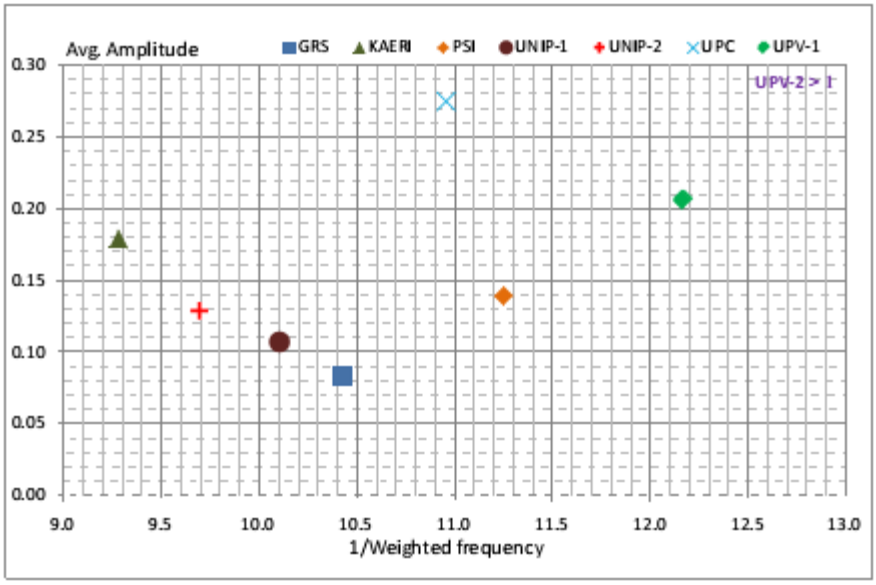

Figure 113 – PKL Test G3.1, benchmark posttest FFTBM application: quantitative accuracy evaluation of the results – from 0 up to 1030 s.

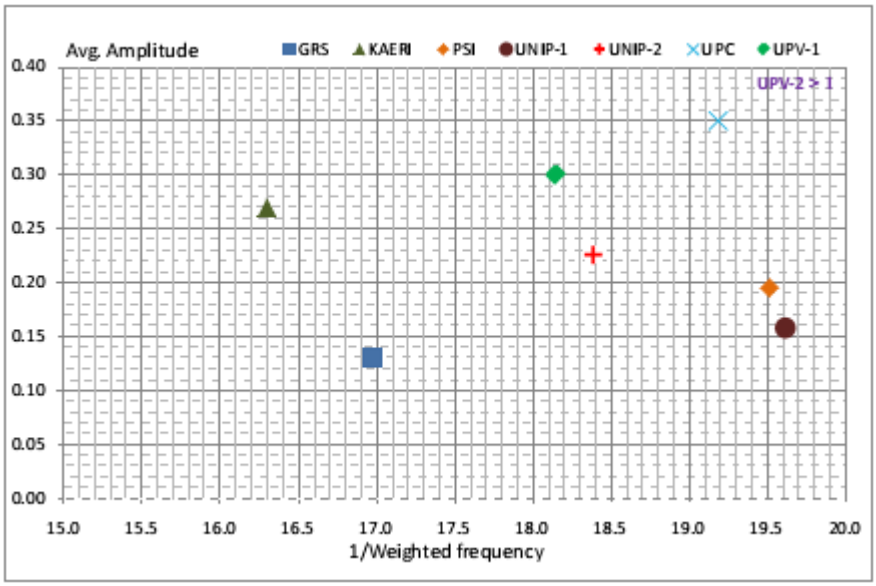

Figure 114 – PKL Test G3.1, benchmark posttest FFTBM application: quantitative accuracy evaluation of the results – overall transient

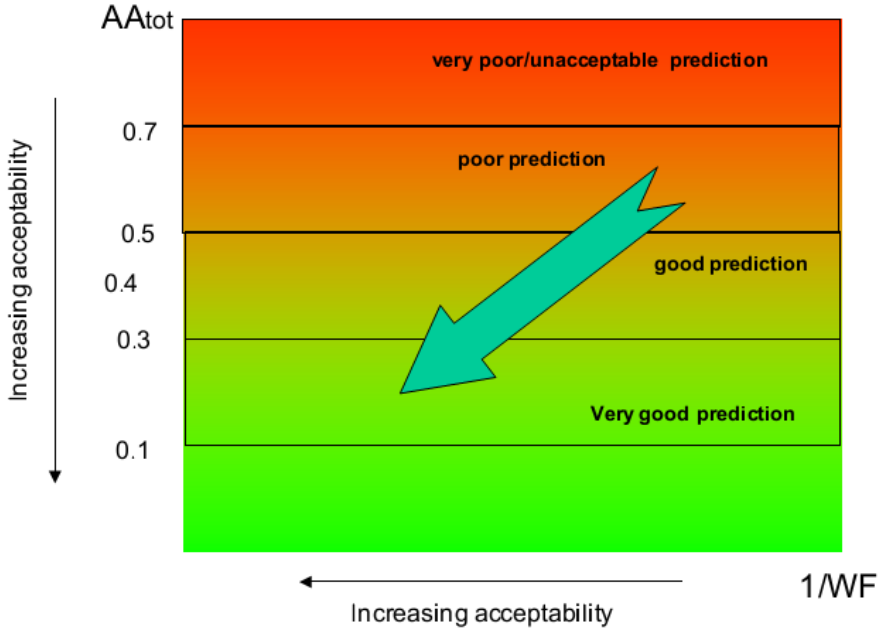

Figure 115 – The Fast Fourier Transform Based Method (FFTBM): evaluation of the quality of the result of the total average amplitude.

6.4. Buoyancy/convective driven flow mixing experiments (ROCOM tests)

As outlined in the chapter 5 and at the beginning of the this chapter the ROCOM tests, carried out in the framework of the PKL experimental activity for investigating the PWR system behavior subject to a MSLB inside containment (test G3.1), serve as complementary experiments for studying buoyancy/convective mixing phenomena in the RPV downcomer annulus and in the lower plenum expected to occur during the postulated accident scenario.

6.5. Description of the ROCOM test facility

The ROCOM (ROssendorf COolant Mixing) test facility models the primary circuit of a German KONVOI-type PWR in a linear scale of 1:5 ([72], [73] and [74]). The test facility was build with the purpose of investigating of a wide spectrum of coolant mixing scenarios occurring inside the primary circuit of a KONVOI-type PWR. The experiments executed in this facility provide experimental data for code validation (mainly CFD but also TH-SYS codes). The reactor pressure vessel was manufactured from acrylic glass and forms the main part of the test facility (Figure 116). The reactor core itself is represented by a hydraulic resistance of the fuel elements, only (see Figure 117). A core basket consisting of 193 aluminum tubes is inserted being a hydraulic short circuit between core inlet and outlet. In the current design, the model of the pressure vessel is equipped with a plane vessel head, which can be replaced by a spherical head according to the original reactor. The upper plenum does not contain any internals. The cylindrical part of the vessel consists of two half shells of acrylic glass with a thickness of 20 mm.

The geometrical similarity between the model and the prototype reactor is fully respected within the region in-between the bends in the cold legs, which are closest to the reactor inlet and to the core entrance. The geometry of the inlet nozzles with their diffuser segments and the curvature radius of the inner wall at the junction with the pressure vessel were modelled in detail. Similarity is also taken into account for the core support plate (CSP) (see Figure 119) with the orifices for the coolant. The KONVOI reactor has a perforated sieve drum (flow skirt below the core barrel), which is also placed in the lower plenum of the vessel in the ROCOM test facility (Figure 118). The hydraulic path of fluid flow is subdivided in four loops with individually controllable pumps (Figure 120) in each loop, which enables the possibility of performing tests over a wide range of flow conditions, from natural circulation to nominal flow rates and this includes the use of ramped flow rate changes to mimic normal or natural operation conditions.

Figure 120 shows the arrangement of the loops in the facility. Further, the positions of the seven loop wire mesh sensors are shown, which have been used during the different tests conducted within the OECD PKL2 project.

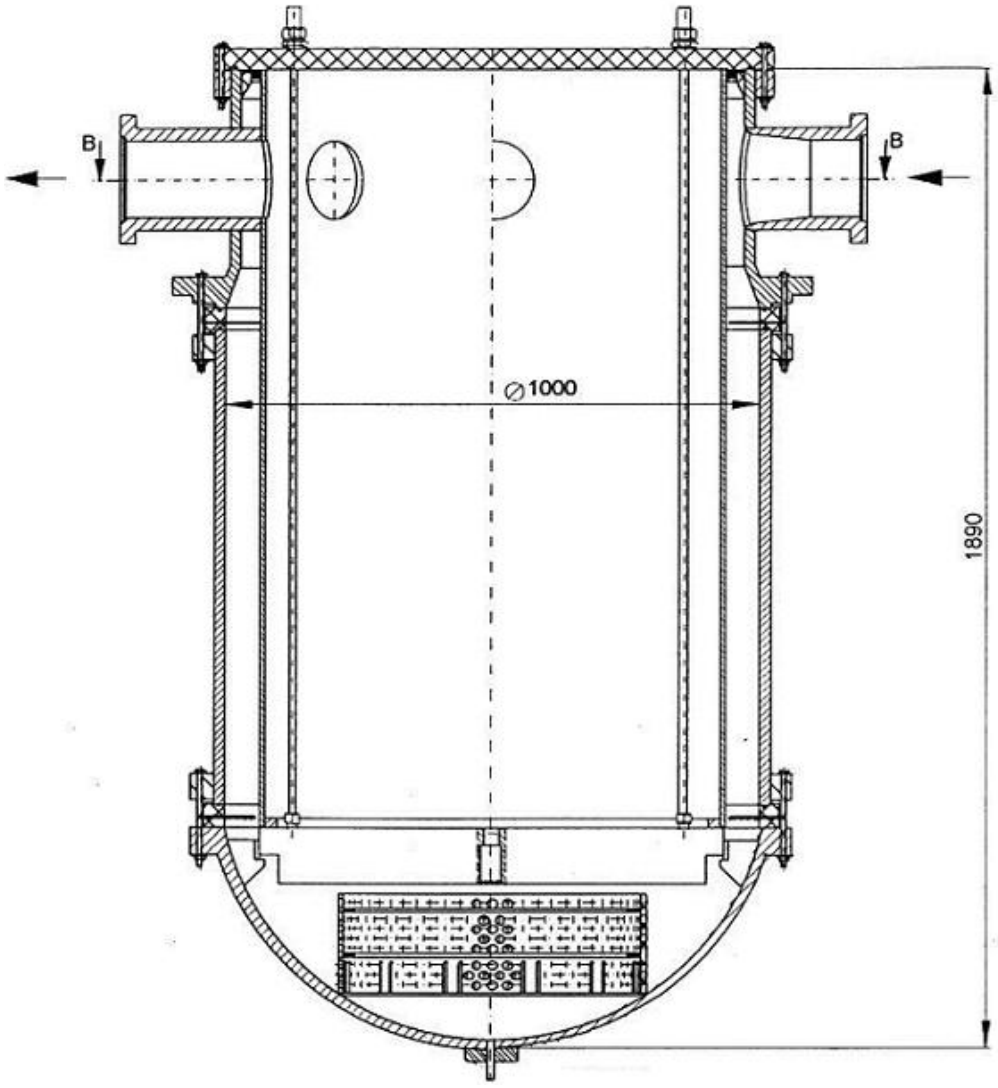

Figure 116 – Model of the reactor vessel, vertical section

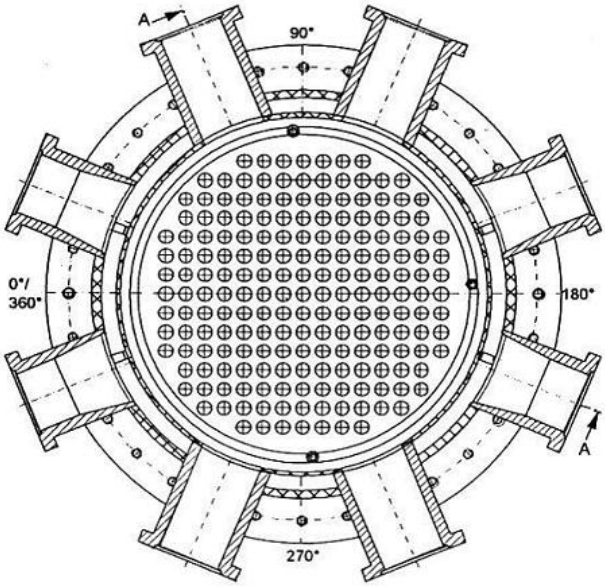

Figure 117 – Model of the reactor vessel, cross section in the nozzle region

Figure 118 – Sieve drum in the lower plenum of the ROCOM test facility

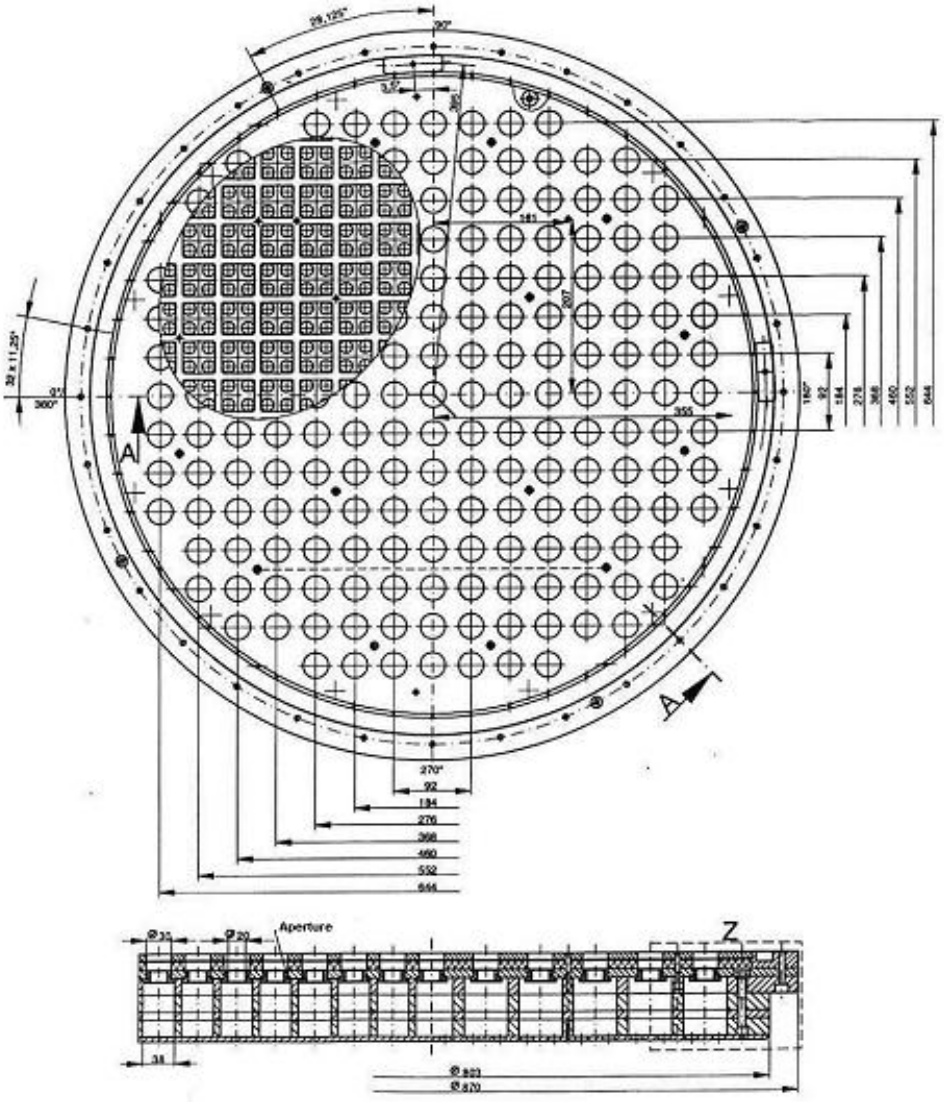

Figure 119 – Model of the lower core support plate

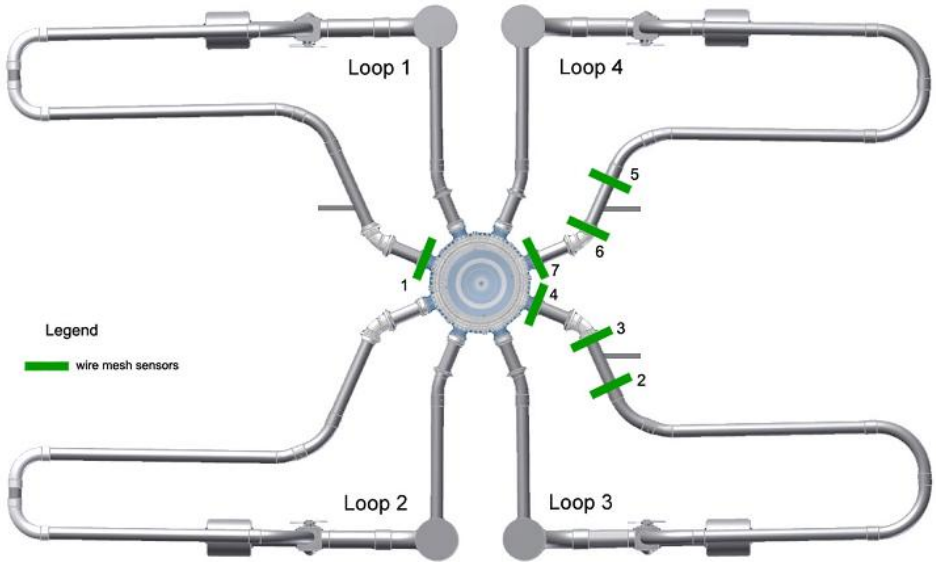

Figure 120 – Schematic of the ROCOM test facility with numbering of the loops and positions of different wire-mesh sensors in the loops

A comparison between the main geometric and operating features of ROCOM and a KONVOI reactor with water at 20° C is shown in Table 32.

Table 32 – Some characteristics of ROCOM facility compared to those of a KONVOI reactor.

Value	Unit	KONVOI design	ROCOM test facility
Inner diameter of the vessel	mm	5000	1000
Height of the vessel	mm	~12000	~2400
Inner diameter of the inlet nozzle	mm	750	150
Width of the downcomer	mm	315	63
Coolant flow rate per loop	m^3/h	23000	350 (max) 185 (nominal)
Coolant inlet velocity	m/s	14.5	5.5 (max) 2.91 (nominal)
Velocity in the downcomer	m/s	5.5	2.1 (max) 1.1 (nominal)
Reynolds number in the inlet nozzle	-	8.4×10^7	8.3×10^5 (max) 4.4×10^5 (nominal)
Re – downcomer	-	2.7×10^7	2.6×10^5 (max) 1.4×10^5 (nominal)
Re – reactor / Re – ROCOM	-	1	~100 (max) ~190 (nominal)
Travelling time Reactor / ROCOM	-	1	1 (nominal)

Regarding the transferability of the measurements obtained for the velocity and scalar quantity (namely boron concentration and the temperature of the coolant) in ROCOM facility to the prototype reactor, that is KONVOI reactor, this could poses a problem because of reduced scale of the experimental rig. On other hand extensive studies (based on numerical investigations) carried out by HZDR specialists shown that the presence of high level of turbulence and negligibility of density effects (conditions always satisfied during the several experiments preformed in the ROCOM facility) guarantee the similarity assumption.

6.6. ROCOM instrumentation

6.6.1. Measurement principles

The facility is usually filled with de-mineralized water. A part of the water is labeled with a tracer (usually the part of the water between the two slug valves; alternatively the ECC water or other externally injected water can be tracered), which changes the conductivity of the coolant. Chemical pure NaCl is used as tracer. The amount of tracer is very small; there is no density effect on the fluid. The conductivity of the tracered water is still considerably less than that of tap water. This is due to the high sensitivity of the wire mesh sensors.

The wire mesh sensor realizes the measurement of the instantaneous local conductivity of the medium in its vicinity. It consists of two planes of electrodes, being a mesh in the flow cross section. The planes are located in short distance one from each other, in most of the cases. The angle between the electrodes is 90°, mainly. All electrodes are insulated against each other and against the wall of the facility and the wall of the sensor base itself. The electrodes of the first plane (transmitter) are provided with short voltage pulses, consecutively. At each single electrode of the second plane (receiver) a current is formed, being directly proportional to the conductivity of the medium in the vicinity of the measuring position. These currents are registered, submitted and stored on a data acquisition PC. The measurement principle is demonstrated on

An error assessment has been performed with the result that the measurement error is up to 3.5 % (see [76])

6.6.2. Location of the wire-mesh sensors in the facility

Wire mesh sensors can be installed at different positions inside the test facility. One sensor is integrated into the core support plate just below the fuel element inlets in such a way that one measurement position for each fuel element inlet is available (Figure 121). Two axial sensor planes are available for the inner and outer wall of the downcomer spawning a measuring grid of 64×29 positions (Figure 122). A third sensor type is available for measurements in the cross section of the loops. In the current experiments between one and six of such sensors were installed in dependence on the investigated scenario (Figure 123).

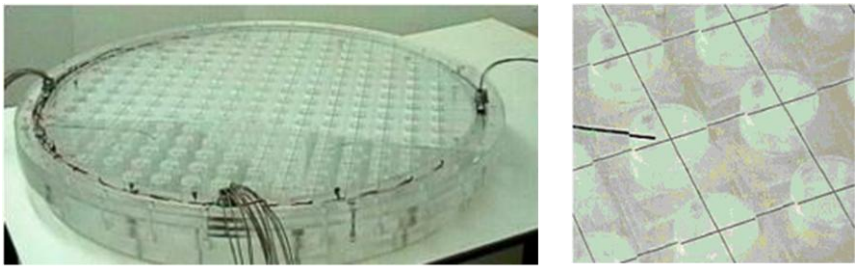

Figure 121 – Core inlet mesh sensor: general view (a), electrode (b).

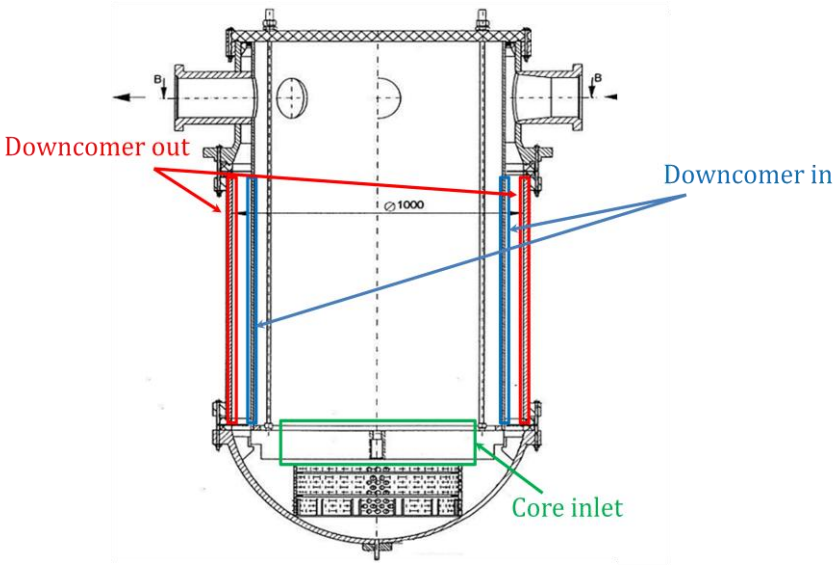

Figure 122 – Core wire mesh sensors position into the downcomer and at the core inlet.

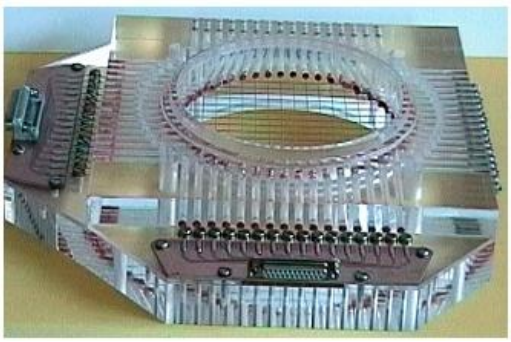

Figure 123 – Wire mesh sensor for pipes.

6.7. Outline of the ROCOM/PKL tests

In the framework of the OECD PKL2 Project to investigate in depth the coolant mixing phenomenon inside the RPV five complementary tests were conducted at the ROCOM test facility focusing on the two most severe thermal hydraulic conditions of the test G3.1, namely the achievement of the maximum overcooling and starting point of the higher ECC mass flow rate injection (see § 6.7.3). These two physical situations characterize the two phenomenological phases in which is subdivided the test (see Figure 124).

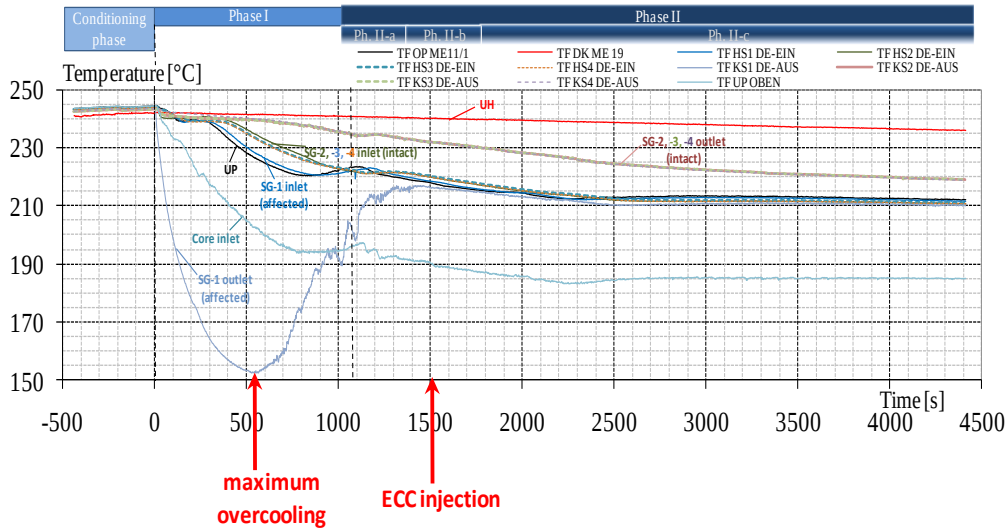

Figure 124 – Measurement loop temperature in the PKL test G3.1.

The tests ROCOM 1.1, 2.1 and 2.2 were dedicated to the overcooling phase of the related transient, different mass flows were imposed through the four cold coolant loops; whilst the tests ROCOM 1.2 and 1.3 are dealing with the ECC injection phase of the transient. A summary of the characteristics of the ROCOM tests are reported in Table 4 (in the table $\Delta\rho/\rho_0$ represent the relative density between the perturbed and the unperturbed flow).

A shortcoming during the conduction of a single experiment is that the time behavior of the injected coolant at identical positions in the pressure vessel differs in each single realization of an experiment with identical boundary conditions. The causes of these deviations between single realizations of one experiment are due to the fluctuations of the flow field that is of turbulent nature. These fluctuations appear randomly to a certain degree. For this reason the experiment are repeated five or more time to have a statistically significant sample for averaging the experimental data over all realizations for dumping statistical fluctuations.

The analytical activity only deal with the tests 1.1, 1.2 and 2.2 which is a sensitivity test for studying the effects of the mass flow rate on the stratification layer, as will show in the description of the test.

Table 33 – ROCOM test matrix

TEST	CONNECTION TO PKL TEST G3.1	NOTES
1.1	**Overcooling phase**	No ECC injection, affected loop (sub-cooled) characterized by higher mass flow rate than the other tree loops (2-4), $\Delta\rho/\rho_0$= 0.12
1.2	**ECC injection phase**	Cold injection with two ECC systems activated (loop 3 and 4), affected loop (sub-cooled) characterized by higher mass flow rate than the other tree loops (2-4), $\Delta\rho/\rho_0$= 0.20
1.3	**ECC injection phase**	No flow in loops 1-4, only one ECC system injection, $\Delta\rho/\rho_0$= 0.20
2.1	**Overcooling phase**	No ECC, affected loop (sub-cooled) characterized by higher mass flow rate than the other tree loops (2-4), $\Delta\rho/\rho_0$= 0.0128
2.2	**Overcooling phase**	No ECC, one loop sub-cooled (loop 1), time dependent flow rates in the non-affected loops (2-4)

6.7.1. Scaling assumptions

The scaling factor of 1:5 must be adopted in the application of the boundary conditions in order to replicate phenomena on the reactor scale, as was mentioned in the section §5.4. The density differences between the different coolants in the facility (reactor) play an important role for the phenomena in these tests. The Froude number *Fr* is the dimensionless similarity number used in order to scale the buoyancy effects:

$$Fr = \sqrt{\frac{\rho v^2}{\Delta\rho \cdot g \cdot L}} \tag{28}$$

where v is the velocity, g is the gravitational acceleration, ρ is the density, $\Delta\rho$ is the density difference and L is the characteristic length.

Taking in account that the Froude number is defined as the ratio between the inertia forces (numerator), whose influence in the fluid medium is characterized by the density, and the gravitational force (denominator) characterized by the density difference, the key parameter which determines the feature of *Fr* is the ratio $\Delta\rho/\rho$. The boundary conditions should be selected in such a way that the Froude number in the ROCOM experiment is identical to the Froude number under reactor conditions. In order to keep the same ratio $\Delta\rho/\rho$ in the ROCOM experiments (1.1, 1.2, 1.3 and 2.2) and in the PKL, the velocity in the ROCOM facility is reduced by a factor $\sqrt{5}$. For the test 2.1 the scaling strategy was different. To ensure the similarity of the Froude number the velocity and density difference measured in the PKL test G3.1 were reduced by a factor of 5 (see [76]).

6.7.2. The ROCOM test 1.1

6.7.2.1. Objectives of the test

The objective of the ROCOM test 1.1 (see [74]) was the investigation of the 3-D flow behavior inside the reactor pressure vessel during the maximum shrinkage of the fluid flow which characterizes the first phase of the MSLB scenario. For that reason the concrete boundary conditions were derived from the corresponding PKL experiment G3.1. Quasi-stationary flow conditions were foreseen to be established derived from the time point of minimum loop temperature in the PKL experiment.

The temperature distribution inside the downcomer represent an important thermal hydraulic parameter for understanding the turbulent mixing induced by the existence of thermal gradients which taking place after entering of the flows from the different loops with different temperatures into the vessel. Another relevant physical aspect concerns the sector formation as a consequence of the asymmetrical loop behavior of the coolant flow. The test should provide information about the following phenomena:

- the position of the transition region between the established a more or less homogeneous temperature distribution and the unperturbed temperature distribution into the downcomer,
- azimuthal temperature distribution at the core inlet.

The main outcomes of this test should allow drawing conclusion on the occurrence of the recriticality but also on the thermal load on the DC wall relevant for triggering PTS phenomenon.

For the ROCOM test the temperature and mass flow rate data from the time $t = 609\ s$ were used (see Figure 124)

6.7.2.2. Initial and Boundary conditions

As mentioned above from the PKL test G3.1 the time point of minimum temperature in loop 1 during the overcooling phase was selected (t=609 s). The thermal hydraulic conditions of the PKL at that time are reported in Table 34, whilst the selected boundary conditions for the ROCOM test 1.1 are shown in Table 35.

Table 34 – Conditions in PKL test G3.1 at t = 609 s (P = 3.8MPa)

Loop	**1**	**2-4**
Temperature, [^{o}C]	153	236.1
Mass flow rate, [kg/s]	267.4	69.2
Normalized mass flow rate	5.46	1.41
Density [kg/m^{3}]	915.9	819.9
Relative Density [-]	1.12	1.00

Table 35 – Initial and Boundary conditions of ROCOM Test 1.1

Loop	1	2-4
Temperature, [^{o}C]	153	236.1
Mass flow rate, [kg/s]	267.4	69.2
Normalized mass flow rate	5.46	1.41
Density [kg/m^3]	915.9	819.9
Relative Density [-]	1.12	1.00

Figure 125 shows the condition of the test rig before and after the starting of the test. The liquid representing the overcooled water and the water in the facility are separated only by a valve, the front valve. When the run is started, the front valve is opened and the injection pump starts running. Loop 1 is closed upstream of the injection position by a valve. The distances of the valves and the injection position are given in relation to the RPV inlet (wire-mesh sensor position).

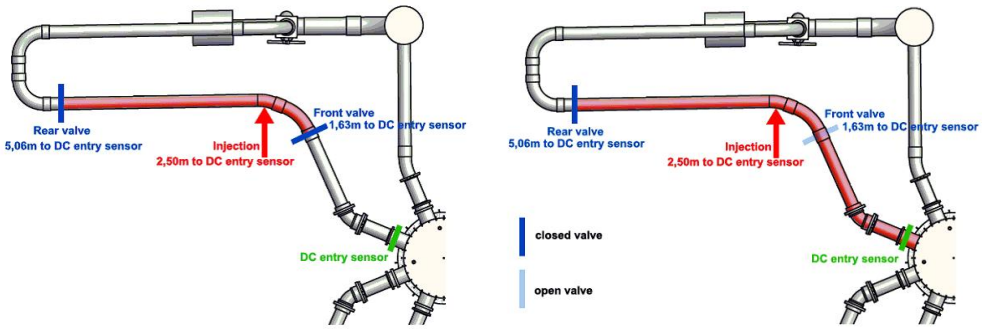

Figure 125 – Configuration before starting the test (a), Configuration of the test facility during run.

6.7.3. ROCOM test 1.2

6.7.3.1. Objectives of the test

The second relevant aspect from the safety point of view, which characterizes the postulated MSLB scenario, is represented by the PTS phenomenon. The objective of the ROCOM test 1.2 (see [74]) was the assessment of the mixing of the ECC water with the ambient water on the way from the injection position to the core inlet. Special attention was put on:

- the stratification in the loops;
- on a possible flow reversal in the loops;
- on the temperature distribution in the downcomer;
- the sector formation at the core inlet;
- coalescence of two ECC water stripes in downcomer

In this test respect the position of the lowest coolant temperature and the possible presence of fluctuations of the ECC water stripe are of special interest. For this test was decided to use the temperature and mass flow rate data from the time interval with higher ECC mass flow rate (see [74] and [76])

6.7.3.2. Initial and Boundary conditions

The initial condition and boundary conditions for the ROCOM test 1.2 (Table 37) are taking as explained above at the time point in which the higher mass flow rate is reached in the PKL facility, namely t=1500 s. The derived boundary conditions, by using the scaling considerations explained in section 6.7.1, for the separate effect facility are shown in Table 36.

Table 36 –Conditions in PKL test G3.1 at t = 1500 s (P = 3.97MPa)

Loop	**1**	**2-4 (Average)**	**ECC**
Temperature, [^{0}C]	-	227.65**(4)**	25
Mass flow rate(3) [kg/s]	133.2	50.1	-
Normalized mass flow rate(1) (%)	2.72	1.02	-
Density [kg/m^3]	-	831.7	998.9
Relative Density [-]	-	1.00	1.2

(1) nominal value: 4900 kg/s
(2) evaluated data
(3) reactor conditions
(4) averaged from loop 2 and loop 3

Table 37 – Initial and Boundary conditions of ROCOM Test 1.2

Loop	***1***	***2***	***3***	***4***	***ECC***
Normalized volume flow rate [%]	2.28	2.28	6.08	2.28	-
Volume flow rate [m^3/s]	4.22	4.22	11.25	4.22	1.87
Volume flow rate [l/s]	1.17	1.17	3.12	1.17	0.52
Relative Density [-]	1.00	1.00	1.00	1.00	1.2

In the procedure adopted for the realization of the PKL experiment G3.1 was planned the injection of one of the ECC systems into the loop affected by the steam line break. From the safety point of this choice is very conservative for the occurrence of the PTS phenomenon. Therefore, to be as close as possible to the PKL experiment it was further decided that also in the ROCOM experiment one of the injections should take place into the loop with the higher flow rate (caused by the break). In the current ROCOM experiment this loop correspond to loop 3, namely to the loop with the break (see Figure 126)

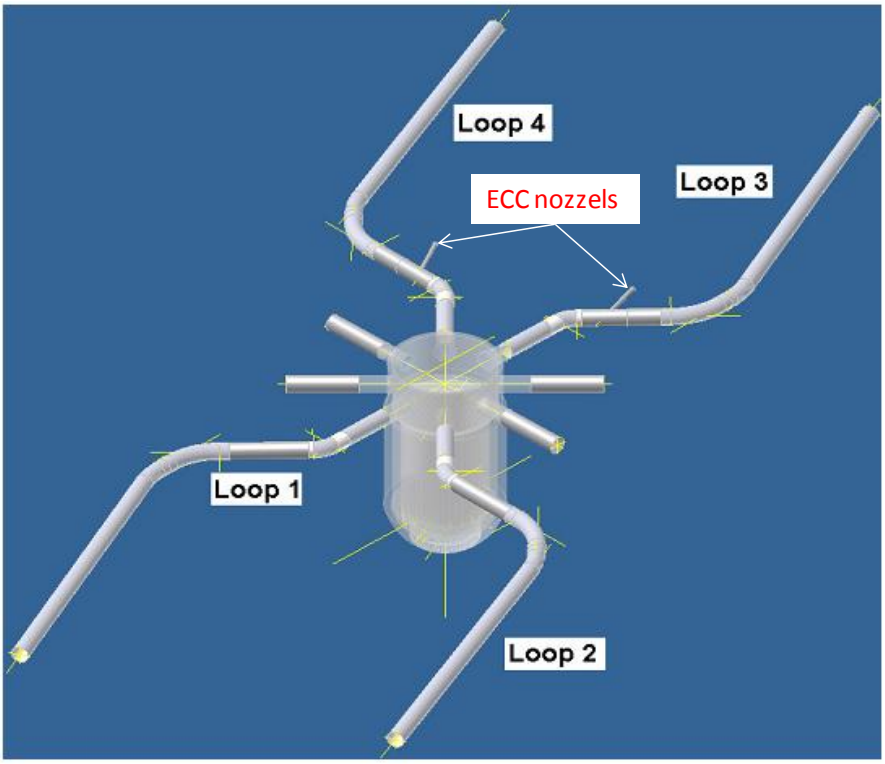

Figure 126 – Schematic of the ROCOM test facility with ECC injection nozzles

6.7.4. ROCOM test 2.2

6.7.4.1. Objectives of the test

The test 1.1 showed the influence of the boundary condition variation (temperature and flow rate) on the obtained flow mixing pattern inside the RPV and especially on the transition region between sector-shaped and nearly homogeneous temperature distribution. Both tests have been conducted under quasi-stationary flow conditions.

In contrast to these quasi-stationary ROCOM tests the test 2.2 was performed under transient conditions (see [75] and [76]). The main objective of this test was the assessment of the influence of changing mass flow rate in the non-affected loops on the position of the transition region between perturbed more or less homogeneous thermal layer and the unperturbed zone in the downcomer region,

6.7.4.2. Initial and Boundary conditions

In order to meet the objectives of the ROCOM Test 2.2 was conducted with changing time-dependent boundary conditions for the flow rate in the non-affected loops (see Figure 127). The initial conditions (see Table 38) were selected in such a way that the results of this test can be compared with those of ROCOM Test 1.1.

Table 38 – Initial and Boundary conditions of ROCOM Test 2.2

Loop	***1***	***2***	***3***	***4***
Normalized volume flow rate [%]	10.2	4.8	4.8	4.8
Volume flow rate [m^3/s]	6.27	6.27	6.27	6.27
Relative Density [-]				
Temperature [°C] (PKL)	153.0	236.1	236.1	236.1

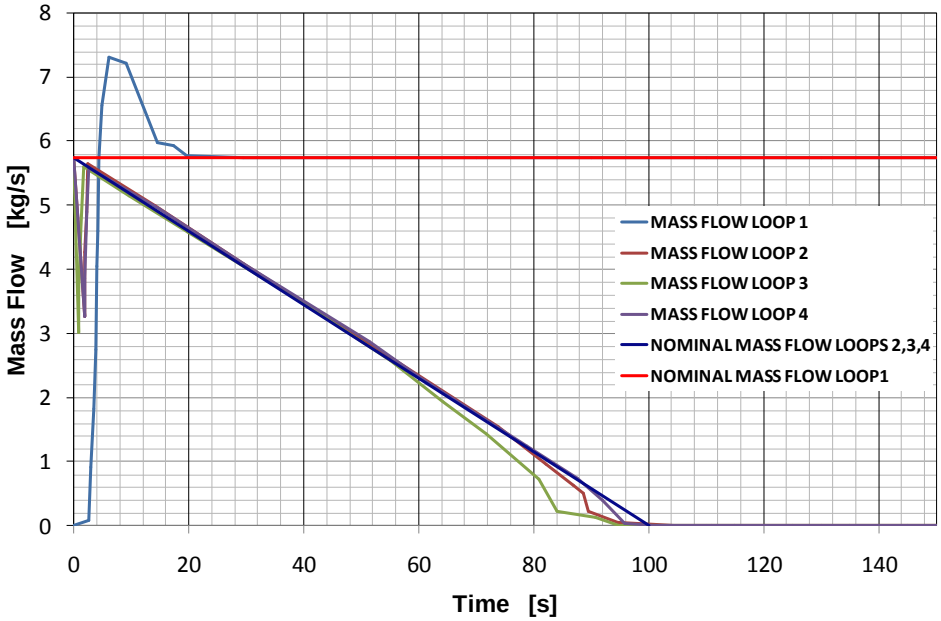

Figure 127 – Measured loop mass flow rates in the ROCOM Test 2.2

6.8. TRACE-V5 code Simulation

The strategy to assess the code results, as outlined in chapter 5, consists first of all in showing the tendency of the results compared to the time behavior of the experimental data with the purpose to evaluate the capability of the computational model to capture the phenomena present in the test. The second phase of the accuracy evaluation consists in quantifying the discrepancy between the computational data and the test results. To characterize the accuracy of the calculations the amplitude of the FFT of the experimental signal and of the difference between the experimental signal and the calculated trend were employed to define the averaging amplitude (see equation), that is a averaging fractional error.

The TRACE model used to simulate these experiments is that described in the APPENDIX D, in which the computational domain is subdivided in 16 axial meshes, 6 radial rings and 8 azimuthal sectors.

To reach the purpose of the assessment process the strategy used was to do a temporal and spatial comparison between the calculated and measured data of the temperature distribution in the downcomer an core inlet. The experiment/simulation temporal comparison is achieved following two approaches:

- *pseudo-local analysis,*
- *averaging analysis*.

In the frame of the pseudo-local analysis the comparison between experimental and calculated temperature distribution in the downcomer has been performed selecting three different axial layers (which are close to the experimental layers (29, 15, 1) see Figure 128): top, middle and bottom of the downcomer zone. Because of the coarse nodalization each layer that includes on average three experimental axial sensors was divided in 8 azimuthal sectors. For each of these sectors an average temperature was obtained to have a consistent comparison between analytical and experimental data. In the core inlet region the comparison between experimental and calculated temperatures (see Figure 129) has been carried out as depicted in the Equation 21, namely computing an average temperature $\bar{T}_{exp}$ obtained averaging the single channel experimental temperature T_i^{exp} over the number of core channels inside the computational meshes $N_{CompMes\ h}$.

$$\bar{T}_{\exp} = \frac{1}{N_{CompMesh}} \sum_{i=1}^{N_{CompMesh}} T_i^{\exp} \qquad (21)$$

The averaging analysis has been carried out to compare the integral behavior (average process over all capturing sensors) of the temperature distributions of the experiment and the simulation on the two probes areas: downcomer outer plane and core inlet plane (see section § 6.6.2 for the analysis of the results).

The spatial comparison has been performed in order to consider a quasi-stationary flow conditions (which are the condition on which the tests 1.1 and 1.2 are performed) is obtained averaging the sensor data at each measurement position in the downcomer and at the core inlet from 73 s to 83 s for the test 1.1 and from 60 s to 70 s for the test 1.2 (the analysis of the results has been reported in the sections § 6.8.2.1.2 and § 6.8.3.1.2).

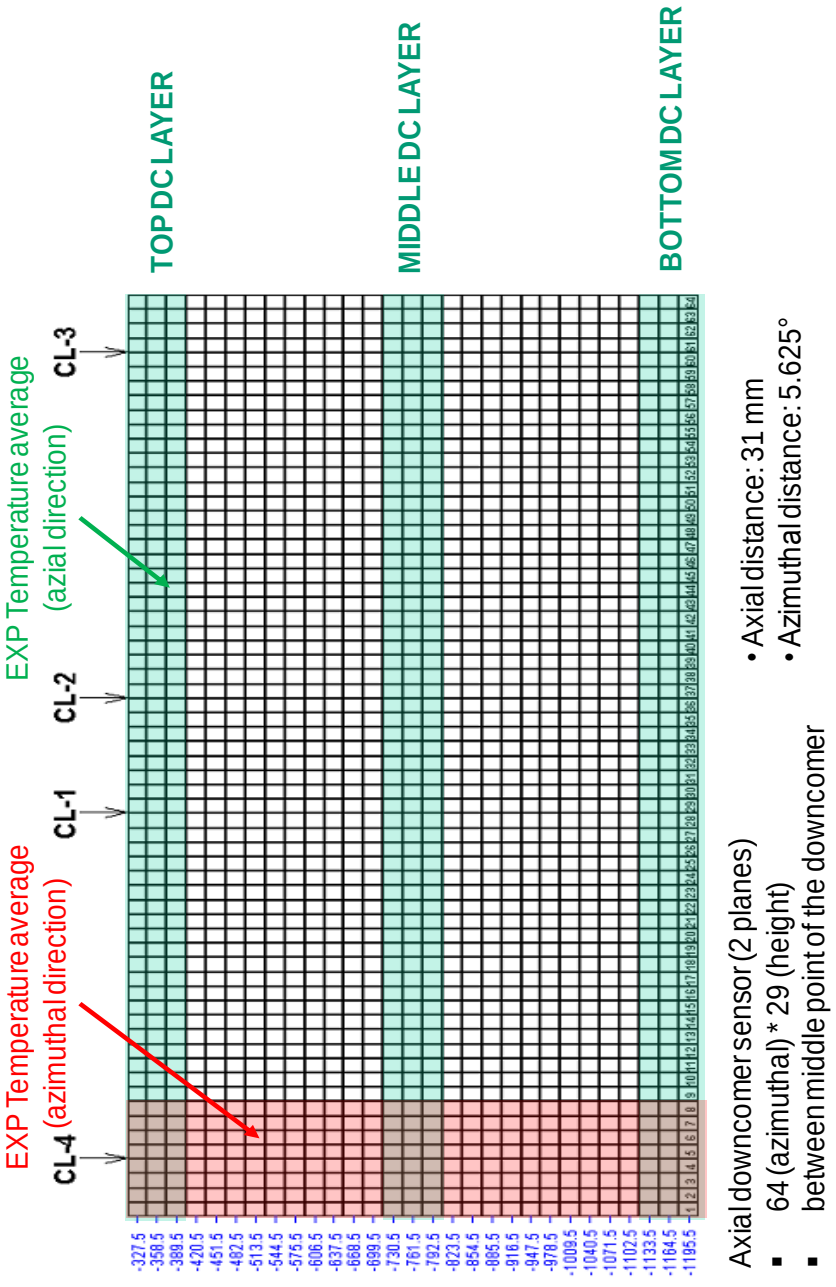

Figure 128 – Spatial resolution of the computational and experimental downcomer sensors

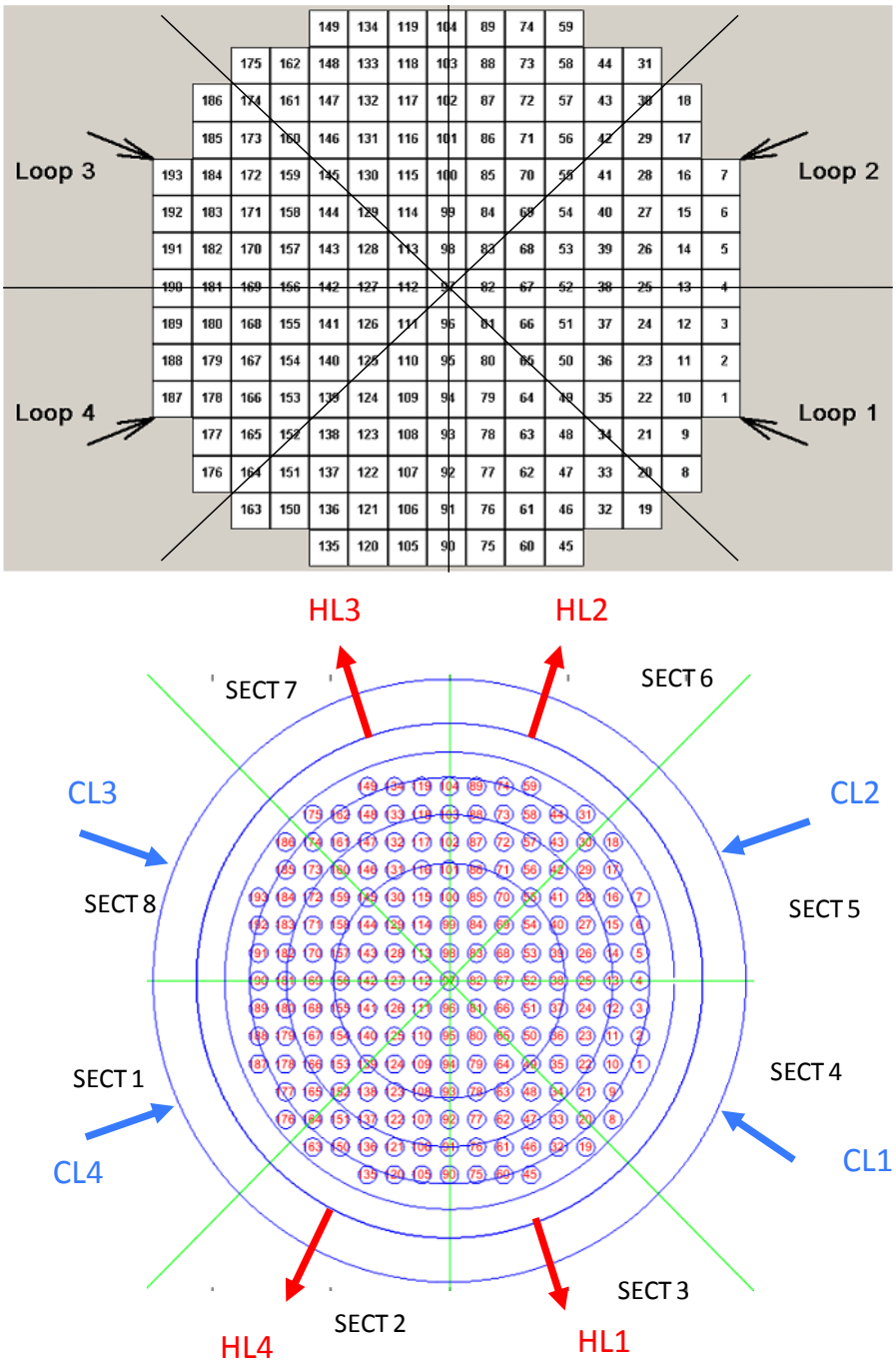

Figure 129 – Spatial resolution of the computational and experimental downcomer sensors

6.8.1. Thermodynamic considerations

The thermodynamic state, in which the ROCOM tests are carried out, is given by atmospheric conditions and the density differences are produced by mixing sugar into the water. The computational analyses presented here are performed in the *real* thermodynamic conditions, namely the pressures and temperatures of the test rig are that corresponding to the PKL experiments. The main reason of this choice is due to the lack of fluid properties for sugar/water solution in the system codes. As thermal conductivity should not play a significant role in any of the simulated experiments, the temperature fields obtained from the simulations are expected to correspond reasonably well to the experimental *temperatures*, which is derived from the mixing scalar Θ and the average temperature of the three intact loops T_{2-4} and the temperature of the overcooled loop T_1.

$$T_{x,y,z} = \Theta_{x,y,z} \cdot \left(T_1 - T_{2-4} \right) + T_{2-4} \tag{22}$$

The mixing scalar is determined using the electrical conductivity σ_0 in the facility before the experiment and the conductivity of the slug water σ_1, namely:

$$\Theta_{x,y,z} = \frac{\sigma_{x,y,z} - \sigma_0}{\sigma_1 - \sigma_0} \tag{23}$$

6.8.2. Simulation of the test 1.1

The numerical investigation has been performed following 100 seconds of *null transient* aimed to reach the stationary and initial conditions of the ROCOM test 1.1. No cold slug is injected from the cold leg 1 (damaged loop) during this 100 seconds steady state and the boundary mass flow rate at the four cold legs has been set in such a way to have the nominal ROCOM mass flow rate. The isobar pressure conditions have been imposed to keep the system at the same condition of the PKL at the time point of interest. (t=609 s), namely the adopted pressure is equal to 3.8 MPa. With a stabilized flow regime, 120 s transient has been performed where the injection of water with lower temperature was maintained throughout the entire transient. The procedure is outlined in the Table 40, the initial and boundary conditions used for running the TRACE input model are reported in Table 39.

Table 39 – ROCOM experiment 1.1: boundary conditions of the TRACE-V5 model (P=3.8 MPa)

Loop	**1**	**2-4**
Temperature, [^{o}C]	153	236.1
Mass flow rate, [kg/s]	5.743	1.328

Table 40 – ROCOM experiment 1.1: adopted procedure

Cal. Time (s)	Event
0 – 100	Establish stationary flow conditions in all loops by controlling boundary pressure (temperatures of all loops are equal, 236.1 ^{o}C)
100	Start of injection of cold water (153 ^{o}C) into loop-1 • Changing inlet temperature of loop-1 from 236 ^{o}C to 153 ^{o}C in 0.5 s • Pressure also controlled to maintain flow rate in each loop
220	End of calculation

6.8.2.1. Analysis of the results: experiment/simulation temporal comparison

6.8.2.1.1. Pseudo local analysis

The analysis of TRACE-V5 calculations on the perdition of the temporal evolution of the stratification region in the downcomer and homogeneous thermal mixing process, that take place in the downcomer and lower plenum because of the cold plum injection (from the affected loop, namely loop 1), has been addressed by comparing the local (referred to the captor position) time history of the experimental and calculated temperature distribution in the vessel. The results are resumed into four set of figures. The first three (Figure 130 to Figure 132) show the temporal behavior of the fluid temperature inside the downcomer at three different axial layers (top, middle and bottom). Form the comparison of the temperature distribution at the top of the of the downcomer axial captor points is highlighted qualitatively well prediction of the temperature trend in the affected sector (namely sector 4) both in terms of onset time of the cooling following the arrival of thermal perturbation and in terms of time trend (see Figure 130(d)). The diffusion of the cold stream in the azimuthal direction affects only the bordering sectors, i.e. sector 3 and 5 at the onset of the perturbation. This effect can be seen in Figure 130(c) and 130(e) by the appearance of overcooling peak versus the unperturbed temperature which has been predicted also by TRACE-V5 simulation. After approximately 13 s from the start of the test the calculated temperatures behavior show a trend toward greater cooling compared to experimental data that remain almost undisturbed in all sectors except sector 4. The physical reason of this behavior is due to the influence of the transition layer between the perturbed (homogeneous thermal mixing) and not perturbed region of the downcomer that in the TRACE-V5 simulation is characterized by large band (of approximately 0.2 m at the end of the test, see also Figure) in which the dispersion of the temperature is related to the diffusion resulting from the virtual turbulence induced by the numerical diffusion, whilst in the experiment the transition between the mixed zone and unperturbed hot layer is almost sharp (approximately 0.1 m). The Figure 133 (four set of figures) pointed out this phenomenon comparing experimental and calculated evolution of the cold plum and the mixing front inside the DC at five time frames, 5 s, 10 s, 15 s, 20 s and 25 s from the start of the test. The artificial

turbulence represents in combination with the advective transport of energy the only mean of thermal mixing that in turn is responsible of the thermal homogenization in the *lower part* of the downcomer. In fact in all sectors of the DC middle and bottom layers the calculated temperature distribution shows a cooling trend similar to the experiment but whit an overestimation of the temperature after 40 s in the middle zone and after 25 s in the bottom zone from the start of the test (see Figure 131 and 132) that is symptomatic of a less thermal mixing compared to the experiment. The cause of this behavior as mentioned above is due to the lack of turbulent diffusion effects replaced by numerical viscosity (or diffusion) inherent in two-phase numerical solution scheme of the TRACE-V5 code.

At the core inlet (CSP zone) the slight anticipation of the disturbance transported by the cold plum affecting the predicted temperature trend in all computational volume (see Figure 134, 135, 136 and 137) is caused by numerical diffusion that in turn determines a smaller mixing than the experiment which results into a more high temperature distribution at the end of the test (this phenomenon is well characterized throughout the averaging approach) as happens inside the DC. A nearly uniform temperature distribution is observed in the core inlet plane in both the experiment and the calculation, but in this last case the temperature distribution is higher than the experimental one. The result is that sector formation as consequence of the asymmetrical loop behavior of the coolant flow not occurs (see Figure 138 and Figure 139 in which are recorded the temperature distribution at the core inlet starting from 25 s to 75 s from the start of the test with a time step of 5 s).

6.8.2.1.2. Averaging analysis

The averaging approach compares the time trend of experimental and calculated temperature averaged over all capturing points, the first set of data, and over all computational meshes the second set of data in the DC and at the core inlet. This comparison aimed to analyze the TRACE-V5 results from the macroscopic point of view filtering the effects of the local turbulent thermal mixing which cannot be detected by the code through the artificial turbulent mixing mechanism induced by numerical diffusion. The Figure 140 and Figure 141 show the averaged temperature evolution inside the DC and at the core inlet. The calculated curve features a qualitatively well prediction of the macroscopic thermal mixing phenomenon in the DC and at the core inlet with a tendency to overestimate the. This means that the simulation is characterized by less thermal mixing than the experiment.

6.8.2.2. Analysis of the results: experiment/simulation spatial comparison

In order to consider a quasi-stationary flow and to compare computation and experiments, the flow probes are averaged from 73 to 83 seconds for the experiments and the computation

In the downcomer, stratification takes place. The experimental result shows sharp transition between the mixing region and the unperturbed zone (see Figure 142(a)), whilst the simulation the transition between the two region perturbed and

unperturbed occurs in a dispersive way characterized by a band (see Figure 142(b)). Two transition zones can be compared:

- horizontal separation is characterized by the transition from hot water to mixed water;
- vertical separation is characterized by the transition from the affected cold leg's stream to hot water on the upper downcomer.

On Figure 144, the two transition zones are represented in the simulation. Two line probes extraction have been extracted on the top of the downcomer probe area and on the left hand side. Figure 145, shows this cut and compare the calculated datum to the average experiment. The horizontal length of the cold stream in the computation is comparable to that in the experiment. For the downcomer, the stream is more diffused in the simulation. On the other hand, for the horizontal separation the two interfaces are separated by 4 captors who correspond nearly to 10 cm, whilst in the TRACE-V5 simulation the horizontal separation between the unperturbed (hot water) and the mixed layers is nearly 20 cm. The final discrepancy is that in the computation, the jet flow is less concentrated and more diffused in the DC compared to the experiment.

In the core inlet plane a nearly uniform temperature distribution is observed. The temperature difference over the core inlet is less than 5.1 K in the experiment. In the simulation the spread between the maximum and minimum temperature is 2.1 K.

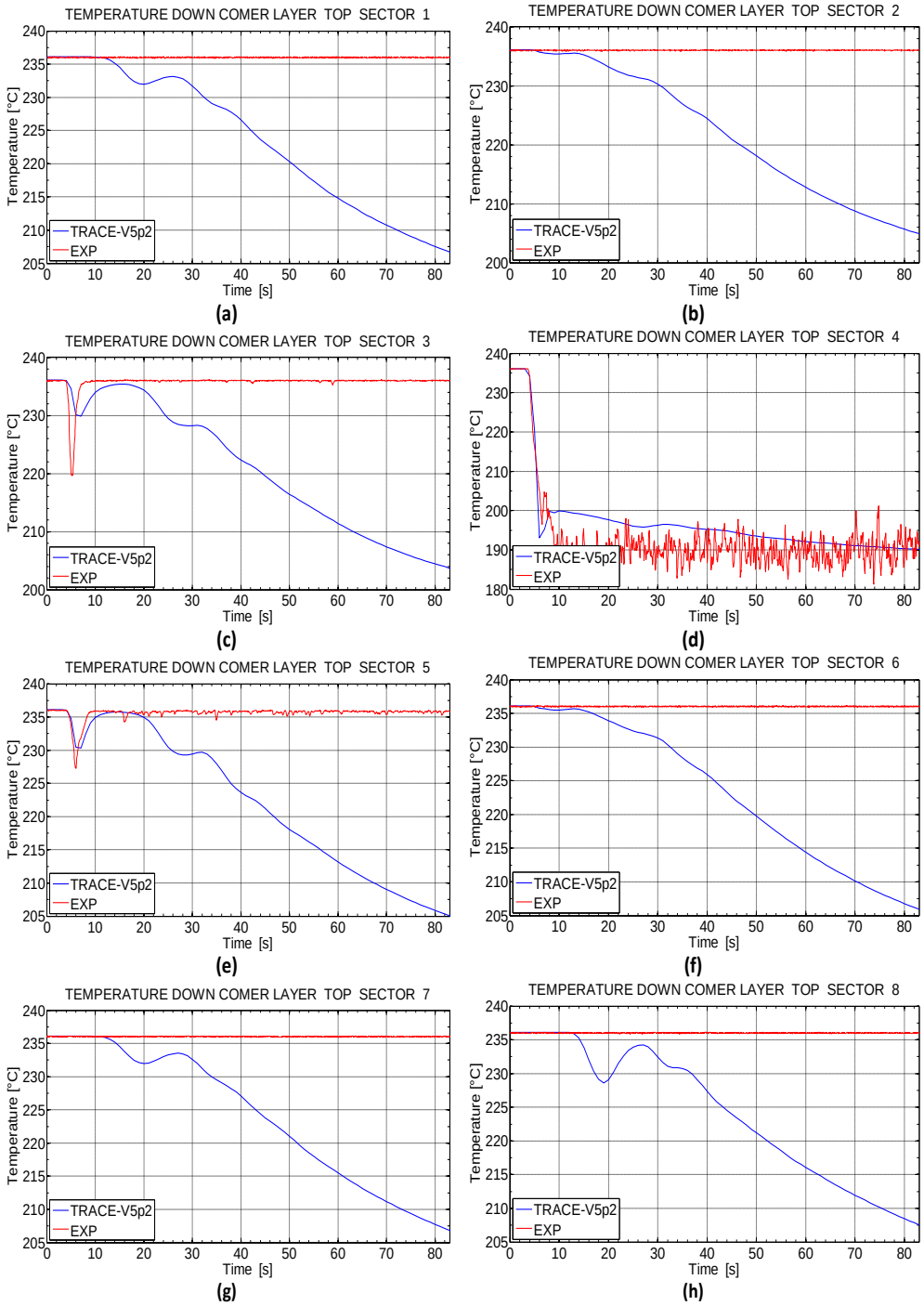

Figure 130 – ROCOM experiment 1.1 reference results: temperatures trends at the downcomer top layer

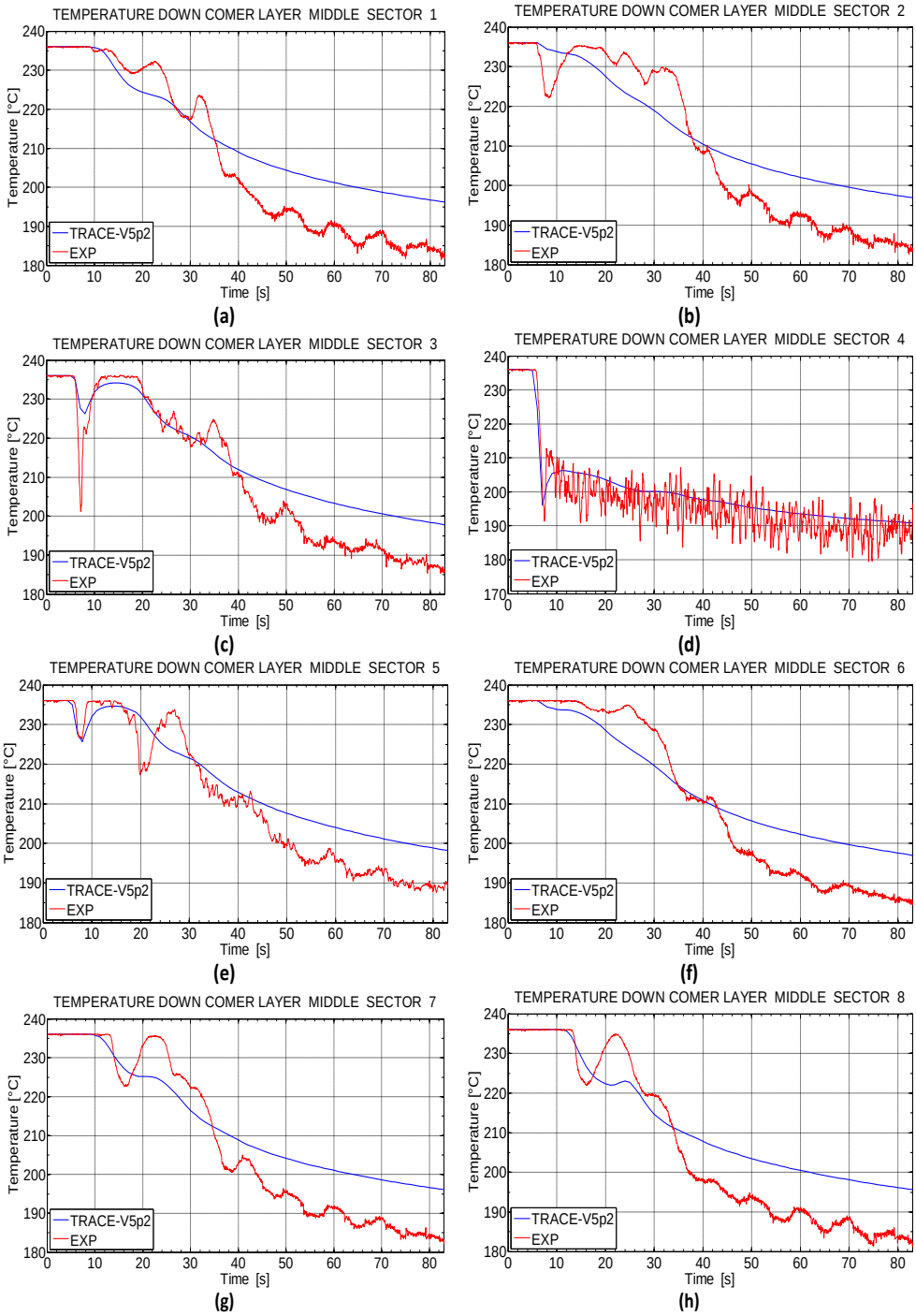

Figure 131 – ROCOM experiment 1.1 reference results: temperatures trends at the downcomer middle layer

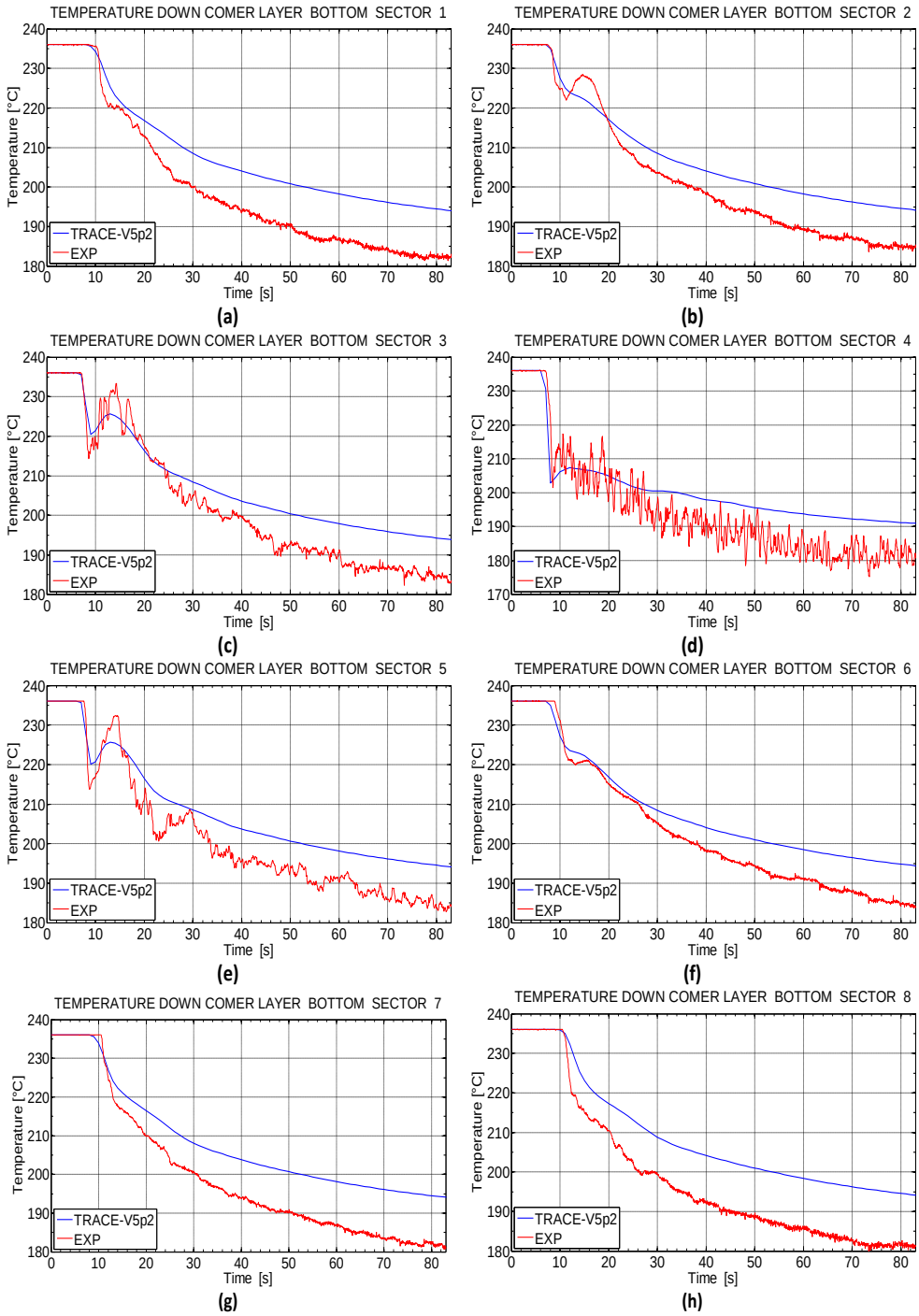

Figure 132 – ROCOM experiment 1.1 reference results: temperatures trends at the downcomer bottom layer

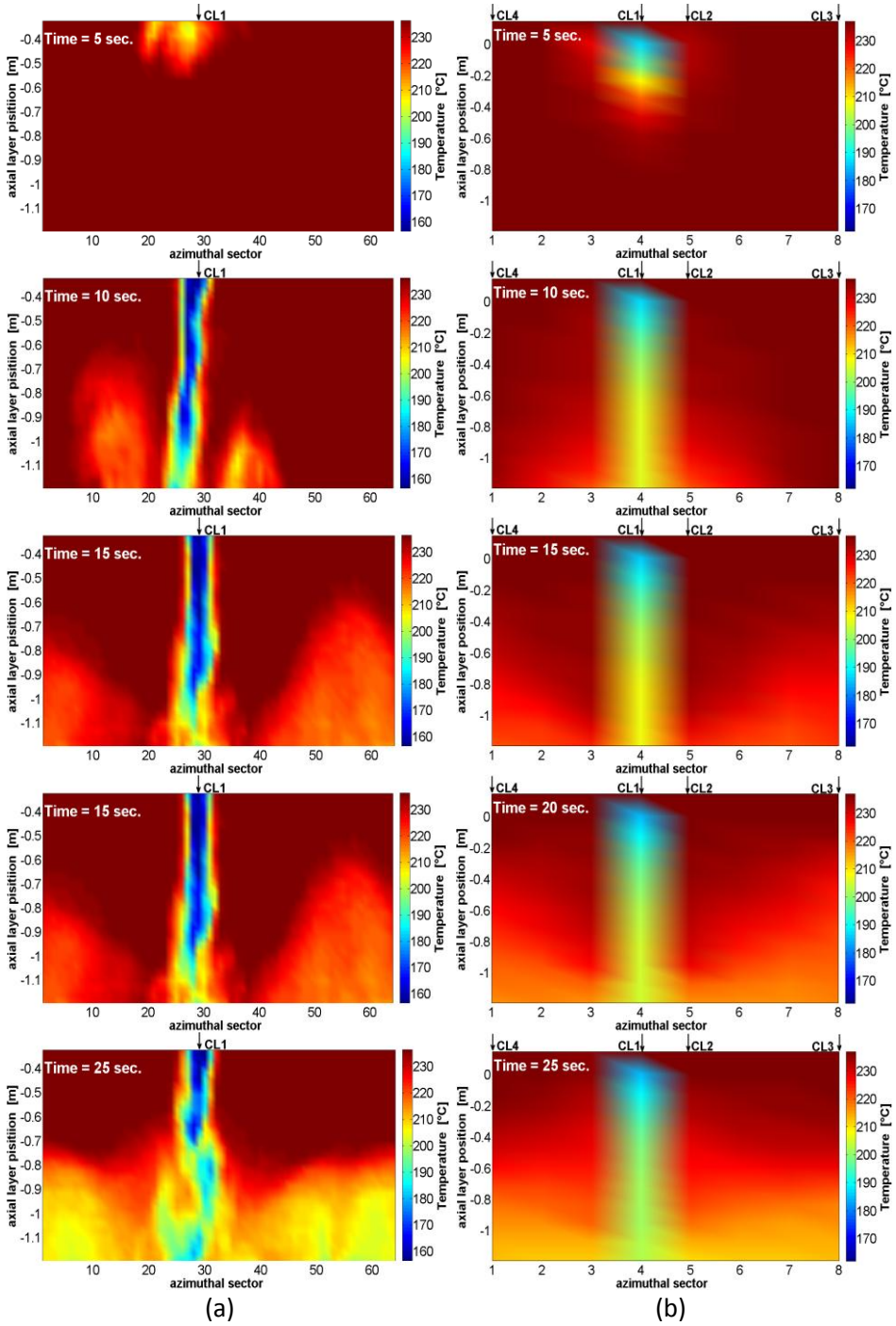

Figure 133 – Snapshots of the temperature distribution in the downcomer (outer plane) at five different time points in tests 1.1 (experimental (a), calculated (b))

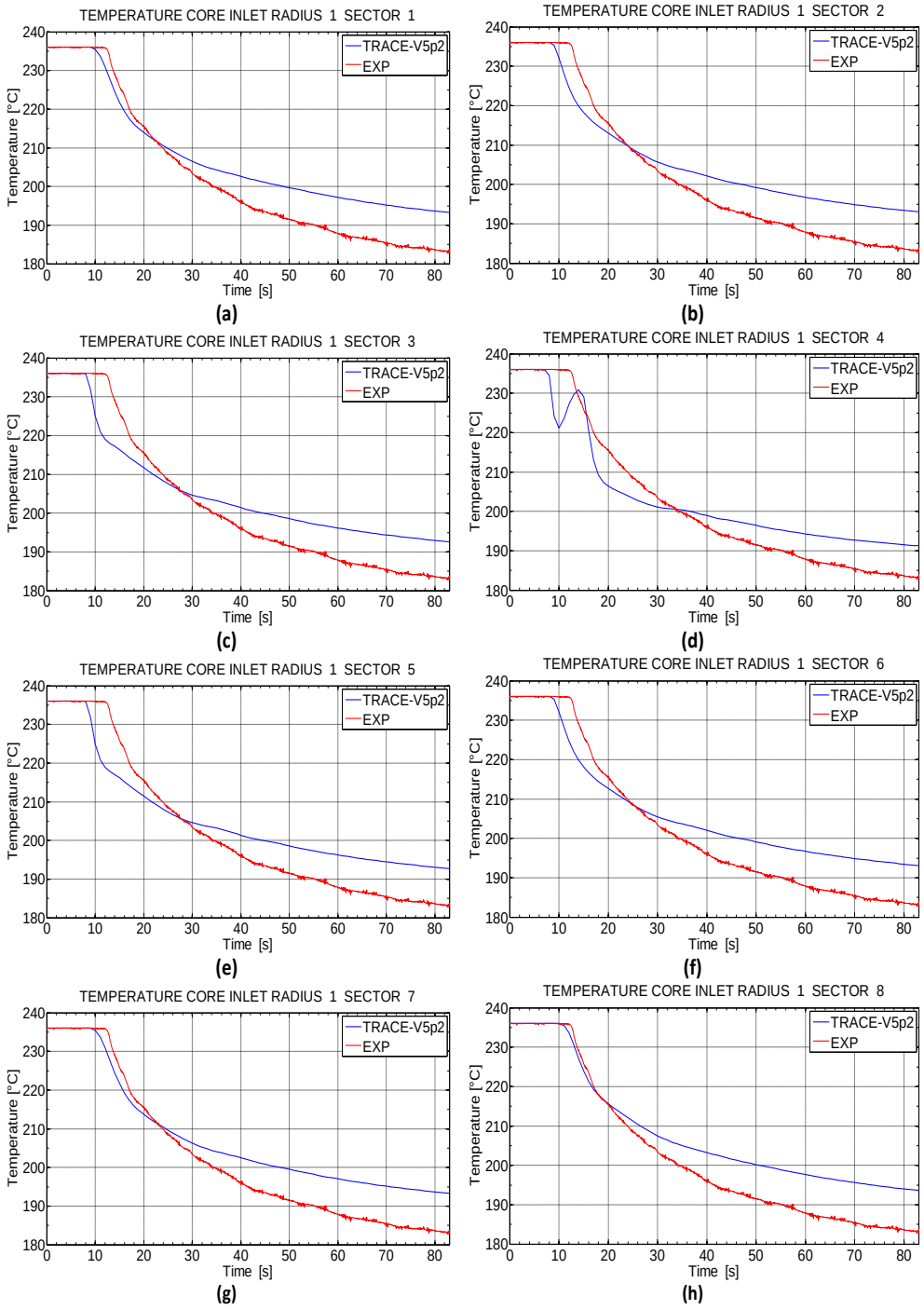

Figure 134 – ROCOM experiment 1.1 reference results: temperatures trends at the core inlet first radial ring, all azimuthal sectors.

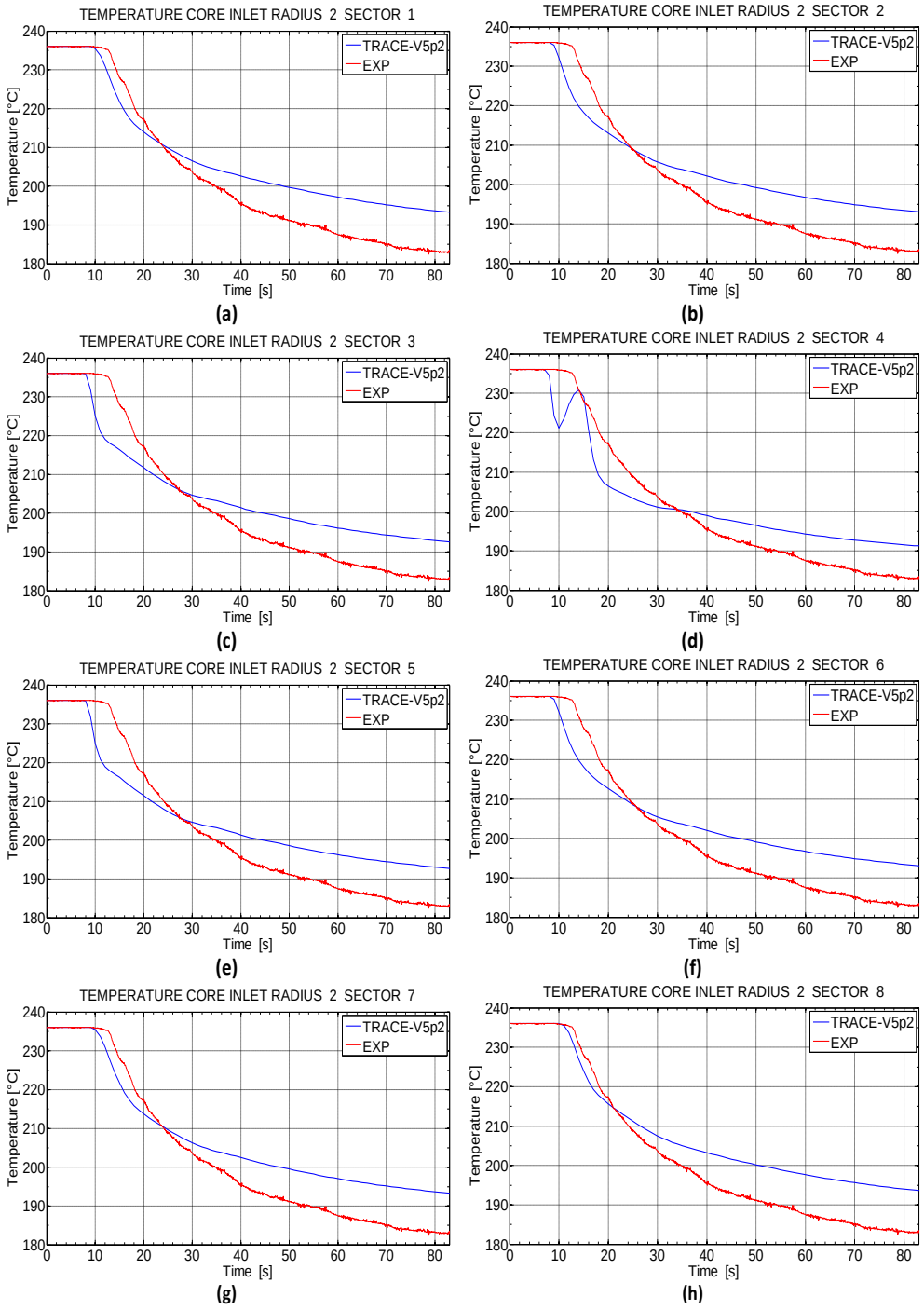

Figure 135 – ROCOM experiment 1.1 reference results: temperatures trends at the core inlet second radial ring, all azimuthal sectors.

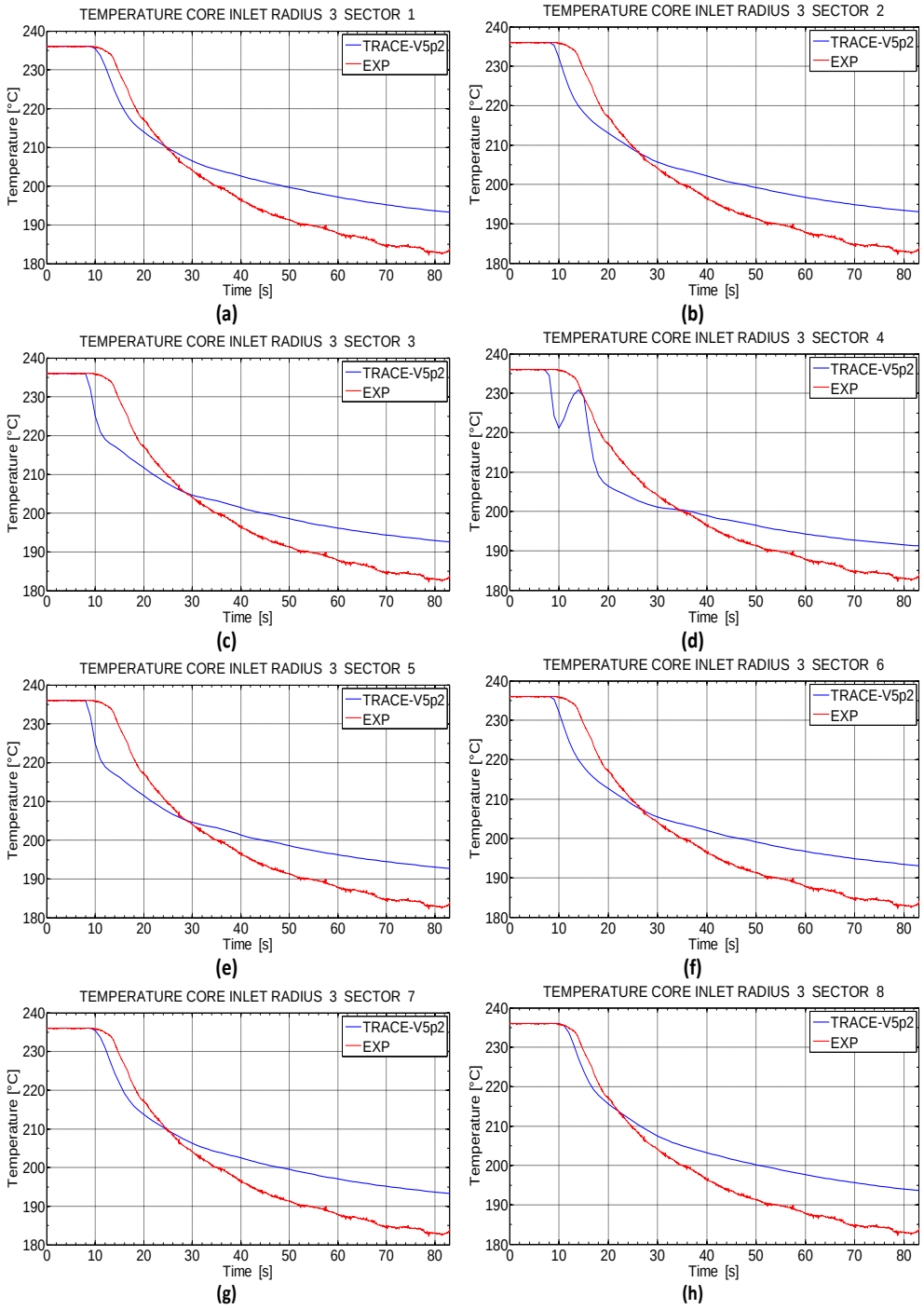

Figure 136 – ROCOM experiment 1.1 reference results: temperatures trends at the core inlet third radial ring, all azimuthal sectors.

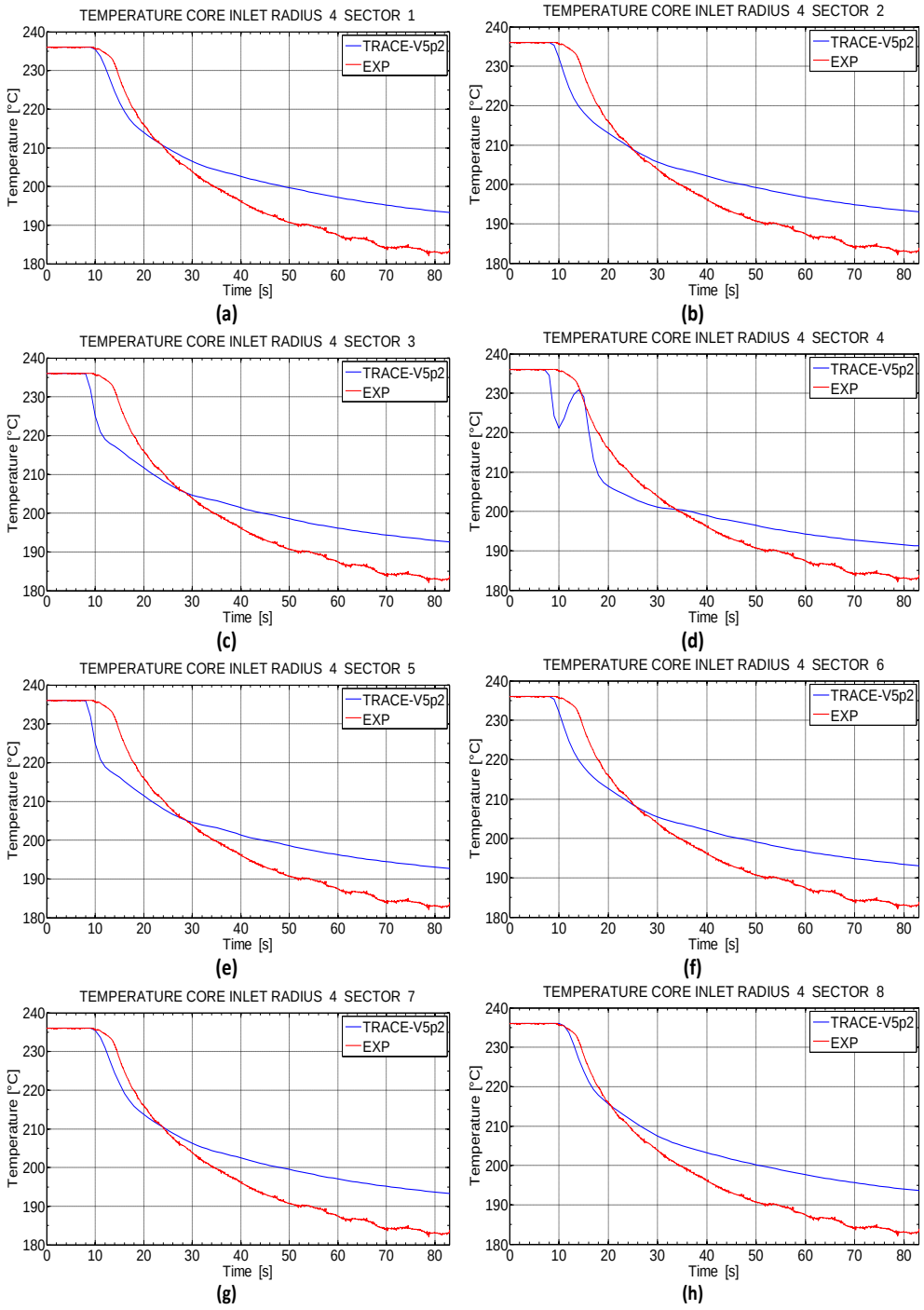

Figure 137 – ROCOM experiment 1.1 reference results: temperatures trends at the core inlet fourth radial ring, all azimuthal sectors.

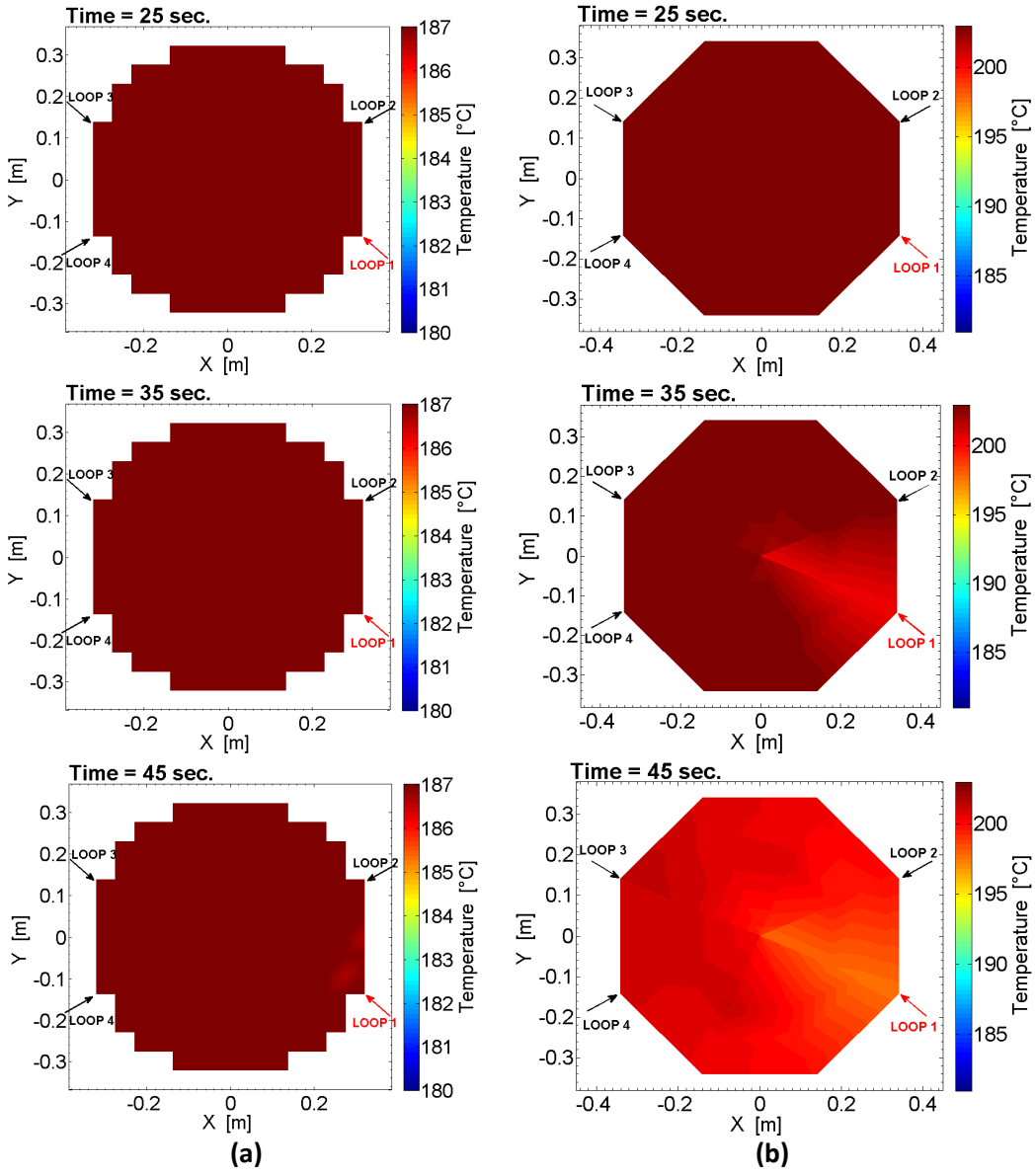

Figure 138 – ROCOM experiment 1.1: snapshots of the temperature distribution in the core inlet at six different time points in tests 1.1. (part 1 of 2) (experimental (a), calculated (b))

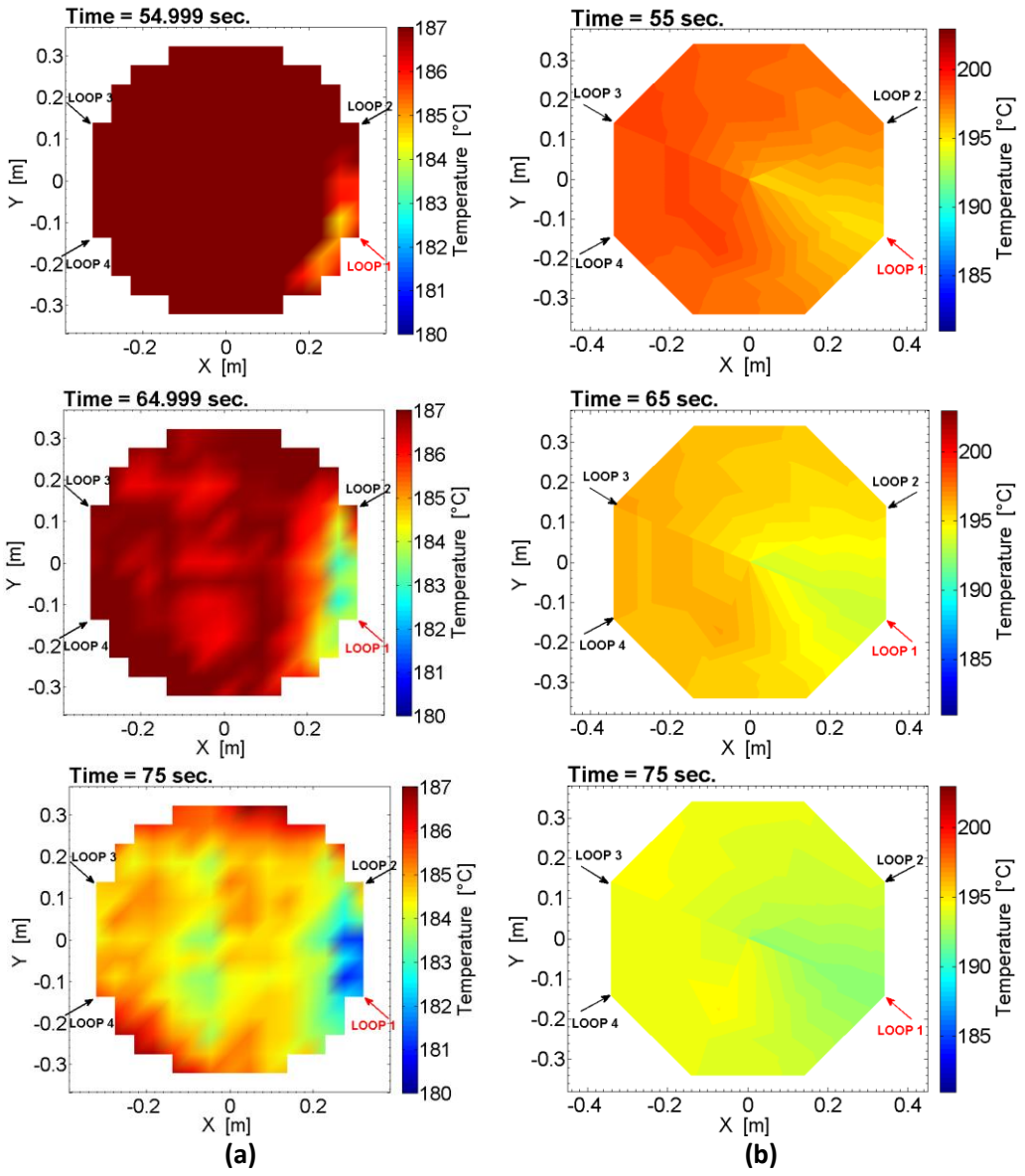

Figure 139 – ROCOM experiment 1.1: snapshots of the temperature distribution in the core inlet at six different time points in tests 1.1. (part 2 of 2) (experimental (a), calculated (b))

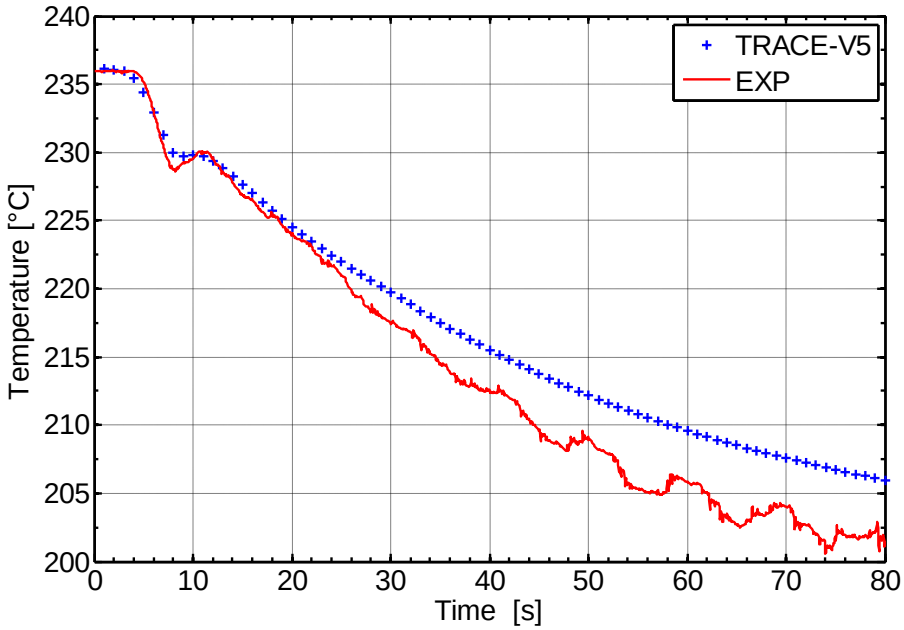

Figure 140 – ROCOM experiment 1.1 averaged temperature evolution inside the DC

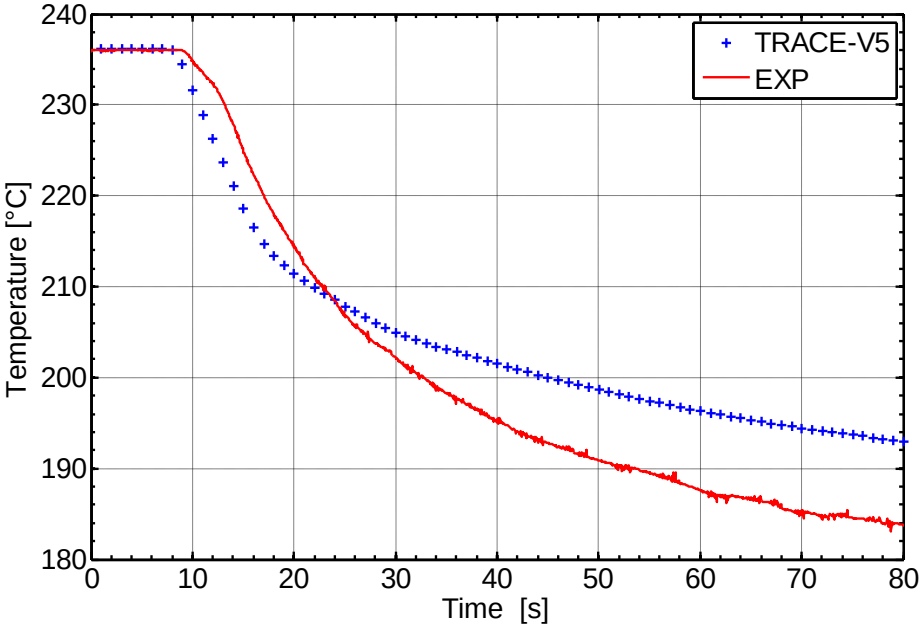

Figure 141 – ROCOM experiment 1.1: averaged temperature evolution at the core inlet

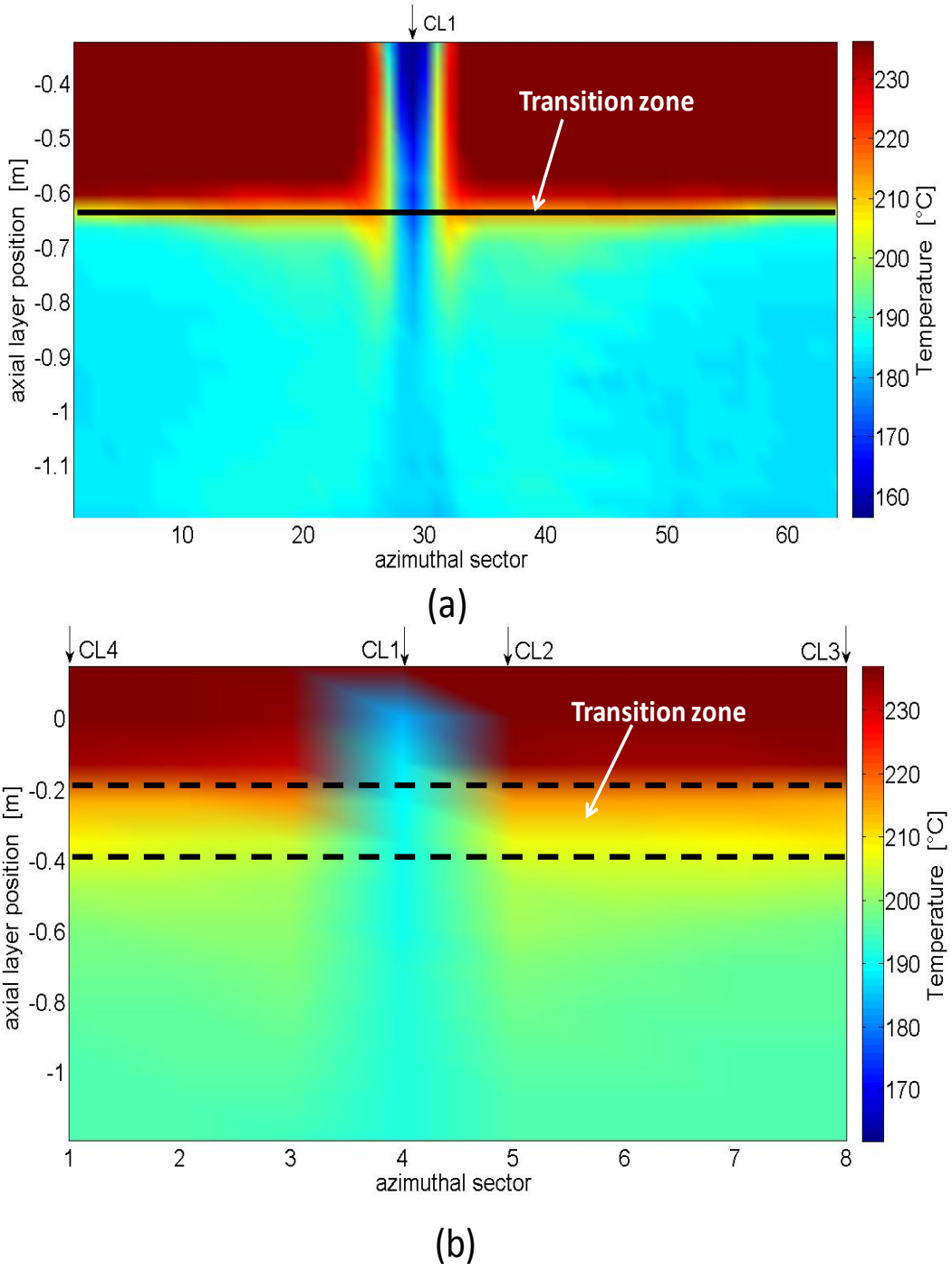

Figure 142 – ROCOM experiment 1.1: experimental (a) and simulated (b) temperature time averaged value in the DC outer plane (time averaging interval: t = 73 s to t = 83 s)

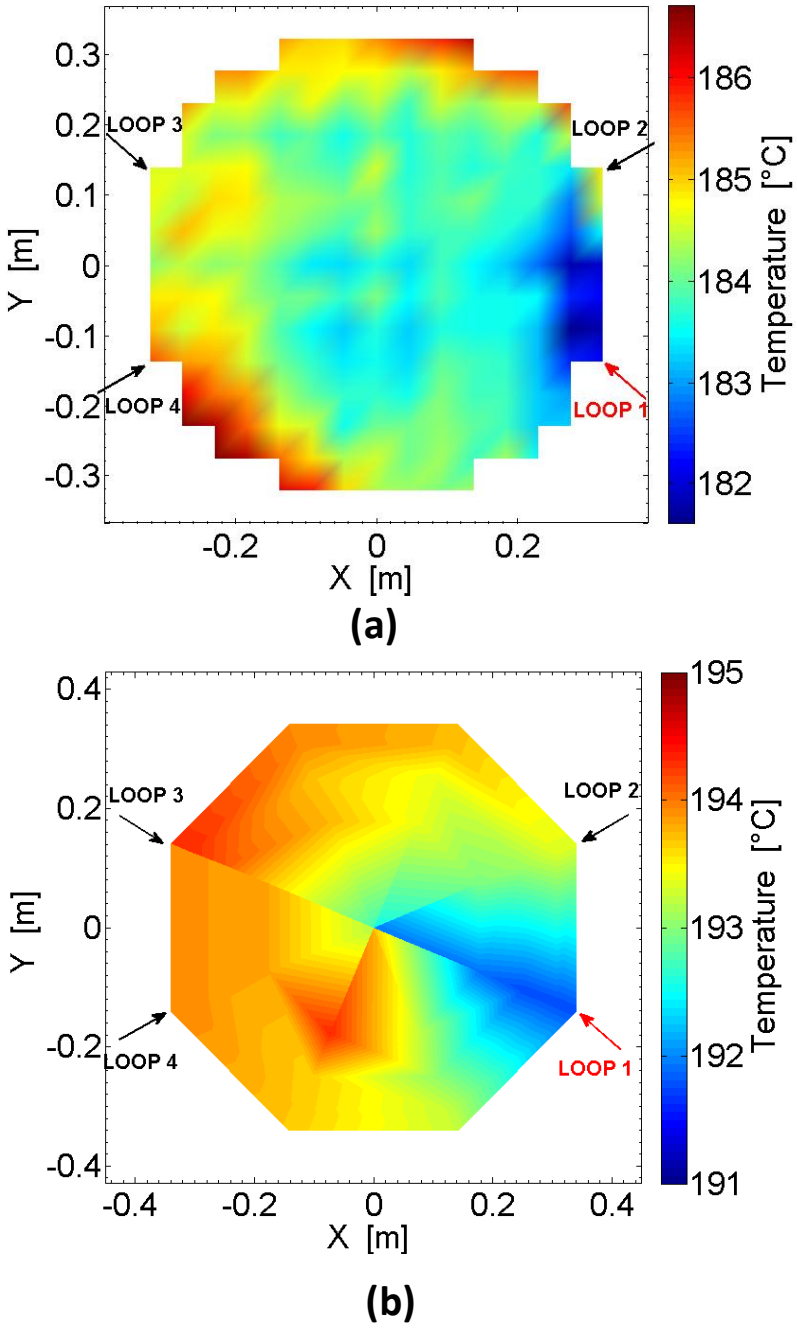

Figure 143 – ROCOM experiment 1.1: experimental (a) and simulated (b) temperature time averaged value at the core inlet (time averaging interval: t = 73 s to t = 83 s)

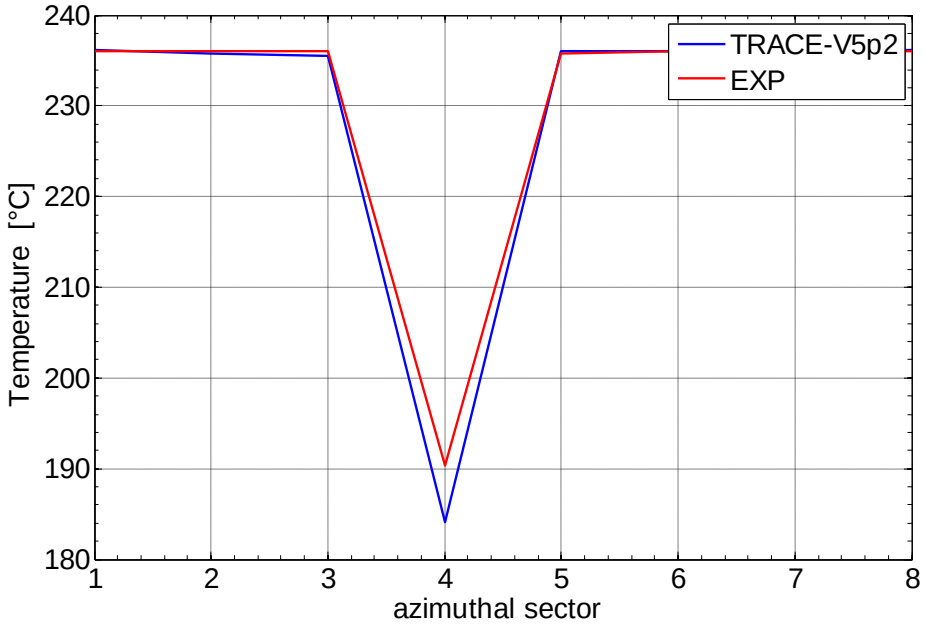

Figure 144 – ROCOM experiment 1.1: downcomer time averaged temperature horizontal cut

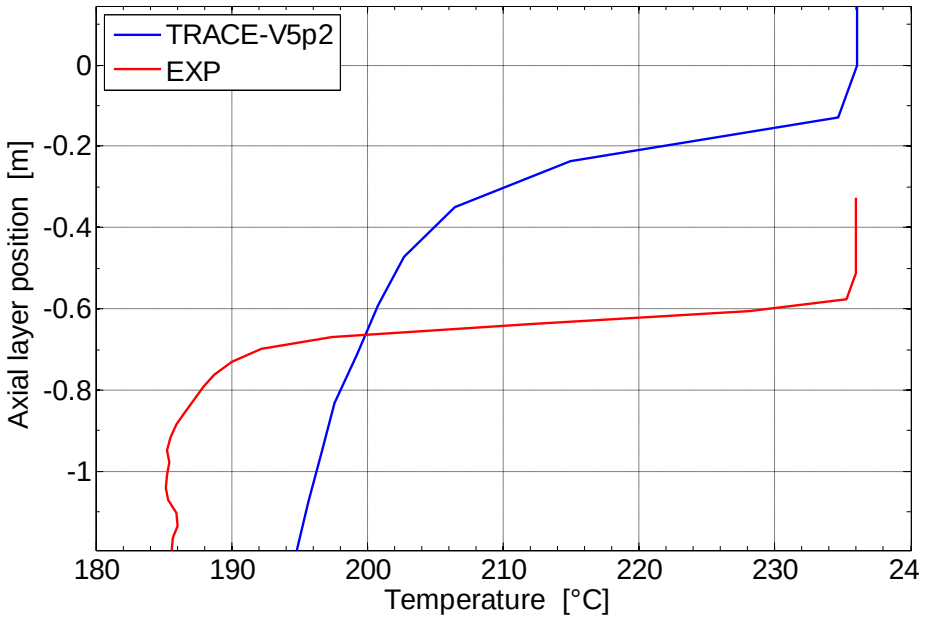

Figure 145 – ROCOM experiment 1.1: downcomer time averaged temperature vertical cut

6.8.3. Simulation of the test 1.2

As addressed in section § 6.7.4.2, the injection of one of the ECC systems takes place into the loop with the higher flow rate which corresponds to the affected loop by MSLB. In the current ROCOM experiment as well as in the TRACE model this loop coincides with loop 3.

The boundary conditions have been set through 100 seconds of null transient (see Table 41 in which are summarized the BC) during which stable steady state flow conditions have been reached in the computational domain. After this time, the injection of the ECC systems in the loop 3 and 4, which are simulated using two FILL components, started. The sequence of events is resumed in the Table 42

Table 41 – ROCOM experiment 1.2: boundary conditions of the TRACE-V5 model (P=3.97 MPa)

Loop	1	2	3	4
Temperature, [^{o}C]	227.65	227.65	227.65	227.65
Mass flow rate, [kg/s]	0.9731	0.9731	2.595	0.9731
ECC injection mass flow rate, [kg/s]	-	-	0.5194	0.5194
ECC injection temperature, [^{o}C]	-	-	25.0	25.0

Table 42 – ROCOM experiment 1.2: adopted procedure

Cal. Time (s)	Event
0 – 100	Establish stationary flow conditions in all loops • Temperatures of all loops are equal, 227.65 °C • Controlling outlet pressure to maintain flow rate in each loop, No ECC
100	Start of injection of ECC water (25 °C) into loop 3 and 4
220	End of calculation

For the assessment of agreement between calculation and measurement a local and integral analysis of the temperature distribution time history based on qualitative but also quantitative evaluation of the accuracy has been performed in the same way as it has been done for the test 1.1.

6.8.3.1. Analysis of the results: experiment/simulation temporal comparison

6.8.3.1.1. Pseudo local analysis

The analysis of TRACE-V5 calculations of the temperature distribution time history in the vessel are performed comparing they with the experimental data at the axial computational points inside the DC and in all the azimuthal sectors of the four radial ring at the elevation of the CSP as for the test 1.1. The temperature trends at the top of the DC in the affected sectors, namely the computational sectors 8 and 1 corresponding to loops 3 and 4 show a well perdition of onset time of thermal perturbation due to the ECC injections of cold water (Figure 146(a) and Figure 146(h)). The injections perturb as well the neighboring sectors, i.e. sectors 7 and 2 (Figure 146(b) and Figure 146(g)). These effects are reproduced in the TRACE-V5 simulation whit asymmetric subcooling peaks compared to the experiment as consequence of the azimuthal thermal diffusion of numerical nature (see Figure xx(b) and (g)). The mixing transition region between perturbed and unperturbed coolant located at higher axial position is the cause of temperature decrease in all sectors of the DC top layer (see Figure 146). In the middle layer the calculations simulated qualitatively a similar trend to the experimental one with a tendency towards lower temperature at the end of the test (see Figure 147). The coalescence of the of two ECC water stripes in downcomer observed at the bottom of the DC in the experiment looking to temperature behavior in the sectors 8 and 1, is also simulated by the code. In fact after approximately 19 s after the start of the test the perturbation reached these sectors at the bottom of the DC causing a sharp decrease of the temperatures that reach in few time approximately the same value, namely 213 °C. In the simulation this effect is virtually flattened by the numerical diffusion (see Figure 148(a) and Figure 148(h)). Furthermore the temperature rise immediately after the subcooling peak in the sector 8 is due to the shifting of the unified stripe towards the position of loop 4 (see Figure 148(h)) that promotes the heat conduction from the unperturbed sectors which in turn begin the cooling phase after a few seconds as result of the rising of the mixing front (see Figure 148(c), (d), (e) and (f)). A possible explanation for this shift is the difference between the loop flow rates; loop 4 is the loop with lower mass flow rate. Looking to the temperature temporal behavior in the same azimuthal position the subsequent heating phase is partial reproduced because of the merging plumes move down with less deviation from the middle between both inlet nozzles. Moreover the simulated strip is more stratified in both azimuthal and axial direction than the experimental one (see Figure 149).

At the core inlet (CSP zone) the results of the TRACE-V5 simulation show an anticipated cooling in almost all meshes and in turn a more intensive mixing that determines a global decrease of the temperature time trend compared to the experimental temperature distribution (Figure 150 to Figure 153). The main reason of this behavior is explained by the fact that the advective transport of energy represents the dominant mixing process in the lower plenum for this test reducing the effects of the numerical diffusion. The greatest influence of the numerical diffusion is linked with time difference of appearance of the perturbation at the core inlet. The Figure 154 and Figure 155 show 2-D temperature map in the core inlet at six different time points the. The appearance of cold sector can be seen in the

simulation in contrast to the experiment in which a homogeneous temperature is observed (see 155(a)).

6.8.3.1.2. Averaging analysis

The averaging analysis has the same goals outlined for the test 1.1, namely the investigation of the macroscopic behavior of the TRACE-V5 results in simulating the mixing phenomenon, and therefore the evolution of the transition region between perturbed and unperturbed fluid in the downcomer and at the core inlet. The results of the analysis are shown in Figure 156 and Figure 157. The integral behavior of the temperature in the DC highlights an anticipated overcooling trend due to the higher dispersion of the transition zone between the cold region and the unperturbed hot region compared to the experimental one.

6.8.3.2. Analysis of the results: experiment/simulation spatial comparison

For establishing quasi-stationary flow conditions derived from the time point of ECCS injection in the PKL test and to compare computation and experimental results, a time-averaging was applied to the sensor data at each measurement position from t = 60 to t = 70 s and at each computational cell inside the DC and at the core inlet.

In the downcomer, stratification takes place. Likewise to the test 1.1 two transition zones can be compared:

- horizontal separation is characterized by the transition from hot water to mixed water;
- vertical separation is characterized by coalescence of two ECC water stripes at an asymmetrical position and transition from the affected cold legs stream to hot water on the upper downcomer. The unified stripe does not move down in the middle between both inlet nozzles. It is shifted towards the position of loop 4.

At the core inlet (Figure 159(a)) again no sector formation is to be seen. As mentioned before, in the simulation sector formation can be seen (Figure 159(b)). A nearly uniform distribution of the temperature with a temperature difference of less than 3 °C is measured; the maximum and minimum temperature difference obtained by the numerical simulation is 4.25 °C. This high discrepancy between calculated and experimental data is attributed to the higher maximum temperature at the core inlet. Namely the maximum temperature observed in the experiment is 216 °C, whilst in the TRACE-V5 simulation the maximum temperature is approximately 218 °C.

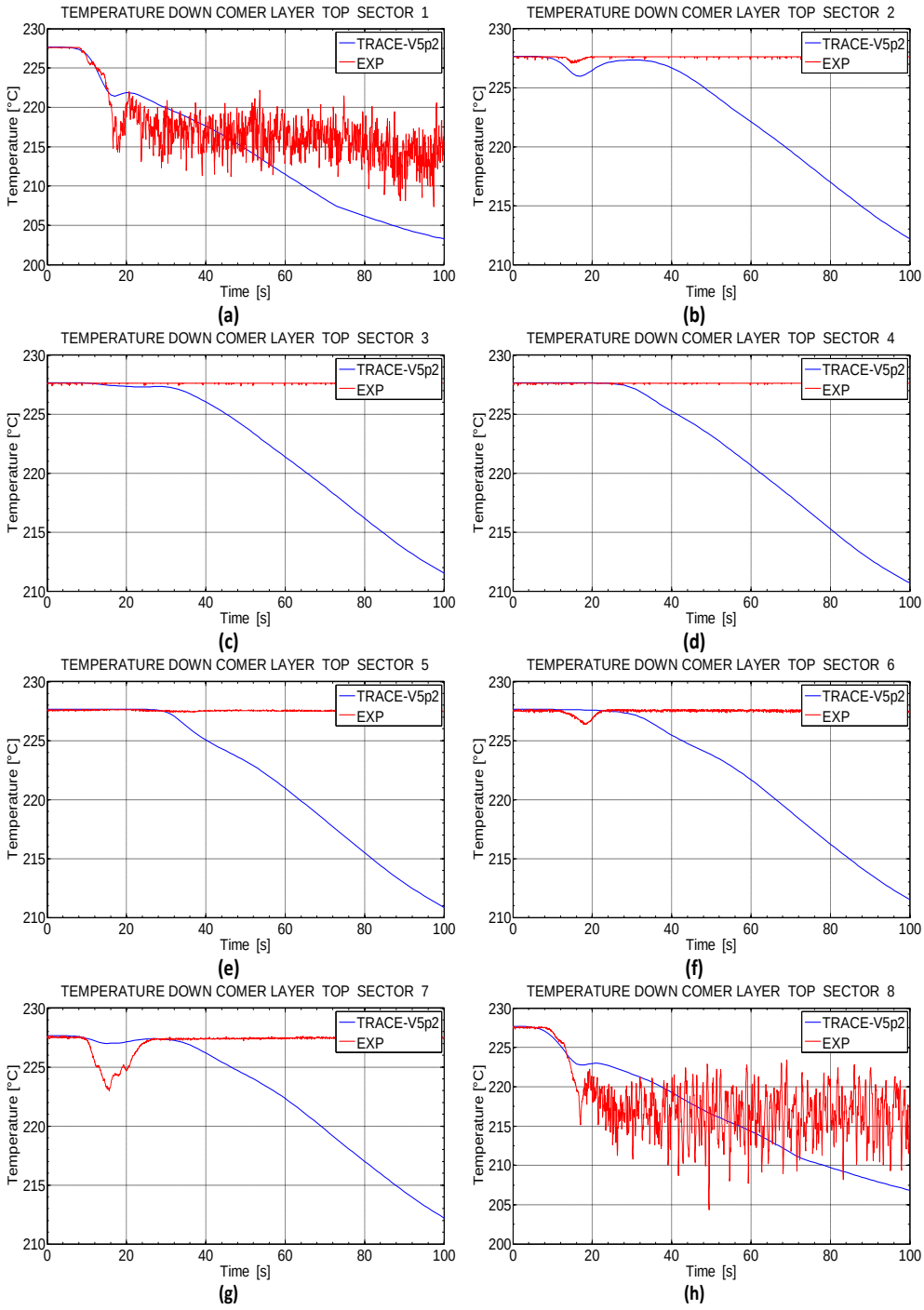

Figure 146 – ROCOM experiment 1.2 reference results: temperatures trends at the downcomer top layer

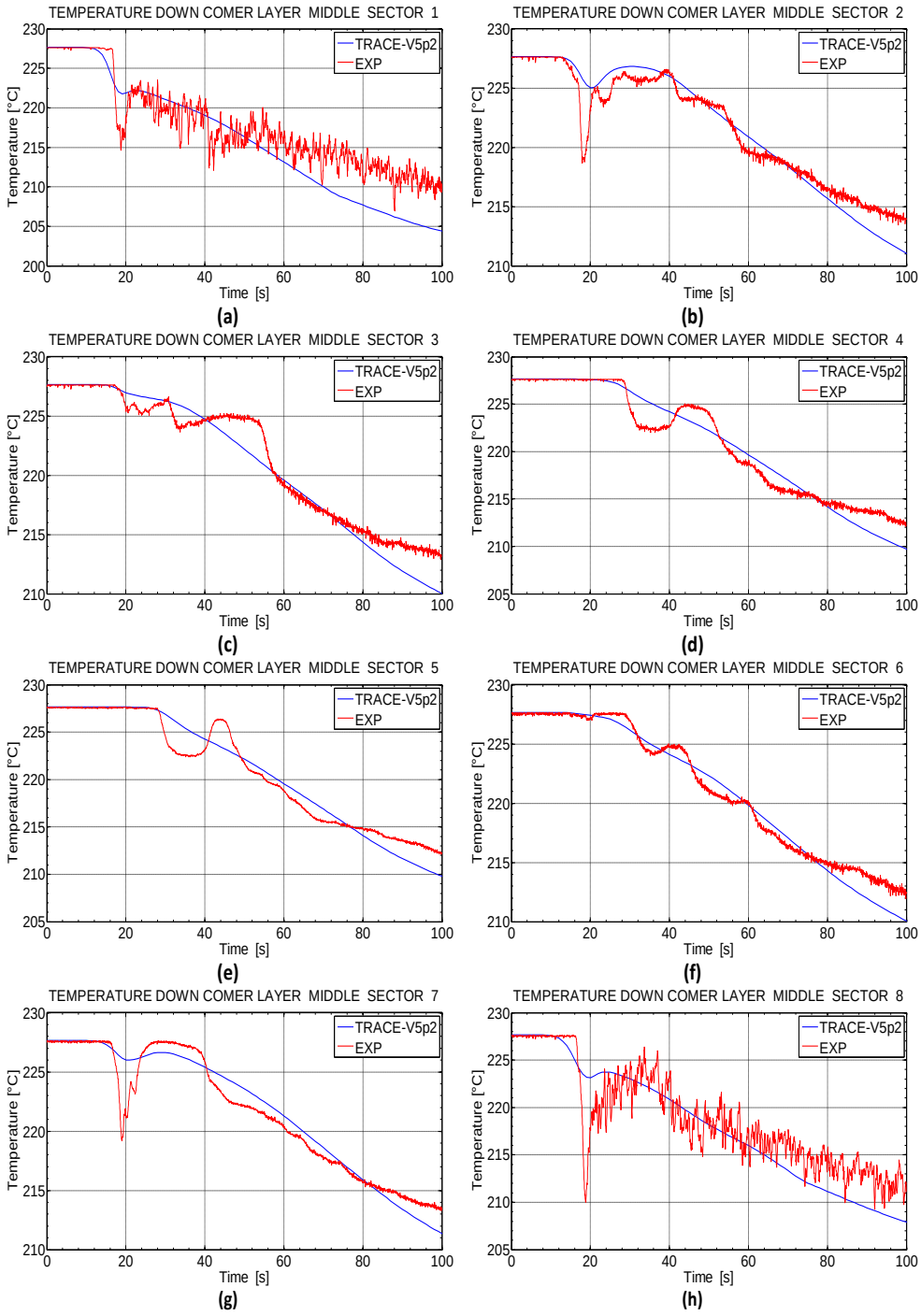

Figure 147 – ROCOM experiment 1.2 reference results: temperatures trends at the downcomer middle layer

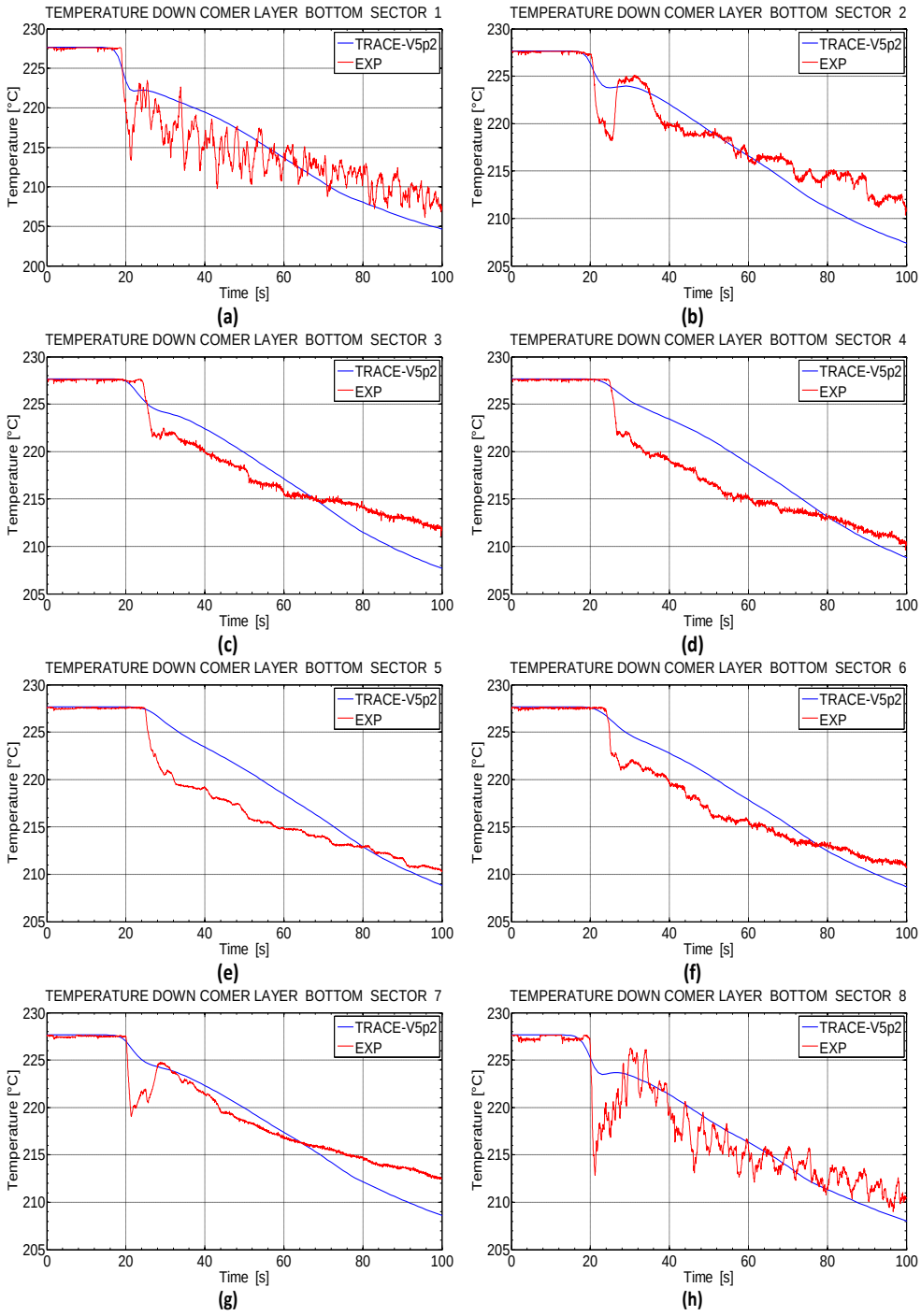

Figure 148 – ROCOM experiment 1.2 reference results: temperatures trends at the downcomer bottom layer

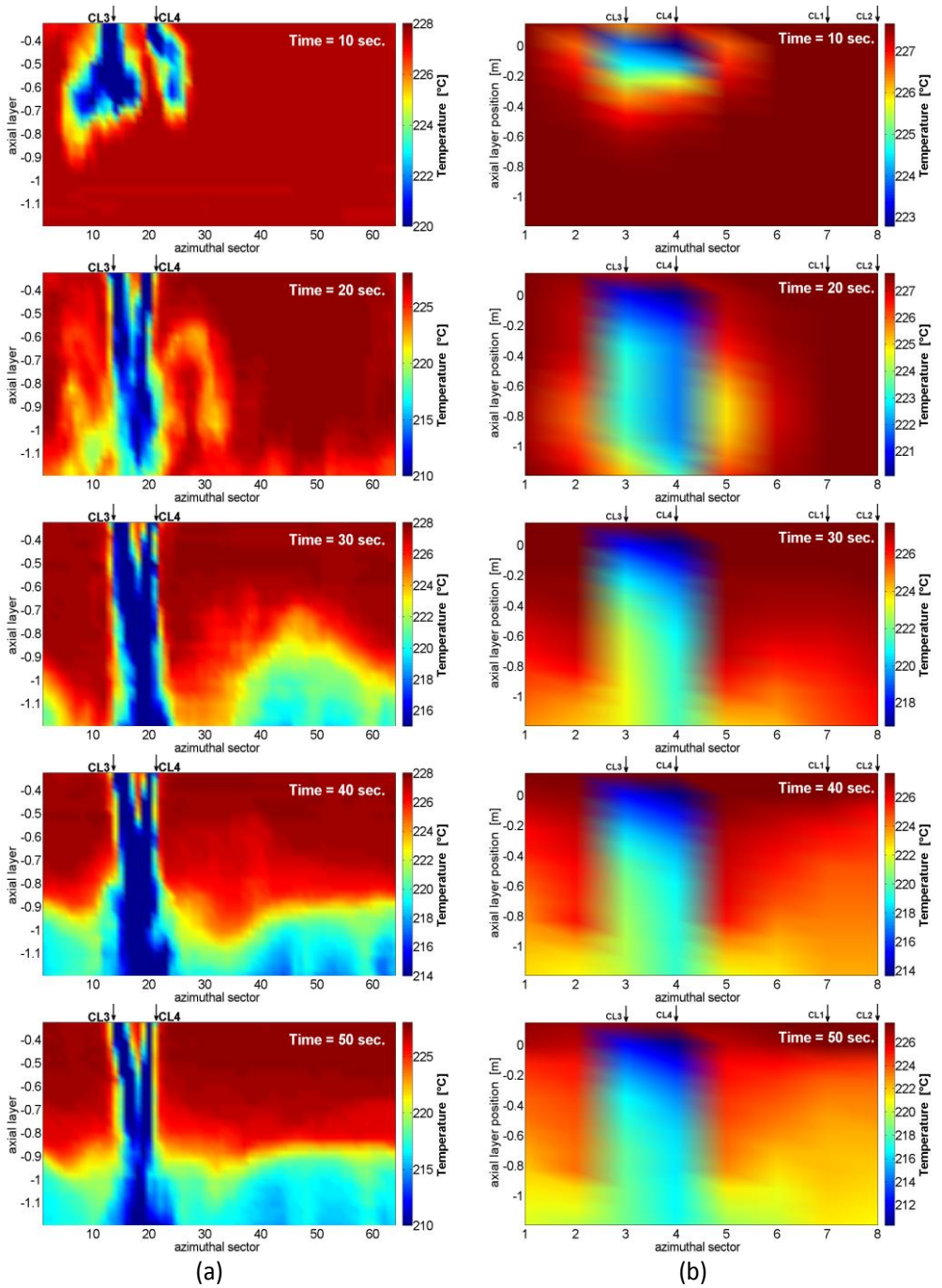

Figure 149 – ROCOM experiment 1.2: snapshots of the temperature distribution in the downcomer (outer plane) at five different time points in tests 1.2 (experimental (a), calculated (b))

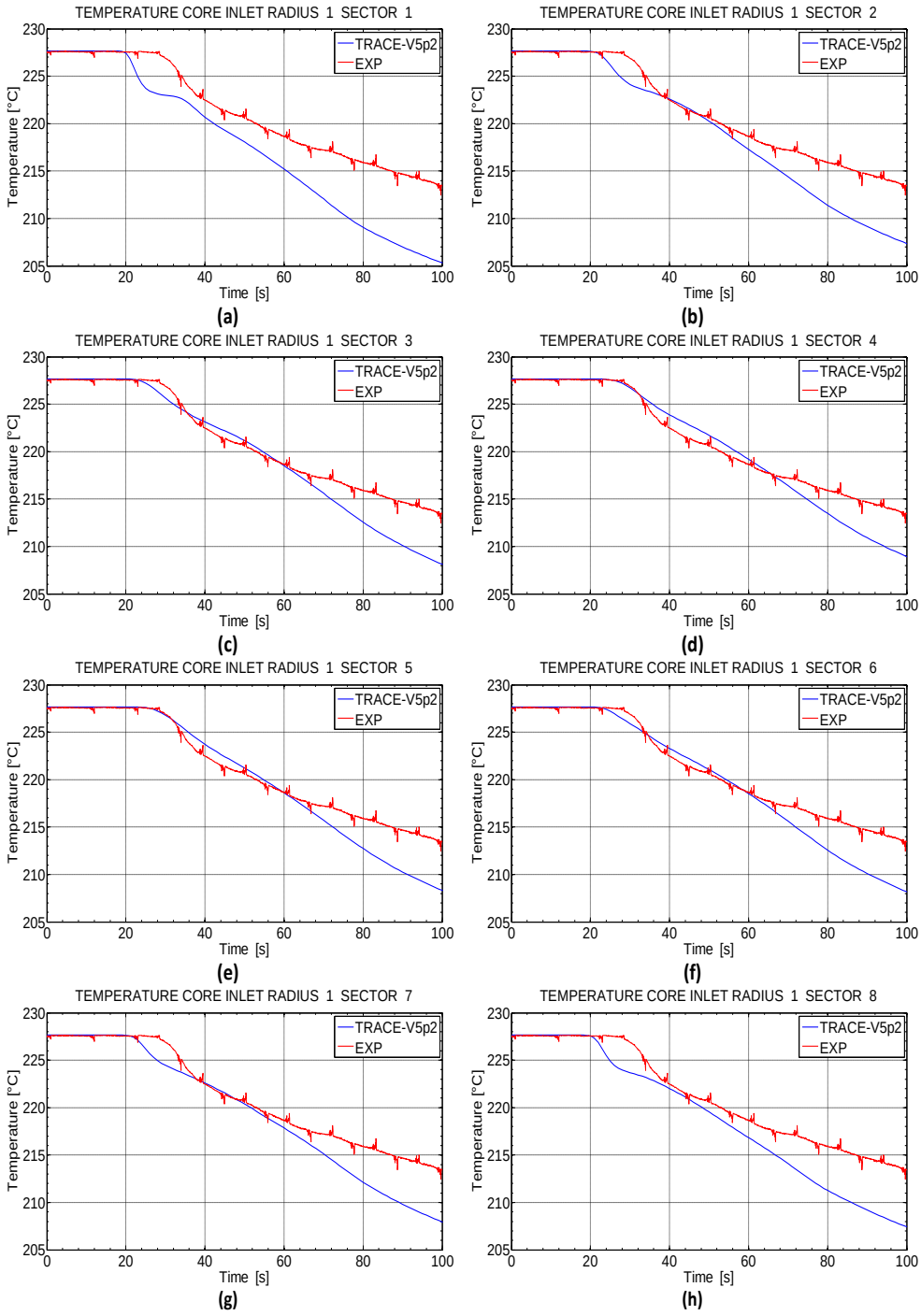

Figure 150 – ROCOM experiment 1.2 reference results: temperatures trends at the core inlet first radial ring, all azimuthal sectors

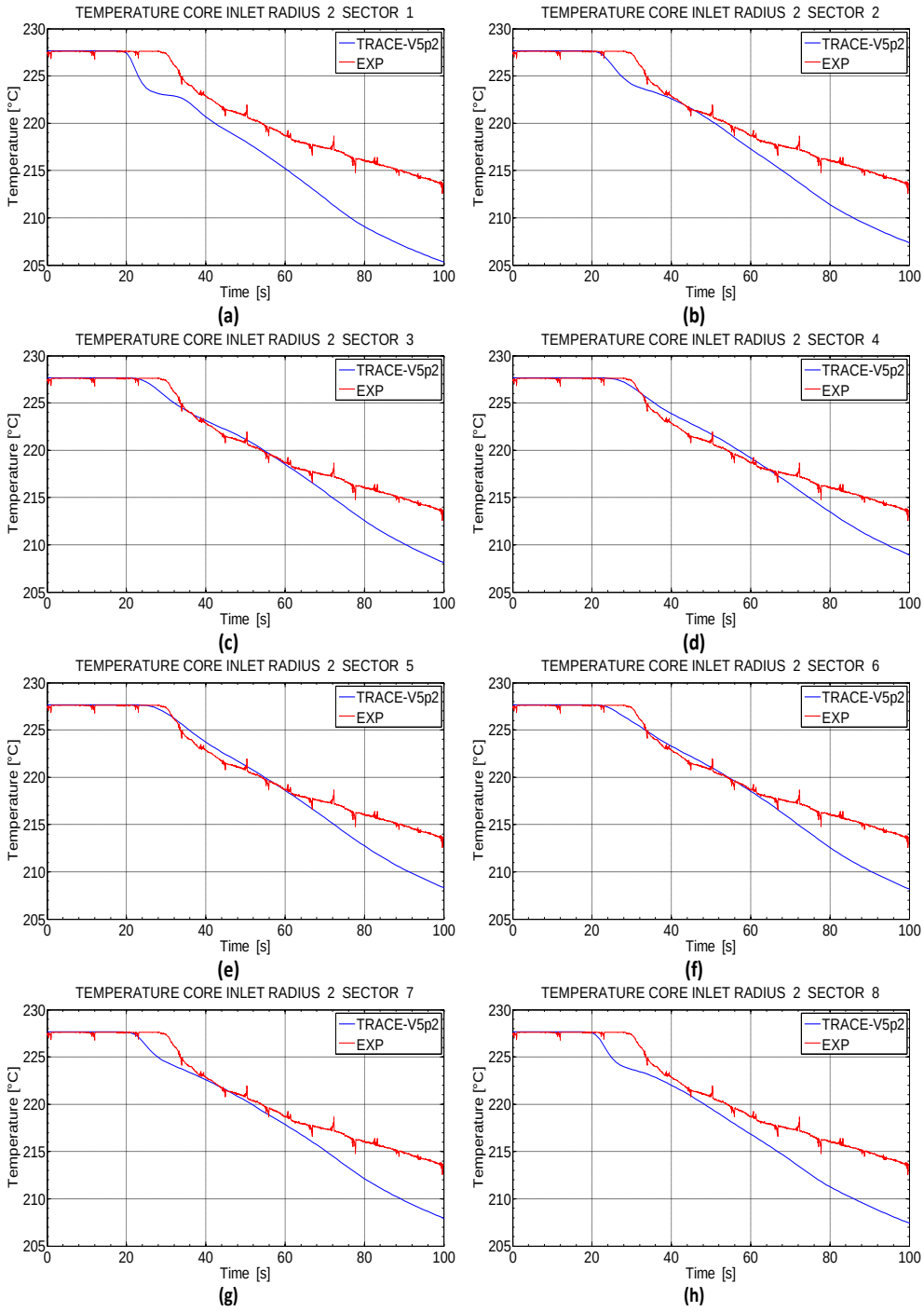

Figure 151 – ROCOM experiment 1.2 reference results: temperatures trends at the core inlet second radial ring, all azimuthal sectors

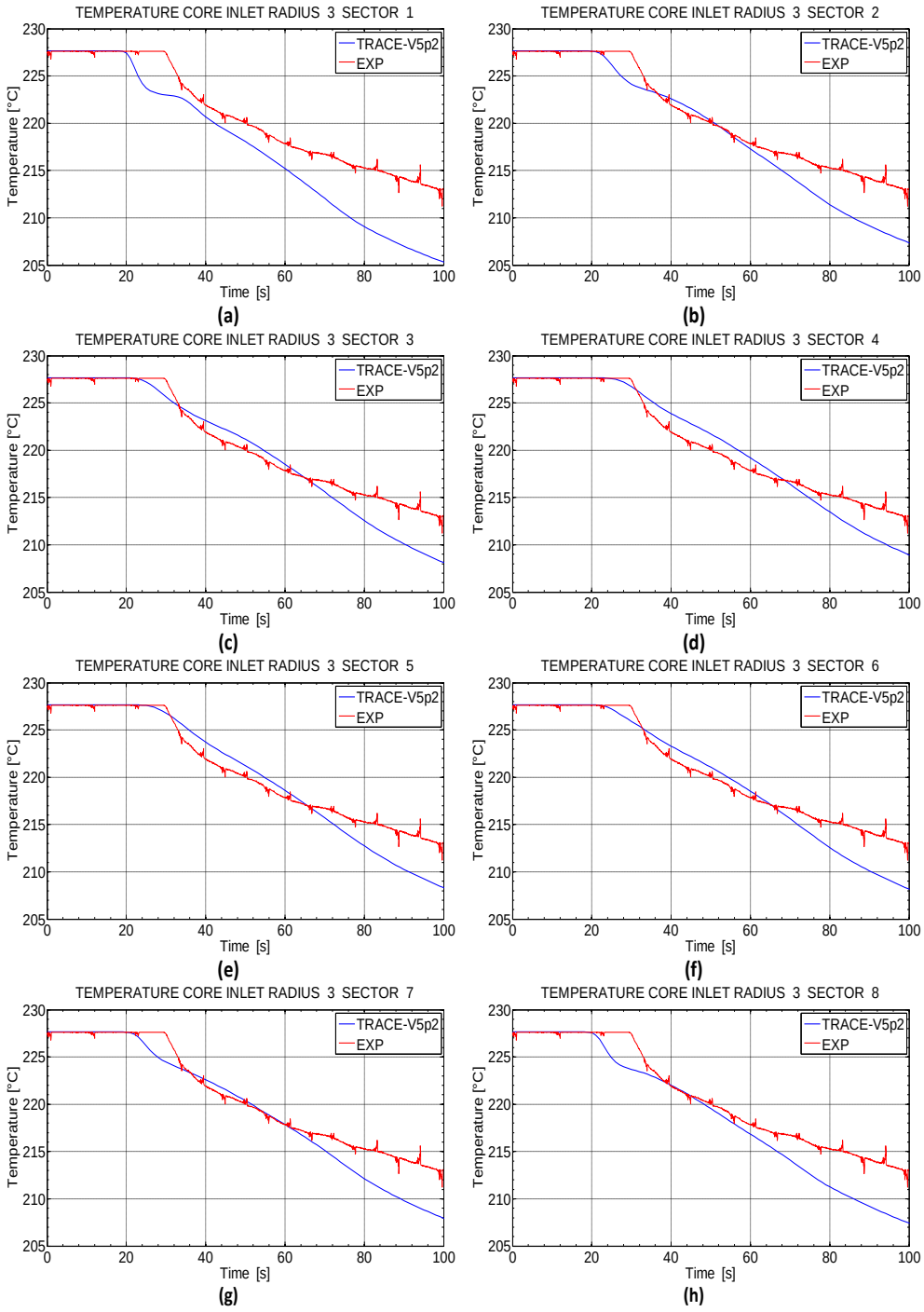

Figure 152 – ROCOM experiment 1.2 reference results: temperatures trends at the core inlet third radial ring, all azimuthal sectors

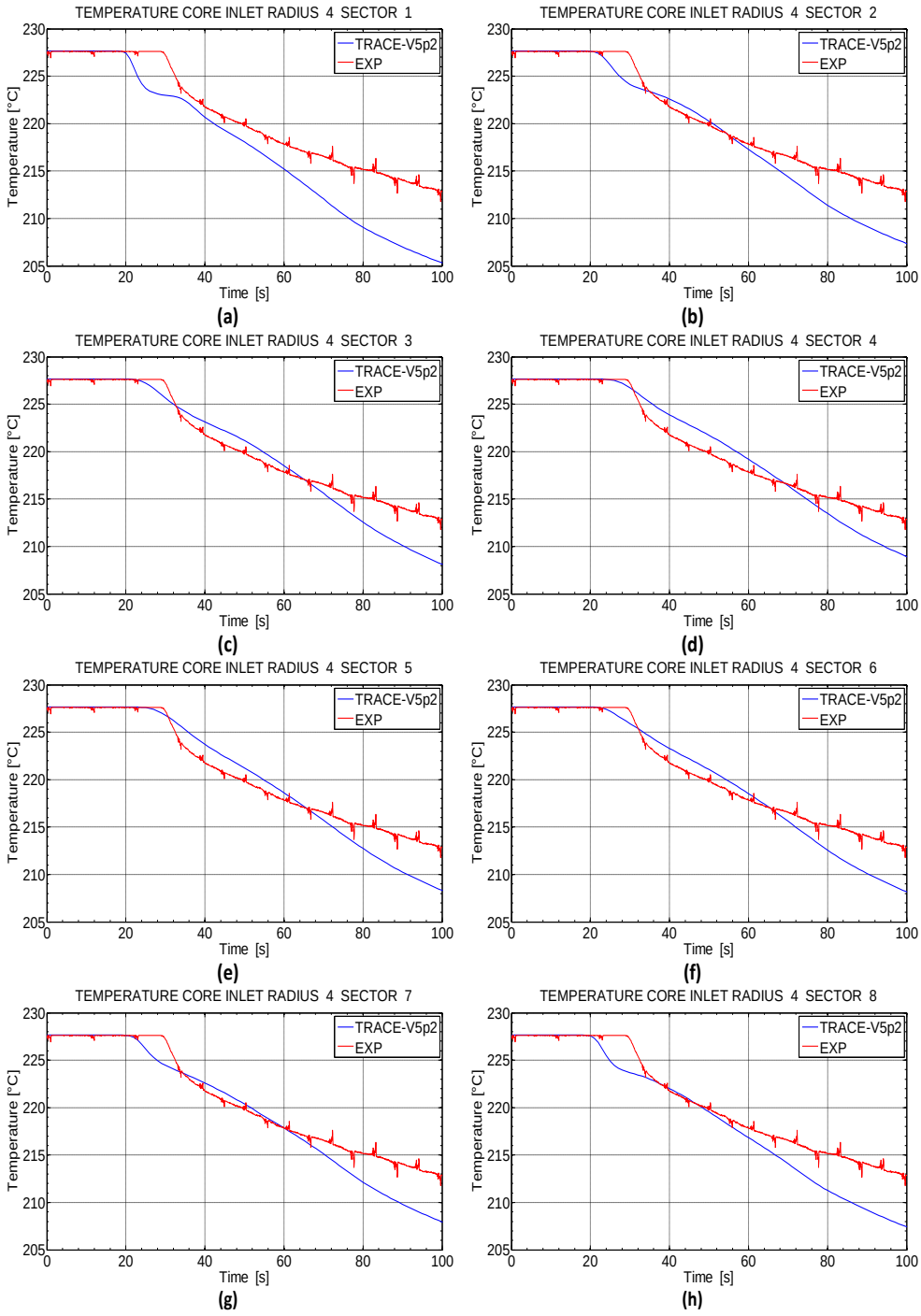

Figure 153 – ROCOM experiment 1.2 reference results: temperatures trends at the core inlet fourth radial ring, all azimuthal sectors

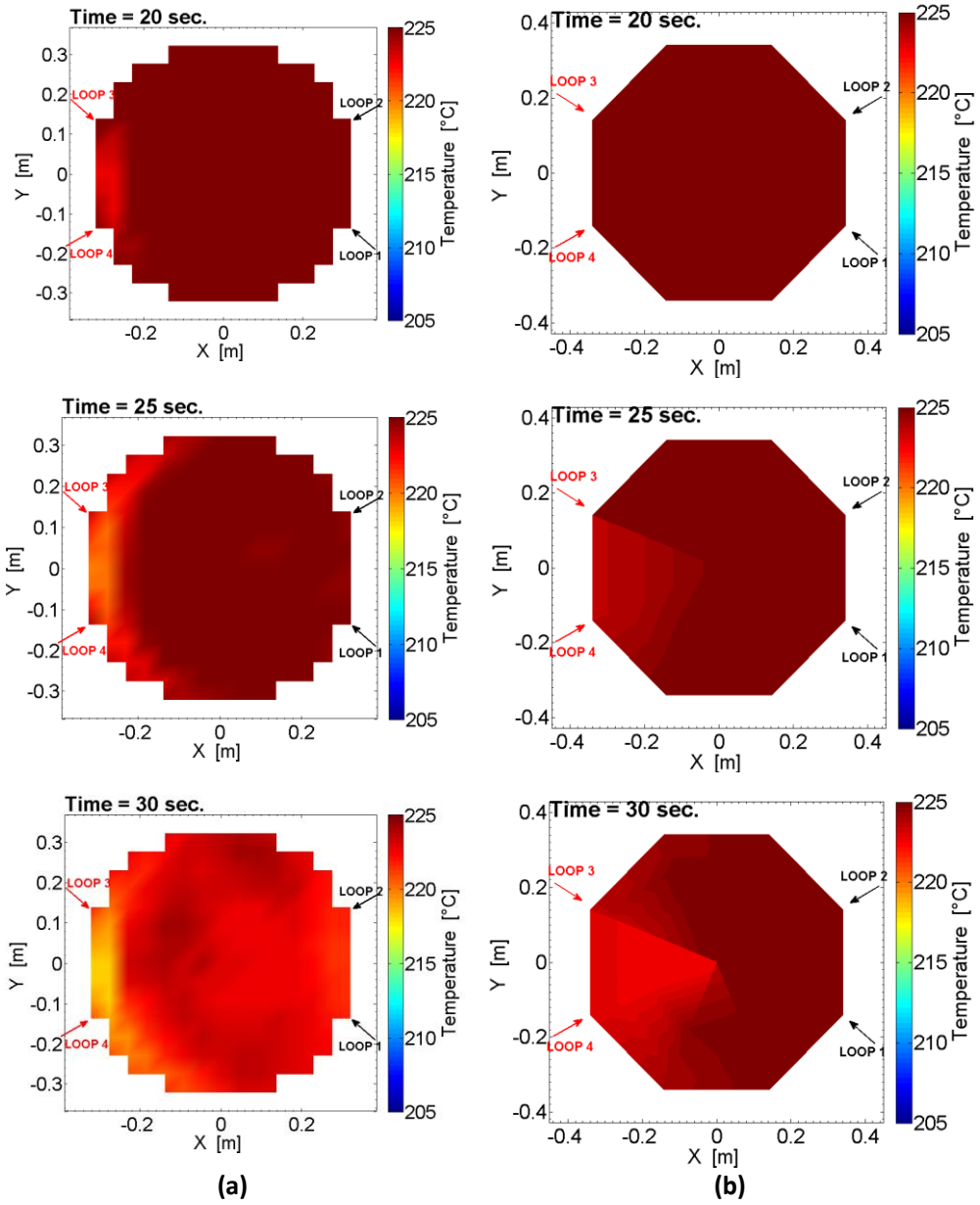

Figure 154 – ROCOM experiment 1.2: snapshots of the temperature distribution in the core inlet at six different time points (part 1 of 2) (experimental (a), calculated (b))

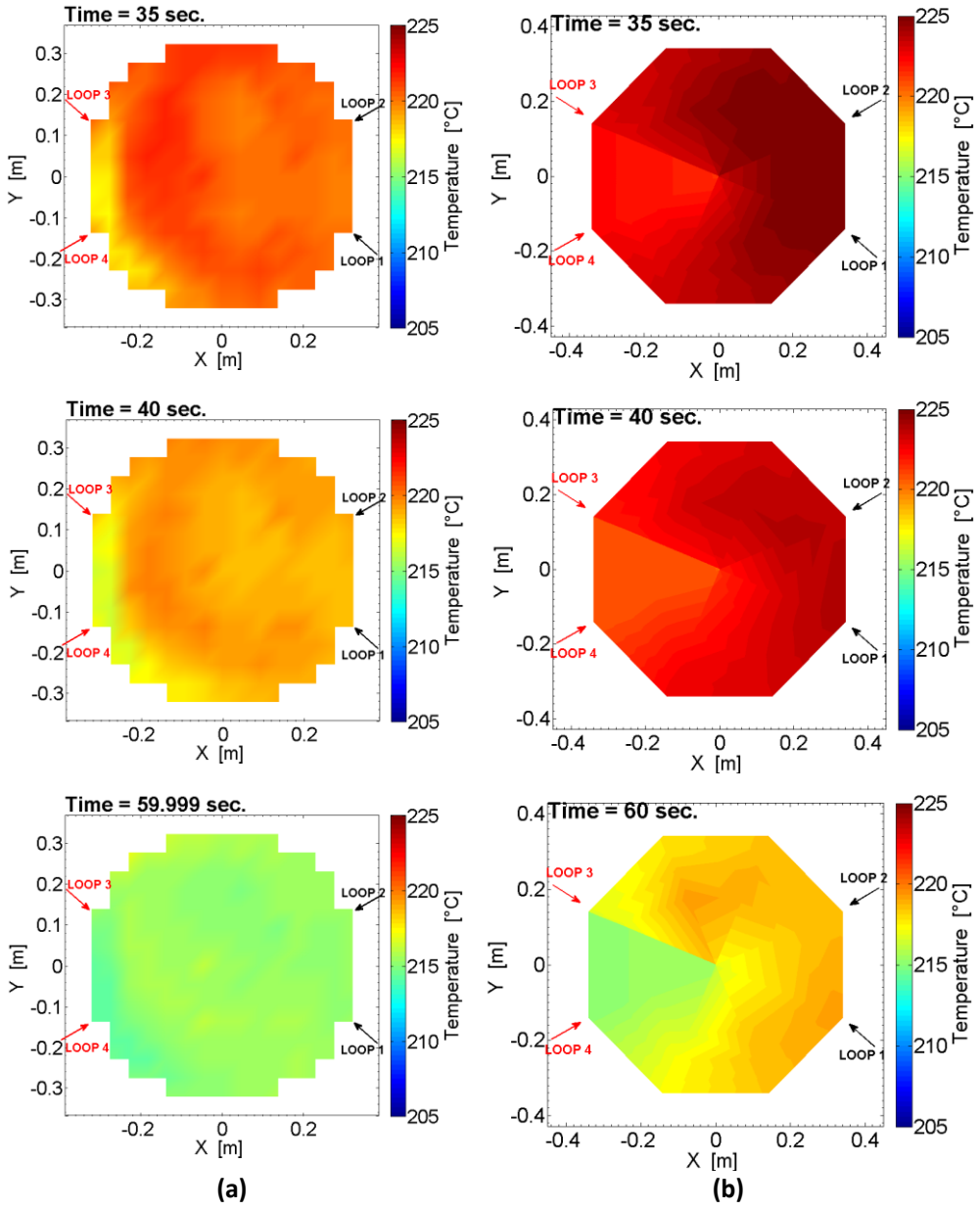

Figure 155 – ROCOM experiment 1.2: snapshots of the temperature distribution in the core inlet at six different time points (part 2 of 2) (experimental (a), calculated (b))

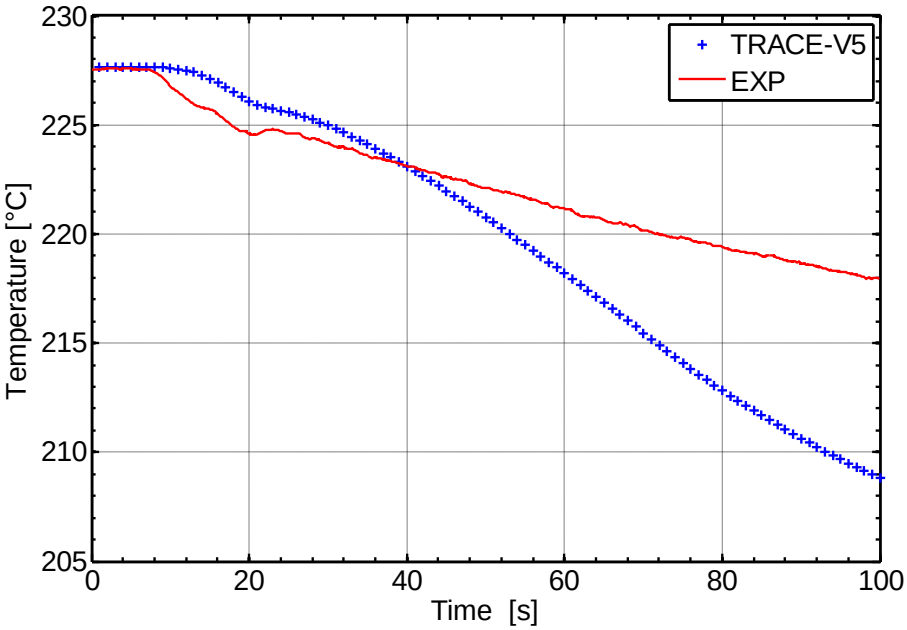

Figure 156 – ROCOM experiment 1.2: averaged temperature evolution inside the DC

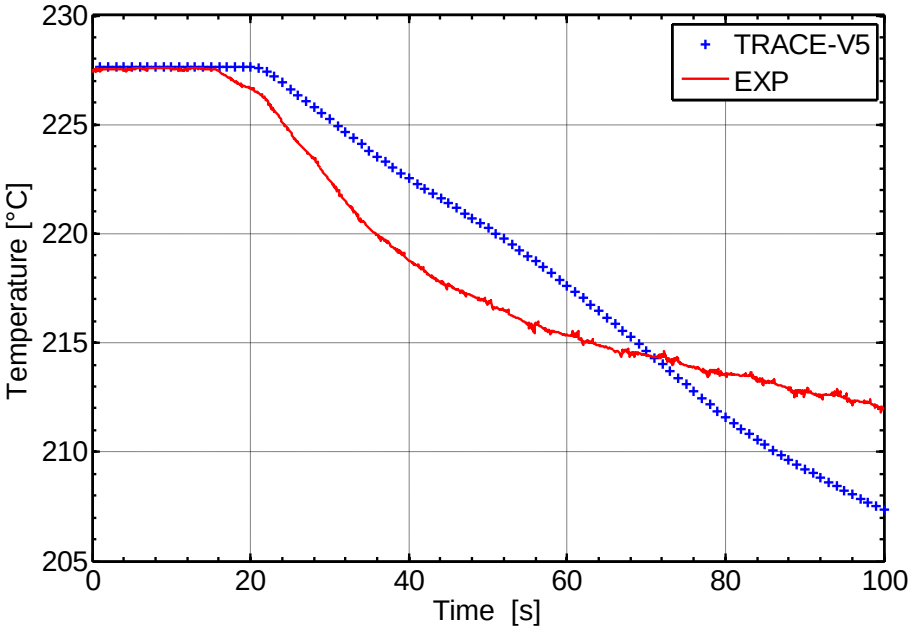

Figure 157 – ROCOM experiment 1.2: averaged temperature evolution at the core inlet

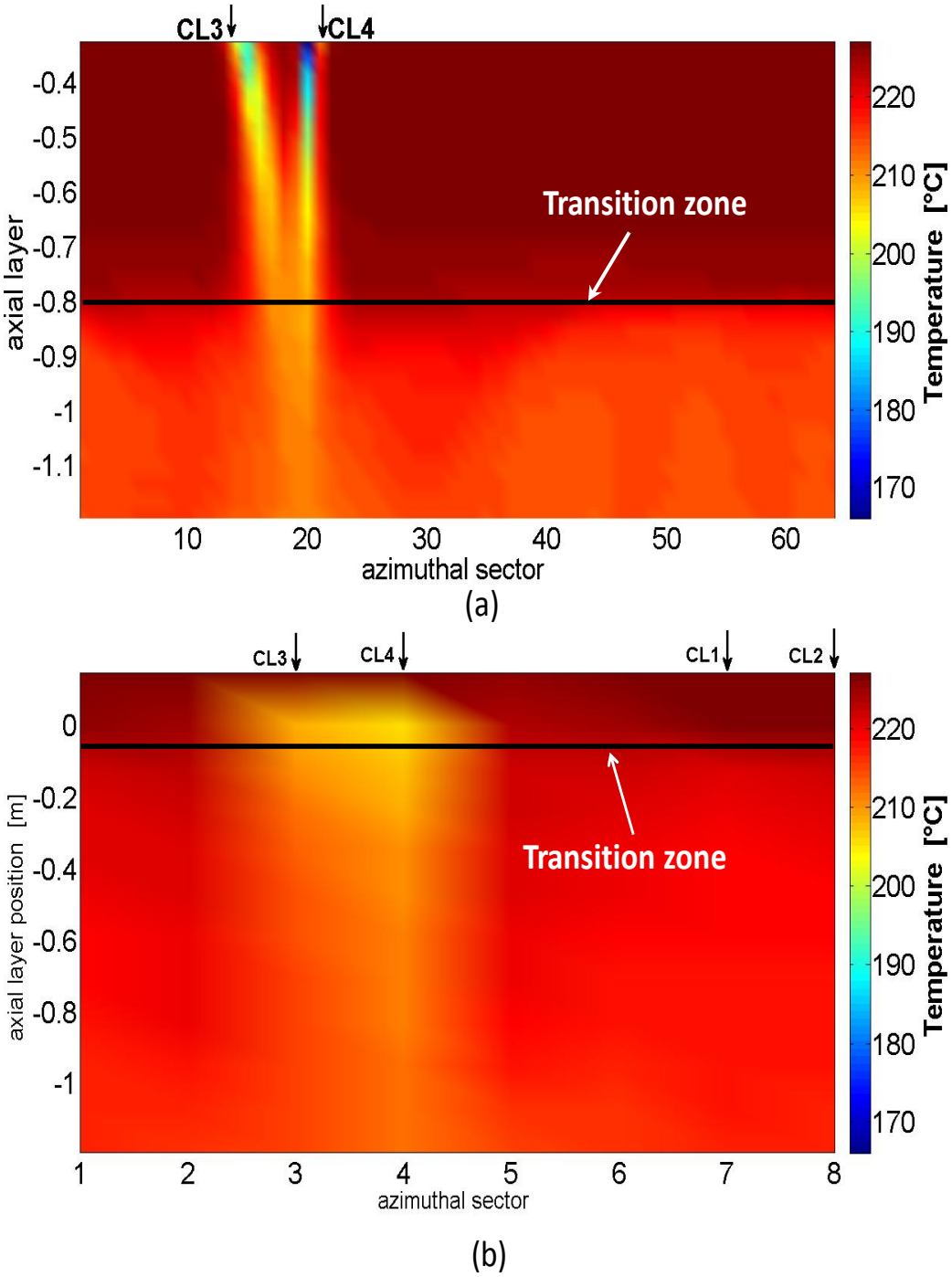

Figure 158 – ROCOM experiment 1.1: experimental (a) and simulated (b) temperature time averaged value in the DC outer plane (time averaging interval: t = 60 s to t = 70 s)

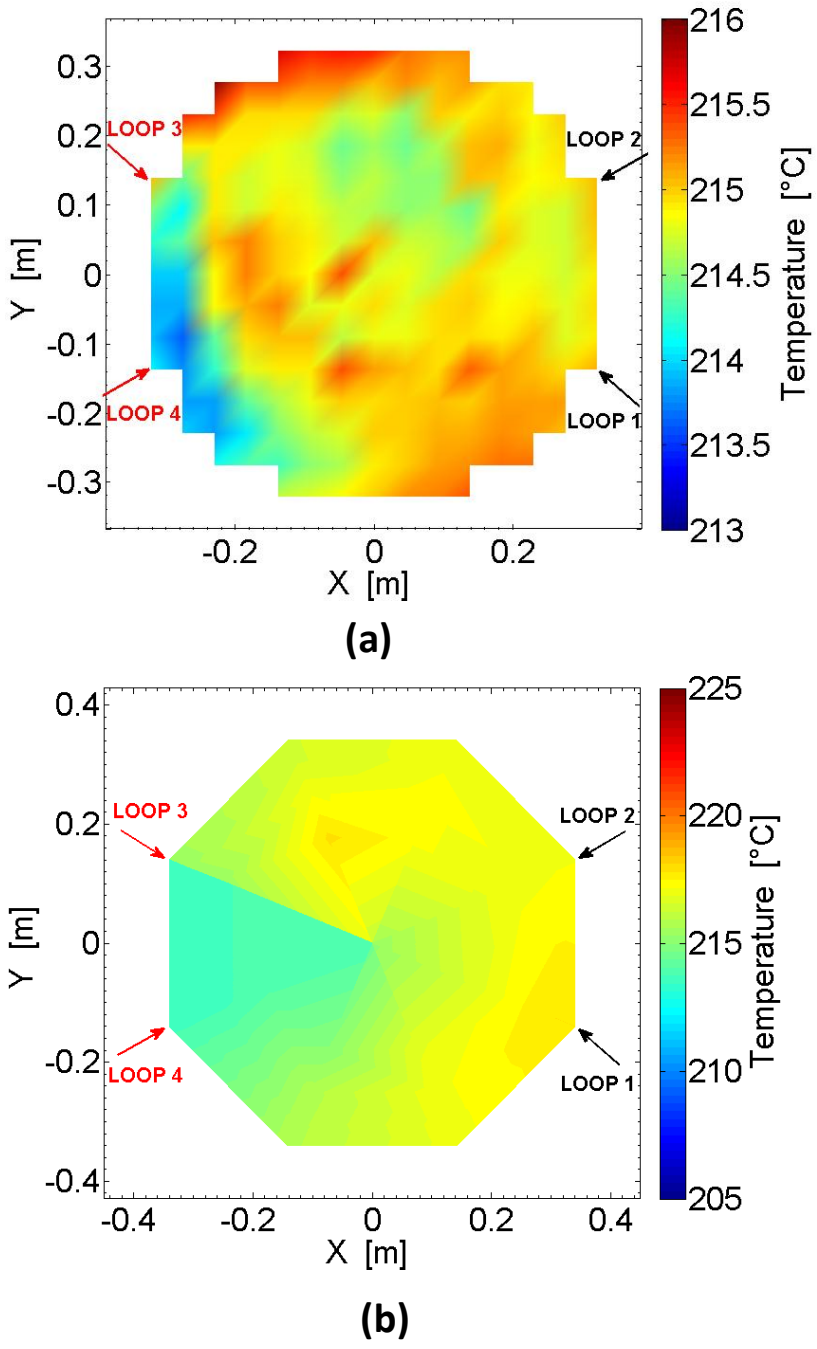

Figure 159 – ROCOM experiment 1.2: experimental (a) and simulated (b) temperature time averaged value at the core inlet (time averaging interval: t = 60 s to t = 70 s)

6.8.4. Simulation of the test 2.2

Section § 6.7.4.2 describes the boundary conditions for the ROCOM Test 2.2 that was conducted with changing time-dependent boundary conditions for the flow rate in the non-affected loops. The initial conditions were selected in such a way that the simulation of this test can be compared with those of ROCOM Test 1.1. Also in this case the numerical investigation has been performed following 100 seconds of *null transient* aimed to reach the stationary and initial conditions of the ROCOM test 2.2. The initial and boundary conditions for the temperature and pressure are same as those implemented in the TRACE-V5 nodalization to simulate the test 1.1. Instead the inlet boundary conditions on the mass flow rate are based on the measured mass flow rates in the cold legs (see Figure 127). After the beginning of transient the mass flow rate in the non affected cold legs started to be reduced until reaching zero flow condition at 100 s after SoT, whilst the flow rate in the affected loop is maintained at nominal conditions. The injection of water with higher density took place over a time span of 150 s. The procedure to perform the simulation of the test 2.2 is listed in Table 43.

Table 43 – ROCOM experiment 2.2: adopted procedure

Cal. Time (s)	Event
0 – 100	Establish stationary flow conditions in all loops by controlling boundary pressure (temperatures of all loops are equal, 236.1 ^{o}C)
100	Start of injection of cold water (153 ^{o}C) into loop-1 • Changing inlet temperature of loop-1 from 236 ^{o}C to 153 ^{o}C in 5 s and reaching the nominal flow rate condition (5.743 kg/s) • Starting mass flow rates reduction in the non affected loops (2 to 4)
200	Zero flow conditions in the non-affected loops (2 to 4)
250	End of calculation

6.8.4.1. Analysis of the results: experiment/simulation temporal comparison

6.8.4.1.1. Pseudo local analysis

The figures from Figure 160 to Figure 162 show the numerical results related to the temperature time trends at the three spatial locations in the downcomer (top, middle and bottom positions) compared against the corresponding experimental time profiles. A qualitative well agreement is obtained at the top of the downcomer in almost all sectors by the TRACE-V5 simulation (see Figure 160) during the first 60 s after the SoT, except for the sector 3 in which the experimental overcooled spike, induced by the cold plume flowing through the affected sector (namely sector 4) is not well predicted and it occurs with a spread of approximately 20 °C (see Figure 160(c)). After approximately 60 s from the SoT the simulated temperature patterns exhibit a decreasing trend earlier than the experimental one

(see Figure 160). The decrease of the experimental temperature trend in the non affected sectors that started after 100 s is due to the stopping of the mass flow in the intact loops and to the continuous injection of cold water in the broken loop that gradually cools down the DC. In turn the anticipated cooling shown by numerical results is a consequence of the discretization scheme which introduce a high numerical diffusion resulting in a higher dispersion and higher position of the transition region between sector-shaped and homogeneous temperature distribution respect to the experimental one (see Figure 164 and Figure 165). In the middle zone of the DC the time behavior of the temperature is similar to the top one but the overcooling process in both experimental and calculated results is triggered in advance (see Figure 161). The thermal mixing process in the lower part of the downcomer (bottom layer) is underestimated in the TRACE-V5 simulation causing warmer temperature trend in all sectors of the computational domain, as can be seen in the Figure 162. Also for this last case the numerical error which acts like an artificial extra diffusion affects the calculated results in the same direction like too large turbulent viscosity used in some turbulence models but whit a lower thermal mixing compared to the experimental results. Figure 163 demonstrates how the overcooled water enters the downcomer. It is clearly to be seen experimentally as well as numerically that this is a transient process. The non stationary behavior of the cooler layer height in downcomer, as a consequence of the transient mass flow behavior, is reproduced by the TRACE-V5 simulation comparing the snapshots between both tests (1.1 and 1.2) as it is shown in Figure 165. In Figure 164, for completeness, is depicted the snapshots of the experimental temperature distribution in the downcomer in tests 1.1 and 2.2. Comparing the snapshots between both tests it can be concluded that the ratio of the flow rates (perturbed flow and sum of the unperturbed flows from the three other loops) is the determining factor for the position of this transition region. A shifting of the position in test 2.2 can be observed only after reducing the flow rate in the unperturbed loops ((see [76])). The positions of the transition region in both tests are also quite close to each other at t = 80 s on the experimental and computational side (see Figure 164 and Figure 165). At last stratification phenomenon in the downcomer and homogeneous mixing in lower downcomer are reproduced by the numerical simulation (see Figure 165).

In the core inlet plane again the temperature distribution because of the numerical diffusion, is overestimated in all computational cells (lower mixing is reproduced in the simulation) as it is depicted from Figure 166 to Figure 169. Furthermore, in the experiment no sector formation can be observed at the time t = 50 s, whilst the simulation highlights the presence of a cold sector at the core inlet (see Figure 170). The measured temperature difference over the core inlet plane at this time point is about 10 K, instead the TRACE-V5 simulation predicted a lower temperature difference, namely about 4 K.

6.8.4.1.2. Averaging analysis

As seen in the test 1.1 the integral temperature distribution in the DC shows an anticipated overcooling trend compared to the experimental one which begins to cool after 50 s from the SoT. Afterwards the temperature distribution seems to be more diffusion in the calculated results than in the real experiment (see Figure 171). In the core this effect is much more emphasized (see Figure 172).

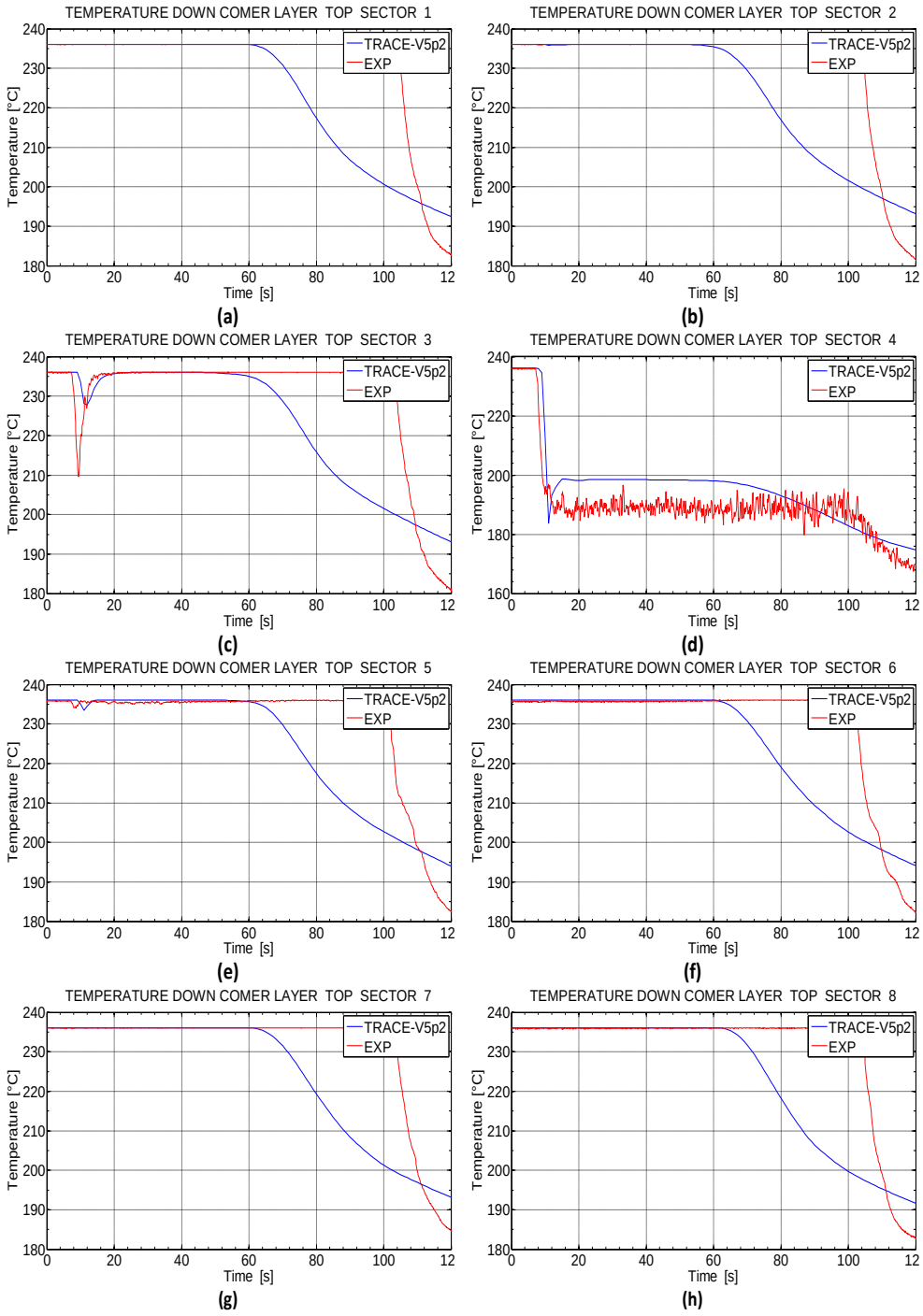

Figure 160 – ROCOM experiment 2.2 reference results: temperatures trends at the downcomer top layer

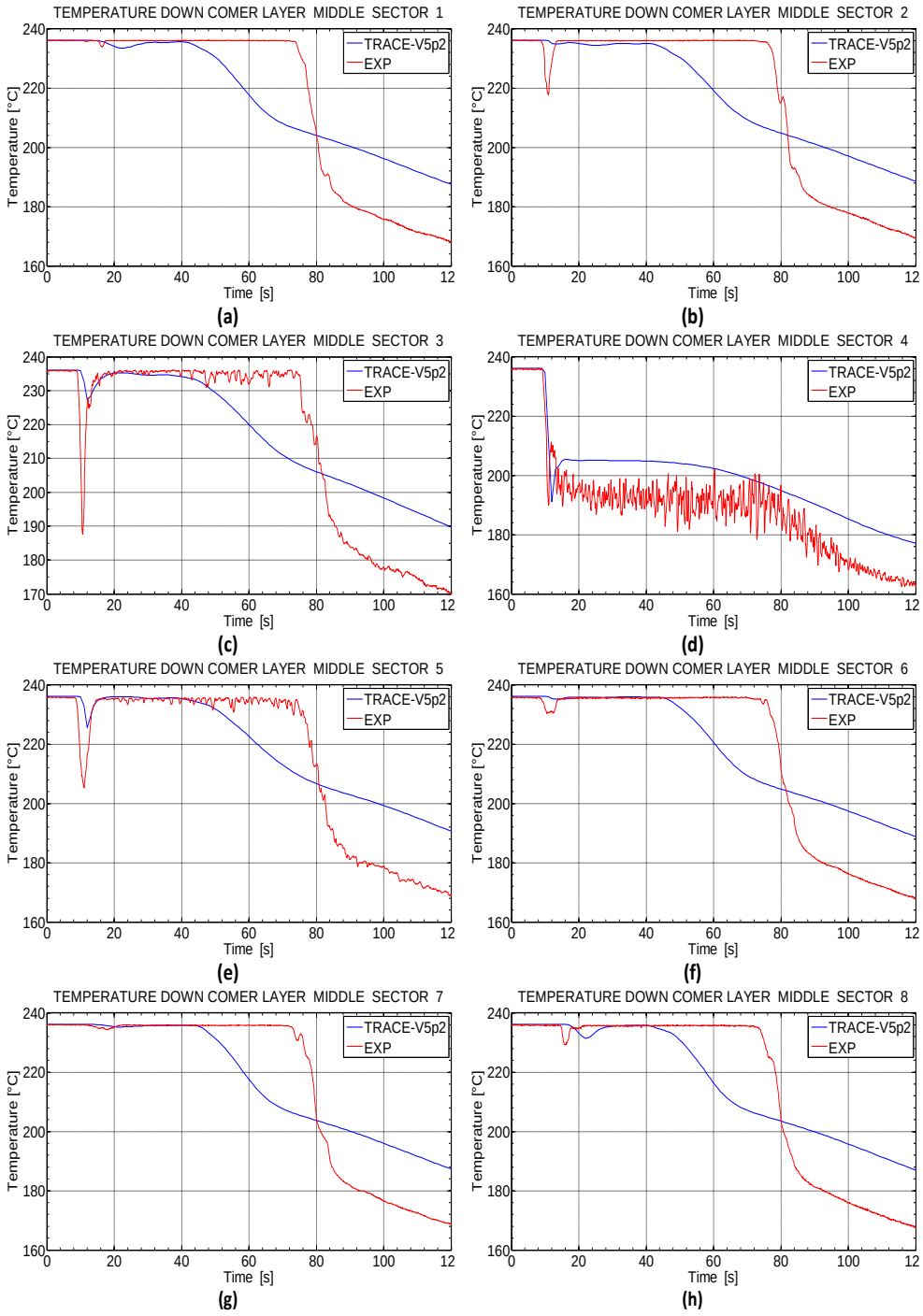

Figure 161 – ROCOM experiment 2.2 reference results: temperatures trends at the downcomer middle layer

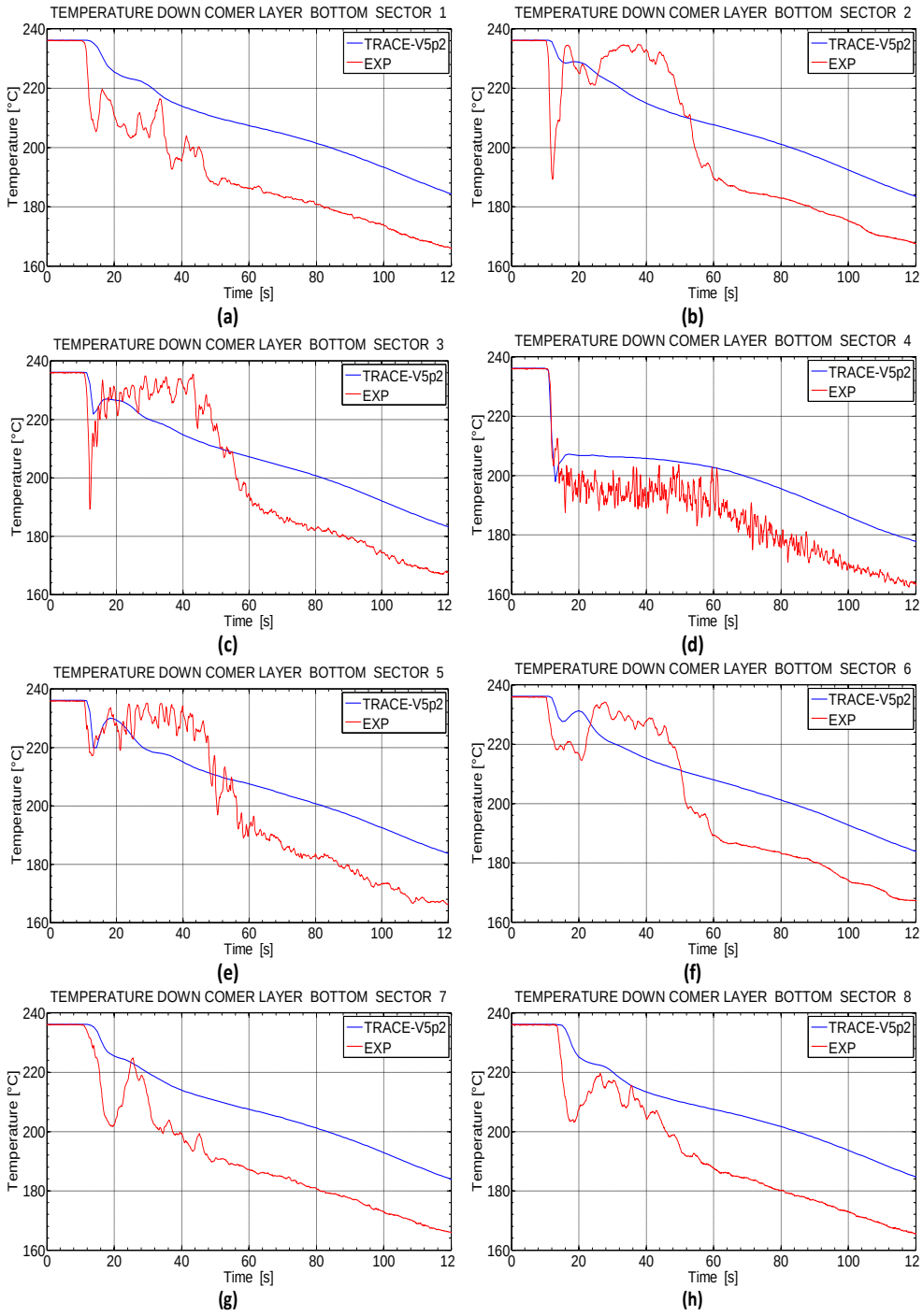

Figure 162 – ROCOM experiment 2.2 reference results: temperatures trends at the downcomer bottom layer

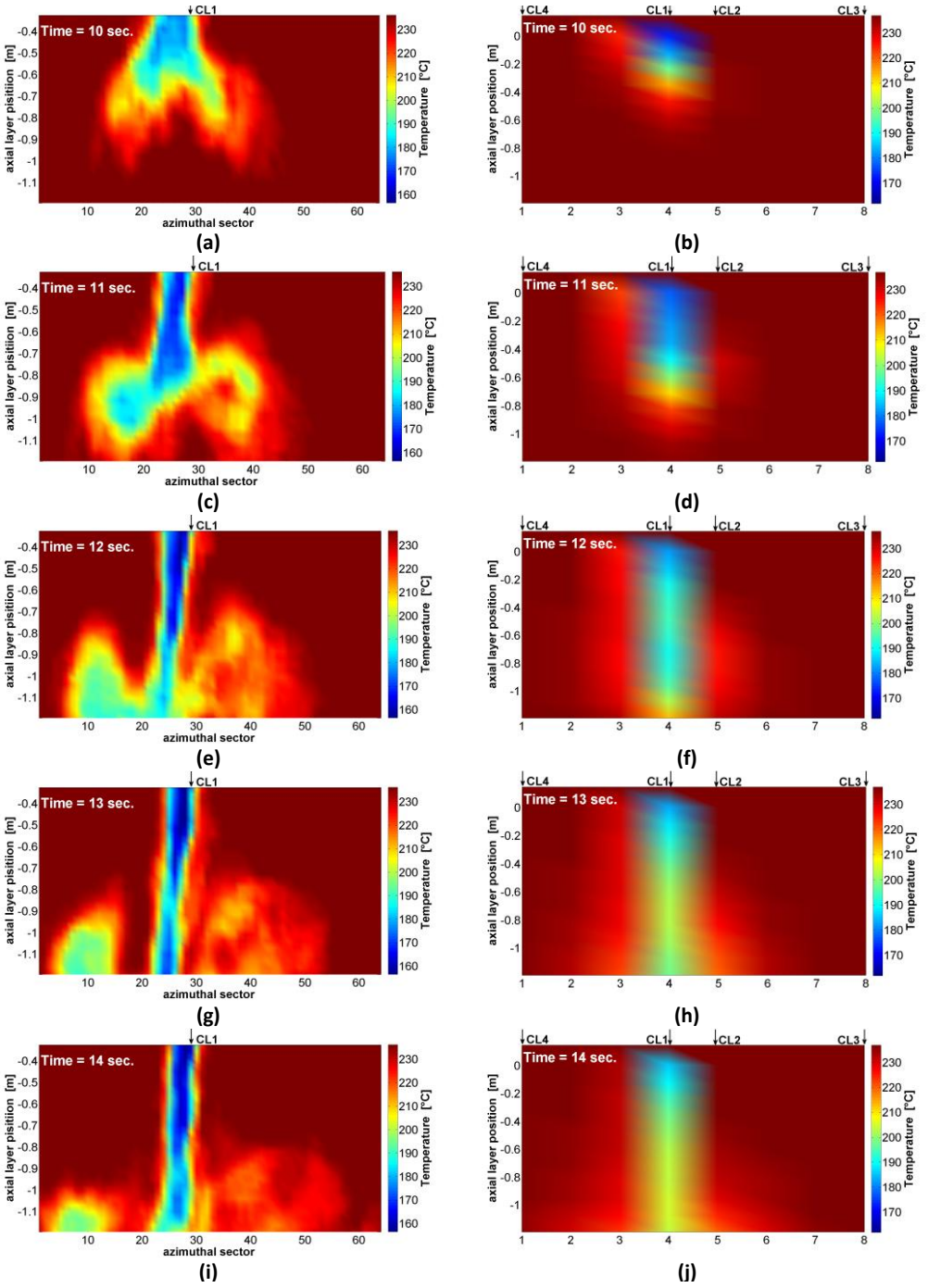

Figure 163 – ROCOM experiment 2.2: snapshots of the temperature distribution in the downcomer (experimental (a), TRACE-V5 results (b)) at different time points (t = 0 s is related to the start of the flow in loop 1)

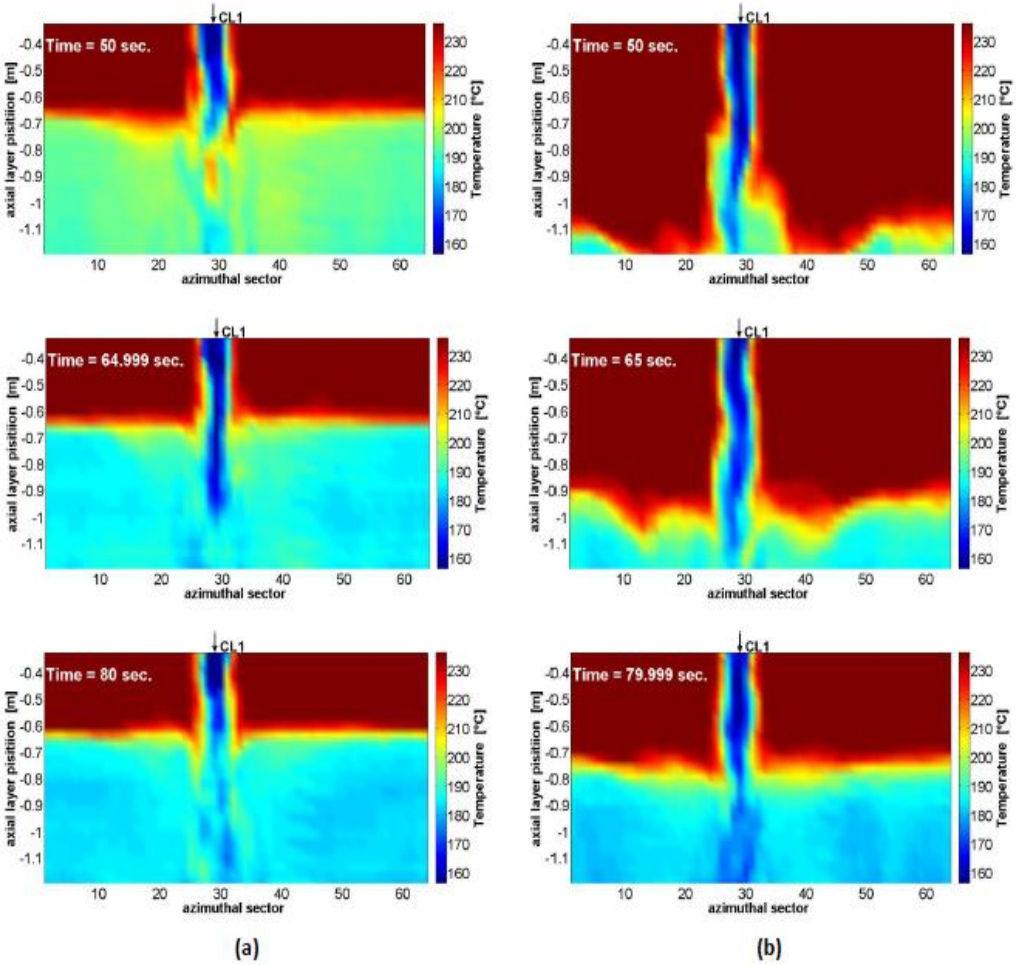

Figure 164 – Snapshots of the experimental temperature distribution in the downcomer (outer plane) at three different time points (t= 50; 65; 80 s) in tests 1.1 and 2.2

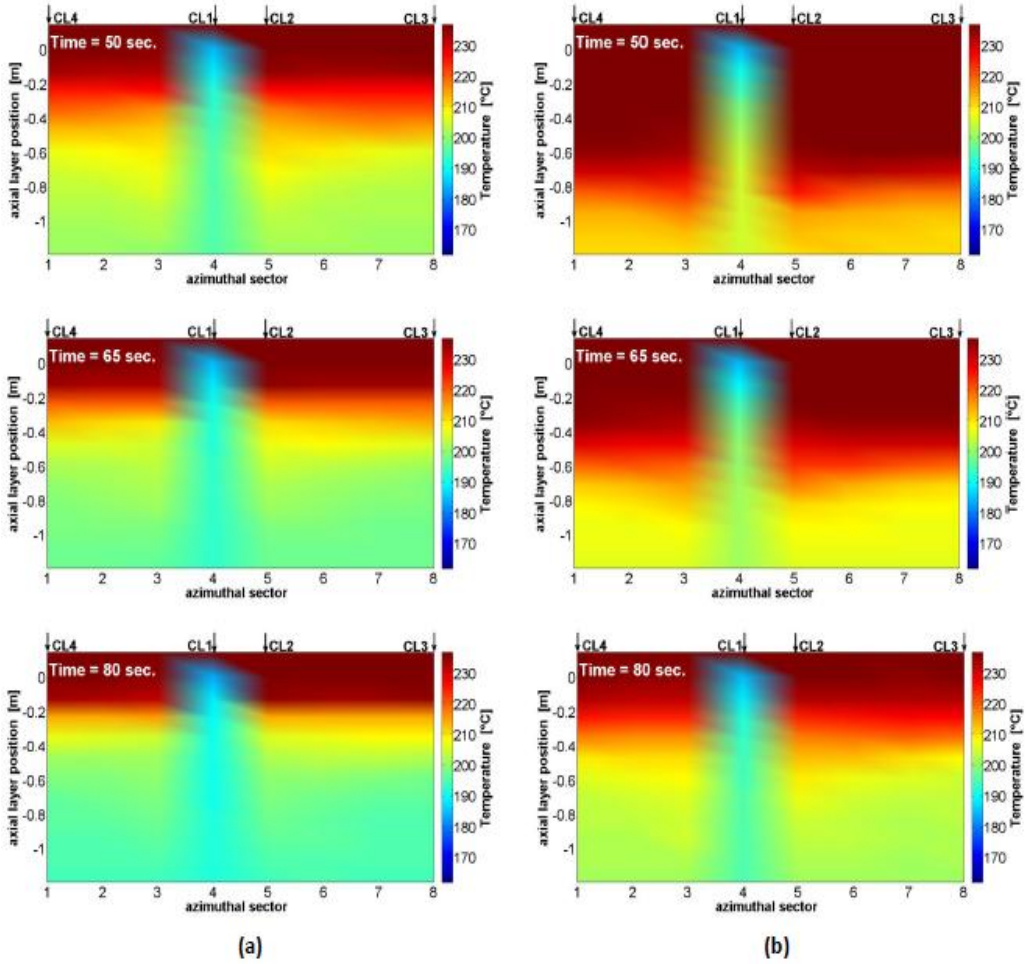

Figure 165 – Snapshots of the simulated temperature distribution in the downcomer (outer plane)at three different time points (t= 50; 65; 80 s) in tests 1.1 and 2.2

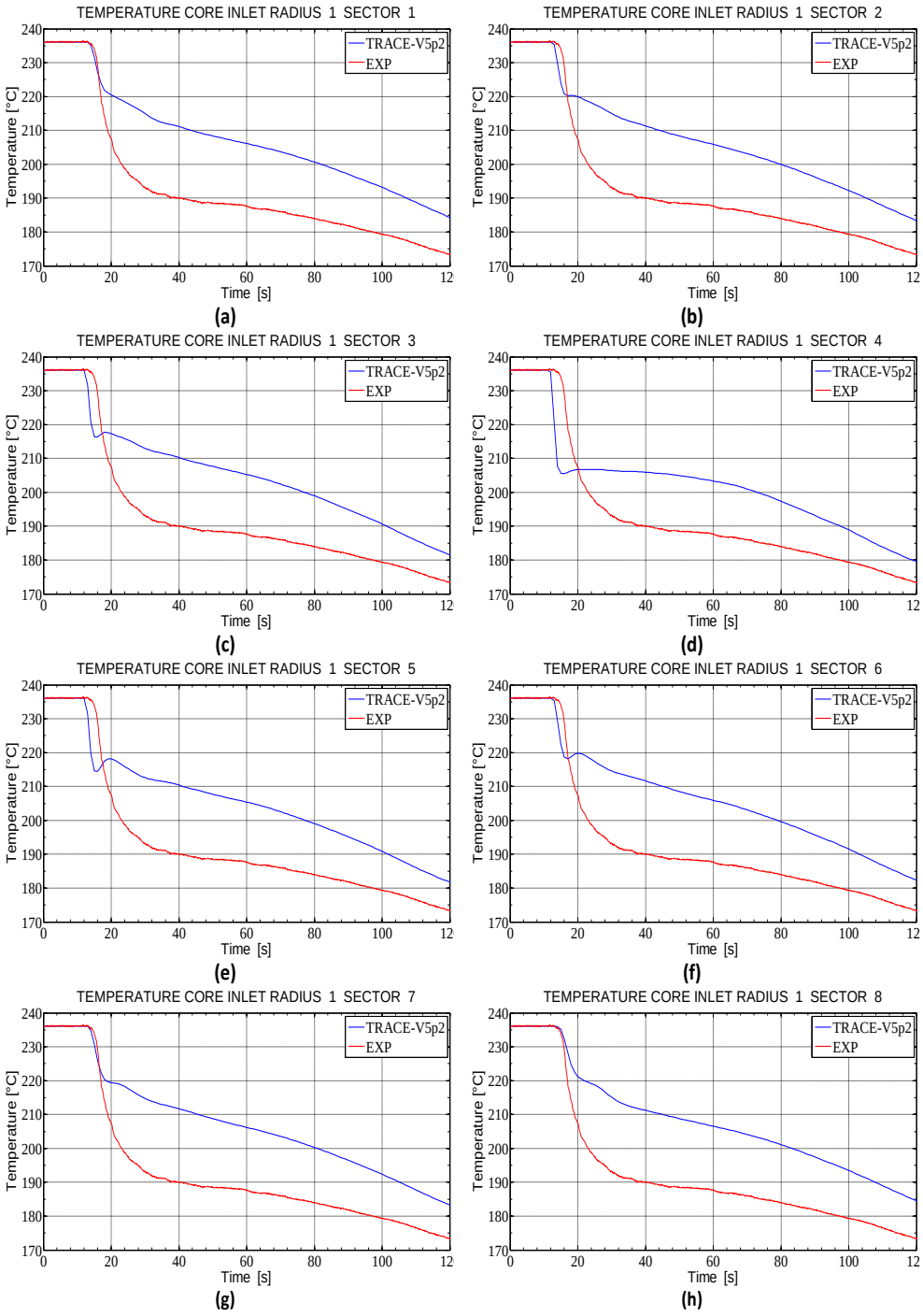

Figure 166 – ROCOM experiment 1.2 reference results: temperatures trends at the core inlet first radial ring, all azimuthal sectors

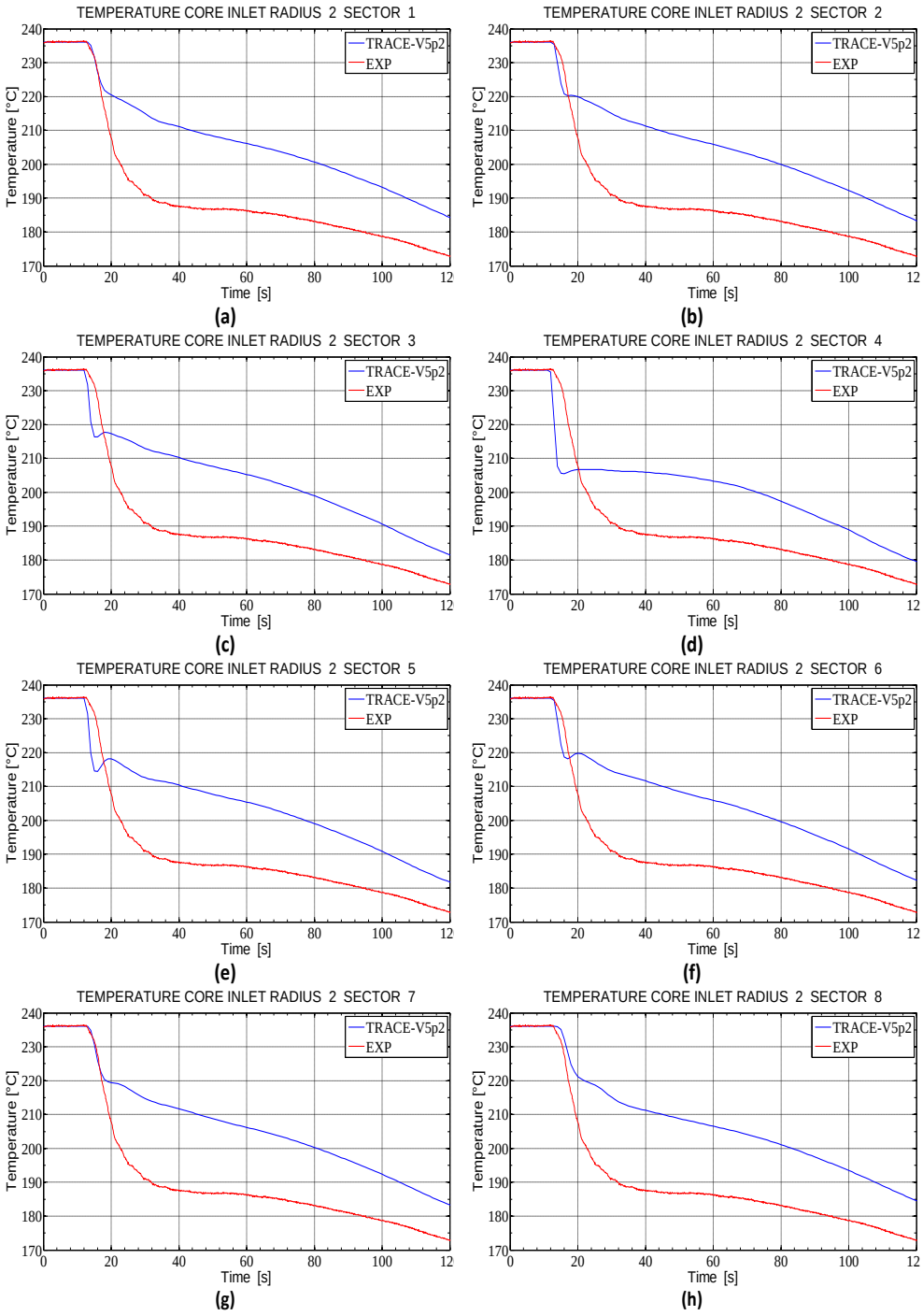

Figure 167 – ROCOM experiment 1.2 reference results: temperatures trends at the core inlet second radial ring, all azimuthal sectors

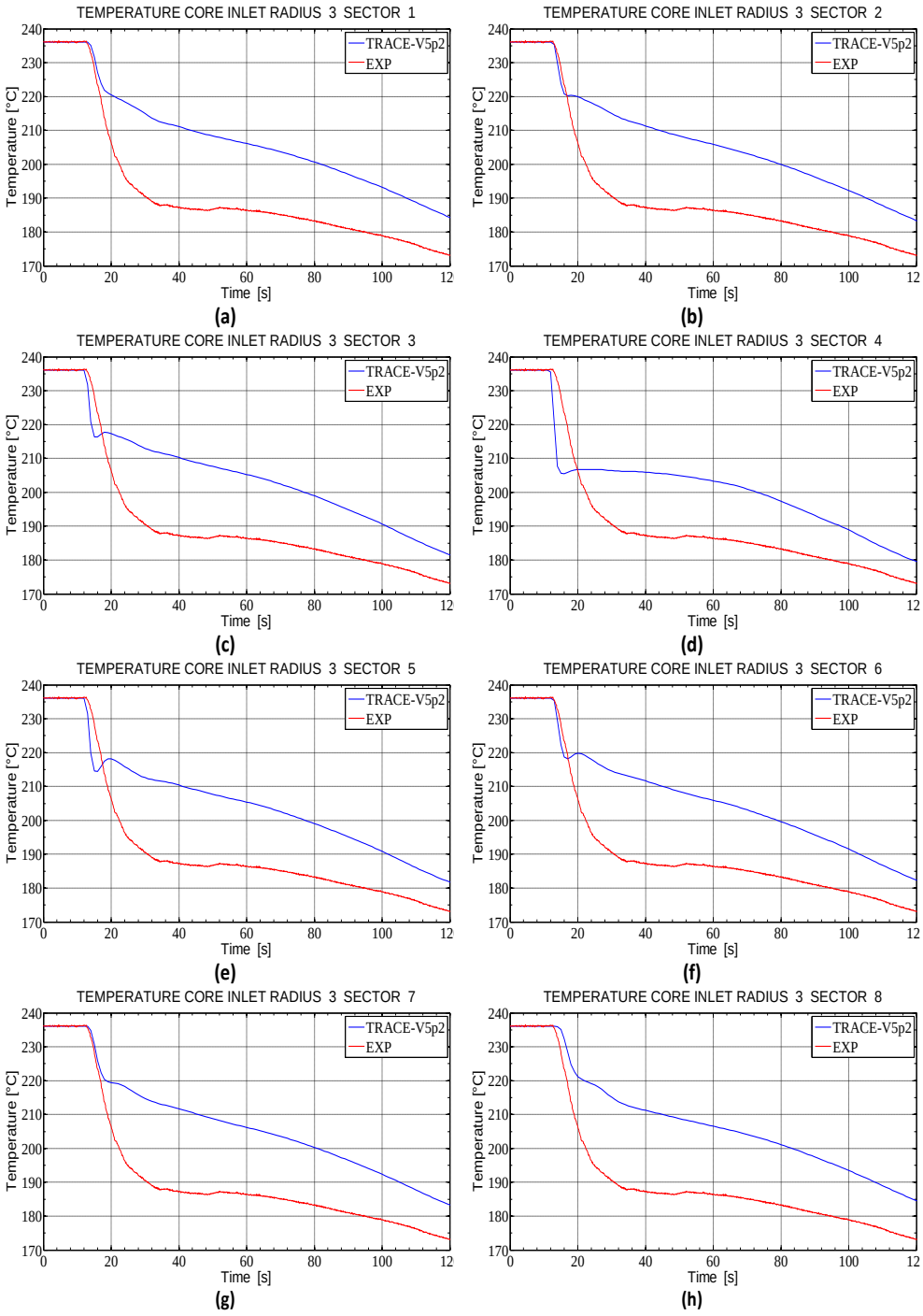

Figure 168 – ROCOM experiment 1.2 reference results: temperatures trends at the core inlet third radial ring, all azimuthal sectors

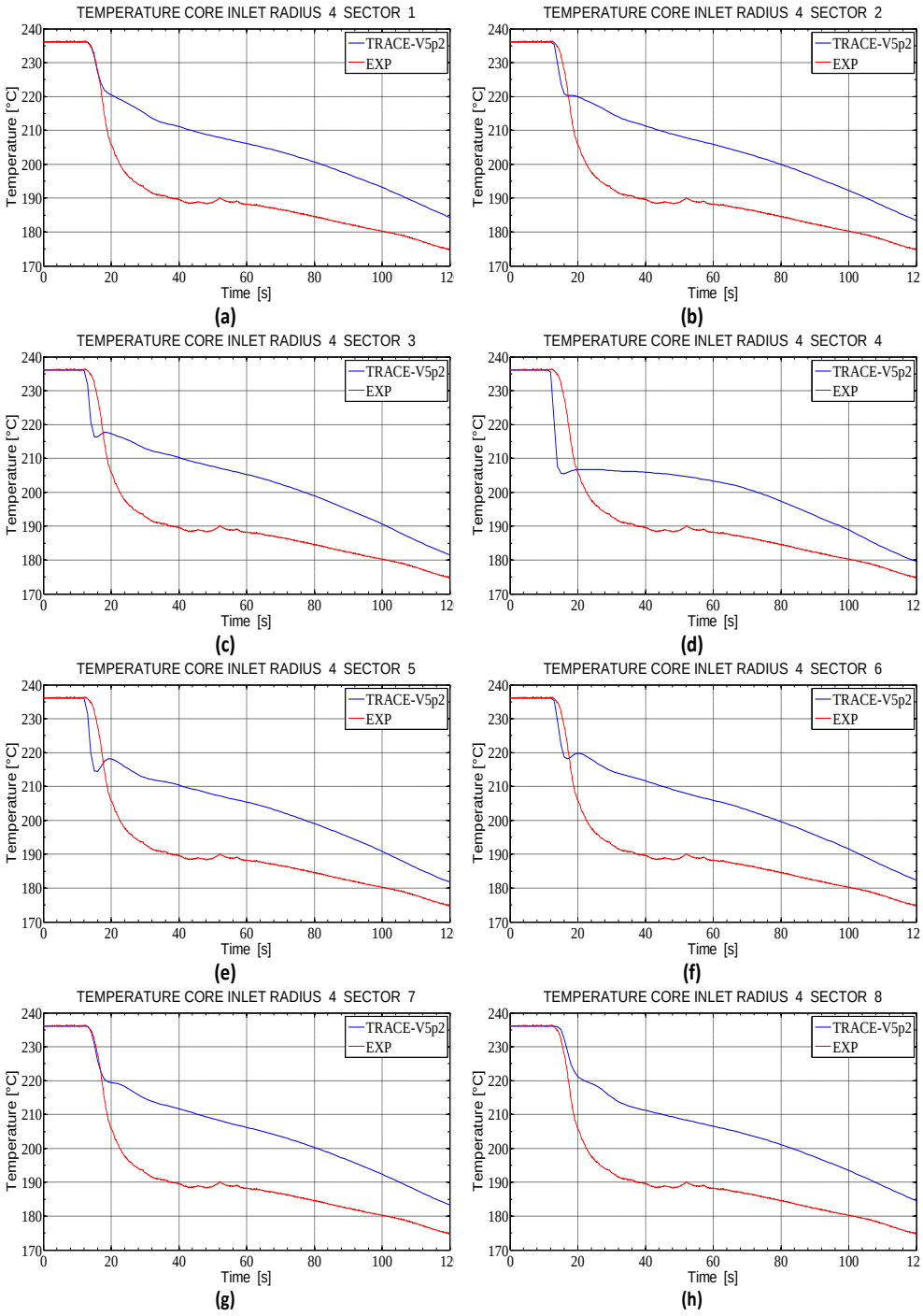

Figure 169 – ROCOM experiment 1.2 reference results: temperatures trends at the core inlet fourth radial ring, all azimuthal sectors

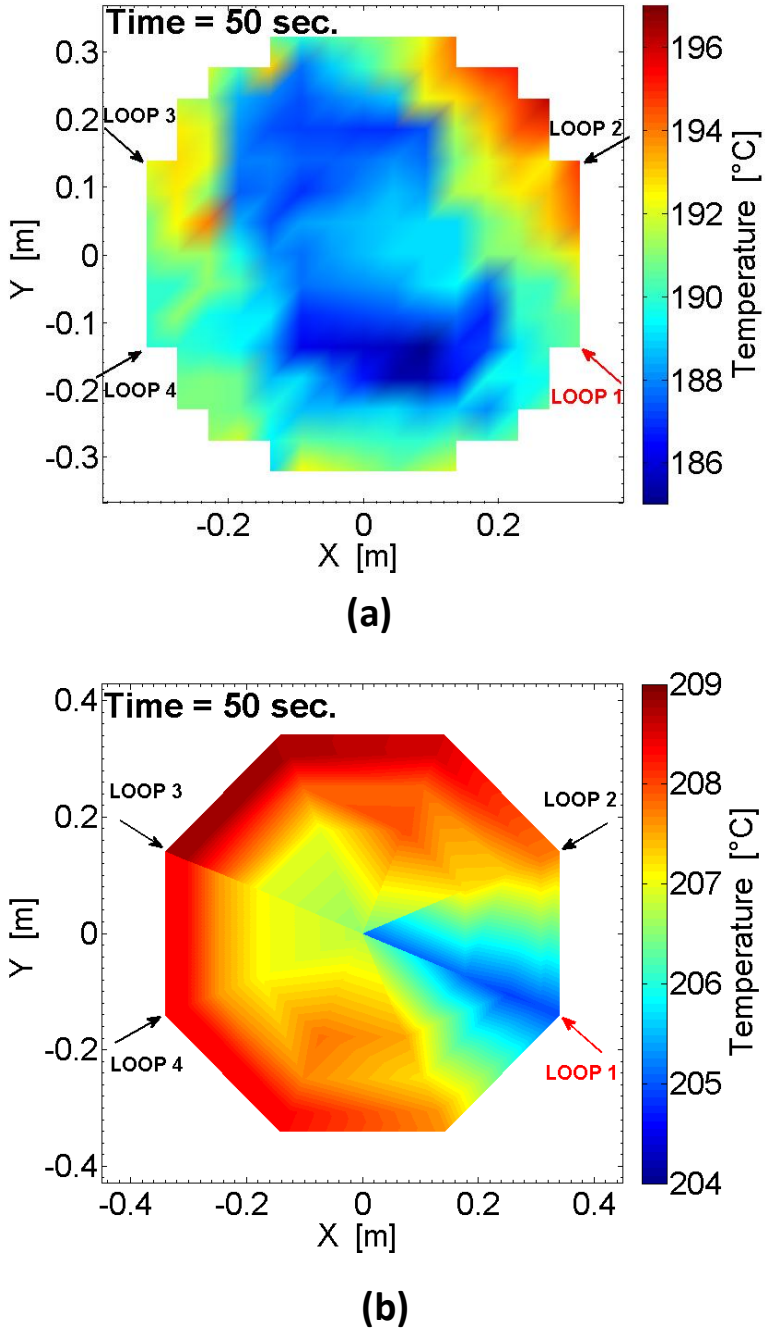

Figure 170 – ROCOM experiment 2.2: snapshot of the temperature distribution in the core inlet plane at t = 50 s in the (experimental results (a), TRACE-V5 results (b)

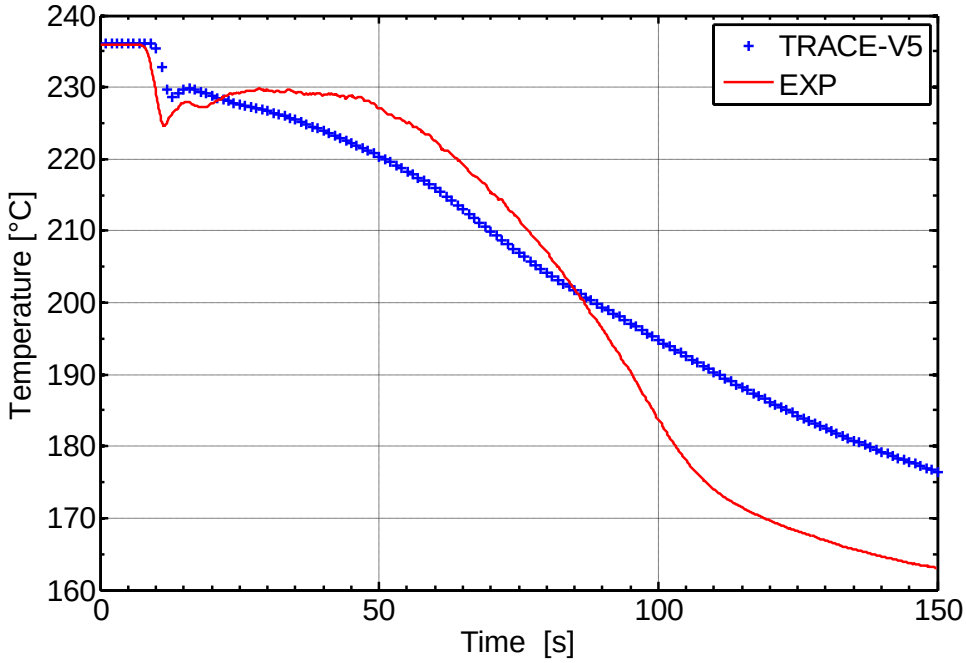

Figure 171 – ROCOM experiment 2.2: averaged temperature evolution inside the DC

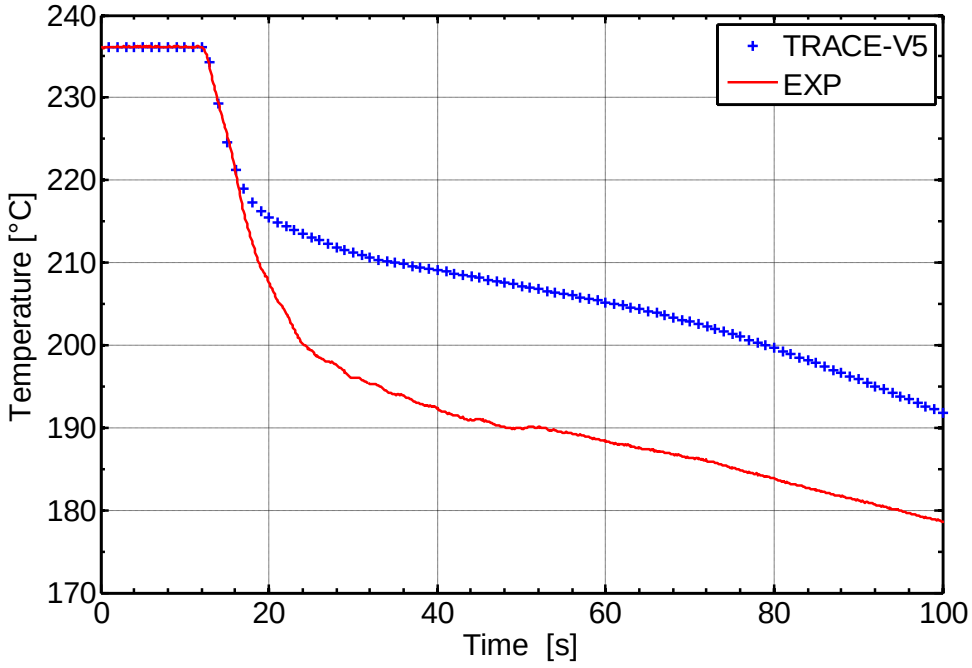

Figure 172 – ROCOM experiment 2.2: averaged temperature evolution at the core inlet

6.8.5. Quantitative accuracy: application of the FFTBM to the simulated ROCOM tests

The FFTBM, as was mentioned in the section § 6.3.3, is a well established tool to quantify the accuracy of system code applications. It is applied to a set of time-dependent scalar quantities featuring the NPP thermal hydraulic behavior (such as primary and secondary pressure, pressure drops, coolant and cladding temperatures, mass flow rates, etc.) and for each of them provides quantification(by the “average amplitude”) of the discrepancy between code prediction and experimental data (see also APPENDIX E).

The information to be analyzed and compared in the present frame has however a completely different nature, as it consists of a temperature distribution over three variables: the time, and two independent spatial coordinates (which define coolant channels locations at the core inlet and the axial and azimuthal position inside the DC). The basic idea is to apply the FFT to the temperature time-history at each computational mesh, so that $N_{CompMesh}$ average amplitudes are obtained: maps of the discrepancies over the core inlet and inside the DC can thus be plotted.

The data processing was performed with the help of MATLAB routine that was coded for this specific purpose. However, a systematic application of the proposed procedure would require the development of a software package that satisfies generality, efficiency and quality assurance requirements (through a suitable Verification and Validation process).

Taking in account that the FFT algorithm requires that the measured and the calculated data are identified by a number of values equally spaced (see APPENDIX E). To fulfill this requirement it is necessary an interpolation to align the two set of data. During the interpolation step, some information could be lost choosing a too low number of points mainly when trends oscillate greatly, as it happens for all tests in the perturbed loops (loop 1 in the tests 1.1 and 2.2, and loops 3 and 4 in the test 1.2). Therefore, to correctly reproduce the experimental signal by linear interpolation, the number of points chosen is given by a power of 2, (namely 2^{14}) to reduce the variation of averaged amplitudes (AA) connected with the oscillatory character of the signal and to increase the accuracy. This approach can obviously be improved using a procedure to smooth the data. Smoothing data removes random variations and shows trends and cyclic components. The simplest way to smooth the data is by taking the averages precisely considering a moving average of the experimental signal that mathematically is an exemple a convolution of the input signal with a rectangular pulse having an area of 1 ([75]).

The figures from Figure 173 to Figure 175 show the results of the application of the FFT method to the three ROCOM tests (namely the tests 1.1, 1.2, 2.2) in order to estimate the error of the *pseudo local approach* considering experimental and calculated the temperature distributions. First aim of the representation is to resume the global behavior predicted by the code making use of a 2D map, which reports the position of each computational core channels in a reference system centered in the CSP centre. The results of FFT for the accuracy evaluation in each mesh of the three layers selected in the DC are summarized in Table 44.

This analysis confirms the outcomes of the qualitative analysis previously performed, namely the lack of turbulent diffusion model emphasizes the high local

discrepancies that are experienced in the computational domain of the two fluid regions that are DC and core inlet.

The shortcoming of the local accuracy analysis highlights that the average amplitude shows values ranging between 0.9 and 1.14 at the core inlet and between 0.87 and 1.38 in the DC, the lower values are obtained from the simulation of the test 2.2, but its sensitivity to accuracy is not particularly evident and certainly needs further assessment.

In turn the outcomes of the spatial averaging highlight a very low error in both regions, i.e. DC and core inlet (see Figure 176, Figure 177 and Figure 178) for the simulation of the tests 1.1 and 2.2. The higher error detected in the test 1.1 at core inlet is mainly due to the anticipated thermal perturbation appearance and to a not complete mixing compared to that in DC, whilst an opposite situation occurs for the test 1.2.

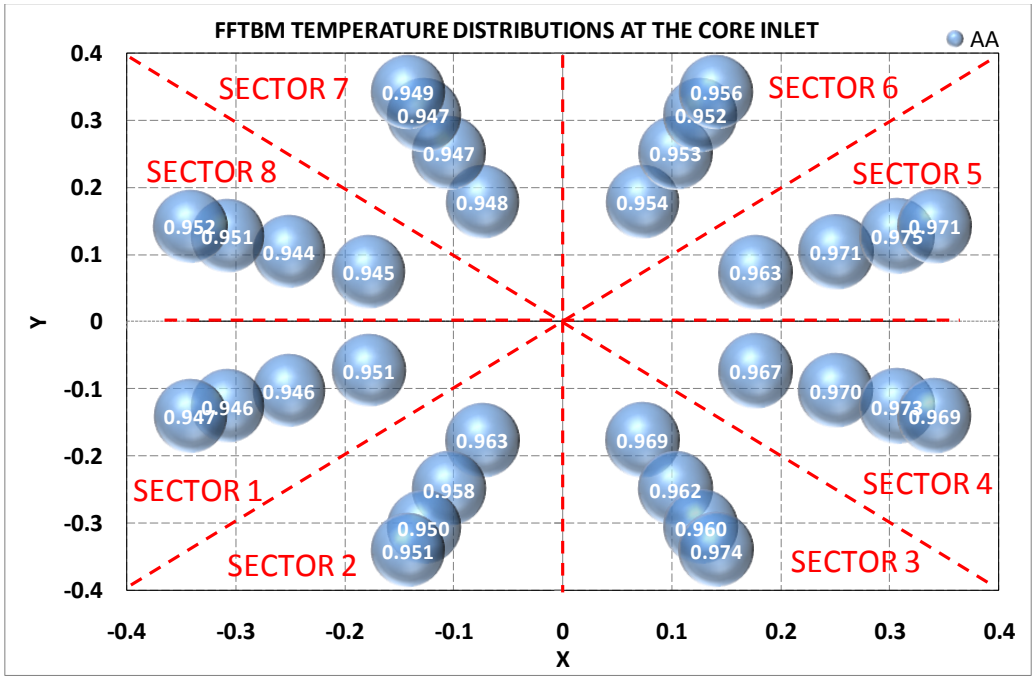

Figure 173 – ROCOM experiment 1.1: application of the FFTBM to the temperature distribution at the core inlet

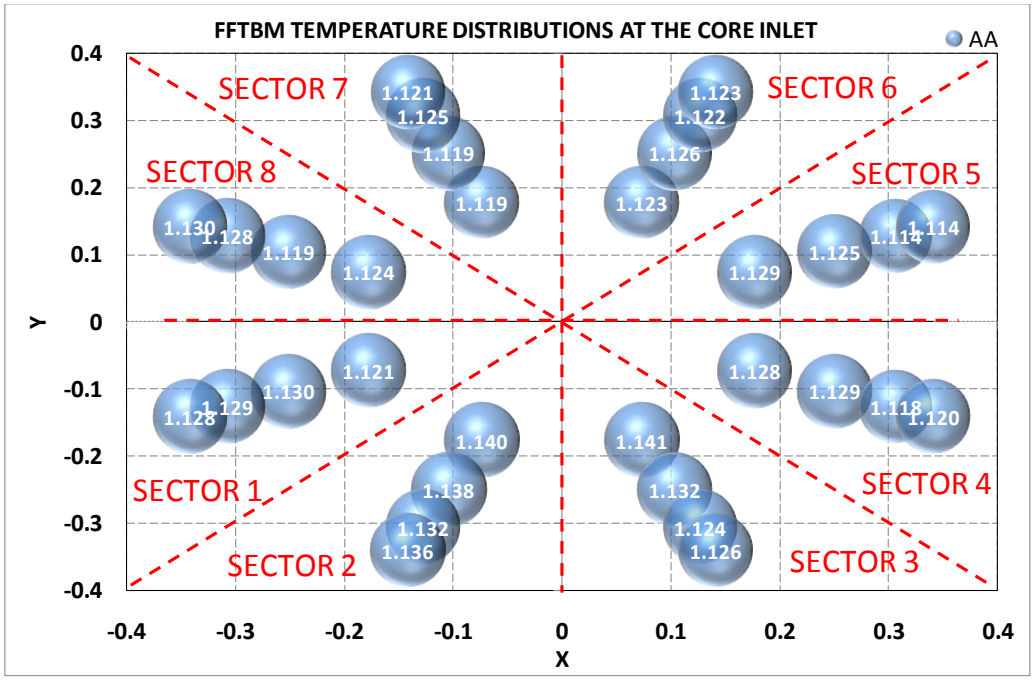

Figure 174 – ROCOM experiment 1.2: application of the FFTBM to the temperature distribution at the core inlet

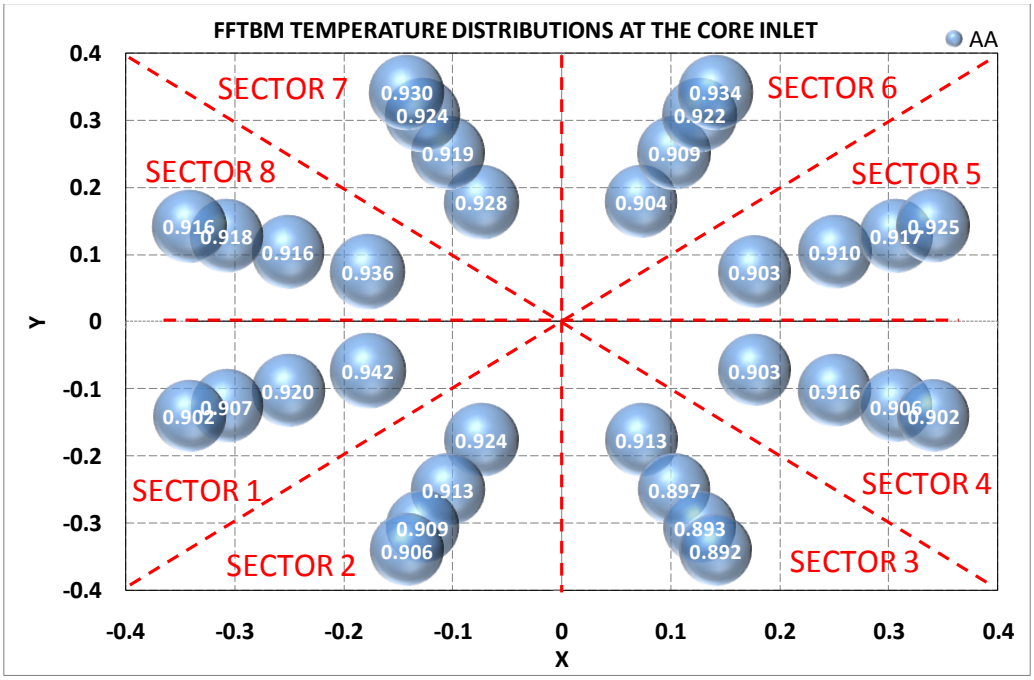

Figure 175 – ROCOM experiment 2.2: application of the FFTBM to the temperature distribution at the core inlet

Table 44 – Results of accuracy quantification in the DC for selected calculations

ROCOM TEST 1.1

DC Axial layer	Azimuthal sector							
	AA S1	AA S2	AA S3	AA S4	AA S5	AA S6	AA S7	AA S8
Top	1.381	1.390	1.313	1.243	1.341	1.386	1.381	1.376
Middle	0.973	0.983	1.007	1.115	1.020	0.956	0.970	0.979
Bottom	0.978	0.969	1.003	1.076	1.006	0.963	0.977	0.988

ROCOM TEST 1.2

DC-Axial layer	Azimuthal sector							
	AA S1	AA S2	AA S3	AA S4	AA S5	AA S6	AA S7	AA S8
Top	1.185	1.318	1.327	1.333	1.330	1.319	1.301	1.183
Middle	1.142	1.126	1.112	1.107	1.105	1.100	1.120	1.156
Bottom	1.129	1.128	1.120	1.108	1.107	1.109	1.130	1.136

ROCOM TEST 2.2

DC Axial layer	Azimuthal sector							
	AA S1	AA S2	AA S3	AA S4	AA S5	AA S6	AA S7	AA S8
Top	0.870	0.868	0.903	1.014	0.865	0.870	0.867	0.872
Middle	0.890	0.902	0.949	0.995	0.929	0.893	0.886	0.890
Bottom	0.958	0.972	0.962	0.973	0.949	0.930	0.937	0.940

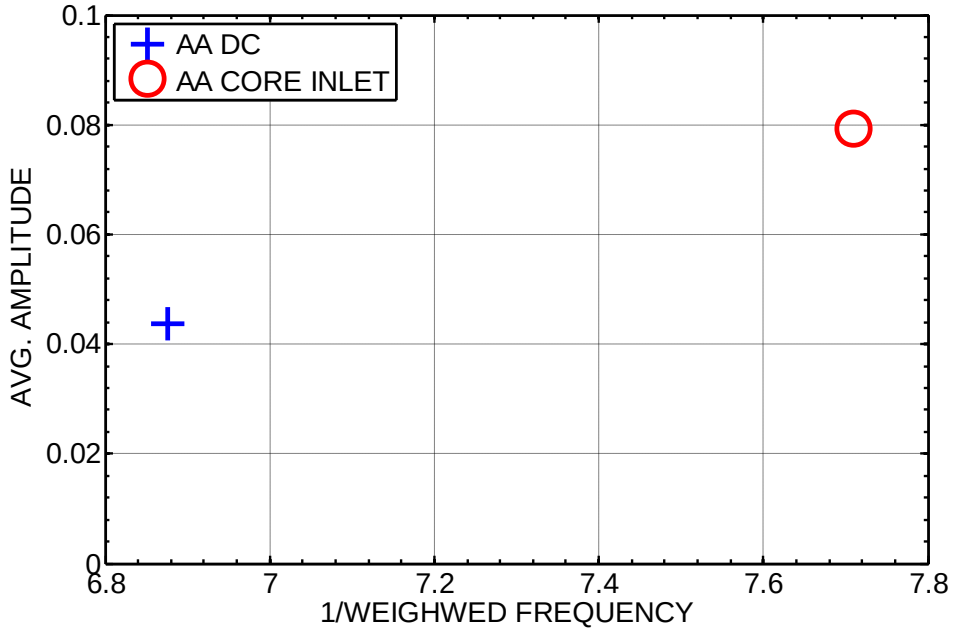

Figure 176 – ROCOM experiment 1.1: application of the FFTBM to the spatial averaged temperature inside the DC and at the core inlet

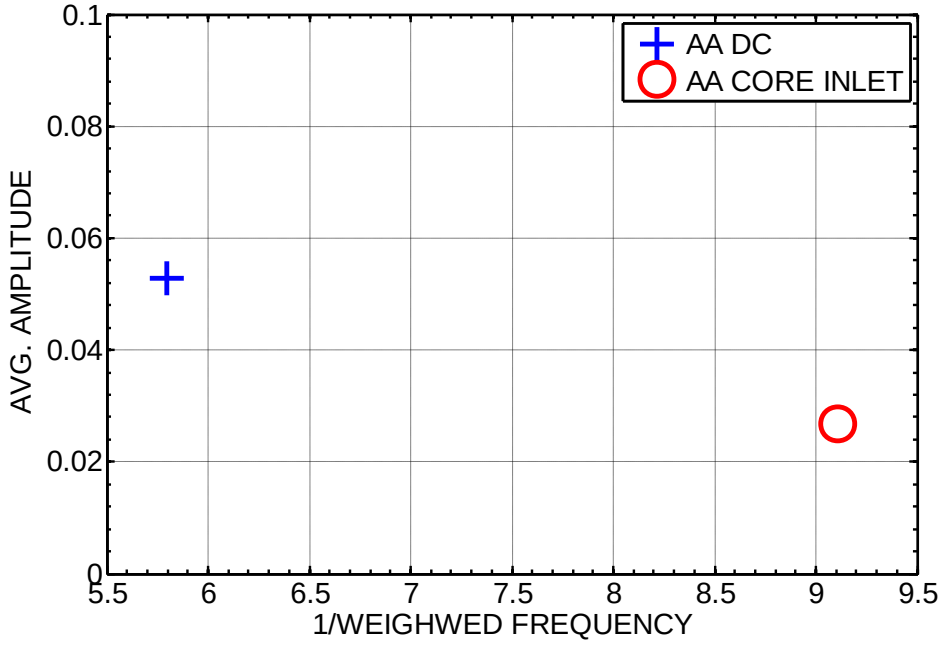

Figure 177 – ROCOM experiment 1.2: application of the FFTBM to the spatial averaged temperature inside the DC and at the core inlet

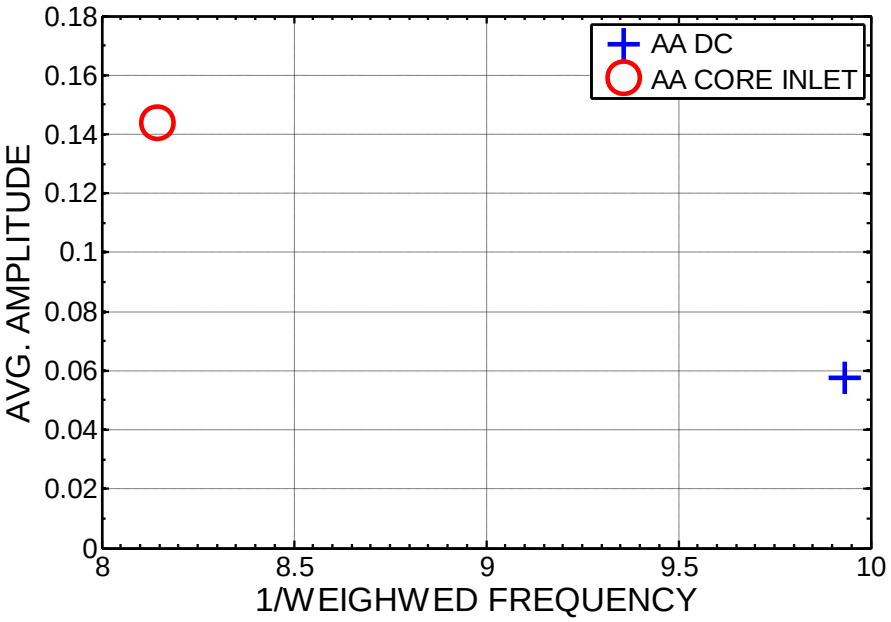

Figure 178 – ROCOM experiment 2.2: application of the FFTBM to the spatial averaged temperature inside the DC and at the core inlet

6.8.6. Effect of the noding scheme on the numerical simulation

In order to assess the influence of the noding scheme on the diffusive character of the numerical schemes used in this work, the simulation of thermal mixing process for the quasi-steady state test 1.1 was made with coarser and finer vessel noding than the reference nodalization (see APPENDIX D). The number of radial rings was maintained in both cases (coarser and finer nodalization). The azimuthal noding was reduced from 8 to 4 in the first case and increased from 8 to 24 in the second case. In the case of mesh refinement the azimuthal nodalization is done in a consistent way with the relative angular locations of the inlet and outlet connections to the vessel. The axial noding was increased only for the finer scheme in the region between the lower plenum and the upper plenum, maintaining for the LP and the UP the same number of cells. Then number of axial cells, for the finer nodalization, is 27. Such refinement mesh refinement is chosen to study numerical diffusion effect in predicting the thermal mixing in the DC region compared to the reference calculation. The resulting vessel noding schemes had 384 cells ($6_{radial} \times 4_{azimut\ hal} \times 16_{axial}$), whilst for the finer noding the number of cells is 3888 ($6_{radial} \times 24_{azimut\ hal} \times 27_{axial}$) versus 768 cells ($6_{radial} \times 8_{azimut\ hal} \times 16_{axial}$) in the original model.

The analysis of the spatial temperature distribution in the DC and at the core inlet leads to the conclusion that the decrease in noding detail results in higher dispersion, whilst the mesh refinement determines a lower dispersion. The Figure 179, Figure 180, Figure 181 , Figure 182 provides a qualitative and quantitative evaluation of the influence of the numerical diffusion on the averaged temperature distribution in the DC and at the core inlet by decreasing and increasing the degree of detail of the original meshing scheme.

In particular, even if the DC averaged temperature curve computed by the coarseness computational scheme seems to be very close to the experimental one, this cannot be considered as a general sign of good performance of the solution, and could be misleading. When one of the parameters that affect the numerical diffusion is changed, e.g. the cell size, the result is that the diffusion increases above what the experimental results suggest is caused by the turbulence of the flow. In turn one could agree that by mesh refinement, the true solution could be achieved but the problem is that usually this solution is unknown. (see [76]). Therefore, it is always advisable to apply methods that produce the least diffusion possible, and try to model the effect of turbulence by using appropriate, physically based models.

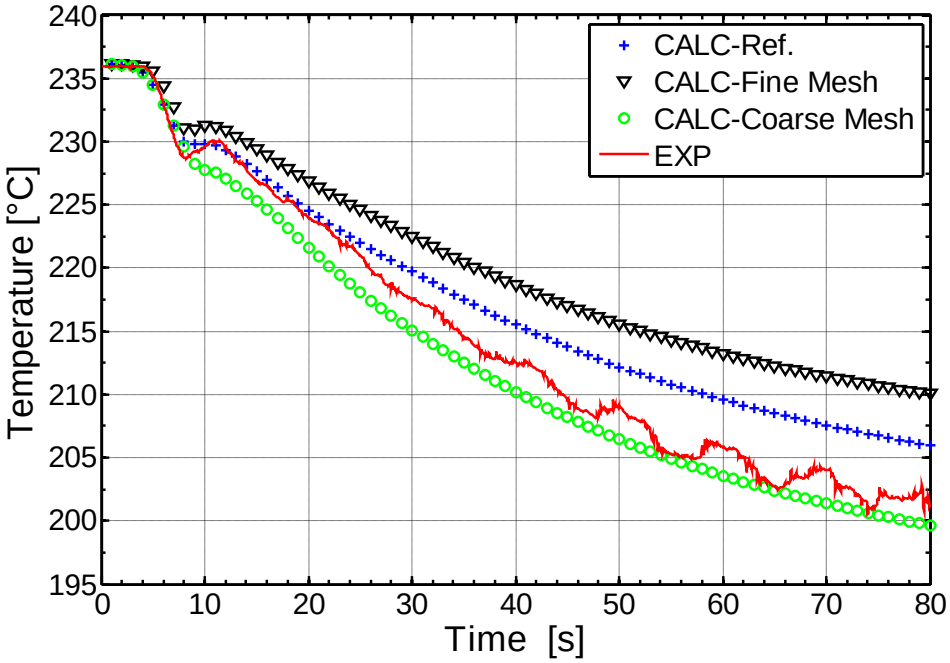

Figure 179 – ROCOM experiment 1.1, noding sensitivity analysis: DC average temperature trends

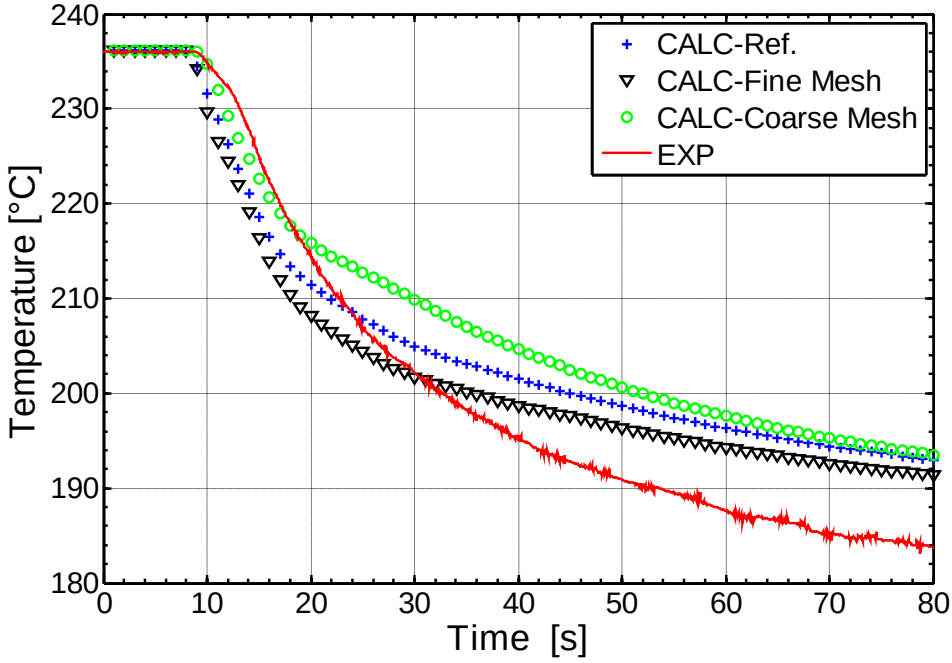

Figure 180 – ROCOM experiment 1.1, noding sensitivity analysis: DC average temperature trends

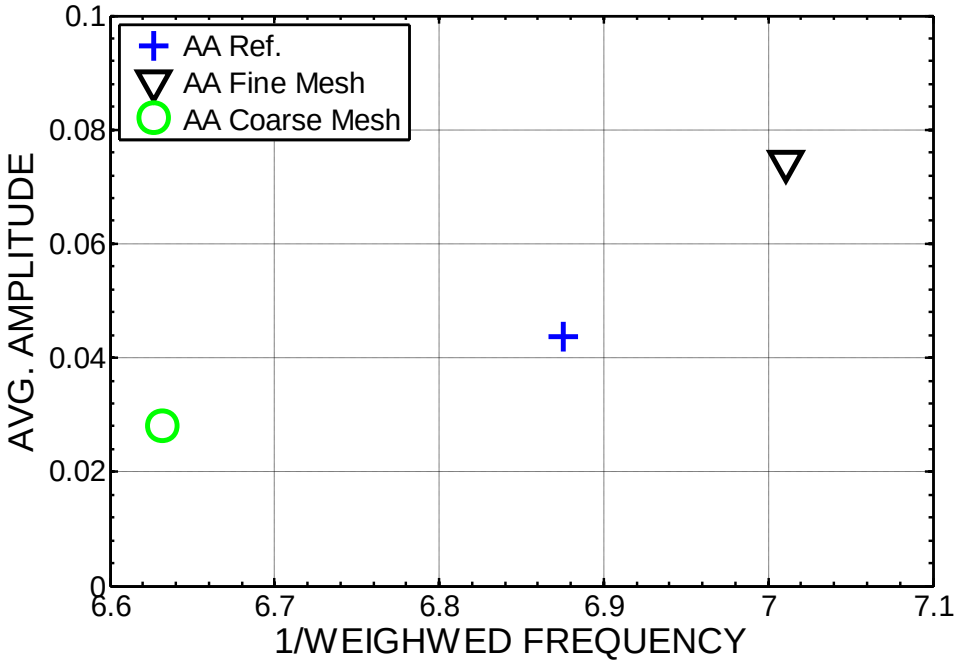

Figure 181 – ROCOM experiment 1.1, noding sensitivity analysis: FFTBM accuracy quantification (DC average temperature trends)

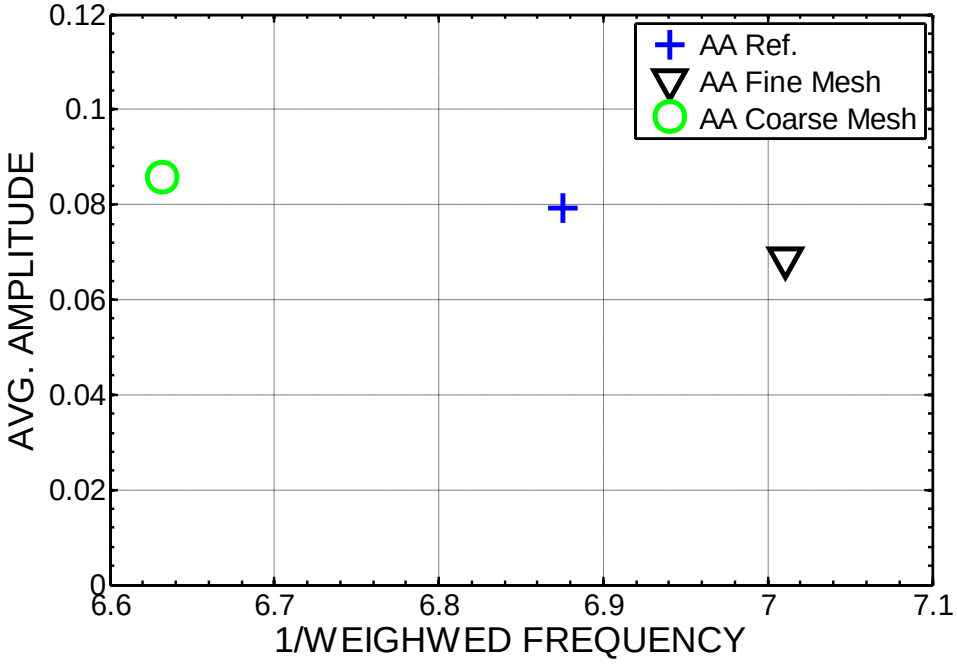

Figure 182 – ROCOM experiment 1.1, noding sensitivity analysis: FFTBM accuracy quantification (DC average temperature trends)

6.9. Concluding remarks on the IA application to the PKL/ROCOM test

The integrated analytical methodology for the assessment of the TRACE-V5 code was applied to the PKL-III test G3.1 and to buoyancy/convective driven flow mixing experiments performed at the ROCOM facility which are complementary tests simulating all thermal hydraulic phenomena relevant for the MSLB scenario.

The initiating event of the test G3.1 is a 0.1A break in the main steam line. The design of the experiment involves two phases: the first is an overcooling transient due to the initiating event; the second, when the affected SG is emptied, consisting in the ECCS injections by means of the HPIS connected with the cold legs 1 and 4. During these two phases two thermal hydraulic conditions are chosen as the most severe to investigate, throughout the ROCOM experiments, the safety issues during a postulated MSLB accident connected with the 3-D flow behavior inside the reactor pressure vessel. Namely the time point when the maximum overcooling in the affected loop occurs and the starting point of ECCS injection. These conditions are related with the possible re-criticality due to colder water entering the core area and with the PTS phenomenon as a consequence of temperature load on the RPV wall due to the safety injection systems.

The objective of this chapter was to analyze and document the analytical activity (posttest) performed, describing the performances of the code simulations and its capability to reproduce the relevant thermal hydraulic phenomena observed in the experiments carried out in the two facilities. The objective is fulfilled through comprehensive comparisons based on the following steps:

- comparison of the features of the analytical models applied;
- verification of the code performance “at steady state level”;
- assessment of the code performance at “on transient level” based on a qualitative and quantitative (FFTBM) accuracy evaluation of the results obtained by the simulation of the integral and separate effect experiments.

Specific outcomes from the analyses of the integrated simulation of the MSLB scenario are argued below.

Considering the two phase, Phase I and Phase II, of the transient regarding the behavior at the system level, the TRACE-V5 is able to capture the relevant physical phenomena, namely the PRZ thermal hydraulic, the intense natural circulation in the affected loop, also stable natural circulation (at lower intensity) in the unaffected loops, heat exchange primary to secondary and in particular the evaporation process of affected SG-inventory. The suitability and ability of the code perdition are validated by means of a qualitative and quantitative analysis. The first one which compares the calculated and experimental trends of the main parameters, demonstrates that TRACE-V5 predations of the break flow, the affected SG depressurization, the heat exchange primary to secondary, the RCS coolant temperatures at U-tubes outlet, and also the primary pressure are in agreement with the experimental evidences. The main discrepancies with the experiment are associated with imperfect set up of the boundary conditions and the differences in the initial conditions. The imperfect knowledge of the operation of the

PRZ valve and limitations due to simplified assumptions in modeling the component constitute the main reasons of the difficulties in simulating the Phase II.

The results of the investigation of the 3-D flow behavior inside the reactor pressure vessel by the analysis of the DC and core inlet temperature distributions show the outcome of TRACE-V5 calculation in simulating the thermal turbulent mixing phenomena taking place after entering of the flows from the different loops with different temperatures into the vessel (minimum temperature in loop 1 during the overcooling phase and cold mass flow rate injection during the activation of the ECCS). Sector formation between the coolants from different loops inside the vessel, position of the transition region between the established sectors and a more or less homogeneous temperature distribution, coalescence of two ECC water stripes in downcomer, sector formation at the core inlet are reproduced by the code. The agreement between numerical predictions and experiment is poor considering the prediction of the local mixing process as consequence of the large numerical diffusion introduced by the numerical scheme and the lack of turbulent diffusion/viscosity models for multi-dimension flow conditions. The integral parameter like the average temperature trend (considered as figure of merit of the whole mixing process) inside the DC and the core inlet as results of the code predictions show a qualitative well agreement compared to the experimental one during the overcooling phase (test 1.1) in both regions, whilst the agreement between numerical predictions and experiment becomes poorer during the ECCS injection phase (test 1.2). Even if, macroscopic point of view (namely space averaging over all probes point and computational nodes), the code result seems to be very close to the experimental one, this cannot be considered as a general sign of good performance of the numerical simulation, and could be misleading. In fact, the agreement between the two set of data, namely experimental and computational results, is fictitious in so far the mechanism which derives the mixing process is mainly of numerical nature, i.e. it related to the truncation error of the numerical scheme (numerical diffusion). Therefore, when one of the parameters affecting numerical diffusion is changed, e.g. the cell size, going from coarse to fine nodalization, the result is that the diffusion decrease (for a numerical scheme of first order in space and time of upwinding nature) and the calculated parameter trend is above what the experimental results suggest by the effect of the turbulence of the flow (see Figure 179 and Figure 180).

Outcomes from the application of the FFTBM, related to the quantification of the accuracy at the system level, highlight excellent quantitative accuracy of the results (slightly above 0.1) in calculating the coolant temperature at the SG outlet of the affected loop during the first phase of the transient. The accuracy rises above 0.2 if the overall transient is considered for the reasons described above. For the mixing phenomena inside the RPV the local average amplitude do not gives clear indication on the quantitative accuracy estimation and certainly needs further assessment.

The availability of the experimental data and of the code applications brought to the following main achievements:

- the test G3.1 constitutes state of the art, high level quality data, available for the improving the validation matrices of advanced computer codes;

- the experimental results are used to provide the boundary conditions of a SETF focused on mixing processes in DC and LP. (i.e. ROCOM). The combination of the PKL-III and of the ROCOM experiment covers almost all TH phenomena relevant for the MSLB scenario;
- the experiment G3.1 complements the tests performed in facility having different layout and scale (i.e. PKL B5.1, LOBI BT-12, LSTF SB-SL-01 and SB-SL-02, Semiscale Mod–2C S–FS–1);
- the capability of TRACE-V5 code to deal with the relevant phenomena involved in the transient is demonstrated for the Phases I and II of the transient;
- the posttest calculation appear to be adequate representation of the test G3.1: few mismatches between the experimental data and code are identified, discussed and understood;
- limitations and shortcomings of the TRACE-V5 code in simulating 3-D fluid dynamic conditions because of absence of terms in the balance equation accounting the turbulent exchange of momentum and energy;
- the assessment database of advanced computer TRACE-V5 system code, in relation to the PWR technology, is enlarged including the complementary tests performed in PKL-III and ROCOM rigs.

7 CONCLUSIONS

This doctoral thesis is a result of three-year work on application of TH-SYS codes in the area of nuclear reactor safety, operation and design, with particular reference to the code assessment issues. In particular, it aims at proposing a synthesis of what has been learned in the activities carried out within an exceptionally stimulating context.

The Author has been in charge of coordinating the thermal hydraulic activities in the framework of the OEDC/NEA/CSNI PKL-2/3 project in which the San Piero nuclear research group of University of Pisa is the Italian representative. Furthermore the Author has been continuously in touch with top-level experts from foreign research centers, institutions and industries (e.g CEA, AREVA, GRS, PSI, KAERI, etc.) in the framework of the FONESYS network.

In these contexts, the experience gained basically relies on two aspects:

1. the efforts spent and the results obtained in generating and validate the TRACE-V5 PKL-III and ROCOM models;
2. understanding weaknesses and limitations of the current generation of TH-SYS codes in simulating complex transient two phase flow as well as investigating their application for nuclear safety analysis.

A large part of the work dealt with the investigation of the TH-SYS code performances in simulating accident scenarios against experimental data, available for code qualification. Integral and separate tests have been simulated, so that different geometries, scales, flow phenomena and levels of complexity had to be dealt with. In addition numerical issues have been addressed through the use of numerical exercises performed to verify the predictive capability of the numerical techniques, with particular regard to TRACE numerical scheme.

Many thermal hydraulic analysis using the TRACE-V5 code addressed experiments conducted by the PKL-III integral test facility and ROCOM separate effect test facility in the frame of a research cooperation agreement between the University of Pisa and OECD/NEA Consortium Program to investigate primary circuit thermal-hydraulics that constitutes the PKL-2 Experimental Program. The international institutions involved in OECD/NEA/CSNI PKL project are: AREVA NP (DE), GRS (DE), BELV, VTT (FI), EDF (F), CEA (F), KFKI (KR), KAERI (KR), etc.

Concerning the numerical aspect of the TRACE-V5 code the analytical activity was performed within context of FONESYS network which comprises leading International institutions in the field of nuclear thermal-hydraulics and related code development (i.e. GRNSPG/UNIPI (IT), VVT (FI), GRS (DE), CEA (FR), AREVA NP SAS (FR), KINS (KR) and KAERI (KR)).

The objective of this research has been to provide a contribution to the assessment of TH-SYS codes (in particular of the TRACE-V5 code) in their application to nuclear reactor safety issues. Namely to the prediction of the time-space thermal-hydraulic conditions through the reactor coolant system considering the simultaneous physical interaction between the different phenomenological levels

(system, component and local), which characterize the thermal hydraulic of two phase flow patterns in the plant as it undergoes to an accident event. This includes, in particular, the simulation of multidimensional regimes, present in the RPV during a transient scenario (namely TMF), using 3-dimensional modules existing as an option in the codes like TRACE-V5 (code used in the framework of the research activity). The aim is to move toward a more realistic representation of the reality improving the best estimate point of view focused to provide a detailed realistic description of postulated accident scenarios based on best-available methodologies and numerical solution strategies. This means qualify the code to predict the global spectrum of concurring phenomena featuring a specific transient and therefore validate its 3-D features to overcome the approach used by strictly one-dimensional codes like RELAP5 or ATHLET that try to model multi-dimensional effects by multiple junction connections to a (one-dimensional) computational cell or by using a parallel channel representation with cross junction connections (results obtained are very sensitive to the chosen nodalization details, and other input parameters like flow resistance and form loss coefficients). The basis for the analysis of this process is a newly developed integrated assessment strategy which allows a complete evaluation of the code performance to accident analysis in PWR systems. The proposed methodology has been applied to main steam line break scenario and the accuracy of the code predicted results has been demonstrated in tests performed in a complementary way in scaled down integral and separate test facilities, that is test G3.1 conducted in PKL-III and ROCOM test rigs.

The application of the integrated approach allowed to assess the TH-SYS code reliability in predicting the phenomenology at the system level as well at the component level expected to occur during an accident scenario like a MSLB (which was the test under investigation) toward simulation capabilities as realistic as possible. Of course the application of this approach can be done only if experimental data, from complementary tests, are available. The performed PKL test G3.1 integrated with ROCOM tests provided the experimental database for the application of IA methodology.

The availability of the experimental data and of the code applications brought to the following *main achievements*.

- The test G3.1 constitutes state of the art, high level quality data, available for the improving the validation matrices of advanced computer codes.
- The experimental results are used to provide the boundary conditions of a SETF focused on mixing processes in DC and LP. (i.e. ROCOM). The combination of the PKL-III and of the ROCOM experiment covers almost all TH phenomena relevant for the MSLB scenario.
- The experiment G3.1 complements the tests performed in facility having different layout and scale (i.e. PKL B5.1, LOBI BT-12, LSTF SB-SL-01 and SB-SL-02, Semiscale Mod–2C S–FS–1).
- The capability of the TRACE-V5 to deal with the relevant phenomena involved in the transient at the system level is demonstrated for the Phases I and II of the transient performed in the PKL-III. In fact the code suitable to provide accurate coolant temperatures and mass flow

rates at RPV inlet besides the primary pressure. These parameters trends constituted the boundary conditions for performing the three dimensional analysis of the flow paths in DC and LP, which is relevant for investigating PTS and recriticality issues of a typical MSLB scenario. In this regard the simulation of multidimensional flow patterns performed using the results of the ROCOM complementary tests highlighted the limitations of the code to deal with mixing processes because of the 3-D modules suffer from the large numerical (artificial) diffusion/viscosity effects and the lack of appropriate bulk (physical) diffusion and turbulence models. Even if, macroscopic point of view (namely space averaging over all probes point and computational nodes), the code result seems to be very close to the experimental one, this cannot be considered as a general sign of good performance of the numerical simulation, and could be misleading. When one of the parameters affecting numerical diffusion is changed, e.g. the cell size, going from coarse to fine nodalization, the result is that the diffusion decrease (for a numerical scheme of first order in space and time of upwinding nature) and the calculated parameter trend is above what the experimental results suggest by the effect of the turbulence of the flow. One could argue that by mesh refinement, the right solution could be achieved but the problem is that usually this solution is unknown. Therefore, it is always advisable to apply methods that produce the least diffusion possible, and try to model the effect of turbulence by using appropriate, physically based models.

- The assessment database of advanced computer codes like TRACE, in relation to the PWR technology, is enlarged including 0.1A main steam line break in PKL-III facility and mixing process in ROCOM facility.

Finally, it is evident that each model or code represents an approximation of the real system or plant. The final use of these codes will therefore largely depend on the progress in validating these computational tools and in quantifying the uncertainty associated with the code prediction of the plant behavior.

REFERENCES

[1] Annunziato A., Glaeser H., Lillington J., Marsili P., Renault C., Sjöberg A., *"CSNI Integral Test Facility Validation Matrix for the Assessment of Thermal-Hydraulic Codes for LWR LOCA and Transients"*, NEA/CSNI/R(96)17, July 1996.

[2] IAEA, *"Accident Analysis for Nuclear Power Plants"*, Safety Reports Series No. 23, Vienna, A, 2002.

[3] OECD/NEA, *"CSNI International Standard Problems (ISP) – Brief Descriptions (1975-1999)"*, NEA/CSNI/R(2000)5, 2000.

[4] Choi K. Y., Baek W. P., Cho S., Park H.S., Kang K.H., Kim Y.S., *"OECD/NEA/CSNI International Standard Problem No. 50 – ATLAS Test, SB-DVI-09: 50% (6-inch) Break of DVI line of the APR1 Draft Comparison Report , Volume I Analysis of Blind Calculations",* NEA/CSNI/R(2010)x, 2010.

[5] Woods B. G., M. R. Galvin, C. J. Bowser, *"Problem Specification for the IAEA International Collaborative Standard Problem on Integral PWR Design Natural Circulation Flow Stability and Thermo-hydraulic Coupling of Containment and Primary System during Accidents"*, OSU-ICSP-10001, Oregon State University, 2010.

[6] Bucalossi A., *"Validation of Thermal-Hydraulic Codes for Boron Dilution Transients in the Context of the OECD/SETH Project"*, Seminar 2, EUROSAFE, Brussels, 2005.

[7] Melikhov O.I., I.V. Elkin, I.A. Lipatov, M.P. Gashenko, A.V. Kapustin, *"Final AE Comparison Report (Test 4) – Final"*, OECD/NEA/CSNI PSB-VVER Project, PSB-29, 2008.

[8] Del Nevo A., Adorni M., D'Auria F., Melikhov O.I., I.V. Elkin, V.I. Schekoldin, M.O. Zakutaev, S.I. Zaitsev, M. Benčík, *"Benchmark on OECD/NEA PSB-VVER Project Test 5a: LB-LOCA Transient IN PSB-VVER Facility"*, University of Pisa, DIMNP, NT 638(08) Rev. 2, Pisa, April 2009.

[9] US AEC, *"Interim Acceptance Criteria (IAC) for ECCS"*, USAEC, Washington (DC), USA, 1971.

[10] IAEA, *"Best Estimate Safety Analysis for Nuclear Power Plants: Uncertainty Evaluation",* Safety Reports Series No. 52, Vienna, Austria, 2008

[11] IAEA, *"Deterministic Safety Analysis for Nuclear Power"*. SSG-2, IAEA, Vienna, Austria, 2010.

[12] USNRC, *"Code of Federal Regulation"*, Washington (US) [continuously updated – see the website of US NRC].

[13] US AEC, *"Interim Acceptance Criteria (IAC) for ECCS"*, USAEC, Washington (DC), USA, 1971.

[14] Guerst J. A., *"Variational principles and two-fluid hydrodynamics of bubbly liquid/gas mixtures"*, Physica, Vol 135A, pp. 455-486, 1986.

[15] Drew D., A. *"Mathematical modeling of two-phase flow. Annual Reviews Fluid Mechanics"*, Vol.15, pp. 261–291, 1983.

[16] Guerst J. A., *"Variational principles and two-fluid hydrodynamics of bubbly liquid/gas mixtures"*, Physica, Vol 135A, pp. 455-486, 1986.

[17] Pauchon C. Smereka P., *"Momentum interactions in dispersed flow: an averaging and a variational approach"*, International J. of Multiphase Flow, Vol. 18, pp. 65-87, 1992.

[18] Bestion D., *"From the direct numerical simulation to system codes-perspective for the multi-scale analysis of LWR thermal-hydraulics"*, NUCLEAR ENGINEERING AND TECHNOLOGY, Vol.42 No. 6, pp. 608-619, December 2010.

[19] Drew D. A., "*Theory of Multicomponent Fluids*", Springer-Verlag Gmbh, 1998.

[20] Staedtke H., *"Gas Dynamic Aspects of Two-phase Flow"*, Wiley-VCH Verlag GmbH & Co. KGaA, Weinheim, 2006.

[21] Ishii M., Hibiki T., *"Thermo-Fluid Dynamics of Two-Phase Flow"*, 3rd edition, Springer, 2010.

[22] Bestion D., *"The physical closure laws in the CATHARE code"*, J. Nuclear Engineering and Design, Vol. 124, pp. 229-245, 1990.

[23] Staedtke H., de Cachard F., Garcia-Cascales J. R., Deconinck H., Franchello G., Graf, U., Kumbaro A., Mimouni S., Paillere H., Ricchiuto M., Romenski E., Romstedt P., Smith B, Toro E. F., Worth B., "*The astar project-status and perspective"*, 8th Int. Meeting on Nuclear Thermal Hydraulics, NURETH-10, Seoul, Korea, October 5-9, 2003.

[24] *"Proceedings of OECD/CSNI Specialist Meeting on Transient Two-Phase Flow - System Thermal-hydraulics"*, Aix-En-Provence (F), 1992

[25] *"Proceedings of OECD/CSNI Workshop on Transient Thermal-Hydraulic and Neutronic Codes Requirements"*, Annapolis, MD, USA, 5-8 Nov. 1996, NUREG/CP-0159, NEA/CSNI/R(97)4.

[26] *"Proceedings of OECD/CSNI Workshop on Advanced Thermal-Hydraulic and Neutronic Codes"* , Barcelona, Spain, April 10-13, 2000.Gf

[27] *"Assessing the Reliability of Complex Models: Mathematical and Statistical Foundations of Verification, Validation, and Uncertainty Quantification"*, Committee on Mathematical Foundations of Verification, Validation, and Uncertainty Quantification, NAS, 2012.

[28] Oberkampf W. L., Trucano T. G., *"Verification and validation benchmarks"*, J. Nuclear Engineering and Design, Vol 238, pp. 716-743, 2008.

[29] D'Auria F., Galassi G. M., *"Scaling in nuclear reactor system thermal-hydraulics"*, J. Nuclear Engineering and Design, Vol 240, pp. 3267-3297, 2010.

[30] Coscarelli E., et al., *"Hyperbolicity and Numerics in SYS-TH Codes, the FONESYS Point of View"*, Internal Report, FONESYS/Rec-04(12) Rev. 4, Pisa, Italy, 2012.

[31] Prosperetti, A., Tryggvason, G., *"Computational Methods for Multiphase Flow"*, Cambridge University Press, 2009.

[32] Zauderer, E., *"Partial Differential Equations of Applied Mathematics"*, New York, Wiley, 2nd edition, 1989.

[33] Kl Mortensen G. A., *"Thermal-Hydraulic Modeling Needs for Passive Reactors",* Proceedings of the OECD/CSNI Specialist Meeting on Advanced Instrumentation and Measurement Techniques, Santa Barbara, CA., 1997.

[34] Kelly, J. M, *"Thermal-Hydraulic Modeling Needs for Passive Reactors",* Proceedings of the OECD/CSNI Specialist Meeting on Advanced Instrumentation and Measurement Techniques, Santa Barbara, CA., 1997.

[35] Ishii M., Kim S., Sun X., *"Interfacial Area Transport Equation and Implementation Into Two-Fluid Model"*, J. of Thermal Science and Engineering Applications, Vol. 1, pp. 011005-1 to 011005-7, 2009.

[36] Staedtke H., *"Advanced modelling and numerical strategies in nuclear thermal-hydraulics"*, International Conference Nuclear Energy in Central Europe, Prtoroz, Slovenia, September 10-13, 2001.

[37] Melikhov V. I., Melikhov O. I., Solov'ev S. L., *"Next-Generation Thermal-Hydraulic Code Present-Day Tendencies for Development"*, High Temperature. Vol. 40, pp. 769-783, 2002.

[38] Talley J. D., Kim S., Mahaffy J., Bajorek S. M., Tien K., *"Implementation and evaluation of one-group interfacial area transport equation in TRACE"*, J. Nuclear Engineering and Design, Vol 241, pp. 865-873, 2011.

[39] IAEA, *"Verification and Validation of System Codes for Nuclear Safety Analyses"*, (the following persons contributed to the present document: Bestion D., D'Auria F., Jeong J. J., Park C. O.), In Press.

[40] D'Auria F., Bousbia-Salah A., Petruzzi A., Del Nevo A., *"State of the Art in Using Best Estimate Calculation Tools in Nuclear Technology"*, Nuclear Engineering and Technology, Volume 38, Issue 1, February 2006, pp 11-32.

[41] Kremin H., et al. *"Description of the PKL III Test Facility"*, FANP NT31/01/e30, FRAMATOME-ANP Erlangen, Germany, July 2001.

[42] Addabbo C., Annunziato A., Aksan N., D'Auria F., Dumont D., Galassi G. M., Nilsson L., Riikonen V., Rigamonti M., Steinhoff F., Toth I., Umminger K., *"Maintenance of European LWR Integral System Test Thermal-Hydraulic Databases"*, EUR Report N. 19937, October 2001.

[43] Umminger K., Mull T., Brand B.*, "Integral Effect Tests in the PKL Facility with International Participation",* Nuclear Engineering and Technology, Vol.41 No.6, August 2009.

[44] D'Auria F., Galassi G. M., W. Giannotti, A. Del Nevo, Araneo D., *"Assessment of CATHARE2V2.5 Code Against Boron Transport Experiment"*, University of Pisa, DIMNP NT 563 (06) Rev. 2, April 2006.

[45] D'Auria F., et al., *"Evaluation of the Data Base from High Power and Low Power Small Break LOCA Counterpart Tests Performed in LOBI, SPES, BETHSY and LSTF Facilities"*, Università di Pisa, DCMN NT 237 (94), Pisa, November 1994.

[46] Del Nevo A., Adorni M., D'Auria F., Galassi G.M., *"Assessment of CATHARE2v2.5 code against PKL-III F4.1 (Run1 and Run2) boron transport experiments",* DIMNP NT 613(08) Rev. 2, Pisa, Italy, 15 October 2008.

[47] Schoen B., *"SB-LOCA with Total Failure of HPSI (Counterpart Testing with ROSA/LSTF)"*, PTCTP-G/2012/en/0008, AREVA NP GmbH, September 2013.

[48] Mull T., Umminger K., A. Bucalossi A., D'Auria F., et al, *"Final Report of the OECD-PKL Project"*, NTCTP-G/2007/en/0009, AREVA NP GmbH, 2007.

[49] .Jasiulevicius A., et al., *"Investigation of Heat Transfer Mechanisms under Shutdown Plant Conditions with TRACEv4.160"*, Proceedings of ICAPP '06 Reno, NV USA, June 4-8, 2006, pp. 1820 - 1828.

[50] D'Auria F., Galassi G. M., *"Characterization of Instability During Two-Phase Natural Circulation in Typical PWR Conditions"*, Experimental and Fluid Science, 1990, 3, pp. 641-650.

[51] Coscarelli E., et al., *"ACCURACY ASSESSMENTS WITH FAST FOURIER TRANSFORM BASED METHOD (FFTBM)"*, 14th Int. Meeting on Nuclear Thermal Hydraulics, NURETH-14, Toronto, Ontario, Canada, September 25-29, 2011.

[52] Coscarelli E., Galassi G. M., D'Auria F., *"Analytical Study of Inherent Boron Dilution Phenomenon During a Small Break LOCA Scenario in a PWR System Using the TRACE V5.0 Code"*, 21st International Conference Nuclear Energy for New Europe, Ljubljana, Slovenia, September 5 – 7, 2012.

[53] Mahaffy, J. H., *"Numerics of codes: stability, diffusion and convergence"*, J. Nuclear Engineering and Design, Vol145, 131-145, 1993.

[54] Mahaffy, J. H., *"A stability-enhancing two-step method for fluid flow calculations"*, J. Computational. Physics. Vol. 46, pp. 329-341, 1982.

[55] Ransom, V., H., *"Numerical Benchmark Tests, Multiphase Science and Technology"*, 3, edited by G.F.Hewitt, J.M.Delhay, and N. Zuber, Hemisphere, Washington, DC, 1987.

[56] Dinh, T.N., Nourgaliev, R.R., and Theofanou,T.G., *"Understanding the ill-posed two-fluid model"*, 10th Int. Meeting on Nuclear Thermal Hydraulics, NURETH-10, Seoul, Korea, October 5-9, 2003.

[57] Coscarelli E., *"PROPOSAL OF NUMERICAL BENCHMARK: WATER FAUCET FLOW"*, 3rd FONESYS Workshop, GRNSPG-UNIPI, S. Piero a Grado, Pisa, Italy, 2011.

[58] Faluomi V., *"Metodologia per l'estrapolazione dell'errore valutazione di singoli fenomeni termoidraulici"*, Tesi di Laurea in Ingegneria Nucleare, Tutors Mazzini M., D'Auria F., Aksan N., Università di Pisa, Pisa, Novembre 1993

[59] D'Auria F., Faluomi V., Aksan N., *"Qualification of the UMAE-SETS Uncertainty Methodology"*, Nuclear Society of Slovenia 3rd Regional Meeting: Nuclear Energy in Central Europe, Portorož, Slovenia, September 16-19, 1996

[60] D'Auria, F., *"Uncertainty Methods Study for Advanced Best Estimate Thermal-hydraulic Code Applications Vol. 2"*, Report from the Uncertainty Analysis Group, CSNI, 1998.

[61] Agnoux C., Coscarelli E., Kliem S., Kovtonyuk A., Marshall S., Sanchez-Perea M., Tóth I., Schollenberger S.P., Dennhardt L., Schoen B., Umminger K., *"OECD-PKL2 Project Solving Thermal Hydraulic Safety Issues for Current PWR and New PWR Design Concepts through Experiments in the Integral Test Facility PKL",* Final Report, PTCTP-G/2012/en/0004, AREVA NP GmbH, 2012.

[62] Glaeser H., *"CSNI Integral Test Facility Matrices for Validation of Best-Estimate Thermal-Hydraulic Computer Codes"*, THICKET 2008, Pisa, Italy, 5-9 May 2008.

[63] Leonardi M., D'Auria F., Pochard R., *"The FFT based method in the frame of the UMAE"*, Spec. Workshop on Uncertainty Analysis Methods, London, March 1994.

[64] Del Nevo A., Coscarelli E., Kovtonyuk A., D'Auria F., *"Analytical Exercise on OECD/NEA/CSNI PKL-2 Project Test G3.1: MSBL Transient in PKL-III Facility: Phase 2 – Post-test Calculation"*, UNIPI/GRNSPG, TH/PKL-2/02(10) Rev. 1, Pisa, Italy, March 2011.

[65] Dennhardt L., *"Test PKL III G3.1: Main Steam Line Break"*, NTCTP-G/2009/en/0009 AREVA NP GmbH, 30 November 2011. PTCTP-G/2011/en/0009

[66] Gauvain J., "*Summary Record of the Third Meeting of the Program Review Group of the OECD PKL2 Project"*, PKL2 PRG/Sec/(09)1, 24 April 2009.

[67] Dennhardt L., *"Additional information on Test G3.1 (Main Steam Line Break)"*, AREVA NP, PKL G3.1 – G3.1-OECDinfoPRZ.ppt, NTCTP-G/De, Erlangen, 20 November 2009.

[68] United States Nuclear Regulatory Commission, *"TRACE V5.0 Theory Manual, Field Equations, Solution Methods, and Physical Models"*, 2008.

[69] United States Nuclear Regulatory Commission, "*TRACE* V5.0 user's manula, volume 2", 2008.

[70] Bonuccelli M., D'Auria F., Debrecin N., Galassi G: M., *"A Methodology for the Qualification of Thermalhydraulic Code Nodalizations"*, Proc. of NURETH-6 Conference, Grenoble (F), October 5-8, 1993.

[71] Bovalini R., D'Auria F., M. Leonardi M., *"Qualification of the Fast Fourier Transform Based Methodology for the Quantification of Thermal-hydraulic Code Accuracy"*, DCMN Report, NT 194 (92), Pisa July 1992.

[72] Kliem S., Franz R., *"Quick-look report of the ROCOM Tests 1.1 and 1.2 conducted within the OECD-PKL2 Project"*, FZD\FWS\2010\07, 2010.

[73] Kliem S., Franz R., *"Quick-look report of the ROCOM Tests 1.3, 2.1 and 2.2 conducted within the OECD-PKL2 Project"*, HZDR\FWO\2012\02, 2012.

[74] Kliem S., Franz R., *"OECD PKL2 Project – Final Report on the ROCOM tests"* HZDR\FWO\2012\03, 2012.

[75] Prošek A., Leskovar M., "*Application of Fast Fourier Transform for Accuracy Evaluation of Thermal-Hydraulic Code Calculations",* in *"Fourier Transforms - Approach to Scientific Principles",* Edited by Goran Nikolic, InTech, April 11, 2011.

[76] Macian-Juan R., Mahaffy J. H., *"Numerical diffusion and the tracking of solute fields in system codes Part II. Multi-dimensional flows"*, J. Nuclear Engineering and Design, Vol. 179, pp. 321-344, 1998.

APPENDIX A. CODES USED WITHIN THE RESEARCH: TRACE-V5 code

A.1. Overview of TRACE

The TRAC/RELAP Advanced Computational Engine (TRACE formerly called TRAC-M) is an advanced best-estimate thermal-hydraulic system code developed by the U.S. Nuclear Regulatory Commission (with the involvement of Los Alamos National Laboratory, Integrated Systems Laboratory (ISL), the Pennsylvania State University (PSU) and Purdue University) with the aim of analyzing the neutron/thermal-hydraulic behavior of light water reactors during operational transient and accident scenarios as loss of coolant accident (LOCA) in light water reactors. The code is the result of merging the capabilities of USNRC many supported codes, such as TRAC-PF1, TRAC-BF1, RELAP-5 and RAMONA. Models for multidimensional two-phase flow, non-equilibrium thermo-dynamics, heat transfer, reflood, level tracking, and reactor kinetics are included.

The two-fluid conservation laws, namely mass, energy and momentum for the liquid and gas field with the closure laws are solved using the finite volume approach. The spatial mesh used for the finite volume equations are staggered, with thermodynamics properties evaluated at cell centers and velocity evaluated at the cell edges. Heat transfer numerical models is based on semi-implicit scheme, while the basic equations of a two-phase flow are solved by a multi-step time differencing procedure SETS, namely stability enhancing two steps method, that has the advantage of eliminating the material Courant stability limit of the semi-implicit method, thus resulting in large time step sizes for slow transients, and fast running capabilities. The resulting system of coupled non-linear algebraic equations is solved by means of a Newton-Raphson iterative method, which strategy is to achieve a set of linearized equations in pressure, whose solution is obtained by direct matrix inversion. A full two-fluid (6-equations) model is used to evaluate the gas-liquid flow, with an additional mass balance equation to describe a non-condensable gas field, and an additional transport equation to track dissolved solute in the liquid field (see [A-1]).

TRACE takes a component-based approach to modeling a reactor system. Each physical piece of equipment in a flow loop can be represented as some type of component, and each component can be further nodalized into some number of physical volumes (also called cells) over which the uid, conduction, and kinetics equations are averaged. The number of reactor components in the problem and the manner in which they are coupled is arbitrary. There is no built-in limit for the number of components or volumes that can be modeled; the size of a problem is theoretically only limited by the available computer memory. Reactor hydraulic components in TRACE include *pipes*, *plenums*, *pressurizers*, BWR fuel channels, pumps, *jet pumps*, *separators*, *tees*, *turbines*, *feed water heaters*, *containment*, *valves*, *vessels* with associated internals (downcomer, lower plenum, reactor core, and upper plenum). Special components are available as well for delivering energy

to the fluid via the heat structures[7], hydraulic component walls or directly to the fluid (such as might happen with gamma heating of the coolant). *Radiation enclosure* components may be used to simulate radiation heat transfer between multiple arbitrary surfaces. Finally, *fill* and *break* components are used to impose flow and pressure boundary conditions, respectively.

The TRACE code is not only modular by component, but also by function, i.e. the major aspects of the calculations are performed in separate modules. For example, the basic 1D hydrodynamics solution algorithm, the wall-temperature field solution algorithm, heat transfer coefficient selection, and other functions are performed in separate sets of routines that can be accessed by all component modules. This modularity allows the code to be readily upgraded with minimal eort, and there is minimal potential for error as improved correlations and test information become available.

A.2. Governing equations

The present two-phase flow model implemented in TRACE is based on a *macroscopic* description of two-phase flow using time and volume averaged values for all state and flow parameters. This leads to what is often called the 'two-fluid model' of two-phase flow with separate balance equations for mass, momentum and energy for both liquid and pas phase. The TRACE two phase flow model is developed for 1-D flow conditions as well as for multi-dimensional flow processes[8].

The thermal hydraulic two fluid conservation laws (1-D and 3-D flow field) describe mass, momentum and energy exchange between the vapor and liquid phases and the interaction of these phases with heat flow from/to the modeled structures. A stratified-flow regime has been added to the 1-D hydrodynamics; a seventh field equation (mass balance) describes a noncondensable gas field; and an eighth field equation tracks dissolved solute in the liquid field that can plated out on surfaces when solubility in the liquid is exceeded. Contributions from the stress tensor due to shear at metal surfaces or phase interfaces within the averaging volume are considered. The two phase flow equations implemented in TRACE are derived rearranging the following space-time averaged two phase flow equations (see [A-1]).

The time and volume averaged mass equations are:

---

[7] Heat structure components, to model fuel elements or heated walls in the reactor system, are available to compute two-dimensional conduction and surface-convection heat transfer in Cartesian or cylindrical geometries.

[8] A 3-D (x, y, z) cartesian and/or (r, θ, z) cylindrical-geometry flow calculation can be simulated within the reactor vessel or other reactor components where 3-D phenomena take place. All 3-D components, such as Reactor Water Storage Tank, where 3-D phenomena are modeled, are named VESSEL although they may not have any relationship with the reactor vessel

$$\frac{\partial(1-\alpha)\rho_l}{\partial t} + \nabla \cdot \left[(1-\alpha)\rho_l \mathbf{v}_l\right] = -\Gamma \tag{A-1}$$

$$\frac{\partial \alpha \rho_g}{\partial t} + \nabla \cdot \left[\alpha \rho_g \mathbf{v}_g\right] = \Gamma \tag{A-2}$$

The time and volume averaged energy equations are:

$$\begin{aligned}\frac{\partial(1-\alpha)\rho_l\left(e_l + v_l^2/2\right)}{\partial t} + \nabla \cdot \left[(1-\alpha)\rho_l\left(e_l + \frac{P}{\rho_l} + v_l^2/2\right)\mathbf{v}_l\right] \\ = q_{il} + q_{wl} + q_{dl} + (1-\alpha)\rho_l \mathbf{g}\cdot\mathbf{v}_l - \Gamma h_l' + (\mathbf{f}_i + \mathbf{f}_{wl})\cdot\mathbf{v}_l\end{aligned} \tag{A-3}$$

$$\begin{aligned}\frac{\partial \alpha \rho_g\left(e_g + v_g^2/2\right)}{\partial t} + \nabla \cdot \left[\alpha\rho_g\left(e_g + \frac{P}{\rho_l} + v_g^2/2\right)\mathbf{v}_g\right] \\ = q_{ig} + q_{wg} + q_{dg} + \alpha\rho_g \mathbf{g}\cdot\mathbf{v}_g - \Gamma h_l' + (-\mathbf{f}_i + \mathbf{f}_{wg})\cdot\mathbf{v}_g\end{aligned} \tag{A-4}$$

The time and volume averaged momentum equations are

$$\frac{\partial(1-\alpha)\rho_l \mathbf{v}_l}{\partial t} + \nabla \cdot (1-\alpha)\rho_l \mathbf{v}_l \mathbf{v}_l + (1-\alpha)\nabla P = (\mathbf{f}_i + \mathbf{f}_{wl}) + (1-\alpha)\rho_l \mathbf{g} - \Gamma \mathbf{v}_l \tag{A-5}$$

$$\frac{\partial \alpha \rho_g \mathbf{v}_g}{\partial t} + \nabla \cdot \alpha \rho_g \mathbf{v}_g \mathbf{v}_g + (1-\alpha)\nabla P = (\mathbf{f}_i + \mathbf{f}_{wg}) + \alpha\rho_g \mathbf{g} - \Gamma \mathbf{v}_g \tag{A-6}$$

To simplify the numerical strategy and to reduce the calculation time , the balance equations are not written in conservation form and, in place of two separate energy equations, one mixture energy and one gas energy equation are solved. The internal energy and motion equations are rearranged from the fully conservative forms of the energy and momentum equations (from Eq. A-3 to Eq. A-6). In particular the internal energy conservation equation for the gas phase is obtained by taking the dot product of the corresponding momentum equation Eq. A-6 with its velocity and subtracting the results from the fully conservative energy equation Eq. A-4:

$$\frac{\partial(\alpha\rho_g e_g)}{\partial t} + \nabla \cdot (\alpha\rho_g e_g \mathbf{v}_g) = -P\frac{\partial \alpha}{\partial t} - P\nabla \cdot (\alpha \mathbf{v}_g) + q_{wg} + q_{dg} + q_{ig} + \Gamma h_w' \tag{A-7}$$

A similar operation is performed on the liquid energy equation, but rather than using it in that form, the result is added to the gas energy equation to produce a mixture energy conservation equation, namely:

$$\frac{\partial\left[\left(1-\alpha\right)\rho_l e_l+\alpha\rho_g e_g\right]}{\partial t}+\nabla\cdot\left[\left(1-\alpha\right)\rho_l e_l\mathbf{v}_l+\alpha\rho_g e_g\mathbf{v}_g\right] \tag{A-8}$$
$$=-P\nabla\cdot\left[\left(1-\alpha\right)\mathbf{v}_l+\alpha\mathbf{v}_g\right]+q_{wg}+q_{wl}+q_{dg}+q_{dl}$$

When included in the finite volume equation solution, the mixture energy equation makes it easier to deal with transitions from two-phase to single-phase flow during a step in the time integration. To fully achieve this advantage during a transition, a similar pair of gas and mixture mass equations must be used in the actual solution.

$$\frac{\partial\alpha\rho_g}{\partial t}+\nabla\cdot\left[\alpha\rho_g\mathbf{v}_g\right]=\Gamma$$

$$\frac{\partial\left[\left(1-\alpha\right)\rho_l+\alpha\rho_g\right]}{\partial t}+\nabla\cdot\left[\left(1-\alpha\right)\rho_l\mathbf{v}_l+\alpha\rho_g\mathbf{v}_g\right]=0 \tag{A-9}$$

Motion equations are obtained by the standard means of multiplying the mass conservation equation for a phase (Eq. A-1 or Eq. A-2) by that phase's velocity, subtracting it from the

$$\frac{\partial\mathbf{v}_l}{\partial t}+\mathbf{v}_l\cdot\nabla\mathbf{v}_l=-\frac{1}{\rho_l}\nabla P+\frac{\left[\mathbf{f}_i+\mathbf{f}_{wl}-\Gamma\left(\mathbf{v}_i-\mathbf{v}_l\right)\right]}{\left(1-\alpha\right)\rho_l}+\mathbf{g} \tag{A-10}$$

$$\frac{\partial\mathbf{v}_g}{\partial t}+\mathbf{v}_g\cdot\nabla\mathbf{v}_g=-\frac{1}{\rho_g}\nabla P+\frac{\left[\mathbf{f}_{wg}-\mathbf{f}_i-\Gamma\left(\mathbf{v}_g-\mathbf{v}_i\right)\right]}{\alpha\rho_g}+\mathbf{g} \tag{A-11}$$

The equations Eq. A-10 and Eq. A-11 are generally referred to as the non-conservative form of the momentum equations, because it is not possible to write a finite volume method that guarantees some numerical integral of momentum over a system does not change from one time step to the next in the absence of force terms. Use of this form permits simpler numerical solution strategies particularly for a semi-implicit method, and can generally be justified because the presence of wall friction makes the fully conservative form of the momentum equation far less useful. When sharp flow-area changes exist, however, numerical solution of the non-conservative motion equations can produce significant errors. For these situations, the motion equations have been modified to force Bernoulli flow.

Because these interactions are dependent on the flow topology, a constitutive-equation package dependent on the flow regime has been incorporated into the code.

A.2.1. Interfacial drag force

The transfer of mass, energy and momentum between gas–liquid phases are modeled by the flow regime dependent thermal-hydraulic equations. In TRACE, there are three categories of flow regimes:

- ***Pre-CHF***: these consist of the bubbly/slug and the annular/mist regimes.

- ***Stratified***: the horizontal stratified flow regime is available for 1-D components that are either horizontal or inclined.
- ***Post-CHF***: this encompasses the "inverted" flow regimes that occur when the wall is too hot for liquid-wall contact.

A.2.2. Wall drag force

TRACE models the fluid-wall shear force using a friction factor approach. Regarding the Pre-CHF regime, wall drag force is only applied to the liquid phase.

A.2.3. Wall condensation and boiling

When the wall temperature above the liquid level is lower than the saturation temperature, condensation of vapor on the wall is calculated. If the wall temperature above the liquid level is higher than the saturation temperature, natural convection in the vapor region occurs. Natural convection in the liquid region is considered when the wall temperature below the liquid level is lower than the saturation temperature. When the wall temperature below the liquid level is higher than the saturation temperature, heat transfer occurs by boiling.

A.2.4. Heat conduction

The thermal history of the reactor structure is obtained from a solution of the heat-conduction equation Eq. A-12 applied to different geometries.

$$\frac{\partial\left(\rho c_p T\right)}{\partial t} + \nabla \cdot \mathbf{q} = q''' \tag{A-12}$$

The Eq. A-12 represents the general form that describes the heat conduction process. In practice, the product ρc_p is assumed to be constant for purposes of taking the time derivative. In turn, the heat flux $\boldsymbol{q}$ can be expressed in terms of the temperature gradient by Fourier's law:

$$\mathbf{q} = -k\nabla T \tag{A-13}$$

Therefore, Eq. A-13 becomes:

$$\rho c_p \frac{\partial T}{\partial t} - k\nabla \cdot \left(\nabla T\right) = q''' \tag{A-14}$$

A.3. Physical phenomena considered

The TRACE code can simulate the following physical phenomena (see [A-1]):

- Emergency Core Cooling (ECC) downcomer penetration and bypass, including the effects of counter-current flow and hot walls;
- lower-plenum refill with entrainment and phase-separation effects;
- bottom-reflood and falling-lm quench fronts;
- multi-dimensional flow patterns in the reactor-core and plenum regions;

- pool formation and counter-current flow at the upper-core support-plate region;
- pool formation in the upper plenum;
- steam binding;
- water level tracking,
- average-rod and hot-rod cladding temperature histories;
- alternate ECC injection systems, including hot-leg and upper-head injection;
- direct injection of subcooled ECC water, without artificial mixing zones;
- critical flow (choking);
- liquid carryover during reflood;
- metal-water reaction;
- water-hammer pack and stretch effects;
- wall friction losses, and reversible and irreversible form-loss ow eects on the pressure
- distribution;
- horizontally stratified flow, including reflux condition mode;
- gas or liquid separator modeling;
- noncondensable-gas effects on evaporation and condensation;
- dissolved-solute tracking in liquid flow;
- reactivity-feedback effects on reactor-core power kinetics;
- two-phase bottom, side, and top off take flow of a T-junction.

A.4. Numerical approach

The numerical method applied is based on a staggered grid/donor cell approach with a partial implicit time integration to eliminate the material Courant stability limit condition. The solution methods applied in TRAC is the Stability-Enhancing Two Step (SETS) method of Mahaffy (see [A-2] and [A-3]) which comprises the following five steps

1) First guesses for the phasic velocities are calculated from the simplified separate momentum equations (equations of motions) using only new-time velocities in the linearized expressions for the drag force. All other values (including pressure) are taken from previous time level.
2) In this step updated (intermediate) phasic velocities are calculated again from the momentum equations (“stabilizer equations of motion”). Intermediate term values include only phasic velocities in the momentum flux and wall friction terms. Using the velocities from step 1 in the drag forces, the two momentum equations are decoupled with respect to each other. The resulting two sets of tri-diagonal systems are directly solved for the phasic velocities.
3) Steps 3 and 4 are the semi-implicit part of the SETS method. In step 3, the momentum equations are used again, now with new-time values for the phasic velocities in momentum flux, wall friction, interfacial drag and interfacial momentum transfer terms associated with mass interfacial

transfer (evaporation/condensation). In addition first estimates for the new-time pressure values are introduced in the spatial pressure derivative terms. As a result, linear expressions are obtained for the new-time velocities as functions of the intermediate pressure values.

4) This step provides intermediate new-time values for the scalar (thermodynamic) variables from the expanded form of the mass and energy balance equations using the phasic velocities as calculated by step 3. The resulting non-linear set of equations for the void fraction, pressure and phasic temperatures is solved by a Newton-Raphson iteration method keeping the phasic velocities and wall temperatures constant.
5) In this final "stabilizer step" the mass and energy equations are used in conservative form to calculate new-time macroscopic values for the phasic mass and energy $(\alpha_i \rho_i)^{n+1}$, $(\alpha_i u_i)^{n+1}$ the phasic velocities from the semi-implicit steps 3 and 4. The expressions for the macroscopic mass and energy are then linearized by a first-order Taylor expansion. The resulting system of 4x4 (or respectively 5x5 with non-condensable gases) linear equations are separately solved for each cell by a direct Gauss elimination to obtain final values for phasic temperature, pressure and void fraction.

The time step control is based on convergence criteria for user-specified threshold values for local pressure and void fraction increments.

A.5. References to APPENDIX A

[A-1] United States Nuclear Regulatory Commission, *"TRACE V5.0 Theory Manual, Field Equations, Solution Methods, and Physical Models"*, 2008.

[A-2] Mahaffy, J. H., "Numerics of codes: stability, diffusion and convergence", J. Nuclear Engineering and Design, Vol. 145, 131-145, 1993.

[A-3] Mahaffy, J. H., *"A stability-enhancing two-step method for fluid flow calculations"*, J. Computational Physics, Vol. 46, pp. 329-341, 1982.

APPENDIX B. DESCRIPTION OF THE PKL TRACE NODALIZATION

B.1. Description of the TRACE-V5 nodalization

The TRACE model of PKL facility, shown in Figure 19, consists of two 3-D vessel components in cylindrical geometry that model the rod bundle vessel (RBV) and the RPV down-comer, four separate loops that reproduce the geometry and the hydraulic configuration of the experimental facility. Each one includes a hot leg (HL) a SG, a pump seal, a butterfly valve, a reactor cooling pump and a CL. The pump seal is nodalized with two pipe components: the first one models the circuit from the SG outlet until the BV while the second one reproduces the connection of the loop seal with the RCP (see Figure 187).

The 3-D vessel component that schematizes the reactor core vessel is composed by 45 axial level, 2 radial rings and 6 azimuthal sectors (see Figure 183 and Figure 184). The radial discretization takes in account the internal configuration of the rod bundle vessel characterized by two main radial regions: the reactor core and reflector gap, that simulates the side mass flow through the reactor (core bypass). The core bypass hydraulic resistance in the 3D component is introduced using a suitable K-factor so that the mass flow at the bypass during the steady state calculation matches the experimental values that correspond to 1% of the total primary side mass flow. The six azimuthal sector in which is subdivided the cross section of the rod bundle vessel is defined considering the loops arrangement and the down-comer upper head bypass piping disposition. In particular the HL 1 and 2 are connected with the sector S4 while the HL 3 and 4 with the sector S1. The sectors S2, S3, S5 and S6 have connections to the cold legs, respectively CL1, CL4, CL3 and CL2.

The fuel rods in the core region are modeled by six powered fuel rod heat structures, which are arranged in the azimuthal direction each one with the power that corresponds to the sector where there is set out. In the axial direction the fuel rods are nodalized with 18 volumes, the first two level and the last one are not powered, because there represent the unheated length of the core region (see Figure 184).

The DC vessel model consists of 7 axial levels, 2 radial rings (the inner radius has zero fraction flow area in the radial direction, to reproduce the annular DC model) while the azimuthal nodalization is the same as that of the rod bundle vessel. The down-comer is connected to the RBV by 1-dimensional components that direct the flow from the down-comer to the lower plenum and from the down-comer to the upper head. The four parallel bypass lines that represent the upper heat bypass are model in TRACE with two equivalent parallel bypass pipes (see Figure 185).

The thermal hydraulic behavior of the pressurizer is simulated through three pipes: the first one, nodalized with one volume, models the bottom of the PRZ, the

second one, composed by 20 volumes, analyses the two phase behavior of the pressurizer, finally the last hydraulic component represents the top of the PRZ, that connects it to the relief steam line, modeled with a pipe. The surge line that realizes the attachment between the PRZ and the HL 2 is nodalized with 1 dimensional component (see Fgure 187).

The primary sides of steam generators are nodalized with a single pipe to represent the U-tube bundle. The modeling of the SG U-tubes in TRACE preserves the flow area and the length (or the volume) with respect to the PKL-III geometry (see Figure 187). The TRACE model of the steam generator secondary side is composed by three pipes: the first one models with 61 volumes the rise zone of the steam generator, the second one, composed by 64 volumes, models both the annular top and bottom part but also the two pipes of the down-comer, finally the third one (11 volumes) reproduces the hydraulic behavior of the dome of the SG (see Figure 186).

The feature of the nodalization in terms of geometry and numbers of computational cells are shown in Table

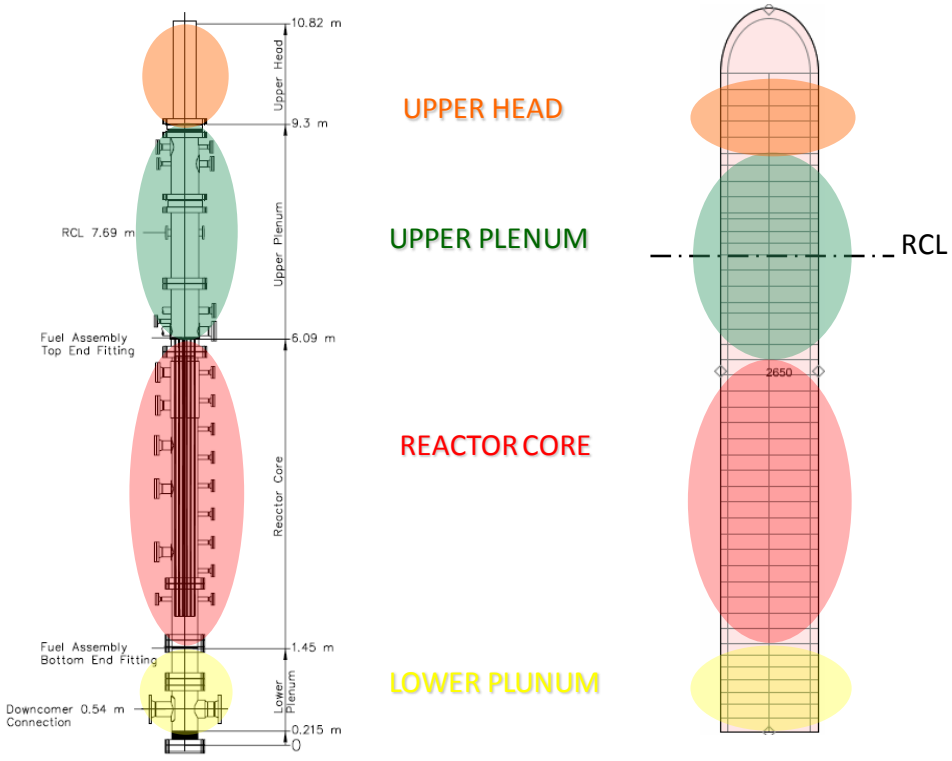

Figure 183 – TRACE nodalization: RBV scheme

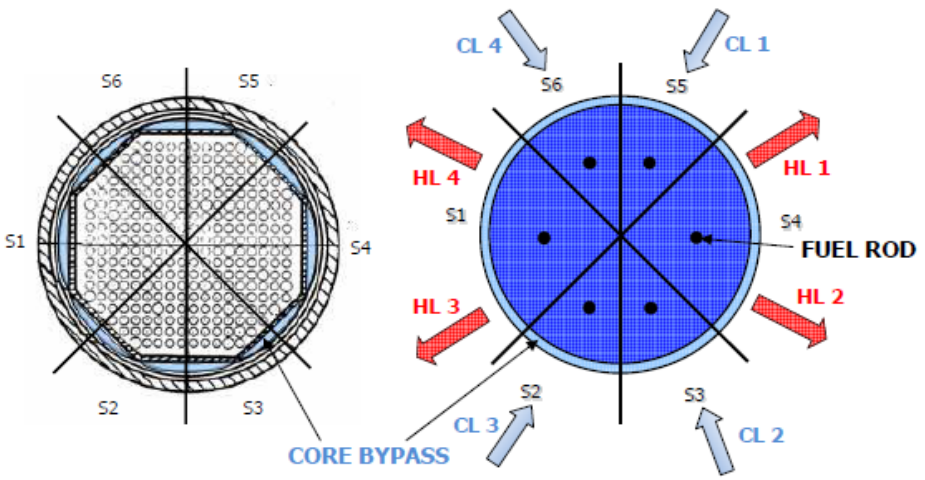

Figure 184 – TRACE nodalization: core

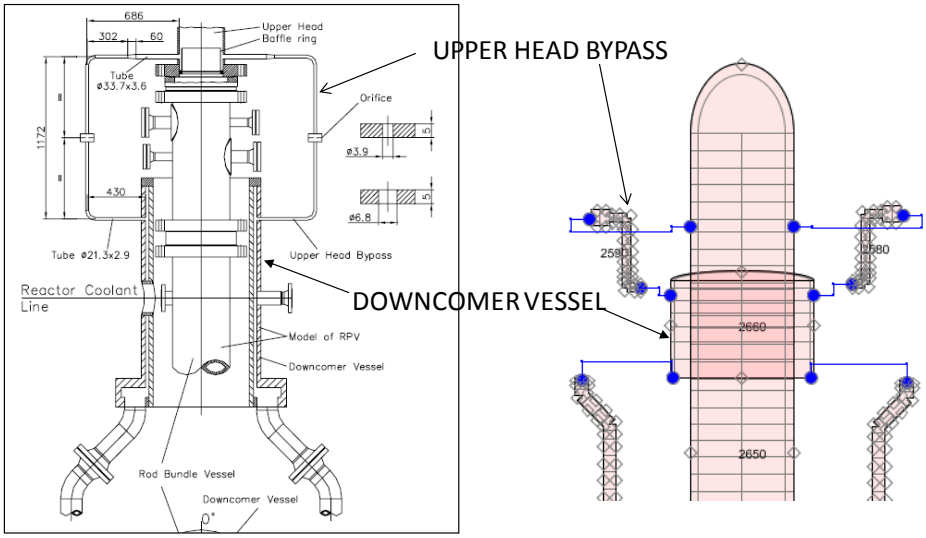

Figure 185 – TRACE nodalization: DC vessel and DC-UH bypass

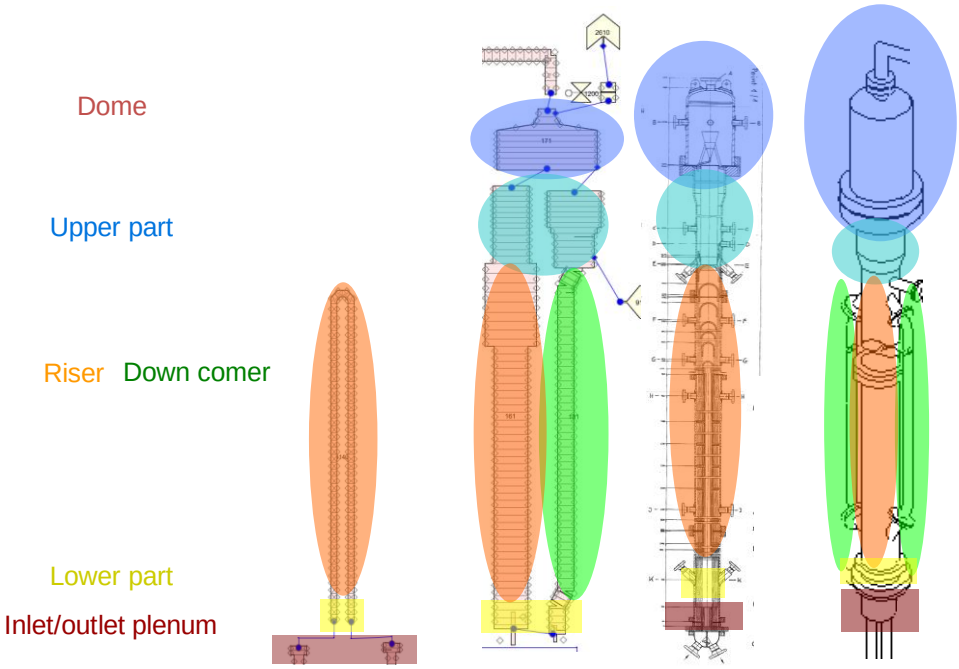

Figure 186 – TRACE nodalization: SG secondary side

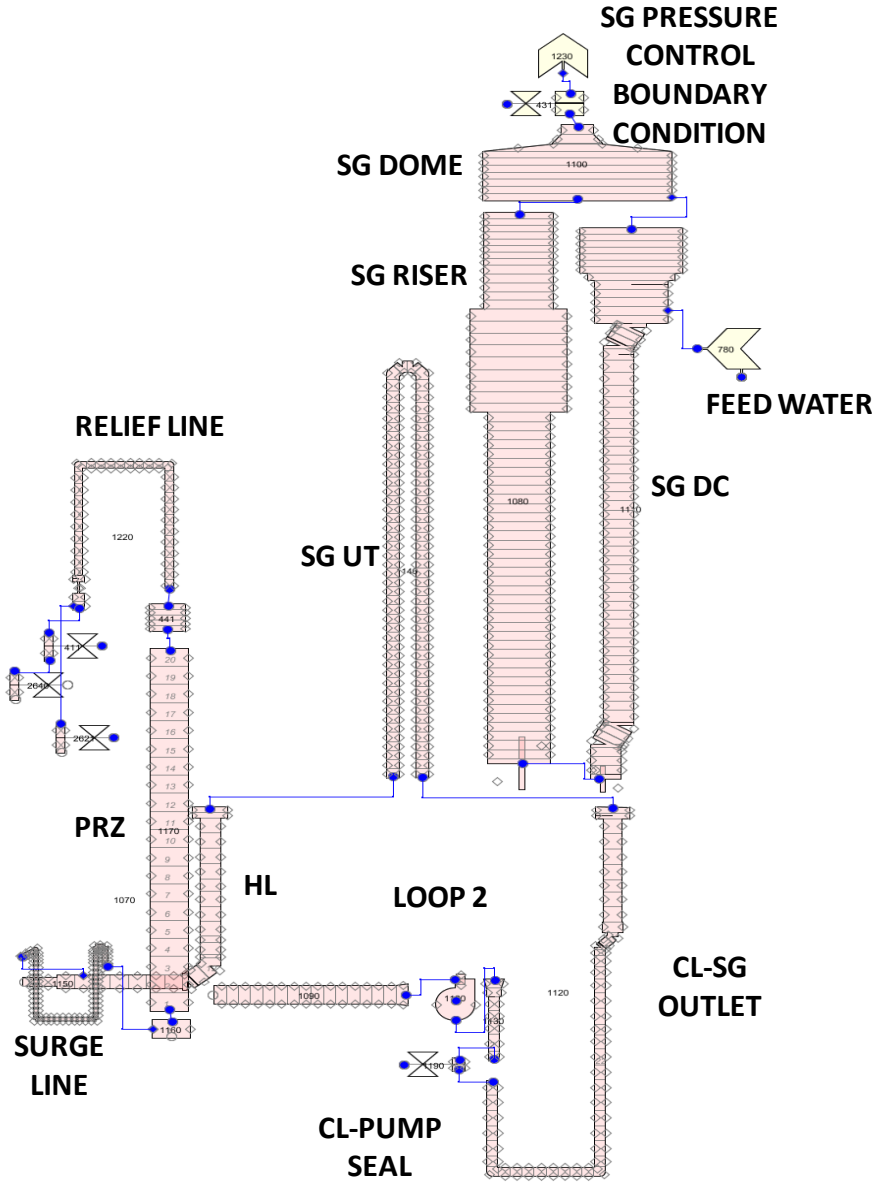

Figure 187 – TRACE nodalization: loop 2, SG 2 primary and secondary side, PRZ system

B.2. Verification of the volumes in the nodalization

The assessment of the individual volumes is a pre-requisite for the validation of the nodalization at the steady state level as well for the interpretation of code results with regard to energy and mass balances.

The individual volumes of the PKL nodalization were calculated and entered as a function of liquid level and compared with the experimental ones (see [B-1]). In Figure 188 to Figure 195 the volume distribution as function of the elevation in each zone of the primary and secondary hydraulic circuits are shown, whilst the individual volumes of all vessels and piping which are part of the RCS were calculated and collated in Table 46.

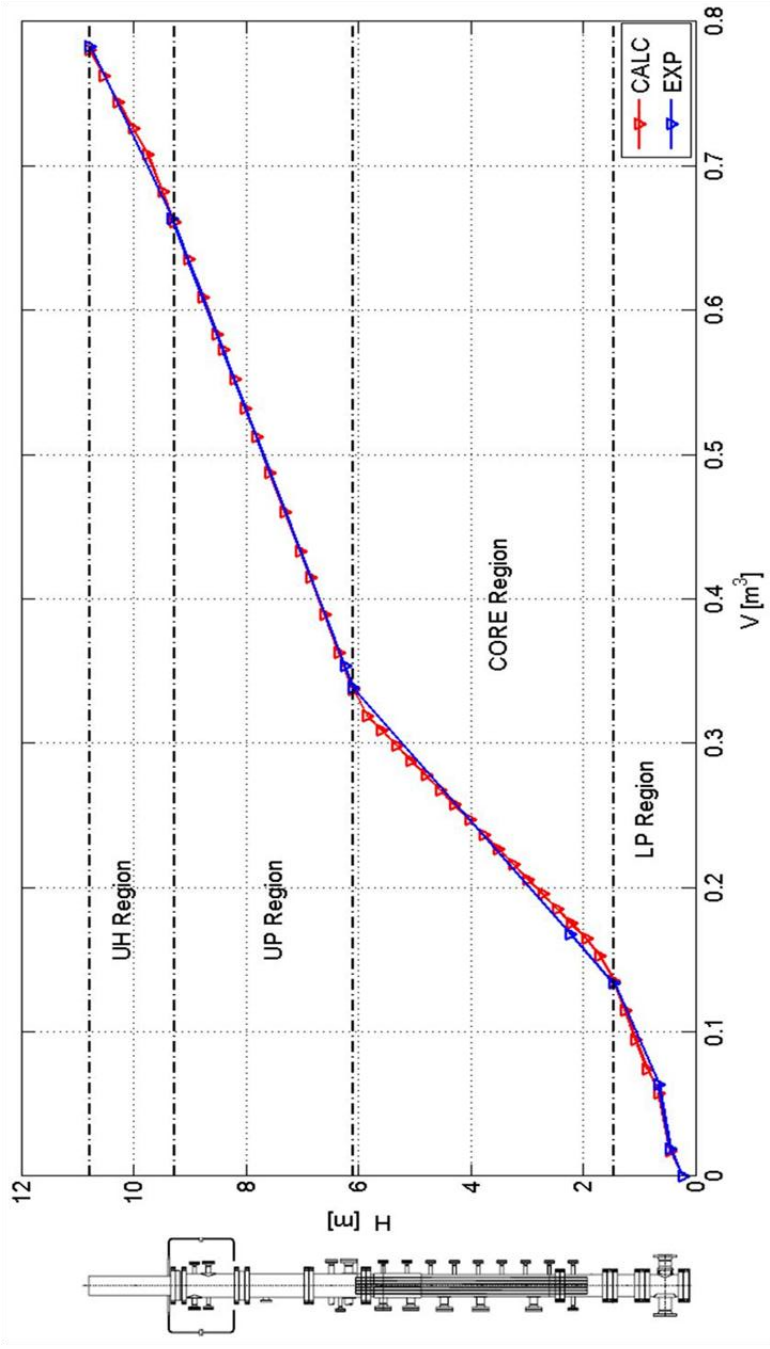

Figure 188 – Volume vs Elevation: Rod Bundle Vessel (without Reflector Gap)

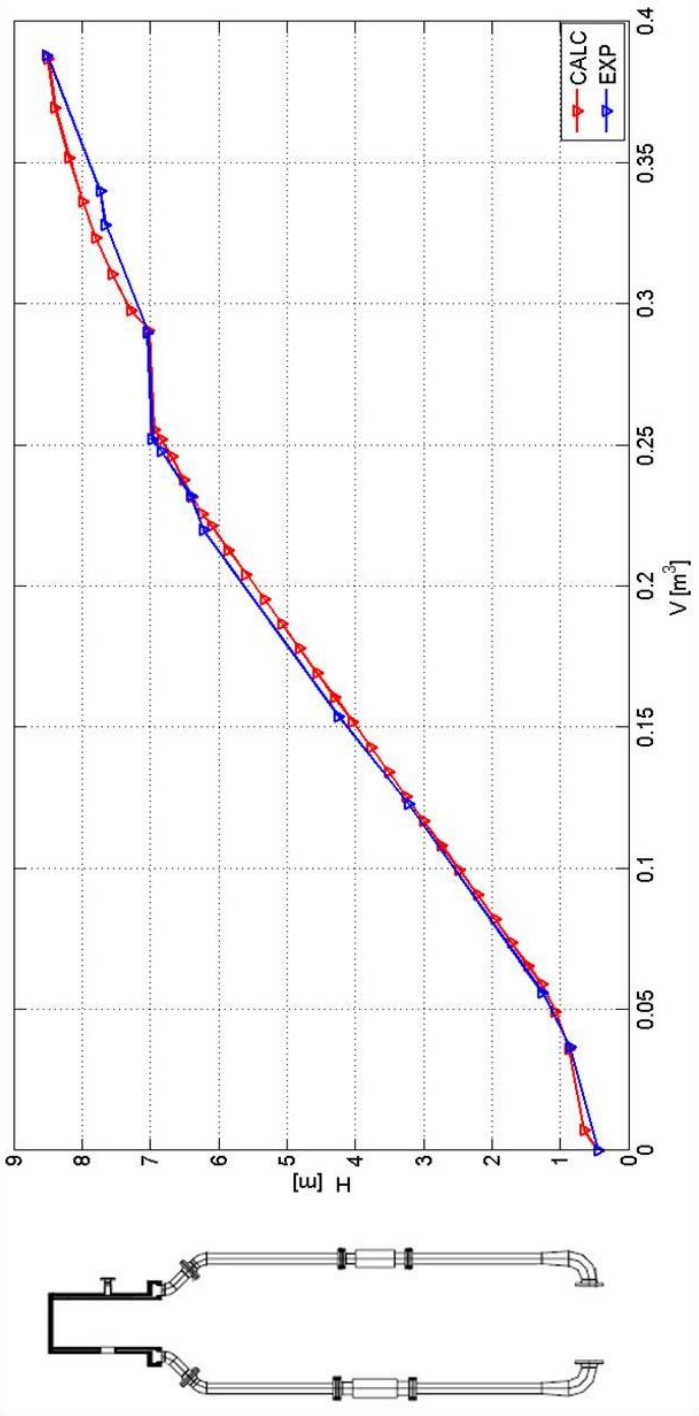

Figure 189 – Volume vs Elevation: RPV Downcomer

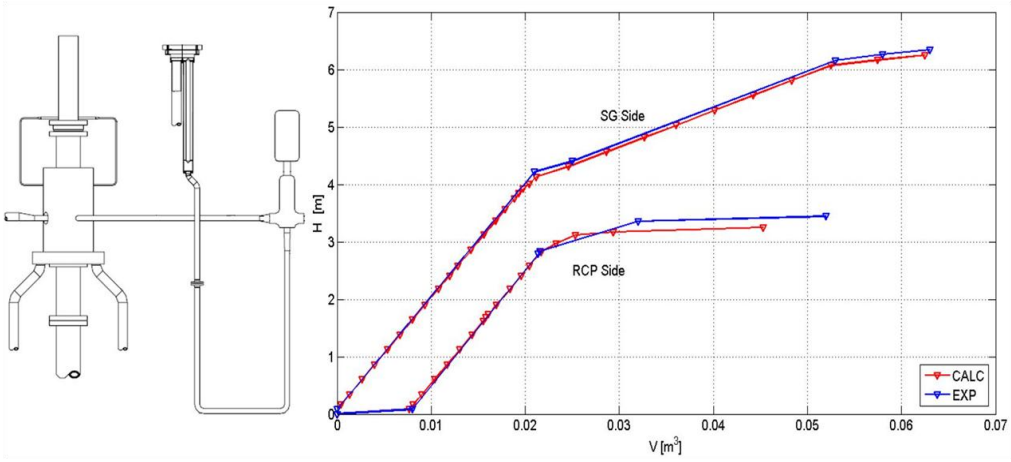

Figure 190 – Volume vs Elevation: Loop 1 (SG Outlet, Pump Seal, Reactor Coolant Pump, Cold Leg Horizontal Section)

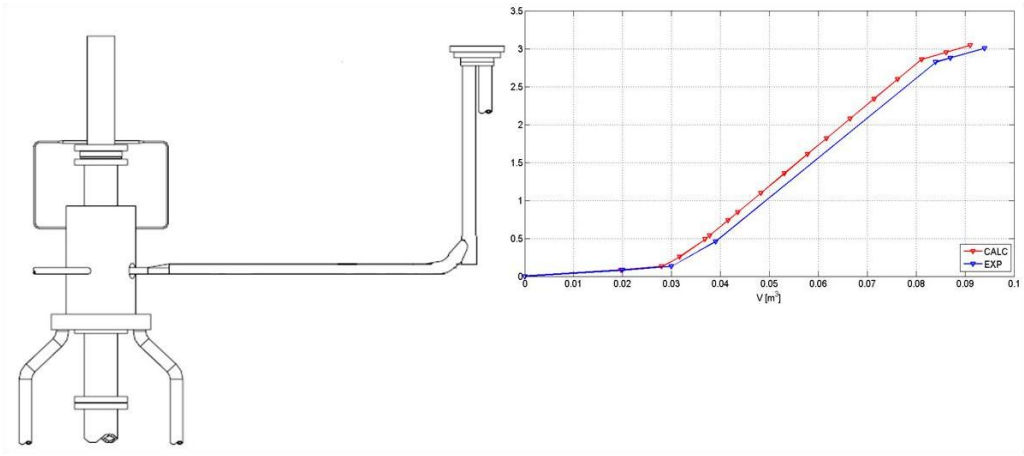

Figure 191 – Volume vs Elevation: hot leg and SG inlet (Loop 1)

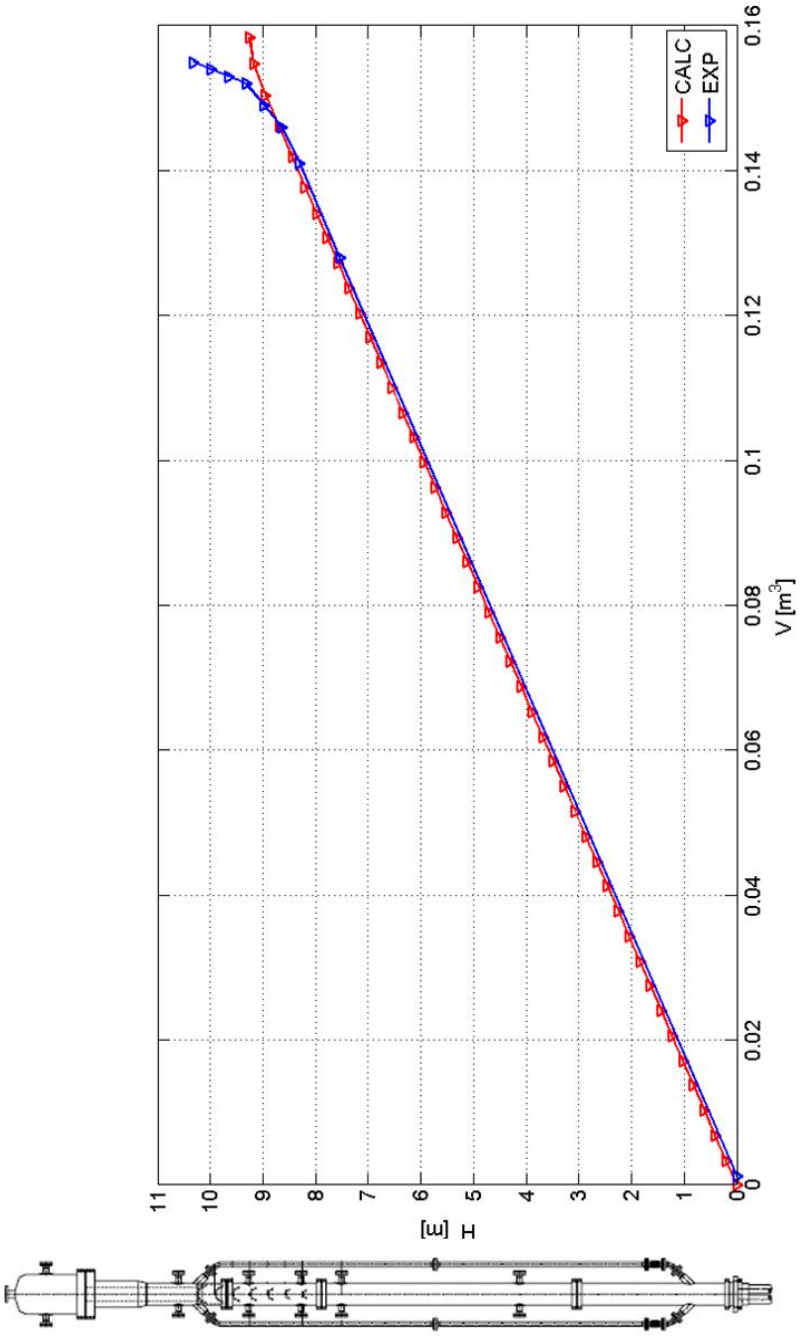

Figure 192 – Volume vs Elevation: Steam Generator primary side (Loop 1)

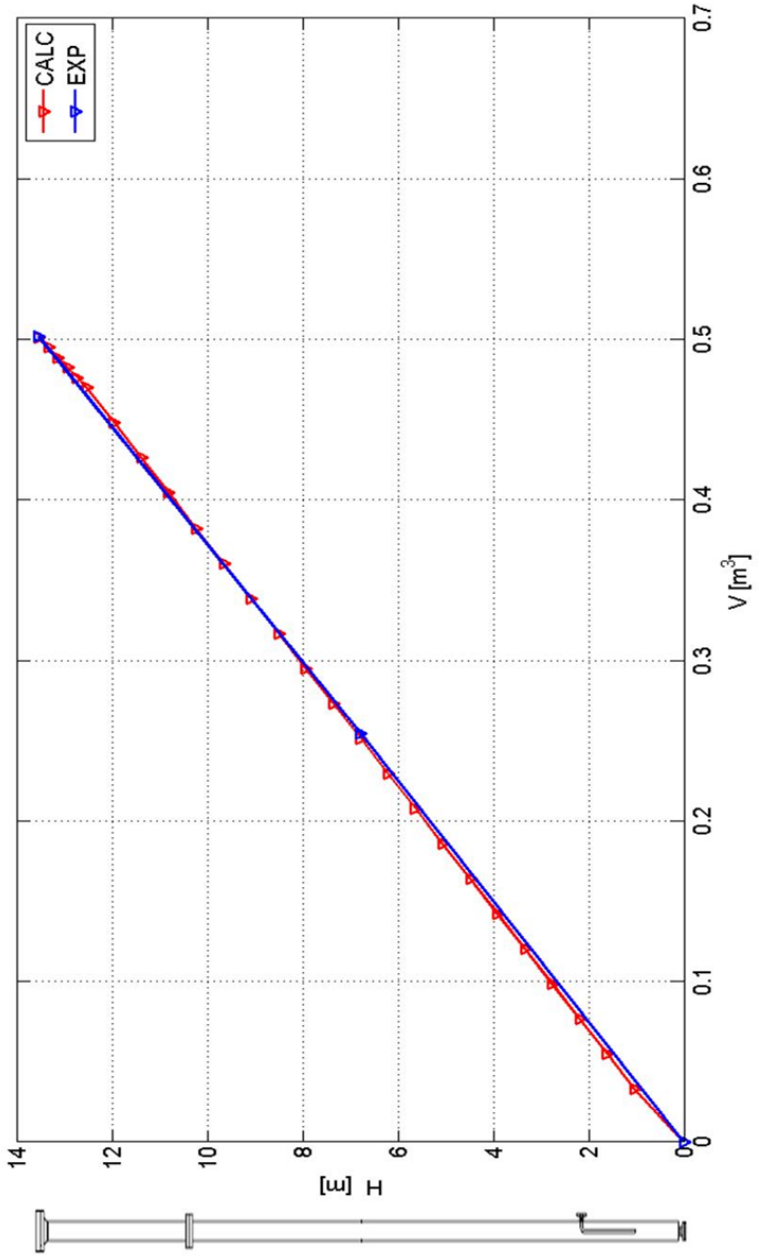

Figure 193 – Volume vs Elevation: Pressurizer

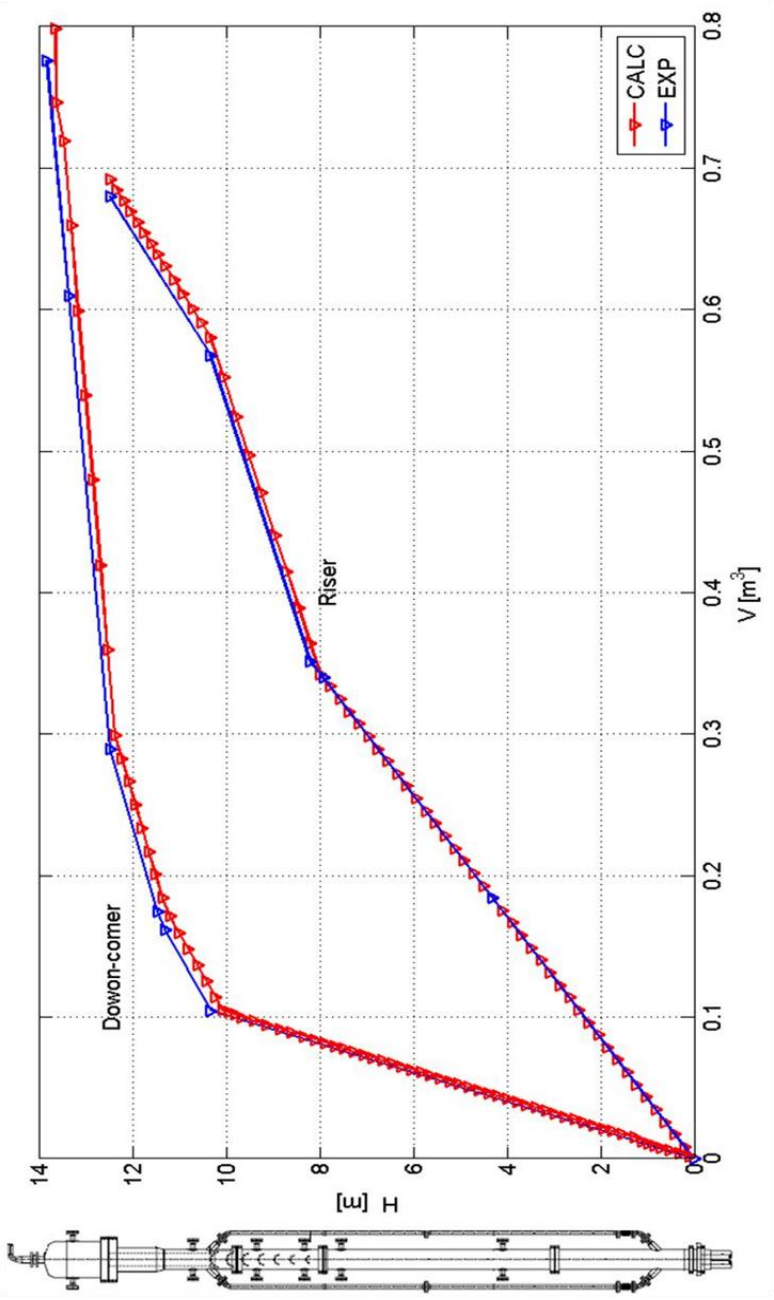

Figure 194 – Volume vs Elevation: Steam Generator Secondary Side

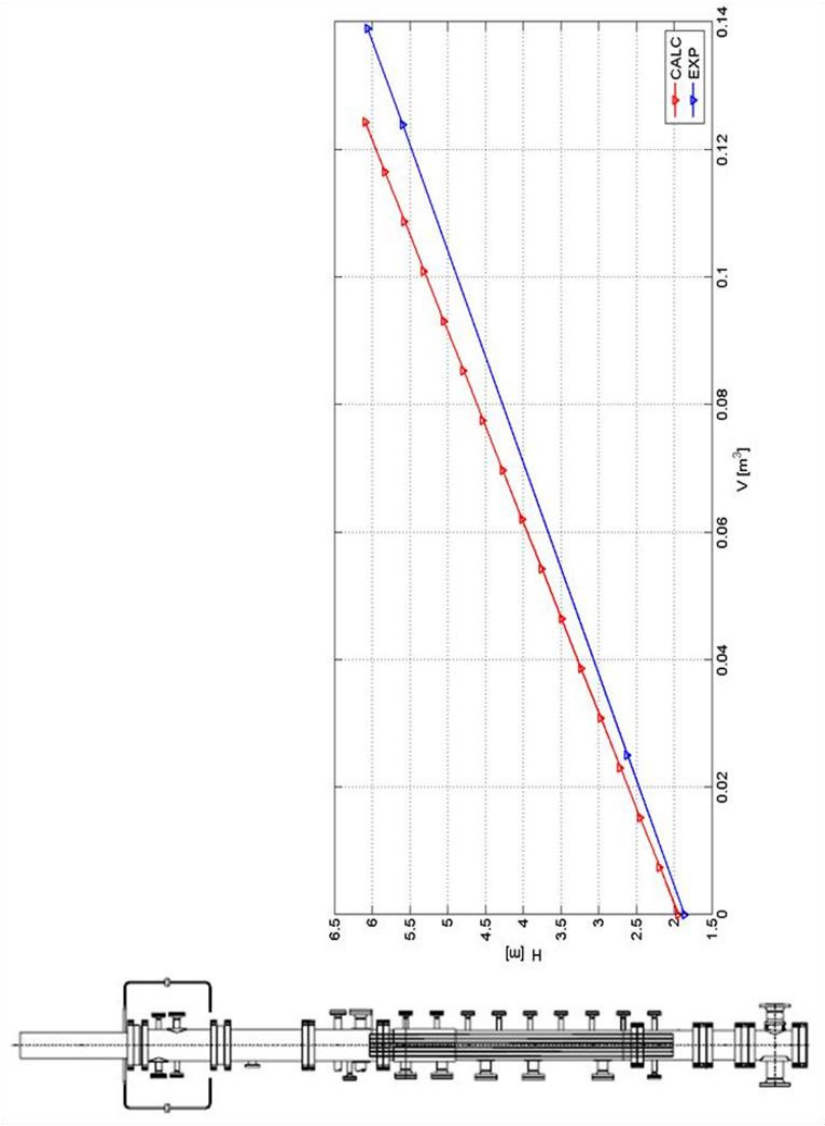

Figure 195 – Volume vs Elevation: Reflector Gap

Table 45 – Nodalization development

1	ADOPTED CODE RESOURCES	
1-1	Total number of hydraulic components primary side	65
1-2	Total number of hydraulic components secondary side (1 SG only vessel)	20
1-3	Total number of hydraulic components	85
1-4	Total number of hydraulic nodes (meshes) primary side	1836
1-5	Total number of hydraulic nodes secondary side (1 SG only vessel)	136
1-6	Total number of hydraulic nodes (meshes)	2380
1-7	Total number of heat structures	258
1-8	Total number of mesh points in the heat structures	--
1-9	Total number of core active structures	6
1-10	Total number of core radial meshes in the active structures	60
2	**NODALIZATION FEATURES**	
2-1	Number of modeled loops	4
2-2	Number of DC tubes modeled	2
2-3	Number of volumes modeling the DC annular region	84
2-4	Number of U-tubes per SG	1
2-5	Number of axial meshes of each SG U-tubes (only one SG)	95
2-6	Length of each SG U-tubes (only one SG), [m]	18.452
2-7	Core model (3-D or 1-D component)	3-D
2-8	N. of hydraulic channels in core region (ring and angular sectors for 3D components)	2-rings 6-angular sectors

Table 46 – Characteristic of the nodalization geometry

#	QUANTITY(*)	UNIT	CALC
1	**PRIMARY CIRCUIT VOLUME**		
1-1	DC (Annular)	m^3	0.0962
1-2	DC (Pipes)	m^3	0.1375
1-3	Lower plenum	m^3	0.148
1-4	Core region	m^3	0.208
1-5	Core bypass	m^3	0.139
1-6	Upper plenum	m^3	0.344
1-7	Upper head	m^3	0.130
1-8	Upper head bypass	m^3	0.0041
1-9	Total vessel	m^3	0.968
1-10	Hot leg (only one loop)	m^3	0.0811
1-11	SG inlet plenum (only one loop)	m^3	0.01
1-12	SG U-tubes (only one loop)	m^3	0.1583
1-13	SG outlet plenum (only one loop)	m^3	0.01
1-14	Loop seal (only one loop)	m^3	0.0187
1-15	MCP (only one loop)	m^3	0.003674
1-16	Cold leg (only one loop)	m^3	0.014685
1-17	Surge line	m^3	0.014209
1-18	PRZ	m^3	0.508123
1-19	Total primary circuit	m^3	3.15271
2	**SECONDARY CIRCUIT VOLUME**		
2-1	FW pipes (only one SG)	m^3	--
2-2	SG DC (only one SG)	m^3	0.29961
2-3	SG riser (only one SG)	m^3	0.692603
2-4	SG dome (only one SG)	m^3	0.516949
2-5	SG steam line (only one SG)	m^3	0.063124
2-6	SG vessel secondary circuit volume (all 4 SGs)	m^3	6.099771
3	**ACTIVE STRUCTURES HEAT TRANSFER AREA (OVERALL)**		
3-1	Core heat structures surface area (total)	m^2	49.2046
3-2	SG U-tubes heat structures external surface area (only one SG)	m^2	36.7933
4	**ACTIVE STRUCTURES HEAT TRANSFER VOLUME (OVERALL)**		
4-1	Core heat structures volume	m^3	0.1322
4-2	SG U-tubes heat structures volume (only one SG)	m^3	0.04372
5	**NON - ACTIVE STRUCTURES HEAT TRANSFER VOLUME (OVERALL)**		
5-1	Total volume of the metallic structures in the vessel (excluding the fuel rod simulator bundle)	m^3	--
5-2	Total volume of the metallic structures in one RCS loop (excluding the SG U-tubes)	m^3	--

5-3	Total volume of the metallic structures in SG vessel (excluding the SG U-tubes)	m^3	--
6	**COMPONENT RELATIVE ELEVATION (WITH REFERENCE TO HLs)**		
6-1	RPV bottom	m	-7.6907
6-2	DC pipe connection bottom	m	-7.1487
6-3	Core active region bottom - BAF	m	-6
6-4	Core active region top- TAF	m	-1.8507
6-5	DC pipe connection top	m	-0.7812
6-6	UH – DC bypass connection bottom	m	0.613
6-7	UH – DC bypass connection top	m	1.6895
6-8	RPV top	m	3.0943
6-9	SG U-tubes inlet / outlet	m	2.9618
6-10	Loop seals horizontal part bottom	m	-3.2098
6-11	MCP (center)	m	-0.1035
6-12	PRZ bottom	m	-0.3432

B.3 References to APPENDIX B

[B-1] Güneysu, R., "*Determination of Individual Volumes and of Total Volume in the PKL Test Facility",* Technical Report, NTCTP-G/2007/en/0011 AREVA NP GmbH, December 2007.

APPENDIX C. ASSESSMENT OF PRESSURE DROPS OF PKL NODALIZATION

C.1. Verification and set up of the pressure drops

The relevance of the pressure losses in the primary circuit and their connection in the qualification process of the nodalization set up plays an important role.

The availability of a new set of experimental data [C-1], related to the determination of the pressure drops in the PKL-III facility has allowed the assessment of the reference input deck.

The data acquired during the characterization tests (dealing with the pressure drop) provides detailed information for very low mass flow rate up to normal RCP operation in the facility (the range of the data available is from 0.8 to 25 kg/s per loop). These data were issued by the experimentalists of AREVA NP GmbH performing three experiments executed at PKL-III facility:

- **PKL III F 2.1 DRUV 1**: (*low range test run*) mass flows from 0,8 up to 3,2 kg/s , butterfly valve BV (covered by MST 198) closed to simulate frictional resistance of RCP at standstill;
- **PKL III F 2.1 DRUV 2**: (*wide range test run*) mass flows from 5 up to 25 kg/s, butterfly valve BV (covered by MST 198) opened, for minimal frictional resistance;
- **PKL III F 2.1 DRUV 3**: (*wide range test run*) mass flows from 5.0 and 7.5 kg/s, only recording RPV total and core section head losses.

The third run was executed for acquiring additional data in the range 5.0 and 7.5 kg/s per loop, which were not satisfactory recorded during the second test.

Only the test DRUV 1 is simulated using TRACE-V5 code. The boundary conditions and time sequence of the events is reported in Table 47. The pressure drop coefficients of the input deck are adjusted in order to improve the agreement with the experimental data. The results of the simulation are summarized from Figure XX to Figure XX.

Two types of figures are presented for the comparisons with the experimental data.

- Form Figure XX to Figure XX the plots of the pressure drop versus the squared mass flow are reported for the different zones of the PKL-III facility. In each figure the measured data, provided in Ref.2 and 4 are compared with the results of the reference nodalization prepared for the simulation of the test PKL III test F4.1.
- Form Figure XX to Figure XX, the plots of the pressure drop versus length are reported at different mass flow rates. In each figure, the values of the pressure drops along the RPV and RCS are plotted and compared with the experimental data, for a specific mass flow rate. This type of figure

addresses the global characteristics of the nodalization from the pressure drop point of view.

The analysis of the experimental data, as well as, the verification and the set up of the nodalization from the pressure drop point of view let to carry out the statements hereafter outlined.

- The experimental data available in [C-1] for the liquid phase, are exhaustive for the different zones of the facility, with an adequate level of detail. Moreover they cover all the relevant mass flow rates.
- In the MCP zone, the first two calculated values of the pressure drop (0.8 and 1.2kg/s) in Figure 200 are not reliable, as it is demonstrated by the fact that the sum of the pressure drop in the loop does not correspond. This is caused by the MCP characteristics, defined in the homologous curves with TRACE-V5, for rotation velocities corresponding at the very low velocities.
- The absolute pressure drops, due to the dynamic and friction terms, are obtained running the CATHARE 2 code and subtracting the term of gravity, as stated above.
- The comparison of the experimental data with the pressure drops calculated using the reference nodalization used in (ref. Eugenio F41) for the former assessment of the TRACE-V5 code against the boron transport experiment F4.1, provides results that can be considered roughly satisfactory with respect to the acceptable criteria for nodalization qualification.

Table 47 – PKL III facility nodalization qualification: Tests DRUV 1 2 boundary conditions and time sequence of the events

DRUV1				
Pressure	**9.4**	**[bar]**		
Temp.	**~ 18.3**	**[°C]**		
Step	**Mass flow rate [kg/s]**	**Time [s]**	**ABS time [s]**	**MCP speed [rpm]**
1	1.60	360	1370.0	289.1
2	2.00	410	1790.0	358.2
3	2.40	360	2160.0	427.2
4	2.80	400	2570.0	495.7
5	3.20	340	2920.0	563.7
6	3.60	500	3430.0	631.7
7	1.20	355	3795.0	219.2
8	0.80	390	4195.0	148.3
9	2.40	320	4525.0	427.2
10	3.20	320	4855.0	563.7

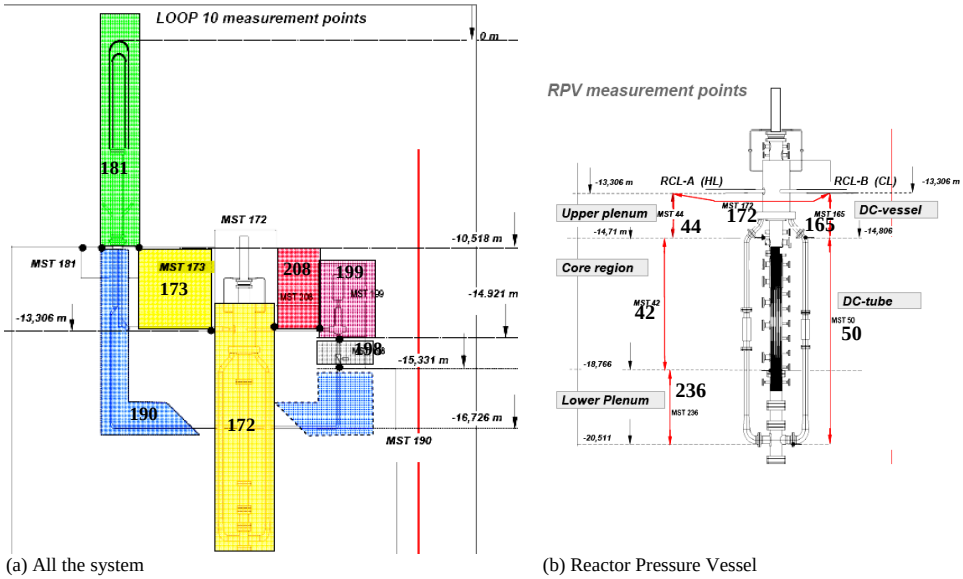

(a) All the system (b) Reactor Pressure Vessel

Figure 196 – Head losses measurement system sketch: identification of the zones

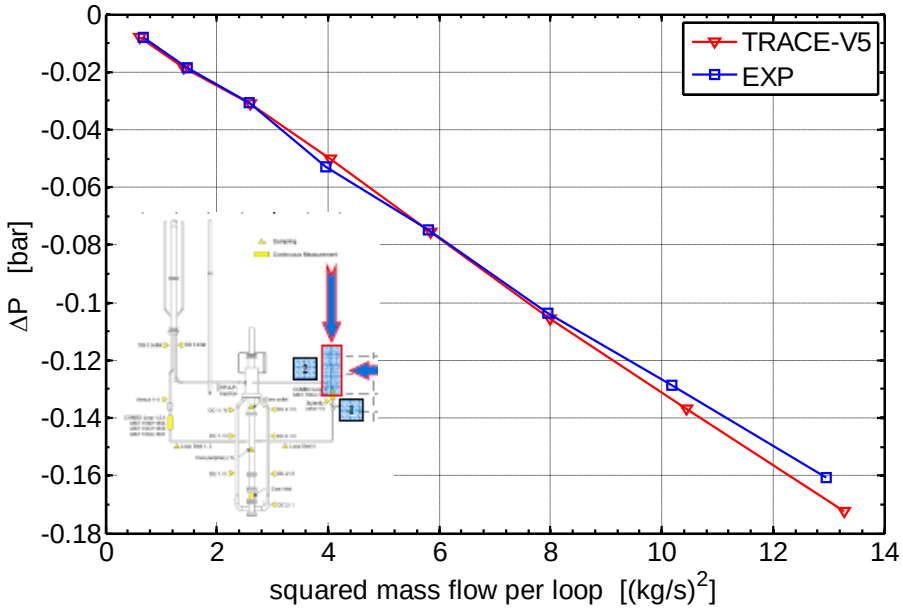

Figure 197 – PKL III facility nodalization qualification: low range, loop mass flow equal from 0.80 to 3.60 kg/s ΔP vs. squared mass flow: MCP zone (MST 199)

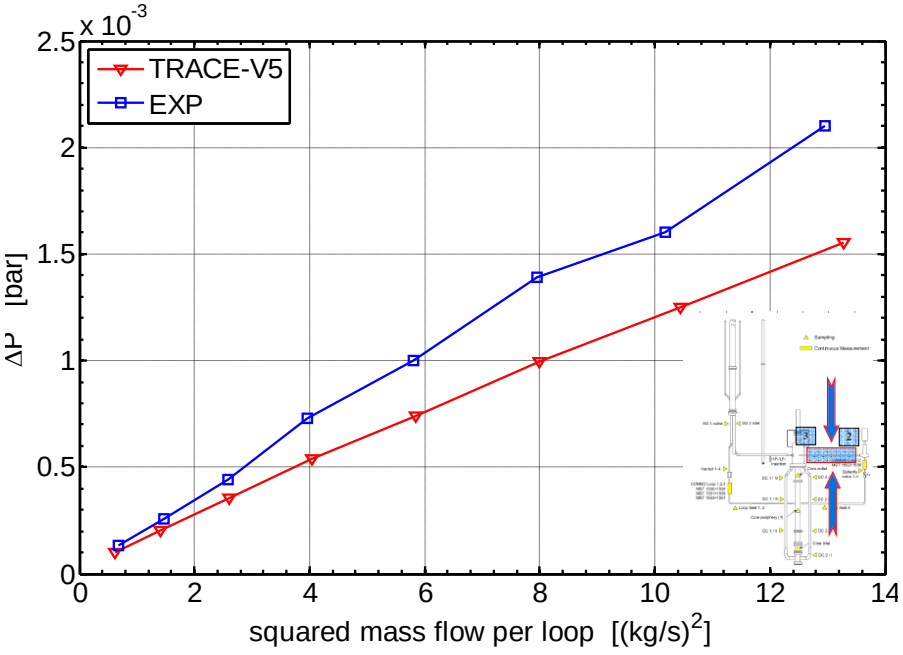

Figure 198 – PKL III facility nodalization qualification: low range, loop mass flow equal from 0.80 to 3.60 kg/s ΔP vs. squared mass flow: CL zone (MST 208)

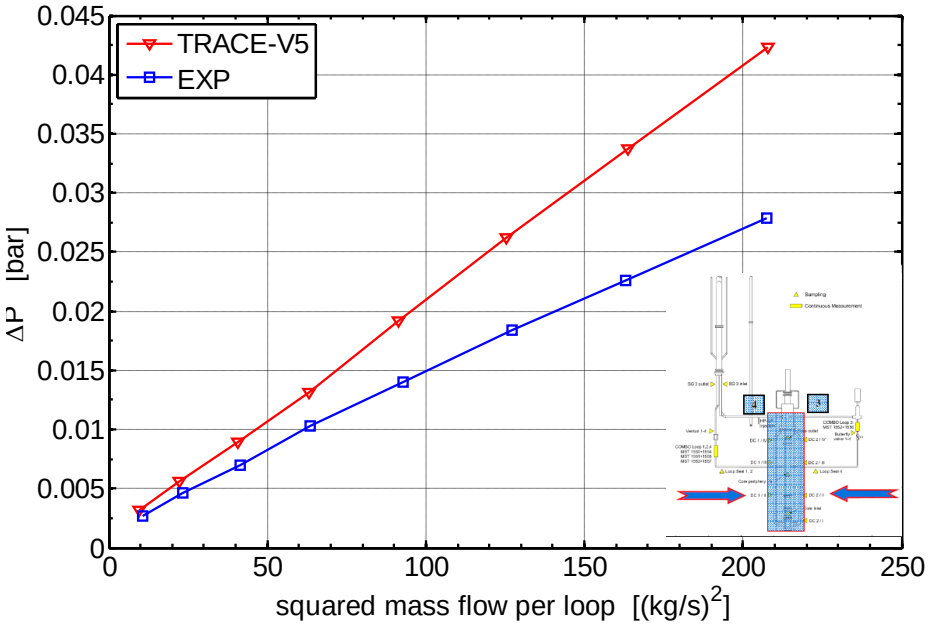

Figure 199 – PKL III facility nodalization qualification: low range, loop mass flow equal from 0.80 to 3.60 kg/s ΔP vs. squared mass flow: RPV zone (MST 172)

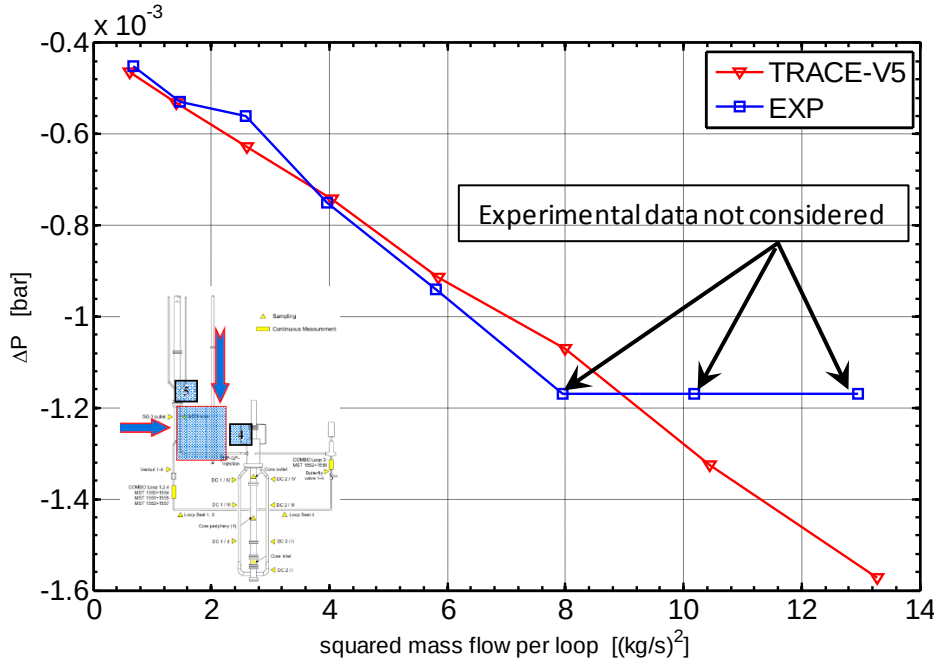

Figure 200 – PKL III facility nodalization qualification: low range, loop mass flow equal from 0.80 to 3.60 kg/s ΔP vs. squared mass flow: HL zone (MST 173)

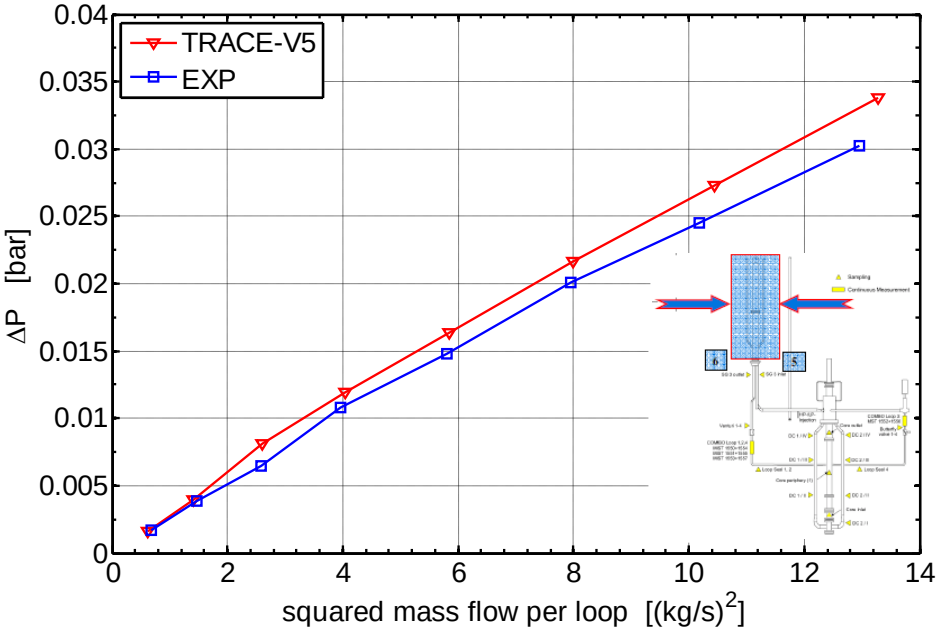

Figure 201 – PKL III facility nodalization qualification: low range, loop mass flow equal from 0.80 to 3.60 kg/s ΔP vs. squared mass flow: SG UT zone (MST 181)

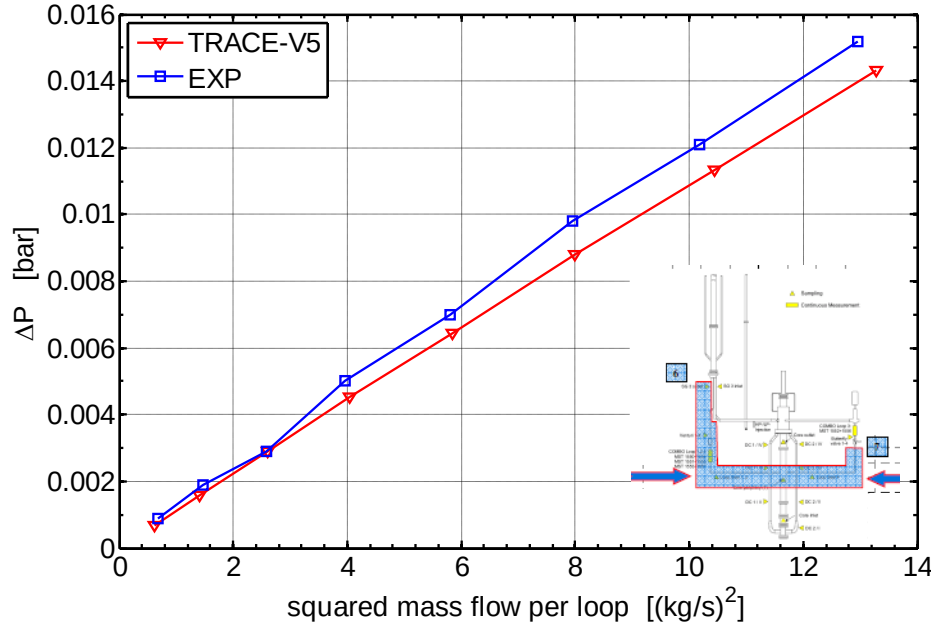

Figure 202 – PKL III facility nodalization qualification: low range, loop mass flow equal from 0.80 to 3.60 kg/s ΔP vs. squared mass flow: LS zone (MST 190)

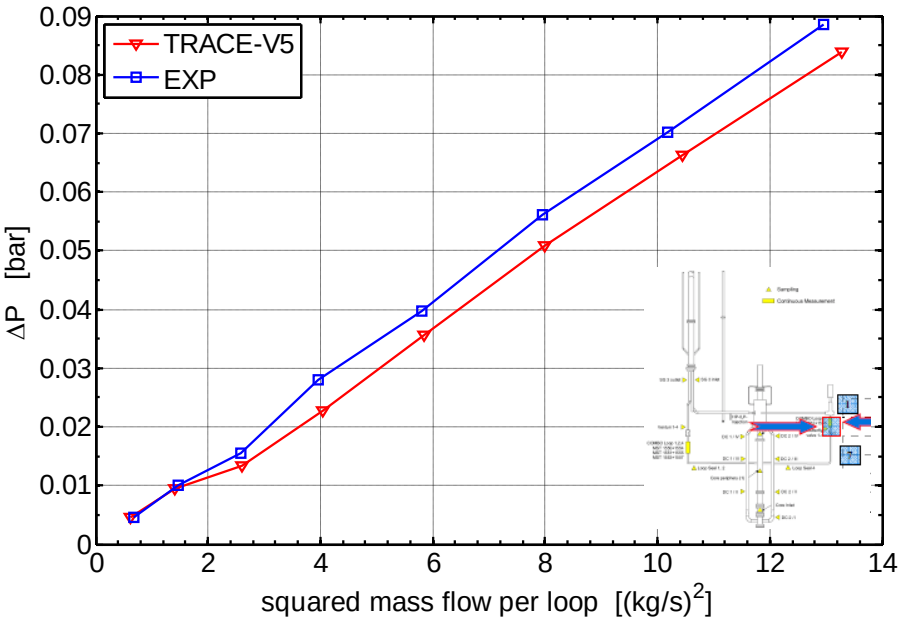

Figure 203 – PKL III facility nodalization qualification: low range, loop mass flow equal from 0.80 to 3.60 kg/s ΔP vs. squared mass flow: BV zone (MST 198)

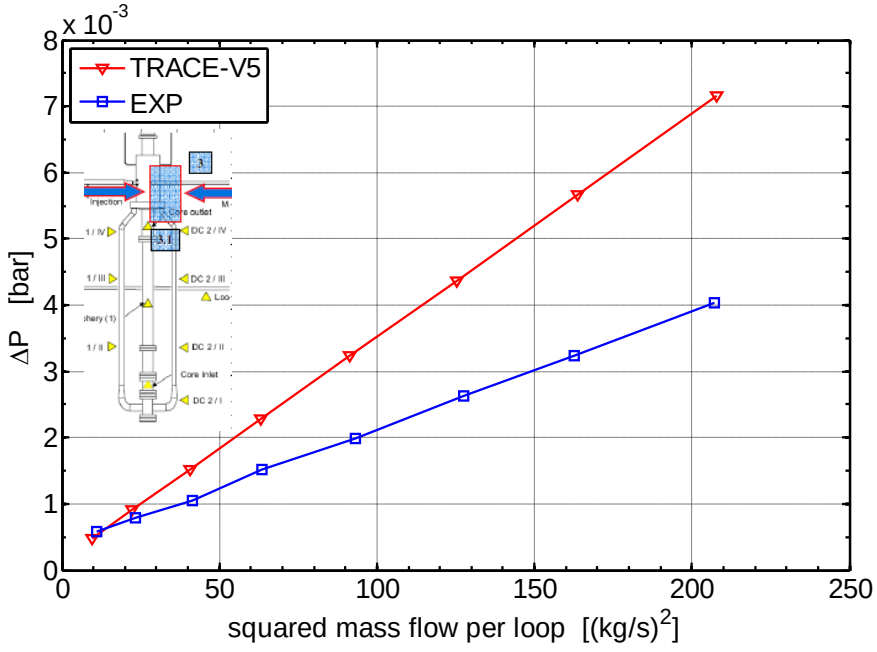

Figure 204 – PKL III facility nodalization qualification: low range, loop mass flow equal from 0.80 to 3.60 kg/s ΔP vs. squared mass flow: DC vessel (MST 165)

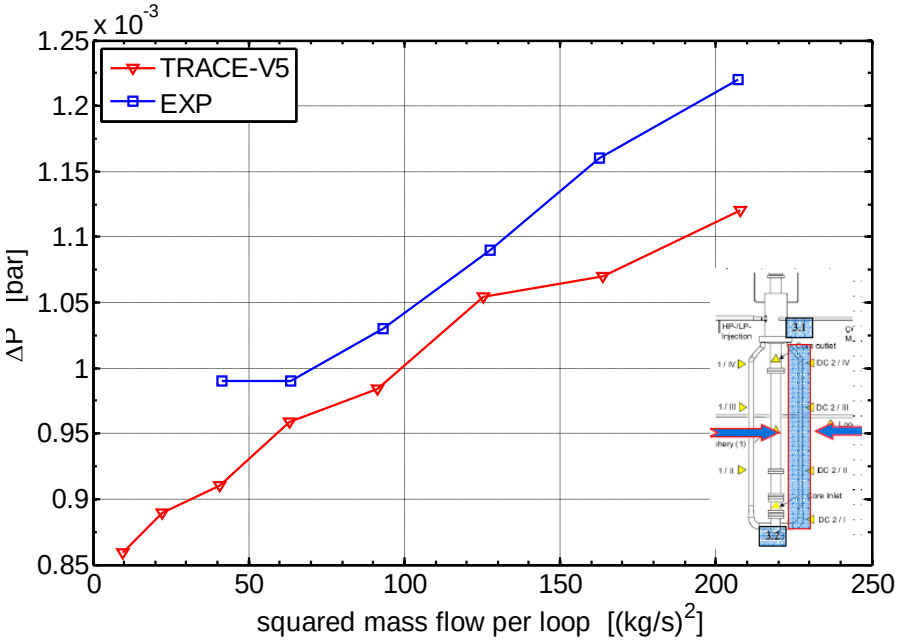

Figure 205 – PKL III facility nodalization qualification: low range, loop mass flow equal from 0.80 to 3.60 kg/s ΔP vs. squared mass flow: DC tube (MST 50)

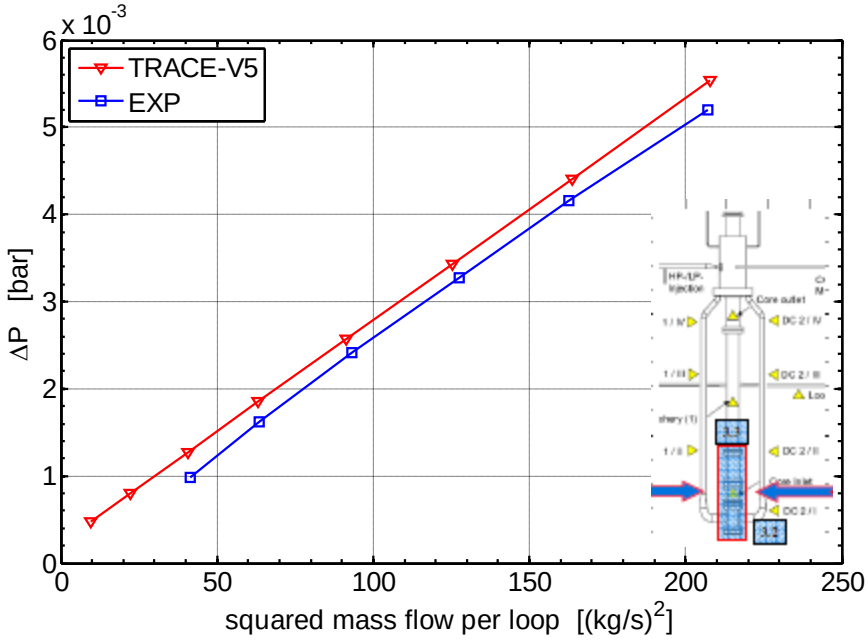

Figure 206 – PKL III facility nodalization qualification: low range, loop mass flow equal from 0.80 to 3.60 kg/s ΔP vs. squared mass flow: LP zone (MST 236)

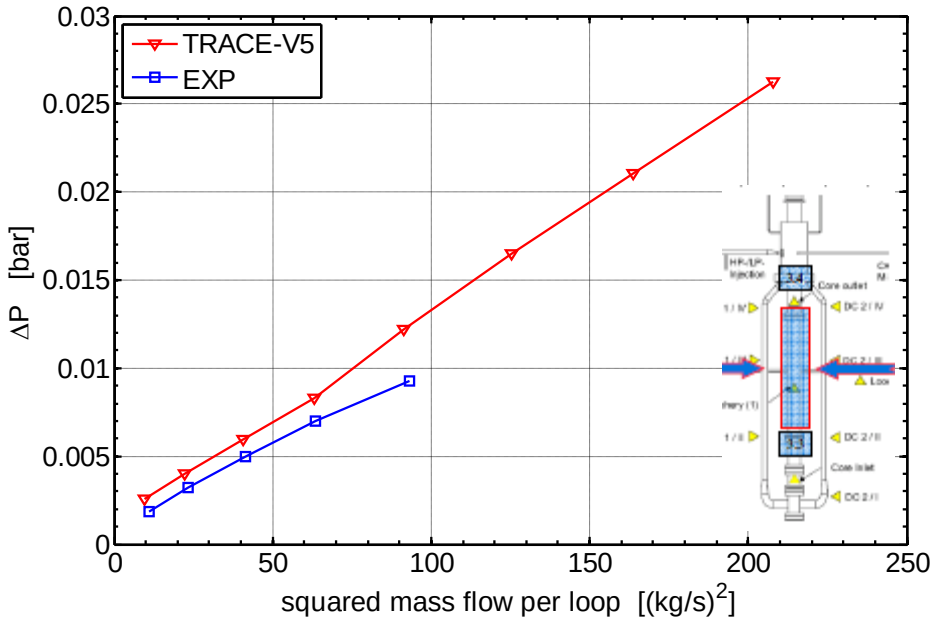

Figure 207 – PKL III facility nodalization qualification: low range, loop mass flow equal from 0.80 to 3.60 kg/s ΔP vs. squared mass flow: core zone (MST 42)

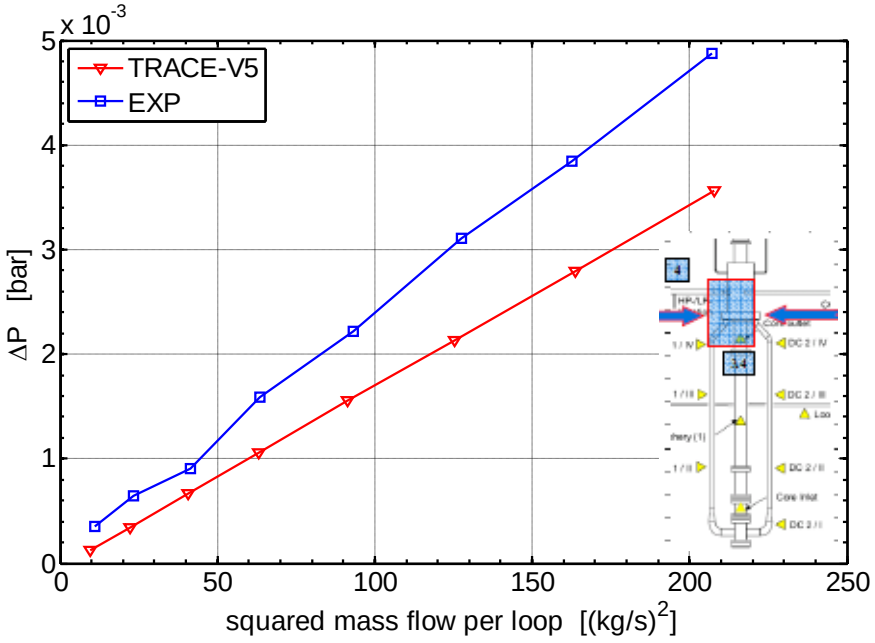

Figure 208 – PKL III facility nodalization qualification: low range, loop mass flow equal from 5.00 to 25.02 kg/s ΔP vs. squared mass flow: UP zone (MST 44)

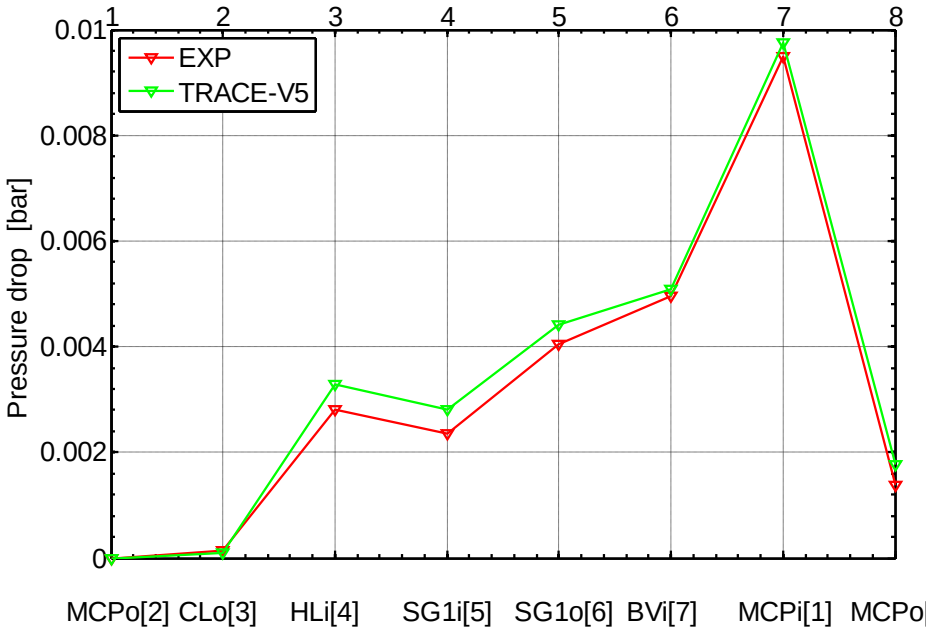

Figure 209 – PKL III facility nodalization qualification: ΔP vs length curve, Loop mass flow equal to 0.80 kg/s

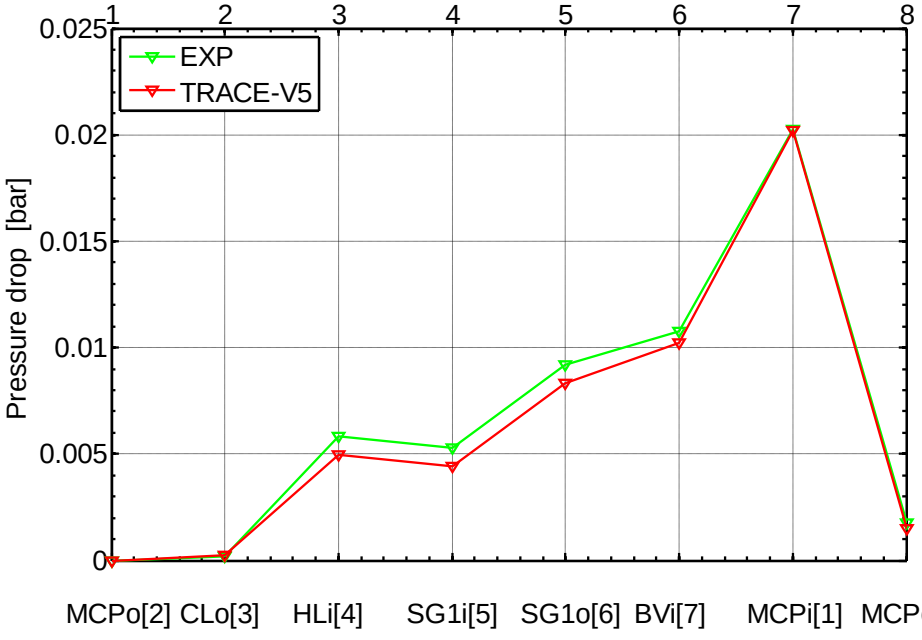

Figure 210 – PKL III facility nodalization qualification: ΔP vs length curve, Loop mass flow equal to 1.20 kg/s

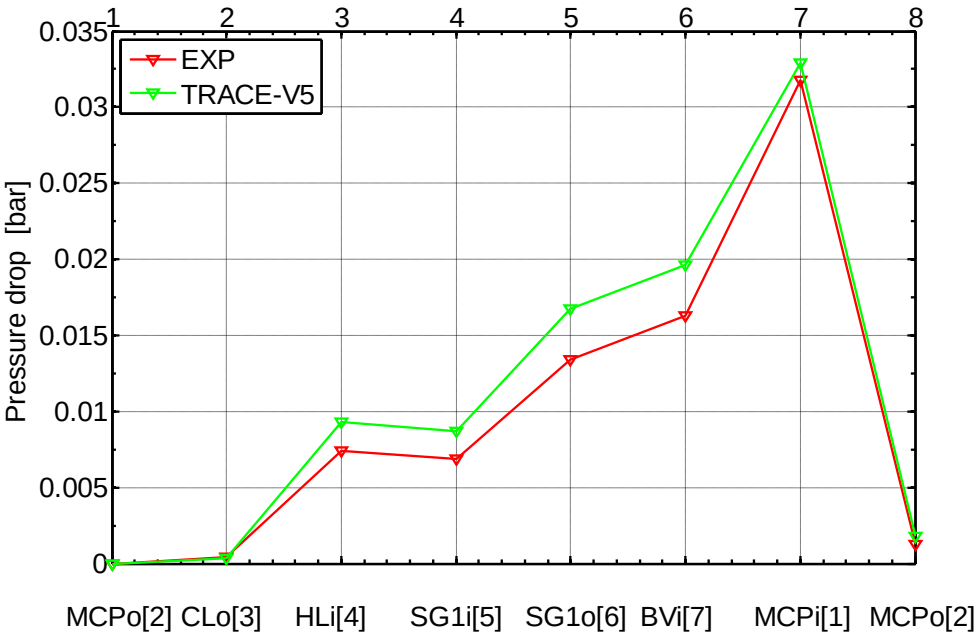

Figure 211 – PKL III facility nodalization qualification: ΔP vs length curve, Loop mass flow equal to 1.60 kg/s

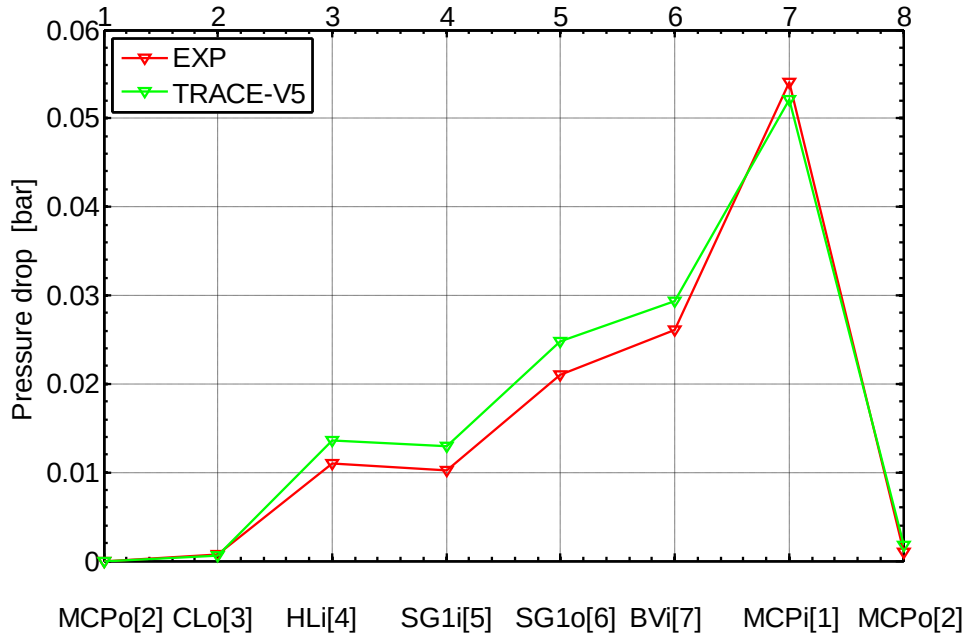

Figure 212 – PKL III facility nodalization qualification: ΔP vs length curve, Loop mass flow equal to 2.00 kg/s

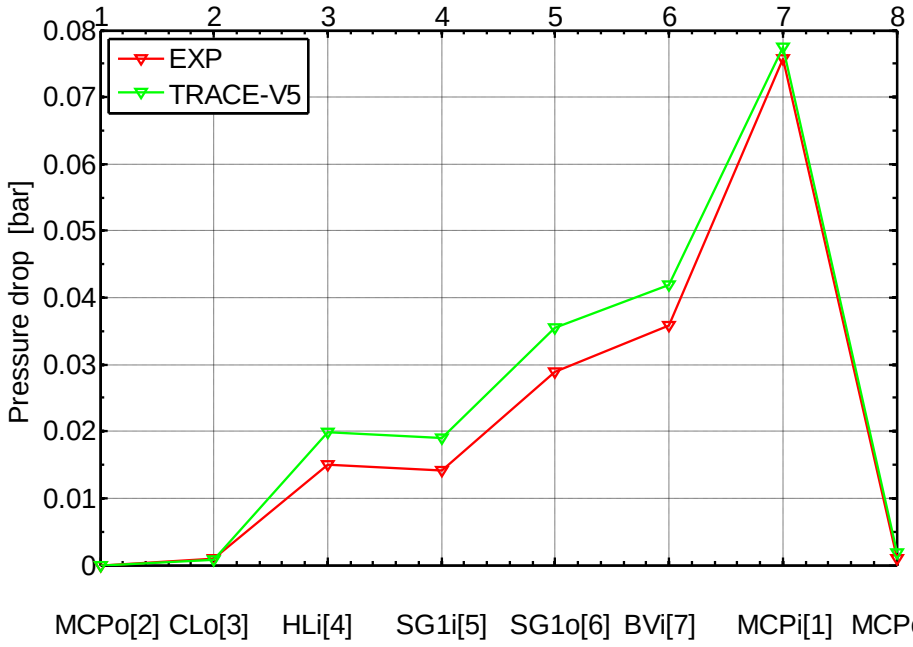

Figure 213 – PKL III facility nodalization qualification: ΔP vs length curve, Loop mass flow equal to 2.40 kg/s

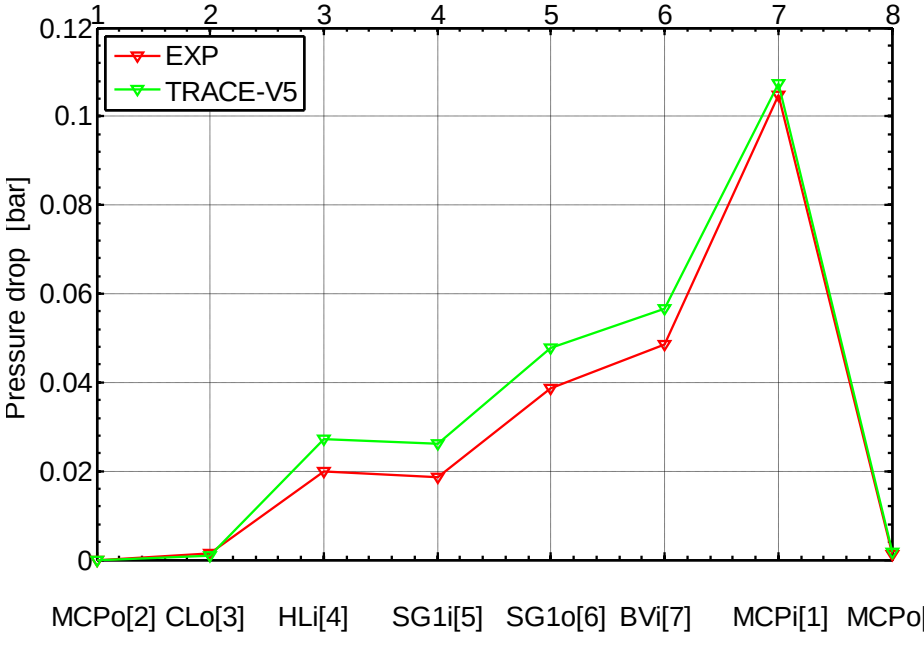

Figure 214 – PKL III facility nodalization qualification: ΔP vs length curve, Loop mass flow equal to 2.80 kg/s

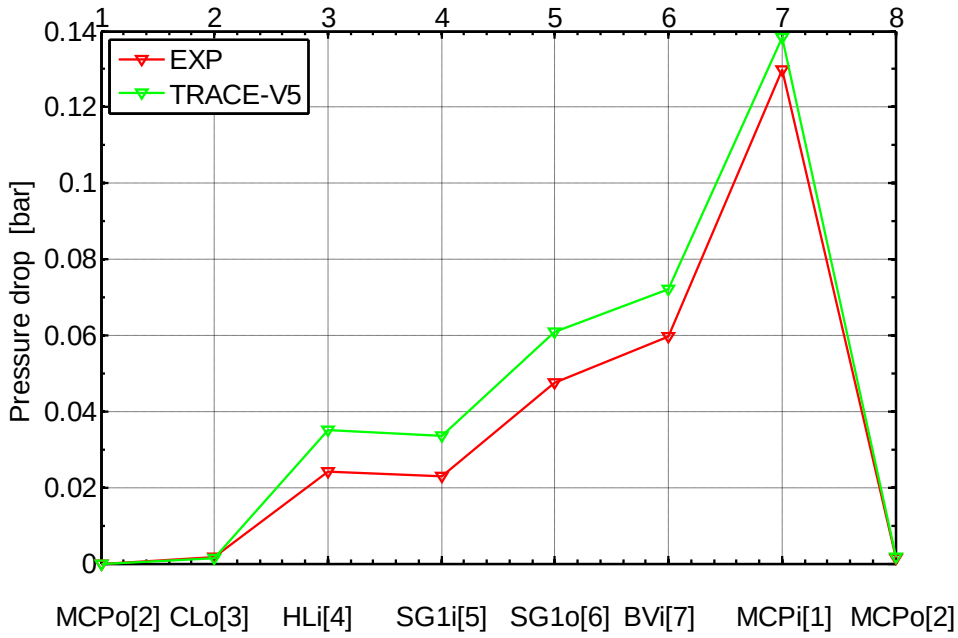

Figure 215 – PKL III facility nodalization qualification: ΔP vs length curve, Loop mass flow equal to 3.20 kg/s

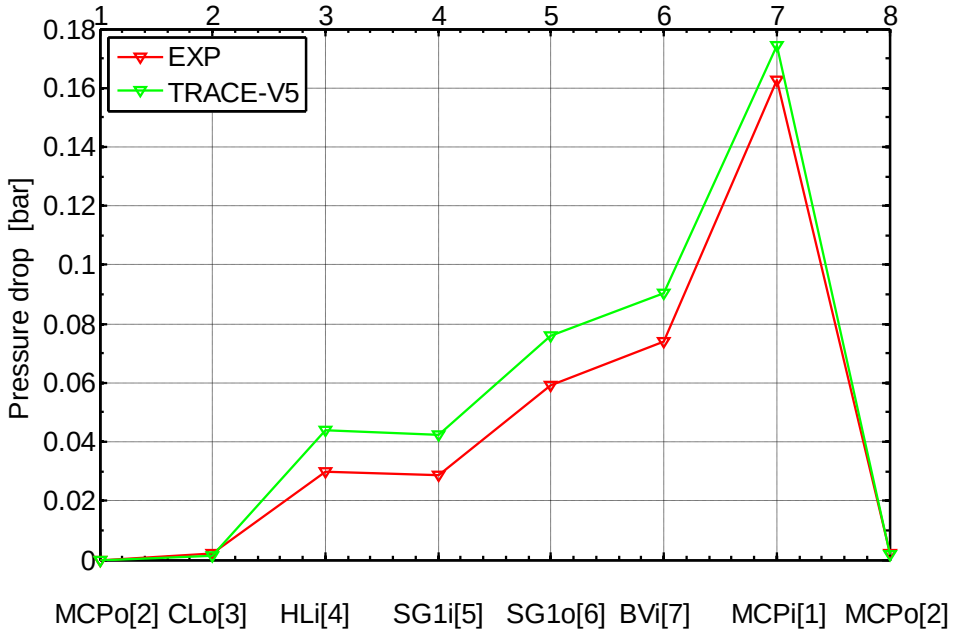

Figure 216 – PKL III facility nodalization qualification: ΔP vs length curve, Loop mass flow equal to 3.60 kg/s

C.2. References to APPENDIX C

[C-1] Schollenberger S. P., *"Determination of the Pressure Losses in the PKL-III Test Facility"*, Technical Report, NTT1-G/2006/en/0066 AREVA NP GmbH, December 2006.

APPENDIX D. DESCRIPTION OF THE ROCOM TRACE NODALIZATION

The general approach followed in setting up the ROCOM nodalization is to make a model suitable to reproduce the facility with a high level of detail and focused on the replication of the vessel. The considered experiments focus on the mixing phenomena occurring inside the reactor vessel and the thermal stratification in the cold legs, then, the related TRACE-V5 model has been set up with the aim to simulate only the flow patters inside the RPV, whereas no attention is paid to the flow phenomena in the other parts of the Reactor Coolant System (RCS) such as cold and hot legs, circulation pumps, and so on). the selected computational domain includes only the following parts of the ROCOM facility:

- downcomer, including 4 inlet nozzles;
- lower plenum
- core simulator;
- upper plenum.

The porous-medium concept is used in the simulation of the three dimensional flow into the RPV taking advantage of the features of the TRACE-V5 VESSEL component in cylindrical geometry. The implementation of the porous-medium approach allows modeling the flow path throughout a domain characterized by the presence flow obstacles such as tube bundle, perforated plate, shell or the shape of the LP.

The definition of the porosity is the ratio between the volume or surface occupied by the fluid and the volume or the surface of the mesh cell (see Equation () and ()). In other words the porosity gives the probability of the presence of fluid in the computational cell.

$$\varepsilon_v = \frac{volume\,occupied\,by\,the\;fluid}{volume\,of\;the\,mesh} = \frac{V_f}{V_m} \qquad ()$$

$$\varepsilon_s = \frac{surface\,occupied\,by\,the\;fluid}{surface\,of\;the\,mesh} = \frac{S_f}{S_m} \qquad ()$$

Only one VESSEL component has been used to model the fluid domain at the core inlet, into the downcomer, lower plenum and in the upper plenum of the ROCOM pressure vessel. The computational grid of 3-D module is composed 6 radial rings, 8 azimuthal sectors and 16 axial layers. The general TRACE-V5 scheme of the ROCOM facility is depicted in Figure 220 and Figure 220.

The LP region has been modeled taking in account both the hemispherical shape and the presence of the drum. To reproduce the fluid distribution inside the hemispherical region, the volume porosity has been considered as function of

radial and axial position (see Figure 217). In Table 49 are reported the value in the LP region of the porosity distribution.

The perforate DRUM is placed in the lower plenum of a KONVOI PWR in order to enhance the mixing in the lower plenum. As shown in Figure XX the perforate drum is cylindrical tube with the following dimension:

- external diameter = 0.58 m
- thickness = 0.008 m
- length = 0.191 m

420 holes, whose diameters are 0.015 m, are uniformly distributed over the cylindrical surface. The drum is approximately in contact to the spherical LP surface (gap of 5 mm), but more important bypass exists between drum and CSP. In order to simulate the flow path as realistic as possible in the TRACE model the perforate drum has been defined throughout the introduction of a surface porosity in the radial direction given by the ration of the total area of the holes and the area of the cylindrical surface. The resulting porosity is: $\varepsilon_s = 0.208$. The pressure head losses throughout the perforate drum have been modeled has singular losses introducing a K-factor in the radial direction (R2) of the vessel nodalization. Furthermore, the bypass between drum and the core support plate is modeled in the TRACE nodalization taking in account the pressure head losses as singular losses at the entrance of the bypass (drum-CSP) region.

The CSP has been modeled using volume porosity equal to the surface porosity variable in the radial direction to reproduce the distribution of the 193 core channels as summarized in Table 48 and depicted in Figure 219.

The core pipes in the core region are modeled and using the same fluid volume distribution set up for the CSP.

Table 48 – Volume porosity distribution in the CSP

Radius	R1	R2-R3	R4	R5 (barrel zone)	R6 (DC zone)
Porosity	0.33	0.35	0.16	0	1

Table 49 – Volume porosity distribution in the LP (subdivided in 3 axial mesh)

	Axial layer	R1	R2	R3	R4	R5 (barrel zone)	R6 (DC zone)
Porosity	1 (LP bottom)	1	1	1	1	1	1
	2 (drum zone)	1.	1	0.9048	0.7155	0.4331	0.0493
	3 (Bypass)	0.5109	0.5158	0	0	0	0

The fluid domain in TRACE-V5 model of the ROCOM facility is represented in Figure 218.

Eight pipes are used to simulate the CL and HL nozzles, radially linked to the VESSEL component preserving their real position. Each of the four pumps are represented by a FILL component. To close the loops four BREAK components are used to treat the pressure boundary of the hot legs.

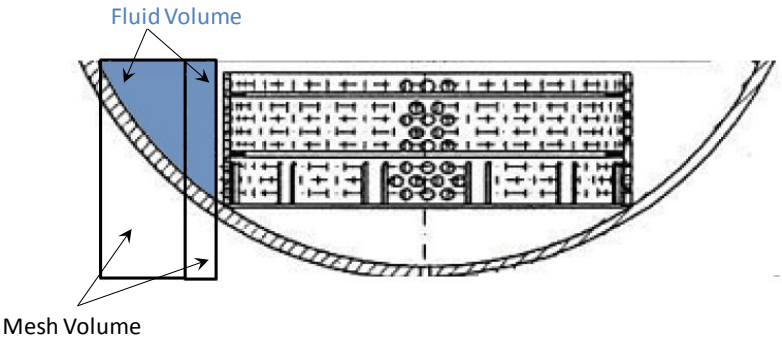

Figure 217 – definition of the 3-D fluid domain in the computational cells

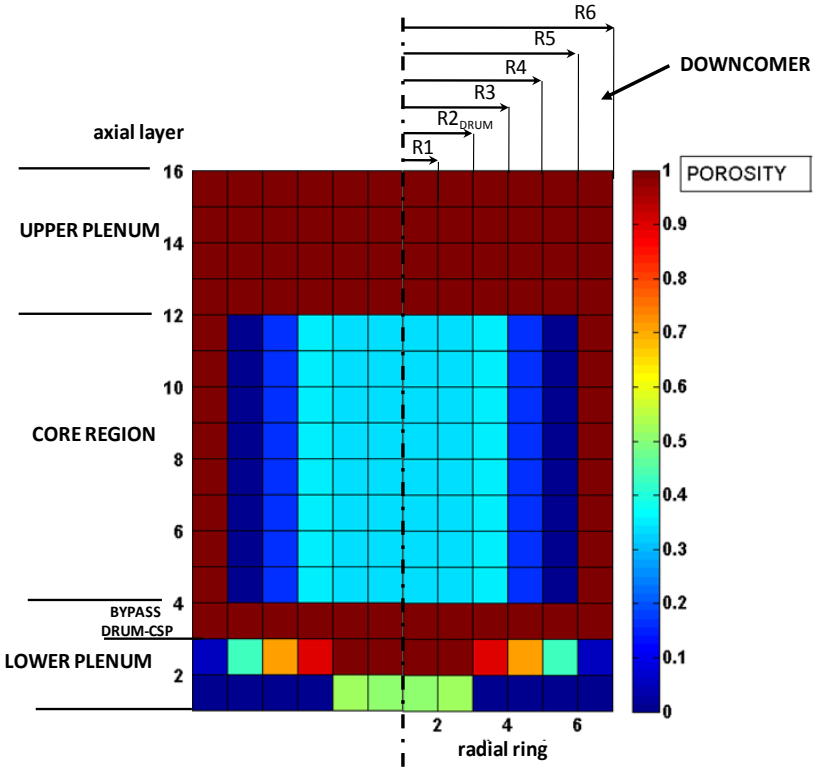

Figure 218 – Volume porosity distribution in the TRACE-V5 vessel model

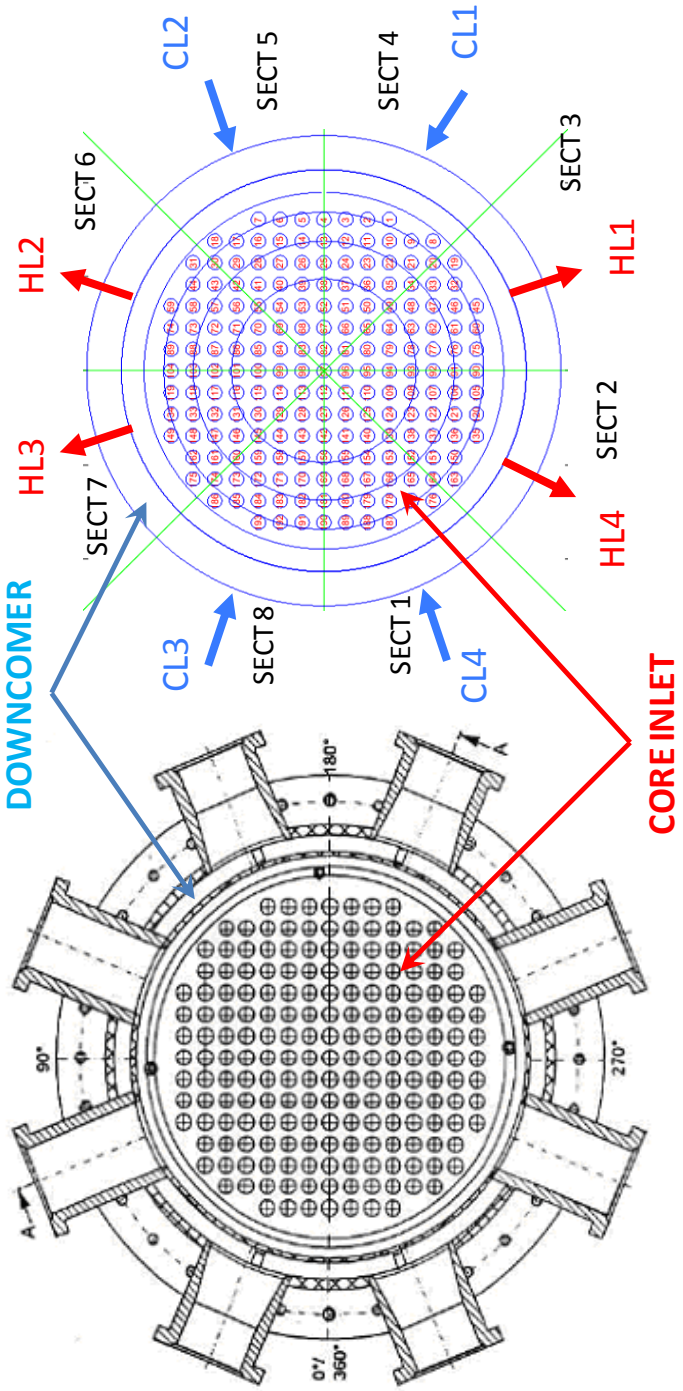

Figure 219 – ROCOM nodalization sketch: top view

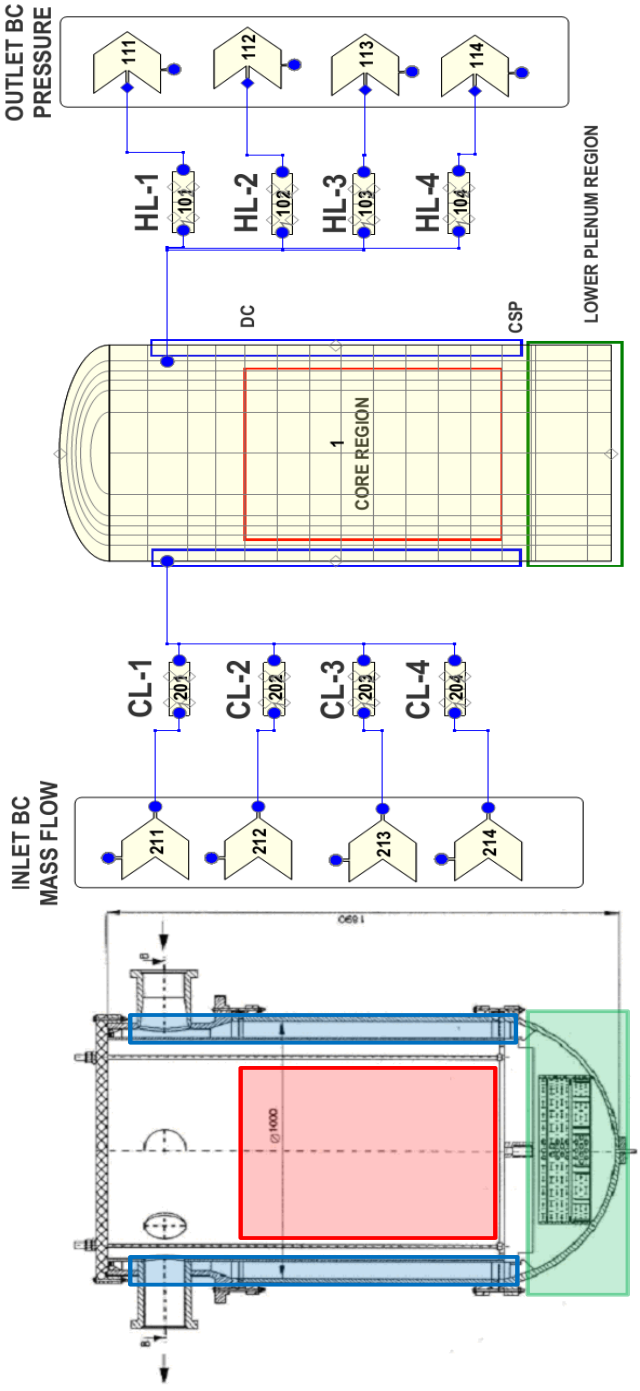

Figure 220 – ROCOM nodalization sketch: front view

APPENDIX E. QUANTIFICATION OF THE ACCURACY: THE FFTBM AND THE APPLICATION

E.1. Description of the Fast Fourier Transform Based Method

E.1.1. Background

Several approaches have been proposed to quantify the accuracy of a given code calculation (information are in [E-1], [E-2] and [E-3]. Even though these methods were able to give some information about the accuracy, they were not considered satisfactory because they involved some empiricism and were lacking of a precise mathematical meaning. Besides, engineering subjective judgment at various levels is deeply inside proposed methods.

Generally, the starting point of each method is an error function, by means of which the accuracy is evaluated. Some requirements were fixed which an objective error function should satisfy:

1. at any time of the transient this function should remember the previous history;
2. engineering judgment should be avoided or reduced;
3. the mathematical formulation should be simple;
4. the function should be non-dimensional;
5. it should be independent upon the transient duration;
6. compensating errors should be taken into account (or pointed out);
7. its values should be normalized.

The simplest formulation about the accuracy of a given code calculation, with reference to the experimental measured trend, is obtained by the difference function:

$$\Delta g(t) = g_{calc}(t) - g_{\exp}(t) \qquad \text{(E-1)}$$

The information contained in this time dependent function, continuously varying, should be condensed to give a limited number of values which could be taken as indexes for quantifying accuracy. This is allowed because the complete set of instantaneous values of $\Delta g(t)$ is not necessary to draw an overall judgment about accuracy. Integral approaches satisfy this requirement, since they produce a single value on the basis of the instantaneous trend of a given function of time. On the other hand, searching for functions expressing all the information through a single value, some interesting details could be lost. Therefore, it would be preferable to define methodologies leading to more than one value in order to characterize the code calculation accuracy. Information that comes from the time trend of a certain parameter, either being it a physical or a derivate one, may be not sufficient for a deep comprehension of the concerned phenomenon; in such a case, it may be useful to study the same phenomenon from other points of view, free of its time dependence. In this context, the complete behavior of a system in periodic regime

conditions (periodic conditions due to instability phenomena are explicitly excluded) can be shown by the harmonic response function that describes it in the frequency domain.

E.1.2. Method development

Time representation of a physical parameter that describes a particular phenomenon is the traditional way to represent a signal. However, the time domain representation may be insufficient to gain insight as to what constitutes a signal. For example, a signal can be affected by the presence of noise or disturbances at particular frequencies that are hidden in the time domain. In this context, the complete behavior of a signal can be understood changing the representation domain, in particular translating a given signal function of the time in the frequency domain that works with the frequency spectrum, that is, with the signal expressed as a function of frequency. The method whereby we may obtain the variation of a quantity as a spectral function is the Fourier Transform (FT). The FT is a powerful tool for signal processing that allows the decomposition of a signal as the sum of a possibly infinite number of sinusoids of different frequencies. The graphical display of a transformed signal is obtained through the two spectral coordinates: amplitude and frequency. In Figure 221 is illustrated an exemple of the Fourier transform of a simple time function. The FT of the exemple function is the two sinusoids that summed together produce the shape of the original time function.

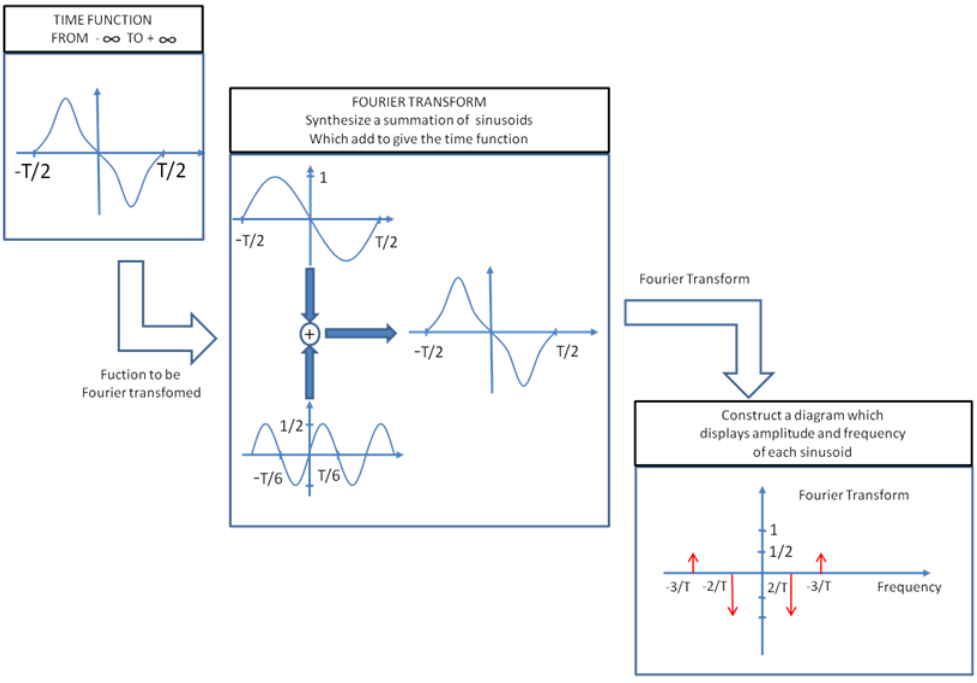

Figure 221 – Sample Fourier Transform representation

The construction of the frequency spectrum of a signal is obtained by means of integral formulation, namely:

$$\tilde{g}(f) = \int_{-\infty}^{+\infty} g(t) e^{-j2\pi ft} dt \qquad \text{(E-2)}$$

If the integral exist for every real value of the parameter f, it defines a function $\tilde{g}(f)$ known as Fourier transform of the function $g(t)$. The back transformation from the frequency domain to the time domain is defined by the inverse Fourier transform (see equation (E-3)).

$$g(t) = \int_{-\infty}^{+\infty} \tilde{g}(f) e^{j2\pi ft} df \qquad \text{(E-3)}$$

is assumed that the time function to which the Fourier transform is applied verify the analytical conditions required by its application theory; i.e., it is assumed that they are continuous (or generally continuous) in the considered time intervals with their first derivatives, and absolutely integrable in the interval (-∞, +∞).This last requirement can be easily satisfied in our case, if the addressed functions assume values different from zero only in the interval (0, T). Therefore:

$$\tilde{g}(f) = \int_{0}^{T} g(t) e^{-j2\pi ft} dt \qquad \text{(E-4)}$$

Generally, in computational work, we do not treat a continuous function $g(t)$ but rather $g(t_k)$ given by a discrete set of t_k's. (For now, we assume that a physical process of interest is described in the time domain.) In most common situations, the value of $g(t)$ is recorded at evenly spaced intervals. In this context, we have to estimate the Fourier transform of a function from a finite number of its sampled points. Suppose that we have a set of measurements performed at equal time intervals of Δt. Then the sequence of sampled values is given by:

$$\{g_0(t_0), g_1(t_1), ..., g_k(t_k)\}, \quad t_k = k\Delta t, \quad k = 0,1,2,..., N-1 \qquad \text{(E-5)}$$

Suppose that we have N consecutive sampled values. With N numbers of input, we can produce at most N independent numbers of output. So, instead of trying to estimate the Fourier transform $\tilde{g}(f)$ in the whole range of frequency f, we seek estimates only at the discrete values $f = f_n$ with $n = 0,1,2, \ldots, N-1$. By analogy with the Fourier transform for a continuous function $g(t)$, we may define the Fourier transform for a discrete set of $g_k = g(t_k)$ ($k = 0,1,2, \ldots, N-1$) as below:

$$\tilde{g}(f_n) = \int_{0}^{T_d} g(t) e^{-i2\pi f_n t} dt \approx \frac{1}{N} \sum_{k=0}^{N-1} g_k e^{-i2\pi f_n t_k} \Delta t = \Delta t \bullet \frac{1}{N} \sum_{k=0}^{N-1} g_k e^{-i2\pi f_n t_k} \qquad \text{(E-6)}$$

In other words to obtain the frequency spectrum of the sampled function we compute the integral through a discrete sum. The equation (E-6) between the discrete Fourier transform of a set of numbers and their continuous Fourier transform when they are viewed as samples of continuous function sampled at an interval Δt can be written as:

$$\tilde{g}\left(f_n\right) = \Delta t \bullet \tilde{g}_n \tag{E-7}$$

The discrete Fourier transform can be computed with an algorithm called the Fast Fourier Transform (FFT), which is algorithm that rapidly computes the discrete FT. To apply it, functions must be identified by a number of values that are a power with base equal to 2 and sampling theorem must be fulfilled. The fulfillment of the sampling theorem is required to avoid distortion of sampled signals due to aliasing occurrence. This theorem, first enunciated by Nyquist in 1928 [E-4] and then proved by Shannon in 1949 [E-5], establishes that any band limited signal can be uniquely determined by its samples as long as the sample rate is at least twice that of the highest frequency found in the signal. The highest frequency of the signal is usually referred to as the Nyquist frequency and twice this, which is the frequency that must be exceeded by the sampling rate, is commonly called the Nyquist rate. Thus, if the number of points defining the function in the time domain $N = 2^{m+1}$ then according to the sampling theorem the sampling frequency is given by the equation (7).

$$\frac{1}{\Delta t} = f_s = 2 f_{\max} = \frac{N}{T_d} = \frac{2^{m+1}}{T_d} \tag{E-8}$$

Where, T_d is the transient time duration of the sampled signal and f_{max} is the highest (maximum) frequency component of the signal. The sampling theorem does not hold beyond f_{max}. From the relation in (E-8) is seen that the number of points selection is strictly connected to sampling frequency. The FFT algorithm determines the number of points, equally spaced, which is a power with base 2 (N range from 2^9 to 2^{12}). Generally, an interpolation is necessary to satisfy this requirement. Taking in account that the available subroutine packages evaluate the FFT normalized to the time duration T_d, from the equations (E-4) and (E-8), it can be easily seen that $|\tilde{g}(0)|$ represent the mean value of the function $g(t)$ in the interval $(0, T_d)$ while $|\tilde{g}(f_n)|$ represent the amplitude of the n-th term of the Fourier polynomial expansion $g(t)$. To apply the methodology described above, after selecting the signals to be analyzed, it is necessary to choose the following parameters: number of points, sampling frequency and cut frequency.

The method developed for the code accuracy quantification of an individual calculation is based on the amplitude of the FFT of the experimental signal and of the difference between this one and the calculated trend. In particular the method introduces the definition of two *figures of merits,* which gives a synthesis of the information inside the error function (1). Indeed any of features that have these figures is to have memory of the discrepancy between the experimental and the analytical time trend of a parameter.

$$AA = \frac{\sum_{n=0}^{2^m} \left|\Delta\tilde{F}\left(f_n\right)\right|}{\sum_{n=0}^{2^m} \left|\tilde{F}_{\exp}\left(f_n\right)\right|} \qquad WF = \frac{\sum_{n=0}^{2^m} \left|\Delta\tilde{F}\left(f_n\right)\right| \cdot f_n}{\sum_{n=0}^{2^m} \left|\Delta\tilde{F}\left(f_n\right)\right|} \tag{E-9}$$

The average amplitude AA represents a sort of average fractional error of the addressed calculation, while the weighted frequency gives an idea of the frequencies which give the greatest contribution to the inaccuracy. The two obtained values can be used to evaluate the accuracy of the code calculation by representing the discrepancies with respect to the experimental data through a point in the AA-WF domain. Of course the most interesting information is given by AA, which represents the relative magnitude of these discrepancies; WF adds a further information allowing to better identify the character of accuracy. As an example, oscillations of the calculated values around an average trend can be readily identified by the method. Moreover, this information can be used, in principle, in the quantification of the accuracy. In fact, depending on the transient and on the variable considered, low frequency errors can be more important that high frequency ones, or vice versa (in thermal hydraulic transient, better accuracy is generally represented by AA low values at high WF values) (see [E-1] [E-6]).

Trying to give an overall picture of the accuracy of a given calculation, average indexes of performance are obtained by defining average performance indices: the total weighted $(AA)_{tot}$ (see Eq. E-10) and the total WF_{tot} (see equation (see Eq. E-11))

$$\left(AA\right)_{tot} = \sum_{i=1}^{N_{\text{var}}} AA \cdot \left(w_f\right)_i \tag{E-10}$$

$$\left(WF\right)_{tot} = \sum_{i=1}^{N_{\text{var}}} \left(WF\right)_i \left(w_f\right)_i \tag{E-11}$$

with

$$\sum_{i=1}^{N_{\text{var}}} \left(w_f\right)_i = 1 \tag{E-12}$$

Where N_{var} is the number of analyzed parameters and $(w_f)_i$ are weighting factors that take into account the different importance of each parameter from the viewpoint of safety analyses.

Following the quantitative evaluation of accuracy, the Quantitative Assessment (QA) can be managed by means of the application of the FFT method. Obviously, the most suitable factor for the definition of an acceptability criterion is the average amplitude AA. With reference to the accuracy of a given calculation, we can define the following acceptability criterion:

$$(AA)_{tot} < K \tag{E-13}$$

Where, K is an acceptability factor that is valid for the whole transient. As lower is the AA_{tot} value, as better is the accuracy of the analyzed calculation. With reference to experience gathered from previous applications of this methodology, K = 0.4 has been chosen as reference threshold value identifying acceptable accuracy of a code calculation.

E.1.3. Methodology implementation

In the following, the FFT method application will be dealt with from an operative point of view. To apply the methodology described in the previous section, after selecting the parameters to be analyzed, it is necessary to choose the following parameters:

- number of points
- sampling frequency
- cut frequency.

All these items are related each other, nevertheless they will be treated in separate sub-sections, in order to allow a better comprehension of their requirements.

E.1.3.1. Sampling frequency

In order to evaluate the discrete Fourier transform, it is necessary, first of all, the sampling of signals to be analyzed. The choice of the sampling frequency depends on transient, kind of parameter trend to be investigated (i.e. pressure, flow rate, clad temperature, etc.); obviously, the fulfillment of the sampling theorem is required to avoid distortion of sampled signals due to aliasing occurrence (see section E.1.2 and Eq. E-8)

$$T = \frac{1}{2 f_c} \tag{E-14}$$

where f_c is the highest frequency component of Fourier transform characterizing the spectrum of the continuous function g(t).Therefore, experimental data acquisition should be characterized by sampling frequency greater than 2 f_c [9] similar frequencies of acquisition should have the corresponding calculated trends. Of course, compared analysis of these data requires that the lowest value of f_c (between the experimental and calculated one) should be taken as limiting value. A typical value of f_c related to parameters of interest in thermal hydraulic transients is 1 Hz; specifically, break flow rates or pressure drops measurements can include higher values.

E.1.3.2. Number of points

Since the FFT algorithm requires that functions are identified by a number of values, equally spaced, which is a power of 2, an interpolation is necessary to satisfy this requirement. On the other hand, the comparison of experimental and calculated signals, and the evaluation of their difference function $\Delta g(t)$, imposes that they have the same time scale.

Furthermore, after selecting the number of points $N = 2^{m+1}$, the maximum frequency of transformed functions by the FFT is given as expressed in Eq. E-8.

[9] Normally 3-4-5 times fc is used.

Then, the number of points is strictly associated with the adopted sampling frequencies; it is meaningless to choose a number of points corresponding to a frequency[10] greater than the f_{max} achievable using a certain f_c. On the other hand, during the interpolation step, some information could be lost choosing a too low number of points. Last, it is worthwhile to remember that the increase of the number of points involves the growth of the array dimensions utilized by the program package set up for the full method application.

Besides, the interpolation introduces an additional effect on signals, i.e. each interpolation, using a linear method, adds a slope. It has been verified that this effect is negligible, because it causes the addition of some spurious frequencies in the original signal spectrum, having values greater than the typical frequencies of thermal hydraulic parameters. On the other hand, most thermal hydraulic quantities are characterized by low frequencies, then high frequency errors (therefore, these spurious contributions too) can be totally avoided considering proper filtering techniques.

E.1.3.3. Cut frequency

To filter any spurious contribution, a cut frequency has been introduced. This cut frequency characterizes the frequency upper value which has to be considered in evaluating the AA and WF factors, as defined by Eq. (E-9).

Typical thermal hydraulic parameter trends (for different kinds of transients) have been analyzed [E-7], aiming at defining an unique suitable value of cut frequency, in such a way to avoid partial loss of information. A cut frequency value of 1 Hz is generally suitable to analyze trends of thermal hydraulics parameters; only flow rates and densities require cut frequency values up to 2 Hz, as a consequence of their higher frequencies, to avoid loss of information in accuracy evaluation.

E.1.3.4. Choice of the weights

In order to give an overall picture of the accuracy of the addressed calculation, the FFT method accounts for the accuracy evaluated for each parameter, and defining some weighting factors $(w_f)_i$ global indexes of code performance are evaluated (see eqs. [E-10] and [E-12]). The need of $(w_f)_i$ definition derives from the fact that the addressed parameters are characterized among other things by different importance and reliability of measurement.

Thus, each $(w_f)_i$ takes into account of:

"experimental accuracy": experimental measures of thermal-hydraulic parameters are characterized by a more or less sensible uncertainty due to:

- intrinsic characteristics of the instrumentation
- assumptions formulated in getting the measurement

[10] Beyond $f_c/2$ the sampling theorem doesn't hold, and we have no further information about these frequencies.

- unavoidable discrepancies existing between experimental measures and the code calculated ones (mean values evaluated in cross-sections, volume centers, or across junctions, etc.);

"*safety relevance*": particular importance is given to the accuracy quantification of calculations concerned with those parameters (e.g. clad temperature, from which PCT values are derived) which are relevant for safety and design.

Last, a further contribution is included in the weighting factors definition; this is a component aiming at accounting for the physical correlations governing most of the thermal hydraulic quantities. Taking as reference parameter the primary pressure (its measurement can be considered highly reliable), a normalization of the AA values calculated for other parameters with respect to the AA value calculated for the primary side pressure is carried out. In other words, the following factor has been defined (for the generic j-th parameter):

$$\left(w_{nom}\right)_j = \frac{\left(AA\right)_{pr}}{\left(AA\right)_j} \tag{E-14}$$

where:

- $(AA)_{pr}$ is the average amplitude calculated for the primary side pressure
- $(AA)_j$ is the average amplitude calculated for the j-th parameter.

So doing, the weighting factor for the generic j-th parameter, is defined as:

$$\left(w_f\right)_j = \frac{\left(W_{exp}\right)_j * \left(W_{saf}\right)_j * \left(W_{norm}\right)_j}{\sum_{j=1}^{N_{var}} \left(W_{exp}\right)_j * \left(W_{saf}\right)_j * \left(W_{norm}\right)_j} \tag{E-15}$$

The $(w_f)_j$ must fulfill the constrain given by the Eq. E-12.

- N_{var} is the number of parameters to which the method is applied
- $(W_{exp})_j$ is the contribution related to the experimental accuracy
- $(W_{saf})_j$ is the contribution expressing the safety relevance of the parameter.

$(W_{exp})_j$ and $(W_{saf})_j$ values have to be assigned using engineering judgment, starting from measuring and safety related considerations. Such an evaluation of a suitable set of weights to be utilized for typical thermal-hydraulic quantities has been performed [E-7]. Some criticism could be raised because engineering judgment is required in weights assignment, but actually, this appears the only practicable way to define the relative importance of the parameters selected to evaluate the accuracy of a code calculation. These weights must remain the same for any comparison between code results and experimental data concerning a same class of transient. Recently, an application of the FFT method to the quantification of the accuracy for containment system codes (based on ISP 35, NUPEC) has been carried out [E-8]. For this application, different considerations were necessary in setting up a suitable set of weights, taking into account design features and safety

concerns related to the containment. On the other hand, once chosen a set of weights with the above described criteria, any variation of some weight involves a homogeneous change of all the calculations analyzed, above all if a sufficiently high number of parameters has been selected for the accuracy evaluation. Obviously, this affects only global accuracy evaluation of a code calculation; no concern is related to the single parameters accuracy.

The weight $(W_{norm})_j$, defined in the Eq. E-14, is given by a factor, which normalizes the AA value calculated for the selected variables with respect to the AA value calculated for the primary pressure. This factor has been introduced in order to consider the physics relations existing between different quantities (i.e. fluid temperature and pressure in case of saturated blow-down must be characterized by the same order of error). The measurement of the primary pressure can be considered highly reliable. Weighting factors have been introduced considering that the quantities that are the object of the accuracy evaluation are not independent from each other. The interdependency among the quantities is complex and is fixed (on the code side) by partial differential equations and by the actual system status (on the experimental side). It is impossible to characterize the function of one quantity versus the others. This function also depends upon the selected transient scenario

E.1.3.5. FFT package

In the first phase of the activities concerned with the definition of the method, some Matlab programs were written in order to perform in an independent way the basic steps of the method. This allowed to better focus the attention on the consistency of the obtained results, further adjusting and improving of the utilized algorithm, and obviously, the validation of each module. On the other hand, during this developmental phase, limited applications (in terms of number of code calculations and parameters analyzed) of the method were carried out, not making necessary the availability of an automatic tool.

Encouraging results achieved by various analyses, related to a wide application range of the FFT based method (see [E-9] and [E-10]) and the occurrence of the large application related to ISP 27 code calculations promoted something like an "assembling" of these programs. This activity was completed during the visiting period at the CEN-FAR, whenever it resulted in the complete development of new modules, allowing a complete use of the method and the execution of various kinds of analyses in a totally automatic way. In practice, an unique source program has been built, managing in the mean time experimental and several calculated data files for the extraction of the variables to be analyzed, application of the FFT method up to getting the evaluation of AA and WF quantities (see Eq. E-9). The results obtained for the single parameters are then processed by another small program in order to get global code accuracy (see Eq. [E-10]).

The program has a modular structure, consisting of a main program supervising the execution of the different tasks, performed by single subroutines, thus allowing the implementation of further modules without main changes in the program. In fact, being available such an automatic tool and from the experience gathered by previous applications, further options were included in the FFT package, increasing

its versatility and applicability. The source program has been coded in FORTRAN 77 standard.

Recently, considering the memory and computing speed performances of current personal computers, a version of the FFT package suitable for such microcomputers has been set up; moreover, running the program on a personal computer implies relatively (a little) slower performances, surely acceptable, taking into account that no data transfer is necessary and that all the results can be immediately processed by means of standard available software (like Microsoft Excel, etc.), taking advantage of the Microsoft Windows environment features. This version has been built utilizing the Matlab routines.

As above mentioned, some new features have been introduced in the program, increasing its flexibility and applicability. The program capabilities can be summarized as follows:

- research and extraction of the addressed variable from data files, allowing various data format;
- conversion of current data units in SI units, or more generally possibility of manipulate data (optional);
- analysis of several time windows in a same execution, where each time window can identify whatever phase in the transient;
- time shifting of data trends to analyze separately the effects of delayed or anticipated code predictions concerning some particular phenomena or systems interventions (optional);
- interpolation of data points to a power of 2 number of points, coherent with sampling frequency and minimum analysis frequency (parameter FFIX);
- FFT evaluation of the signals to be processed;
- evaluation of the AA and WF quantities (see see Eq. E-9);
- output files generation, including information to be processed by standard software in order to trace any desired graphic concerning data curves, error curves, interpolated curves, FFT signals transforms, FFT data spectra, AA-WF data (optional).

E.1.4. Application of the method to sample curves

The curves in Figure 222 can be considered to understand the main the features of the adopted method. The experimental signal is a constant while two possible calculated curves are considered. The first (Curve 1) is a constant with a value different from the experimental one; in this case the average amplitude, AA, is equal to the ratio between the absolute value of the difference to the experimental value. Curve 2 has a sinusoidal shape, the amplitude of the oscillation being equal to the difference between the Curve 1 and the experimental value; it can be verified that AA has in this case the same value as for the Curve 1.

Despite of this, the two cases are characterized by a different value of WF. In fact, for Curve 1 is WF = 0, whilst for Curve 2 it is WF = =1/T. This demonstrates that the selected method allows to distinguish between discrepancies of the same magnitude at different frequencies.

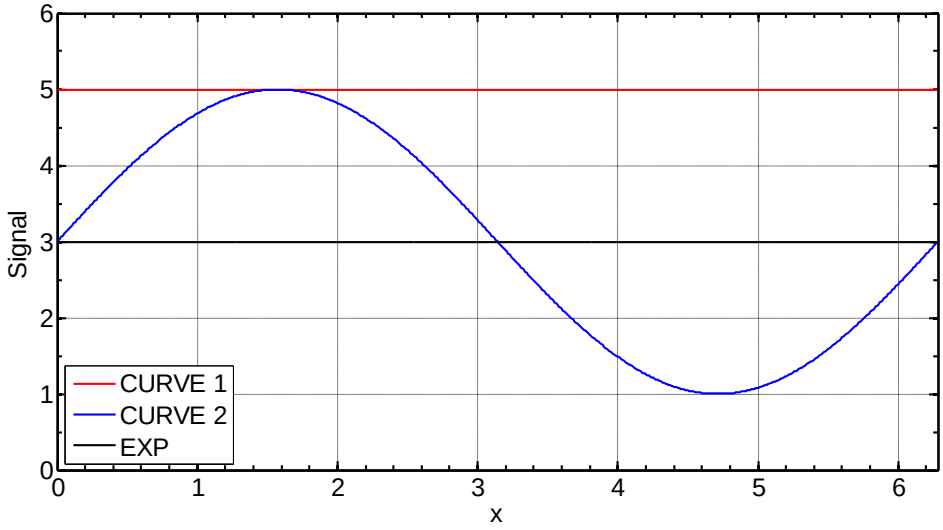

Figure 222 – Sample Problem 1: considered experimental and calculated cirves

The meaning of AA and WF can be clarified also by second exemple. We suppose that the experimental signal and the calculated signal are given by:

$$F_{\exp}(t) = t \qquad if\ \ 0 < t \le 15$$

$$F_{cal}(t) = \begin{cases} 1.4t & if\ \ t \le 5 \\ 4.5 + 0.5t & if\ \ 5 < t \le 15 \end{cases} \tag{E-16}$$

Using the Eq. E-1 the error function is given by the following expression:

$$\Delta F(t) = \begin{cases} 0.4t & if\ \ t \le 5 \\ 4.5 - 0.5t & if\ \ 5 < t \le 15 \end{cases} \tag{E-17}$$

and its graphical representation is shown in Figure 223.

For applying the FFT algorithm the time signal must be interpolated in according to the sampling theorem which states that discrete time signal is identify in digital form by a number of values which is a power of 2, (in particular from 2^9 to 2^{12}) depending on the numbers of discrete points. Choosing $N = 512$ and $T_d = 15s$ being, the maximum frequency is equal to 17.066 Hz. It is suppose that the cut frequency is 0.5 Hz. In this way the amplitude spectrum obtained by means the FFT algorithm generate eight amplitudes for the three signals:

$$\begin{aligned}
\tilde{F}_{exp}(f_n) &= \{7.485 \quad 4.775 \quad 2.387 \quad 1.592 \quad 1.194 \quad 0.955 \quad 0.796 \quad 0.682\};\\
\tilde{F}_{cal}(f_n) &= \{7.488 \quad 3.394 \quad 2.077 \quad 1.273 \quad 0.922 \quad 0.790 \quad 0.637 \quad 0.535\};\\
\Delta\tilde{F}(f_n) &= \{0.002 \quad 1.853 \quad 0.414 \quad 0.318 \quad 0.282 \quad 0.171 \quad 0.159 \quad 0.149\}.
\end{aligned} \tag{E-18}$$

The spectrum of these functions can be seen in Figure 224, Figure 225 and Figure 226.

The AA calculated following the Eq. E-9 is:

$$AA = \frac{\sum_{n=0}^{7}\left|\Delta\tilde{F}(f_n)\right|}{\sum_{n=0}^{7}\left|\tilde{F}_{\exp}(f_n)\right|} = \frac{0.002+1.853+0.414+0.318+0.282+0.171+0.159+0.149}{7.485+4.775+2.387+1.592+1.194+0.955+0.796+0.682} \tag{E-19}$$

While WF is obtained applying the Eq. E-9

$$\begin{aligned}
WF &= \frac{\sum_{n=0}^{7}\left|\Delta\tilde{F}(f_n)\right|\cdot f_n}{\sum_{n=0}^{7}\left|\Delta\tilde{F}(f_n)\right|} = \frac{0+0.1235+0.0551+0.0636+0.0751+0.0569+0.0636+0.0696}{0.002+1.853+0.414+0.318+0.282+0.171+0.159+0.149} \\
&= \frac{0.508}{3.349} = 0.152
\end{aligned} \tag{E-20}$$

When looking at the amplitude spectra of the difference signal (see Figure 226) we can observe that it is exponentially falling function of the frequency. Then we can conclude that a small value for WF means that the discrepancie between the measured and the calculated trends is more important at low frequencies. When WF is large, the discrepancy comes from various kinds of noise and consequently is less important.

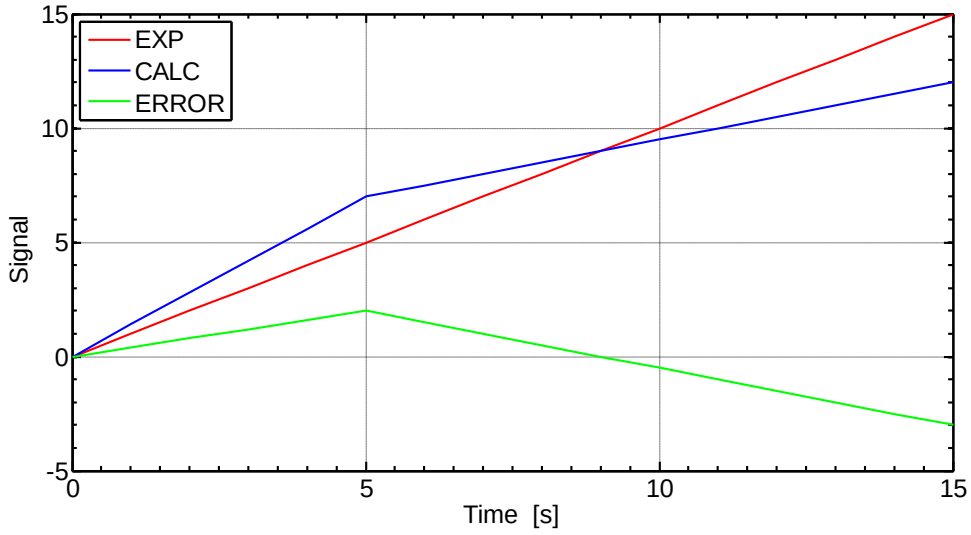

Figure 223 – Accuracy evaluation using FFTBM: graphical representation of functions (experimental, calculated and error) in time domain

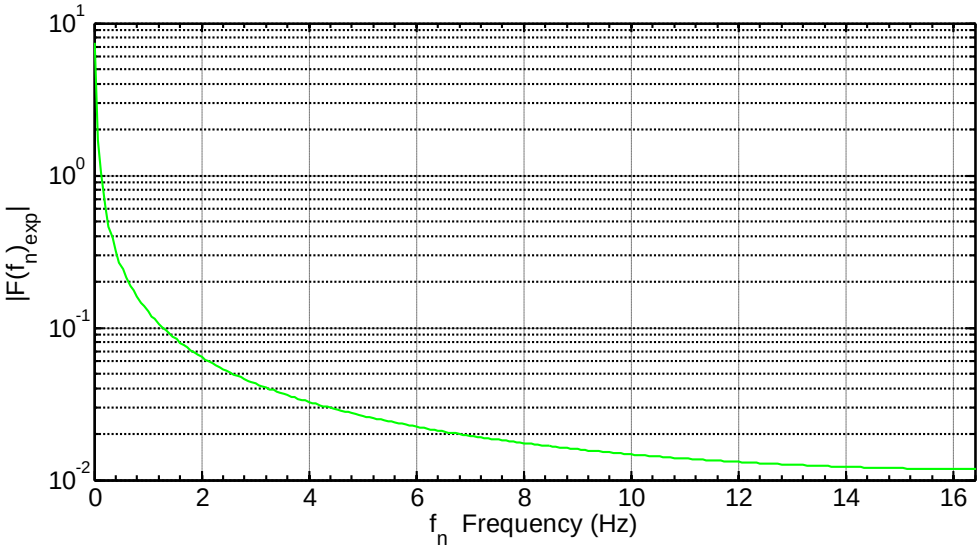

Figure 224 – Accuracy evaluation using FFTBM: spectrum of the experimental function

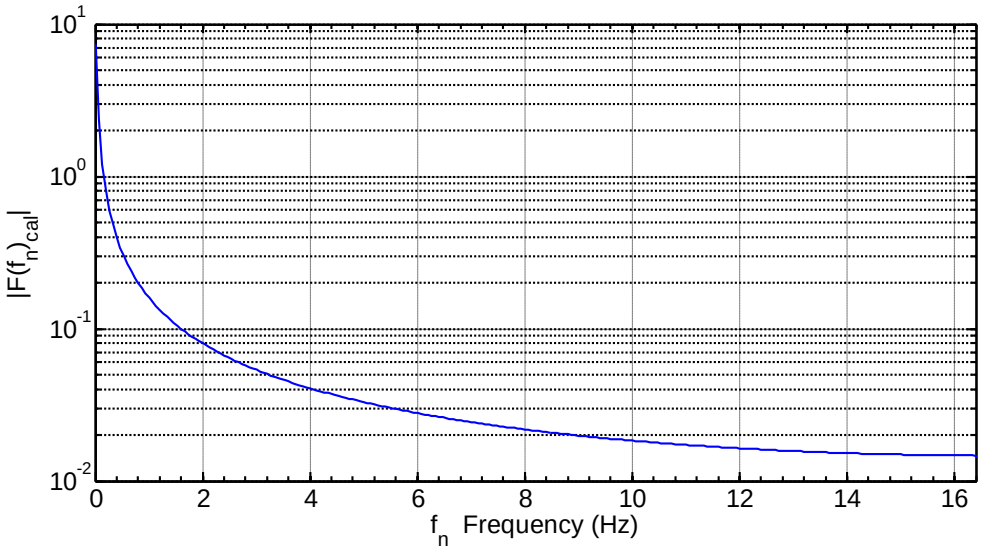

Figure 225 – Accuracy evaluation using FFTBM: spectrum of the calculated function

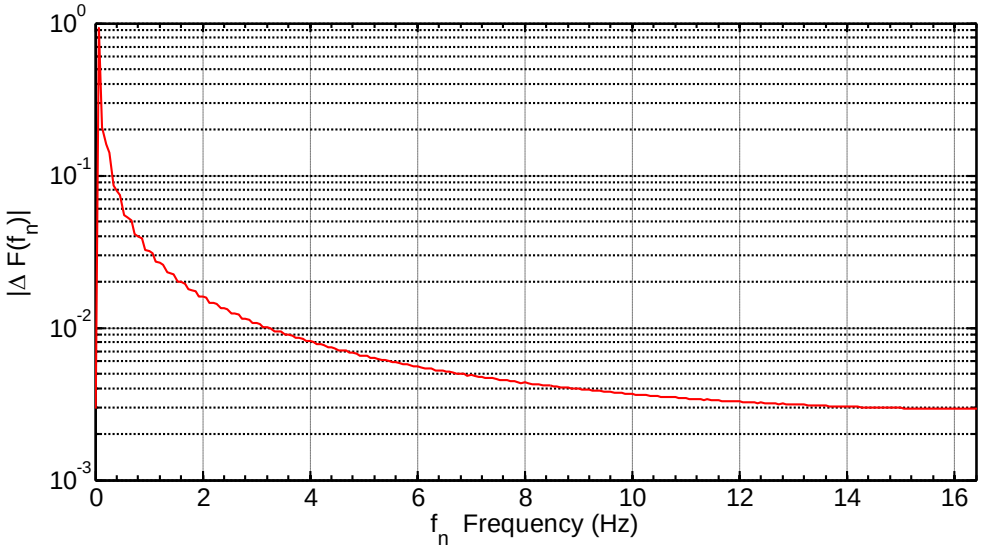

Figure 226 – Accuracy evaluation using FFTBM: spectrum of the error function

E.1.5. References to APPENDIX E

[E-1] Ambrosini W., Bovalini R., D'Auria F., *"Evaluation of accuracy of Thermal-hydraulic code calculations"*, J. Energia Nucleare,vol. 2, 1990.

[E-2] Riebold W., *"Minutes of the OECD/CSNI SACTE Task Group Meeting"*, Paris, December 1987.

[E-3] Pochard R., Porracchia A., *"Assessment closure proposal"*, OECD/CSNI SACTE Task Group Meeting, Paris, December 1986.

[E-4] Nyquist H., *"Certain topics in telegraph transmission theory"*. Transactions AIEE, vol. 47, 1928, pp. 617–644.

[E-5] Shannon C. E., *"Communication in the presence of noise"*. Proceedings Institute of Radio Engineers, vol. 37(1), 1949, pp. 10–21.

[E-6] Prošek A., D'Auria F,, Mavko B,, *"Review of quantitative accuracy assessments with fast Fourier transform based method (FFTBM)"*, Nuclear Engineering and Design, vol. 217, 2002, pp. 179-206.

[E-7] Bovalini R., D'Auria F., Leonardi M., *"Qualification of the Fast Fourier Transform based methodology for the quantification of thermal-hydraulic system code accuracy"*, DCMN NT 194(92), Pisa, 1992.

[E-8] Leonardi M., Oriolo F., Paci S., Villotti A., *"ISP 35 on NUPEC M-7-1 test: evaluation of codes accuracy"*, DCMN RL 633(94), Pisa, 1994

[E-9] D'Auria F., Leonardi M., Pochard R., *"Methodology for the evaluation of thermahydraulic codes accuracy"*, Int. Conf. on 'New Trends in Nuclear System Thermohydraulics', Pisa, May 30 - June 2, 1994.

[E-10] Leonardi M., D'Auria F., Pochard R., *"The FFT based method in the frame of the UMAE"*, Spec. Workshop on Uncertainty Analysis Methods, London, March 1994.